Synthesis and Magnetic Properties of Cobalt Nickel Nanoparticles Prepared by Chemical Reduction Methods

Jalpa Dipesh Patel

Thesis submitted to the University of London, University College London in partial fulfilment of the requirements for the degree of

Doctor of Philosophy
In Chemistry

Supervised by:

Prof Ivan P. Parkin, Department of Chemistry, University College London

Prof Quentin A. Pankhurst, London Centre for Nanotechnology, University College London

June 2007

UMI Number: U592381

Dissertation Publishing

Declaration

I, Jalpa Dipesh Patel, confirm that the work presented in this thesis is my own. Where information has been derived from other sources, I confirm that this has been indicated in the thesis.

ABSTRACT

The purpose of this work was to prepare and characterise Co_xNi_{1-x}/CoNiO core-shell magnetic nanoparticles which showed magnetic exchange bias. The particles were synthesised using a variety of stabilising surfactants and nucleating seeds, via the polyol reduction method. The surfactants were used to coat nanoparticles of various diameters, to prevent agglomeration and oxidation. A mixture of 1:1 oleic acid: oleylamine was found to be the best stabilising agent for the particles as it protected against complete oxidation whilst allowing a partial oxide shell to form. Phosphine-based surfactants yielded particles with spherical morphologies. However, these particles were too small to support oxide-shell growth, and oxidised fully to antiferromagnetic phases. The nucleation of particles was probed using homogeneous and heterogeneous methods. Homogeneous nucleation resulted in particles which had predominantly oxidised to the core, and therefore did not yield pronounced exchange bias effects. Heterogeneous nucleation was attempted using various seeding techniques and seed materials. Platinum seeds were found to be the most effective in controlling the size of Co_xNi_{1-x} nanoparticles. They yielded larger particles with core-shell morphology. Following optimisation of the synthesis conditions, a compositional series of Co_xNi_{1-x} nanoparticulate composite alloys were made. All samples were analysed using TEM to determine the size and structure of the individual particles. A number of other techniques including X-ray diffraction, X-ray photoelectron spectroscopy, Energy-dispersive X-ray analysis, Electron energy loss spectroscopy and Thermogravimetric magnetic analysis, were also used to fully characterise the phase, crystallinity, composition and oxidation in individual particles. The magnetic properties of the particles, made using the various reaction conditions, were measured using the SQUID technique. Exchange bias has been observed in several of the alloyed samples in additional to the cobalt particles made using the polyol technique. Nickel particles did not display any characteristic exchange bias properties.

Acknowledgements

I would firstly like to thank my supervisors, Prof. Ivan Parkin and Prof. Quentin Pankhurst, for their support, guidance and insight over the last few years. I also would like to thank Dr Dorothy Farrell for her guidance which has been invaluable. Dorothy also helped obtain the SQUID measurements that are reported in this thesis, training in TEM analysis and particle synthesis. I thank Dr Ana Garcia Prieto for her effort and insight into characterisation of the synthesised particles using XRD analysis. Dr Steve Firth provided a great deal of assistance with technical aspects relating to the TEM and in particular, helped with my understanding of the TGA technique. Robert Palgrave is thanked for carrying out XPS measurements on the samples reported in this thesis, as is Mrs Jillian Maxwell for elemental analysis. Kevin Reeves is also thanked for helping to refresh my memory on the SEM and EDX analysis of nanoparticles. John Hill, Dave Knapp, Dave Ladd, Joe Nolan and Phil Hayes are thanked for kindly taking the time to help me with various technical problems I have had over the years. Their effort and enthusiasm is much appreciated.

All members of the Parkin and Carmalt research groups are thanked for making the lab an enjoyable place to work, and in that respect I would particularly like to thank Robert Palgrave, Sobia Ashraf, Nicolas Boscher, Dr Jesus Gil-Tomas, Plaboni Hasan and Uzma Qureshi, Kristopher Page, Stephen Potts, Naima Narband, Dr Clara Piccirillo, Paulo Melgari who have been fun to work with. Dr Chris Blackman, Dr Russell Binions, Dr Geoff Hyett and Dr Troy Manning are thanked for many useful discussions over the past four years, and for general help with Schlenk line work, synthetic methods and analysis. I would particularly like to thank Dr Siama Basharat, Dr Ashti Rampaul and Dr Dina Solanki for being the great colleagues and friends that they are. The advice they have given me over the past few years has been more important than they probably realise.

There are always so many friends and family members to thank, however I would like to begin by taking the opportunity to thank my paternal grandparents, Mr Bhanubhai and Mrs Bhanuben Patel, for their love and encouragement over the years. Their encouraging phone calls from India have always been valued, as has the advice they have given me. I would also like to thank my maternal grandparents, Late Mr

Table of Contents

List of figures

-11-

Chapter 2. Polyol synthesis of Co_xNi_{1-x} magnetic nanoparticles

[1] Gallagher, P. K.; Blaine, R.; Charsley, E. L.; Koga, N.; Ozao, R.; Sato, H.; Sauerbrunn, S.; Schultze, D.; Yoshida, H., Magnetic temperature standards for TG. *Journal of Thermal Analysis and Calorimetry* **2003**, 72, (3), 1109-1116.

---

[2] Becker, J. J., Surface Effects on Hysteresis Loop Shapes in High-Coercive-Force Crystallized Amorphous-Alloys. *Ieee Transactions on Magnetics* **1982**, 18, (6), 1451-1453.

List of tables

List of schemes

List of abbreviations

acac	Acetylacetonate
acet	Acetate
AFM	Antiferromagnet
Ag	Silver
Au	Gold
CNT	Classical nucleation theory
Co	Cobalt
EDXA	Energy dispersive x-ray analysis
EELS	Electron energy-loss spectroscopy
eV	Electron volts
EXAFS	Extended X-ray absorption fine structure
FC	Field-cooled
fcc	face-centred cubic
Fe	Iron
FM	Ferromagnet
FTIR	Fourier transform infrared spectroscopy
H	Magnetic field strength
H_C	Coercivity
hcp	hexagonal close packed
HDA	Hexadecylamine
H_E	Exchange bias field
k	Boltzmann's constant
K	Anisotropy constant
M	Mass magnetisation
M_r	Remanent magnetisation
M_s	Saturation magnetisation
N	Nitrogen
Ni	Nickel
nm	nanometer
O	Oxygen
OA	Oleic Acid

Oe	Oersted
OY	Oleylamine
Pt	Platinum
SQUID	Superconducting quantum interference device
TBP	Tributylphosphine
TEM	Transmission electron microscopy
TGA	Thermogravimetric analysis
TOPO	Trioctylphosphine oxide
UV-Vis	Ultraviolet-Visible Spectroscopy
XRD	X-ray diffraction
ZFC	Zero field-cooled
T_b	Blocking temperature
T_c	Curie temperature
T_n	Néel temperature
χ	Magnetic susceptibility
XPS	X-ray photoelectron spectroscopy

1. Introduction

This thesis reports the synthesis and magnetic functional properties of core-shell $Co_xNi_{1-x}/(CoNi)O$ composite alloy nanoparticles, fabricated using the polyol method. The aim was to produce alloyed metallic nanoparticles, so the magnetic properties of the materials can be tuned by varying composition. In order to achieve this, the key objectives are to gain an understanding of the synthetic process and examine the effectiveness of specific reaction conditions, on the size, shape, structure and stability to oxidation of the nanoparticles. In addition to this, the exchange bias magnetic interactions between the ferromagnetic metallic "core" and antiferromagnetic "oxide" shell will be probed.

This chapter begins by outlining the theory behind the polyol reduction technique, and gives some background of nucleation theory and the variables that can affect nanoparticle growth. This is followed by a brief overview of magnetism, with a focus made upon the magnetic properties associated with core-shell nanoparticles, with reference to the literature. Having investigated the background theory in this chapter, Chapter 2 investigates the synthesis of Co_xNi_{1-x} particles. The synthetic process is

examined with variable factors such as nucleation methods, surfactant stabilisers and composition, investigated thoroughly. Following on from this, the magnetic properties of the particles described in Chapter 2 are characterised and explained in Chapter 3. This chapter addresses the exchange bias properties of the particles, and how they are manifested in terms of the features on a hysteresis plot. Chapter 3 also links back to the effects of specific reaction conditions on the magnetic properties of the particles. Chapter 4 gives conclusions and suggestions for future work. Chapter 5 documents the experimental methods used to fabricate the magnetic nanoparticles and the analytical techniques used to characterise them.

1.1 Background

Magnetic nanoparticles with well-defined morphology and size are desirable due to their use in a wide range of applications including ferrofluids[1-4] and high-density recording devices.[5-9] Particles with magnetic properties have recently been employed in efforts to combat cancer, utilising a technique known as magnetic "hyperthermia". The particles can be used as contrast agents for magnetic resonance imaging or therapeutic agents for less destructive treatments, as an alternative to chemotherapy.[10-12]

Intensity of research in the field of magnetic nanoparticles is due to the variation in physical properties, in comparison to that of bulk materials.[13, 14] Recent works have detailed progress in this field, with various procedures allowing relatively high yields of magnetic materials, with a strong magnetic response and anisotropy tailored to the memory-storage application.[15]

The focus of research in this particular field, thus far has been on FePt, CoPt and cobalt nanoparticles. These materials have been highlighted as having the potential to be of use in high-density memory storage devices.[13, 14, 16-22] Some work has been carried out on the synthesis of thin film Co_xNi_{1-x} systems.[23] Attempts to make individual monodisperse Co_xNi_{1-x} particles have yielded particles with large mean diameters of several microns,[24] or more recently as small as 10 nm particles.[25] However, those reactions have taken place in a basic solution, with the polyol acting as the solvent and reducing agent. Synthesis of Co_xNi_{1-x} particles, using a modified version of the polyol method reported in this thesis, is aimed at tuning the magnetic properties for

development in memory-storage applications and is a novel direction on work already carried out in this field.

1.2   Polyol reduction synthesis

The chemical reduction of transition metal salts in the presence of surfactant stabilisers, to generate zero-valent metal colloids in aqueous or organic media, was first published by Michael Faraday[26] in 1857. Faraday produced the first fully characterised gold nanocrystals, whilst endeavouring to investigate the optical properties of gold. Prior to this, gold and α-Fe_2O_3 nanoparticles had been produced by workers making coloured panes for stained glass windows. But they had not been identified as nanoparticles, until very recently.[27] Following on from work conducted by Faraday, the first reproducible method for metal colloid preparation was established by Turkevich et al,[28, 29] also for gold nanoparticle preparation.

The polyol reduction technique has been very successful in producing monodisperse particles of a tuneable size, with good control of shape and useful magnetic properties. It builds upon other synthetic methods that have been used in the past to produce magnetic nanoparticles, by introducing various methods of control for particle sizes, shapes and stability to oxidation. This in turn allows a better control of the magnetic properties in core-shell ferromagnetic-antiferromagnetic particles. This chemical reduction procedure is described as a wet-chemistry "bottom-up" method, and relies upon the reduction of metallic salts. An analogous "bottom up" approach features the controlled decomposition of organometallic compounds such as metal carbonyls.[15, 30]

Polyols are mild reducing agents that have an ability to reduce ions of noble metals, copper and more electropositive metals such as cobalt and nickel to the zero valence state. Polyols cannot directly reduce iron (II) or iron (III) ions to a zero-valence/metallic state. However, they are able to produce iron or iron-based particles via the disproportionation of iron (II).[31] Polyols in other instances have acted simultaneously as a solvent, reducing agent and nanocrystal growth medium. In some cases it has been known to act as a complexing agent for metallic cations.

Various finely divided metallic powders have been prepared by the reduction of a suitable precursor using polyol reduction. Fine metallic particle formation proceeds in a liquid medium with the following key steps: (i) initial dissolution of precursors; (ii) chemical reduction of the dissolved species by the polyol; (iii) nucleation and growth of nanoparticles from a supersaturated solution.

The main benefit of this procedure is the control it allows, so that monodisperse metal particles with a defined shape, controlled size and narrow size distribution (<20%) can be made. These high-quality particles will only be formed if the nucleation and growth steps are separated from one another.

1.3   Particle formation mechanism

The earliest work reported, which endeavours to explain nanoparticle growth, was research led by LaMer and Dinegar[32] into the mechanism of formation of monodisperse hydrosols. Their model can be used to explain the formation of nanoscaled particles or larger amorphous spheres.

In order to precipitate a solid from solution, its solubility must be exceeded. In ionic solutions, the products of the concentrations (activities) of the reactants must be greater than solubility product of the resulting compound at a given temperature. In this supersaturated condition, reactants precipitate from solution, forming atomic or molecular clusters. These clusters are the seeds for further particle growth in a homogeneously nucleated particle synthesis.

This supersaturation condition does not predetermine the properties of the resultant precipitate, as the solid-phase formation proceeds through a series of stages, each of which can affect the composition, size and shape of the final particles. However, in ambient conditions, diffusional growth and aggregative growth pathways may lead to "monodispersed" systems.

Figure 1. LaMer reaction scheme for the formation of monodispersed colloids, showing dissolved molecular precursor before and after nucleation as a function of time.[32]
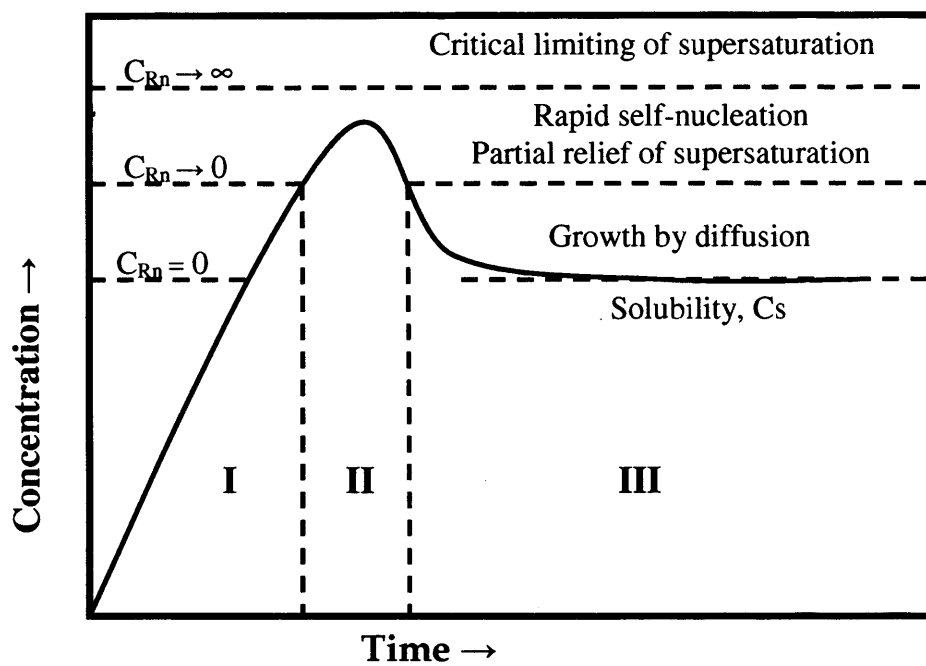
Turkevich et al[28] built upon this work and proposed a mechanism based on nucleation, growth and coalescence of gold nanoparticles. A fast supersaturated–burst nucleation, followed by slow growth without agglomeration, is the key to achieving monodisperse particles with a narrow size distribution.[33] Using modern data on kinetics and thermodynamics, this model can be refined further.[34] A schematic detailing the preparation mechanism is detailed in Figure 2.

Figure 2. Formation of metal nanoparticles via "salt reduction" method. The particles shown in the diagram below are $Co_{80}Ni_{20}$ particles made using the polyol method of synthesis in this study.[34]
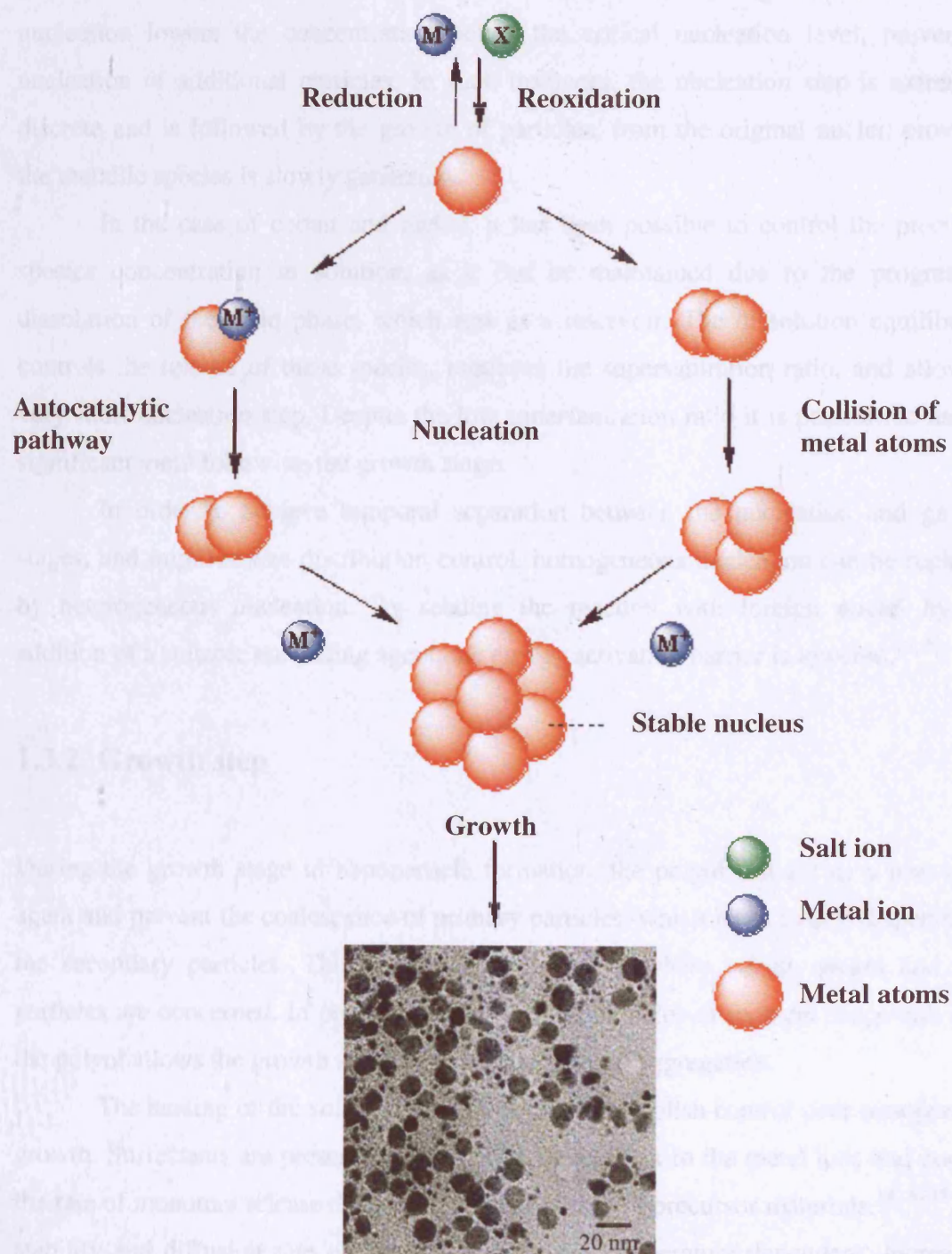
1.3.1 Nucleation step

When the concentration of the metal species generated by reduction, reaches critical supersaturation, spontaneous nucleation of particles occurs. If the metal nuclei are generated slowly and the rate of nucleation is sufficiently high, then the sudden nucleation lowers the concentration below the critical nucleation level, preventing nucleation of additional particles. In such instances, the nucleation step is extremely discrete and is followed by the growth of particles, from the original nuclei, provided the metallic species is slowly generated.

In the case of cobalt and nickel, it has been possible to control the precursor species concentration in solution, as it can be maintained due to the progressive dissolution of the solid phase, which acts as a reservoir. The dissolution equilibrium controls the release of these species, regulates the supersaturation ratio, and allows a very short nucleation step. Despite the low supersaturation ratio it is possible to have a significant yield following the growth stage.

In order to achieve temporal separation between the nucleation and growth stages, and improve size distribution control, homogeneous nucleation can be replaced by heterogeneous nucleation. By seeding the reaction with foreign nuclei by the addition of a suitable nucleating agent, the energy activation barrier is lowered.[24, 35]

1.3.2 Growth step

During the growth stage in nanoparticle formation, the polyol can act as a protective agent and prevent the coalescence of primary particles, which leads to polydispersity in the secondary particles. This is particularly relevant where cobalt, nickel and iron particles are concerned. In order to obtain metallic particles of uniform shape and size, the polyol allows the growth stage to propagate without aggregation.

The heating of the solution is key in order to establish control over nanoparticle growth. Surfactants are present in the solution to complex to the metal ions and control the rate of monomer release during the decomposition of precursor materials.[14, 36-39] The stability and diffusion rate of these complexes are temperature dependent. Increasing the temperature of the reactants in solution leads to a decrease in stability of the complexes, and this encourages nucleation and growth of the particles.[24, 35] If the

temperature increase is too high, this can result in uncontrolled growth and hence lack of control of particle sizes and distributions. Determining the correct temperature range is also a key to producing monodisperse, spherical particles with a narrow size distribution.[40, 41]

1.4   Homogeneous nucleation

Modified forms of the LaMer[32] method have been used to produce metallic nanoparticles, particularly cobalt, using a hot coordinating solvent containing a surfactant mixture that is injected with an organometallic precursor salt.[14] The reactions are typically carried out in an inert atmosphere. The rapid injection of precursor leads to a separation of the growth, and nucleation stages. Therefore, a temporally discrete homogeneous nucleation occurs. The absence of seeds in this type of reaction is notably important. This type of reaction arises from the self-nucleation of particles.[32, 42]

The high temperature of the solution decomposes the precursors, resulting in supersaturation of reagent species in solution, which is relieved by the burst nucleation that occurs. The rapid rate of addition raises the precursor concentration above the nucleation threshold. At the point of nucleation, the concentration of these species dips below that of the critical concentration required for nucleation, and therefore further reagent species can only bind to the particle nuclei that have been formed.[43, 44]

Thermal decomposition of cobalt carbonyl has been successfully used to produce cobalt nanoparticles, via a homogeneous route, by many research groups. Petit[45] adopted this method when synthesising passivated cobalt nanocrystals. Controlling the reaction parameters has an effect on the size and shape of the particles in this type of reaction.[15, 46, 47] Many of the reactions that have previously been attempted, have involved the rapid injection of an organometallic precursor into a hot boiling coordinating solvent, to achieve homogeneous nucleation.[48]

Puntes et al [49] modified this concept and developed a new synthetic procedure. The group succeeded in producing ε-cobalt nanoparticles that are single crystals and defect free by using the rapid pyrolysis of the cobalt carbonyl precursor. Their study introduced a new method of producing magnetic ferrofluids via homogeneous nucleation. The size distribution of these particles was narrow (< 5%), due the discrete nucleation event that took place. These particles however, did not show evidence of the

formation of an oxide layer which is not ideal for exchange bias properties. The pyrolysis of carbonyls is a clean route, as elemental cobalt is the only non-volatile product synthesised in the reaction: $[Co_2(CO)_8] \rightarrow 2Co + 8CO$.[50] The size distribution of particles made using this synthesis was controlled by changes to the reaction temperature, surfactant-type and concentration.[14, 51, 52]

Dinega et al[50] decomposed dicobalt octacarbonyl, to produce cobalt nanoparticles in the presence of trioctylphosphine oxide (TOPO). They reported an interesting result in the discovery of a new crystal structure of cobalt, which was subsequently named epsilon-cobalt, and had a similar unit cell to β-manganese (a high temperature phase of manganese). This was a breakthrough in the area of cobalt chemistry, as cobalt had only been known to have two crystalline phases; face-centred cubic (fcc) and hexagonal close-packed (hcp) prior to this. The fcc structure is thermodynamically favourable at high temperatures (above 450 °C), whilst hcp is favoured at lower temperatures. Both phases coexist at room temperature, however, for smaller particles the fcc structure is preferred below room temperature.[53]

Puntes et al[54] also reported the formation of ε–cobalt through the pyrolysis of the dicobalt octacarbonyl using TOPO, oleic acid and lauric acid as stabilising agents. Particles produced, using thermal decomposition or pyrolysis techniques, have proven to be monodisperse with a narrow size distribution. Disks, platelets and nanorods were formed by controlling the reaction parameters, and reproducibility is well-established using this method.[14, 49, 54, 55]

The polyol method of synthesis is different to the thermal decomposition methods adopted by others, and the formation of monodisperse self-assembled arrays of particles is not as prevalent, due to issues with reproducibility. Homogeneous nucleation via the polyol method has been attempted by Viau et al,[24] where nucleation and growth arises from the solution without the presence of external nuclei. In order to control the particle shape and size, surfactants of varying steric bulk are used. The temperature of the solution is monitored to allow for a short nucleation period and subsequent slow growth. However, control of particle size and shape using the polyol method is much more difficult due to the nature of the reaction.

The nucleation and growth steps are even harder to control in alloy particles, where the underlying chemistry and decomposition temperatures of each salt are different. Decomposition pathways tend to determine the success of a synthesis, due to the mechanism and reaction kinetics of supersaturated solutions.[40] Therefore,

homogeneous nucleation using the polyol synthetic technique is at present a challenging process.

1.5   Heterogeneous nucleation

The synthesis of nanoparticles is challenging due to the numerous variables involved. Size control is critical, when considering potential applications, the material may be suited to. Control of the size distribution is also important in order to maintain reproducibility, so that particles can be modelled in terms of their functional properties and behaviour.

The use of seeds in synthetic procedures such as polyol synthesis is well established.[24, 35, 56] The seeds act as nuclei around which the growth of a nanoparticle may occur by lowering the barrier to nucleation. Noble metal seeds form particles at lower temperatures in comparison to transition metals, and act as preferential growth sites for precursor atoms in solution.[35] The high interfacial energy of transition metals in comparison to the noble metals, means that the lower energy path created by the noble metal nuclei is much more favoured.[57] The concentration of seeds helps to determine the particle size and influence size distribution of the nanoparticles. The more seeds there are, the greater the number of nucleation sites, and hence a larger number of smaller nanoparticles are formed. The inverse is true for a lower concentration of seeds, where you would expect a smaller number of larger nanoparticles to be formed. [35, 56]

Classical nucleation theory (CNT) kinetically favours heterogeneous nucleation over homogeneous, and this is evident in the equation describing nucleation rate of the particles, equation (5).[58] The spontaneous formation of small crystal nuclei occurs only if their size exceeds a critical value, the so-called critical nucleus size, otherwise they re-dissolve into their mother phase. The rate of nucleation is dependent upon the probability function P_{crit}, the probability of the critical nucleus forming spontaneously, and on a kinetic factor (B), which measures the rate at which the critical nuclei then grow.[59]

The probability per particle of the formation of a critical nucleus, is exponentially dependent upon the free energy ΔG_{crit} that is needed to form such a nucleus:

$$P_{crit} = exp(-\Delta G_{crit}/k_B T) \qquad (1)$$

Where T is the temperature and k_B is the Boltzmann constant. Classical nucleation theory also details the total Gibbs free-energy required, to form a spherical crystallite with radius R as being

$$\Delta G = 4/3\ \pi R^3 \rho_s\ \Delta\mu + 4\pi R^2 \gamma \qquad (2)$$

Where ρ_s is the density of the solid, $\Delta\mu$ (<0) is the difference between chemical potential of the solid and liquid, and γ is the solid-liquid interfacial free energy density. The function ΔG passes through a maximum of $R = 2\gamma/(\rho_s[\Delta\mu])$ and the height of the nucleation barrier is:

$$\Delta G_{crit} = (16\pi/3)\ \gamma^3/\ (\rho_s[\Delta\mu])^2 \qquad (3)$$

The crystal nucleation rate per unit volume, J, is the product of P_{crit} and the kinetic prefactor B:

$$J = B\ exp\ (-\Delta G_{crit}/k_B T) \qquad (4)$$

The crystal nucleation expression for the nucleation rate then becomes:

$$J = B\ exp\ [-f\ (16\pi/3)\gamma^3/\ (\rho_s[\Delta\mu])^2\ with\ 0<f<1 \qquad (5)$$

Where, f, describes the influence of foreign nuclei or seeds, on the nucleation barrier. In the case of homogenous nucleation, f , may be counted as being equal to 1 and therefore, has the largest possible energy barrier to nucleation.[58] Equation (5) provides a representation of crystal nucleation theory to date. It is by no means an absolute

explanation of the formation of crystallite spheres in solution, but is a good approximation to make when analysing nucleation theory.

1.6   Surfactant contributions

Surfactants play an important role in nanoparticle synthesis. Metallic nanostructured colloidal particles need a protective surfactant to prevent aggregation and oxidation. There is a great difficulty associated with ensuring nanoparticles, once made, remain separated from one another. This is due to attractive interparticle interactions which arise from van der Waals forces. Nanocrystals remain stabilised if the repulsive force provided by the surfactant is sufficient to prevent the intrinsic van der Waals forces between the particles.[15, 43, 60] Balancing the concentrations of surfactants in such nanoparticle fluids is important as too much can cause coalescence and aggregation, whereas too little causes particles to "precipitate out" of the solvent and complete oxidation. The surfactants can also control interparticle distances in large-scale self assembled arrays.[61, 62]

Magnetic dipole interactions can also be evident in metal nanoparticle suspensions, although this effect is negligible in dilute superparamagnetic particle suspensions. Superparamagnetic nanoparticles form stable ferrofluids where the particles remain suspended in the solvent.[63-65] Ferrofluids are attracted to magnets and are displaced upon the application of a magnet.[64-66]

Shape control by the addition of surfactants is well reported in the cases of CdS and CdSe nanoparticles.[67-69] A wide range of different shapes including rods, teardrops and tetrapods have been synthesised with a controlled change in surfactant concentration and composition.[70] The effects of surfactant on cobalt nanoparticle shape has been investigated with fervour, due to the interest in the magnetic memory storage capabilities of arrays consisting of cobalt-based nanoparticles and the potential for high magnetic anisotropy in non-spherical particles.[71-74] When particles are coated with a close packed monolayer of organic surfactant, the surfactant has the ability control the shape of nanoparticles.

When adjustments are made with the metal precursor-to-surfactant ratio, particle size correspondingly changes. A greater amount of surfactant yields small particles, whereas a decrease in surfactant concentration produces large particles. Bulkier

surfactants such as tributylphosphine and trioctylphosphine inhibit particle growth and hence also form smaller particles. Therefore, steric bulk in surfactants is also an important factor to consider when designing a synthesis. This was demonstrated by Sun *et al*[13] in their work on the formation of monodisperse cobalt nanocrystals.

Surfactants complex with metal ions in solution, and the decomposition temperature of these complexes determine the nucleation point of the particles. Different surfactants, complex well with specific types of metal ion species e.g. nickel and oleylamine.[75] These complexes act as the monomer precursor species in the reaction. The choice of surfactant used in a reaction is therefore an important issue to consider. Many different types of surfactant including alkylphosphines, alkylphosphine oxides and carboxylic acids have been used to control particle shapes.[15] The surfactants produce a protective organic shell that mediates growth, stabilises the nanoparticles in solution and limits the oxidation after synthesis. In many typical syntheses, two surfactants are used concurrently, where the first binds tightly to the surface (e.g oleic acid) promoting slow growth, and the second allows rapid growth by binding weakly to the surface (e.g. trioctylphosphine and tributylphosphine)[13, 43, 44] The surfactants work together to tune the overall nanoparticle size.

1.7   Magnetism

Interest in magnetic nanomaterials is driven by the fundamental applications of devices which harness the magnetic properties for use in modern technology. Greek writings around 600 BC first described magnetic phenonema in Lodestone (magnetite, Fe_3O_4), a natural non-metallic solid, which seemed to attract iron. The significance of this discovery was not realised until much later, when it was used as the first technical magnetic material for the formation of the first compass.[76]

1.7.1 Fundamentals of magnetism

The magnetisation (M) of a sample is defined as;

$$M = N <\mu>$$ (1)

Where;   **N= number of atoms**

$<\mu>$ = average magnetic moment per site

However, in most magnetic systems, the magnetic moment is dependent upon the field so magnetic susceptibility is used. The magnitude of the moment is dependent upon the amount of material. The magnetic susceptibility, χ is a measure of the magnetic response or magnetisation, M, of a material in an applied magnetic field, H. The susceptibility or magnetisation is an intrinsic property of the material.

$$M = \chi H$$ (2)

The dimensionless volume magnetic susceptibility, χ, is closely related to the molar magnetic susceptibility, χ_m:

$$\chi_m = \chi V_m$$ (3)

where V_m is the molar volume of the substance. The magnetic flux density, B, is related to the applied field strength and the magnetisation by

$$B = \mu_0(H + M) = \mu_0(1+ \chi)\, H \qquad\qquad (4)$$

Where μ_0, is the vacuum permeability and $(1+ \chi)$ is the relative permeability. The magnetic flux density can be thought of as the density of magnetic force lines permeating the medium. Materials for which χ is positive, are either paramagnetic or ferromagnetic, and those for which χ is negative are diamagnetic. The superconducting quantum interference device (SQUID) is one of a few methods, which can be used to measure magnetic susceptibility. The permanent magnetic moment can be determined from susceptibility measurements by plotting χ against $1/T$.[77]

1.7.2 Classes of magnetic materials

In nature, there are six main types of magnetic material; (I) diamagnetic (II) paramagnetic (III) ferromagnetic (IV) antiferromagnetic (V) ferrimagnetic (VI) superparamagnetic. Additional classes include antiferrimagnets and spin glasses, amongst several others. The schematic in Figure 3 illustrates the atomic magnetic behaviour of some of these particular classes of magnetic material.[7,78]

Figure 3. Generic shapes of hysteresis loop for some of the different classes of magnetic material, at room temperature; (a) ferromagnet (b) paramagnet (c) superparamagnet.

(a)   (b)

(c)
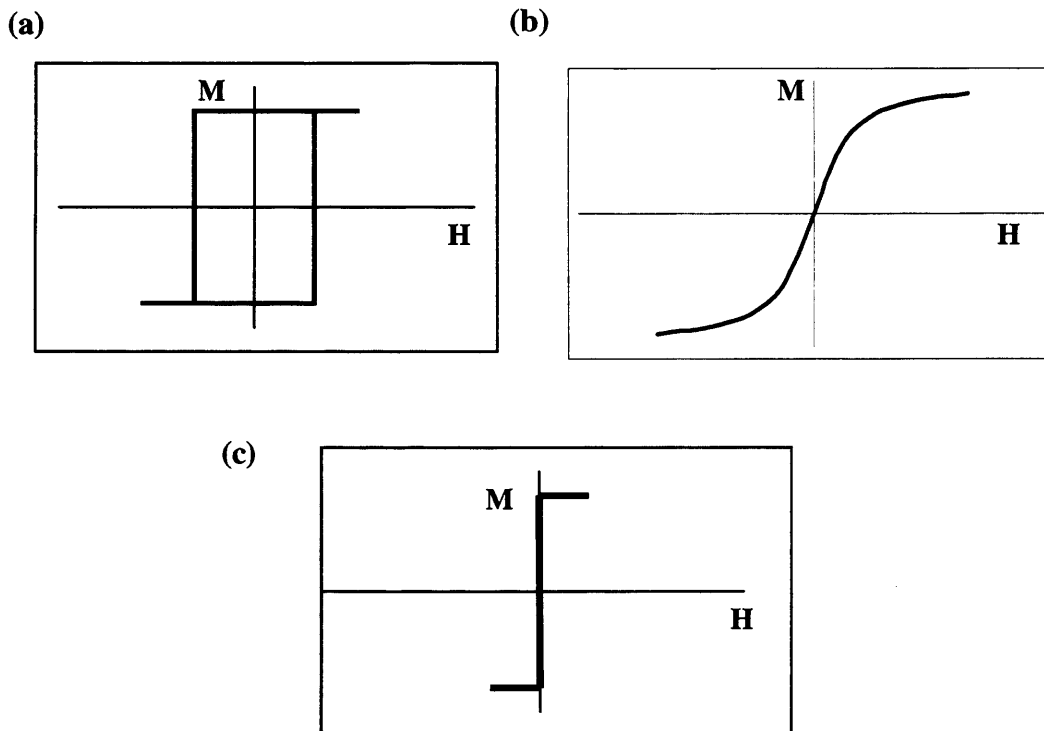
(I) Diamagnetism occurs in materials with no permanent magnetic dipole. Hence, they have no magnetisation in a magnetic field. Materials that are conventionally considered to be "non-magnetic" such as water, DNA, oil and many plastics are diamagnetic in nature. In an applied field, a small negative magnetic moment (M) is induced on the diamagnetic atoms, which is proportional to the applied field strength (H).[7,79]

Diamagnetism is independent of temperature and arises due the effect of applied magnetic fields on the motion of the inner electrons of the atoms present. This is shown

in Figure 4(a). The electronic orbits surrounding the atomic nucleus are often considered as if they are an electric current. In an applied magnetic field, the electronic motions are modified and this leads to a change in the magnetic moment due to the currents. This is called an "induced magnetic moment". Lenz's law of electromagnetic induction states that currents induced by a magnetic field are in such a direction that their magnetic fields tend to oppose the original inducing field. This means the induced magnetisation is negative, as is the susceptibility.[78, 80]

(II) Paramagnetism occurs in atoms or molecules with a permanent magnetic dipole moment, even in the absence of an applied field, where the widely separated neighbouring atoms do not interact. This occurs in the presence of unpaired electrons in atomic/molecular orbitals. In zero-applied magnetic fields, the moments are randomly orientated and fluctuate due to thermal agitation, resulting in a zero net moment. When an external field is applied, the spins align with the field, but this magnetisation effect is weaker than that exhibited by a ferromagnetic material. The spins remain predominantly oriented in a random manner, with some moments aligning with the field (II). However, there is a small net magnetisation in the direction of the externally applied field. [78, 80]

Above their Curie temperature, ferromagnetic materials become paramagnetic and their susceptibility depends on temperature.[80]Antiferromagnetic materials also behave as paramagnets above their Neel temperature. Key points to note are that upon the removal of a magnetic field, magnetisation will disappear. Also, at low temperatures thermal fluctuations are obviously reduced, therefore paramagnetic materials are easier to magnetise (align spins) than at higher temperatures.[79, 81]

Figure 4. Schematic representation of electron orbitals in a (a) diamagnet and; spin arrangements in a (b) paramagnet (c) ferromagnet (d) antiferromagnet (e) ferrimagnet (f) superparamagnet with an externally applied field.
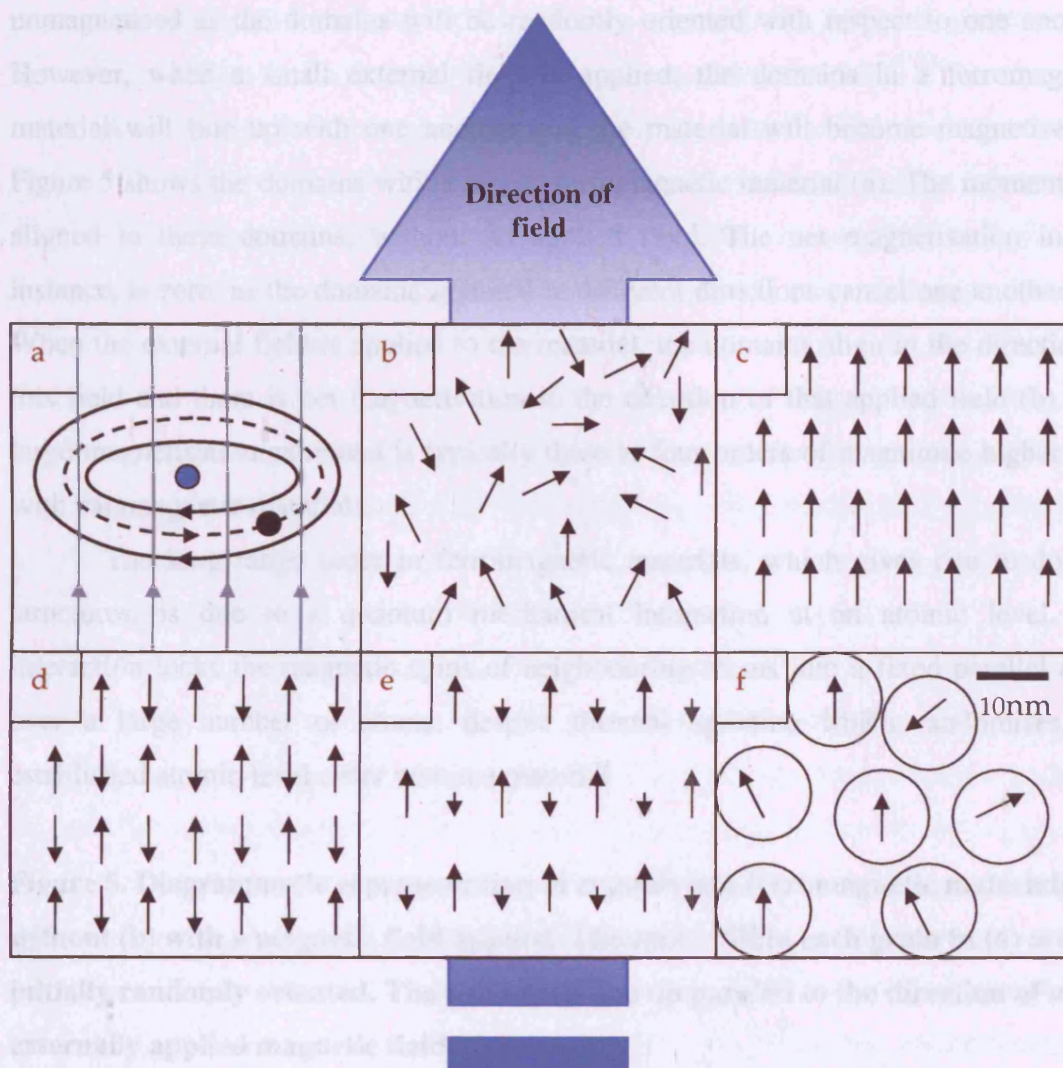
(III) **Ferromagnetism** is inherent in elements such as iron, cobalt, nickel and it arises from coupling between electron spins. This spin coupling leads to long range magnetic order, as a result of the exchange energy, which promotes spin alignment. All ferromagnetic materials lose their ferromagnetic behaviour at a specific temperature due to thermal agitations. The temperature at which this occurs is called the Curie temperature (T_C).

Ferromagnets are long-range ordered systems on an atomic scale, due to the presence of unpaired electron spins which align parallel to one another in regions known as domains. The unpaired electrons, from the d shell (partially filled shells) in

transition metals, give rise to this spin coupling. There is a strong intrinsic magnetic field within the magnetic domains, and this can exist when there is no external magnetic field applied. In a bulk sample the material, without an applied field, will be unmagnetised as the domains will be randomly oriented with respect to one another. However, when a small external field is applied, the domains in a ferromagnetic material will line up with one another and the material will become magnetised. [81] Figure 5 shows the domains within a bulk ferromagnetic material (a). The moments are aligned in these domains, without an applied field. The net magnetisation in this instance, is zero, as the domains oriented in different directions cancel one another out. When the external field is applied to the material, the domains align in the direction of this field and there is net magnetisation in the direction of that applied field (b). The large magnetisation exhibited is typically three to four orders of magnitude higher than with paramagnetic materials.

The long range order in ferromagnetic materials, which gives rise to domain structures, is due to a quantum mechanical interaction at an atomic level. The interaction locks the magnetic spins of neighbouring atoms into a fixed parallel order over a large number of atoms, despite thermal agitation which randomises any established atomic-level order within a material.

Figure 5. Diagrammatic representation of crystals in a ferromagnetic material; (a) without (b) with a magnetic field applied. The spins within each grain in (a) are initially randomly oriented. The spins then line up parallel to the direction of an externally applied magnetic field.

(a)   (b)

Direction of
magnetic field
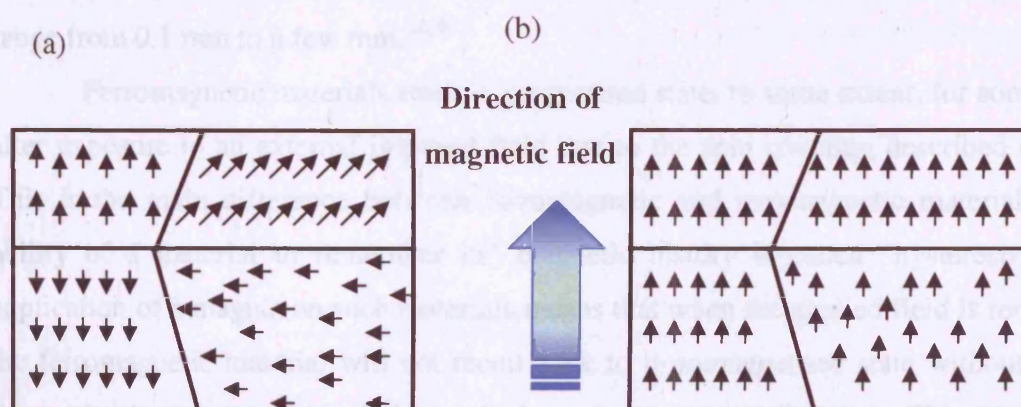
Weiss first gave an answer to the riddle of why a piece of iron, at room temperature and well below its' Curie temperature, does not yield a macroscopic total moment in the absence of an externally applied field. Weiss proposed that a macroscopic magnetic material will break into domains that align themselves in a manner that will minimize the total effective moment of the material. [80, 82]

A magnetic field contains energy proportional to the field squared and its volume. Therefore, the magnetostatic energy of a monodomain of parallel spins can be decreased by breaking it into smaller, oppositely aligned domains. This decrease in energy is beneficial, as it would further continue to divide into more and yet smaller domains, were it not for the exchange energy that increases with declining size. Exchange energy occurs at the boundary between oppositely aligned domains which, by the ferromagnetic nature of the coupling, battles against the anti-alignment. Domain formation is the balance between the spin coupling, which prefers parallel orientation and magnetic dipole interactions which prefer antiparallel alignments. This is why domains are formed at all, rather than whole material having aligned spins.

The opposition between the magnetostatic energy and what is known as a domain wall, limits the division of the material to domains of a finite size. The boundary between domains, the domain wall, is due to another competition of energies between the exchange interaction energy and magnetocrystalline anisotropy energy. The energy required to form a domain wall is larger than the energy cost of uniform magnetization in very small particles. Therefore domain magnetism occurs in bulk materials and is not applicable to the fine particles produced in this thesis, where single-domain behaviour is much more likely. The crystals in ferromagnetic materials must be relatively large for domain behaviour to become apparent. In fact sizes of domains can range from 0.1 mm to a few mm. [82, 83]

Ferromagnetic materials retain a magnetised state, to some extent, for some time after exposure to an external imposed field due to the spin coupling described earlier. This is the main difference between ferromagnetic and paramagnetic materials. The ability of a material to remember its' magnetic history is called "hysteresis." The application of a magnet on such materials means that when the applied field is removed, the ferromagnetic material will not recoil back to it unmagnetised state without being driven back to zero by a field applied in the opposite direction. This hysteretic behaviour in magnetic materials will be discussed later (Figure 9).

(IV) **Antiferromagnetism** is characterised in materials which consist of sublattices of atoms that exhibit an anti-parallel alignment of moments. Antiferromagnets (AFM's) are long-ranged ordered systems and have a small positive magnetic susceptibility due to this anti-parallel arrangement of spins. An applied field tends to align the spins and this induced alignment is larger than the diamagnetism of electron orbitals. Exchange coupling between neighbouring spins exists in AFM materials. That causes the system to align in an antiparallel fashion, and is exactly opposite to a ferromagnet.

Transition metal compounds and certain transition metal oxides are examples of antiferromagnets, including α-Fe_2O_3, CoO and NiO. However, there is a critical temperature above which these materials lose their AFM character and become paramagnetic in nature. This is known as the Néel temperature (T_N).

Figure 6 shows that a powder of this type of material, behaves antiferromagnetically at low temperatures. However, as the temperature increases, the Néel transition temperature is reached (illustrated by the peak maxima) and after this the material behaves paramagnetically. The paramagnetic region fits the Curie-Weiss law. The qualitative trace in the graph represents the zero-field cooled (ZFC) and field cooled (FC) plots overlapping. This is typical in the case of antiferromagnetic materials.[78, 79, 81]

Figure 6. The Néel temperature transition(T_N) illustrated by a peak shown in a plot of temperature versus magnetic susceptibility, in a typical AFM material.[78, 80]
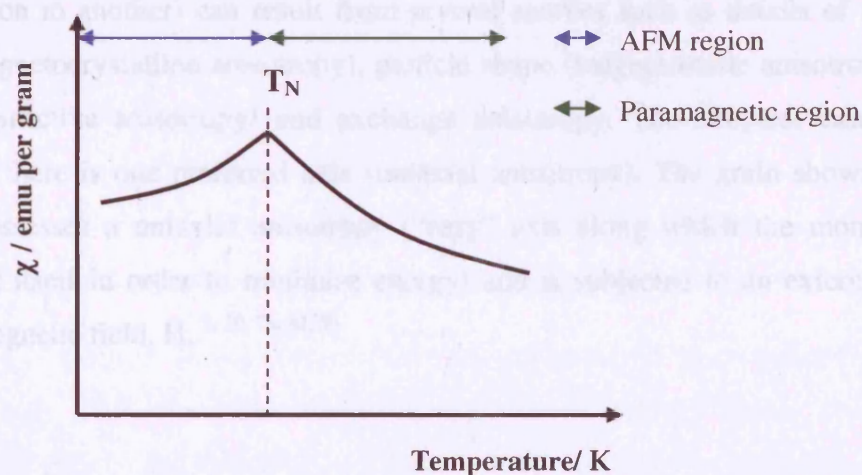
(V) **Ferrimagnetism** is similar to antiferromagnetism, as the spins are aligned anti-parallel with respect to one another. However, the moments are of a different

magnitude, and therefore there is a net overall magnetisation, as they do not cancel each other out. The magnetisation of this type of material is similar to a ferromagnet in terms of its hysteretic behaviour.[78, 81]

(VI) **Superparamagnetism** occurs in materials composed of small crystallites. If spins in a material move coherently together, they are represented collectively as M_s. The coherent rotation of the magnetisation was first considered by Stoner and Wohlfarth,[84] who recognised that the response of the saturation magnetisation (M_s) to an applied field, was limited by the anisotropy (shape, stress, crystalline, exchange).

When the physical size of a magnetised particle is made smaller, the relative contribution of the domain boundary energy, to the total energy increases. A point is eventually reached, whereby it becomes energetically unfavourable for a domain boundary to be formed at all. The particle then behaves as a single-domain and its' properties differ from the properties of multi-domain particles, where domain walls are present. [7, 82]

The Stoner-Wohlfarth[84] model (coherent rotation) describes a ferromagnet represented by a single magnetic grain. The material is considered to be a single magnetic domain particle. At T = 0 K the domain grain carries a single moment, M, and is elliptical in shape, as a material with uniform magnetisation should maintain an ellipsoid form. Superparamagnetic particles are very small and have one or more "easy" axes along which the energy is lower than the intervening "hard" axes. The so-called anisotropy energy (the energy required to change directions of the magnetisation from one easy direction to another) can result from several sources such as details of spin interactions (magnetocrystalline anisotropy), particle shape (magnetostatic anisotropy), stress (magnetostrictive anisotropy) and exchange anisotropy. The simplest case to model is where there is one preferred axis (uniaxial anisotropy). The grain shown in Figure 7 (a) possesses a uniaxial anisotropy ("easy" axis along which the moment prefers to orient itself in order to minimise energy) and is subjected to an externally applied static magnetic field, H. [7, 30, 78, 82, 85]

Figure 7 (a) Single domain grain shown with magnetisation (M) and an applied magnetic field (H). The grain's easy axis, or anisotropy axis, makes an angle (Φ) with the applied magnetic field [78] (b) Coercivity as a function of mean particle volume.[7]
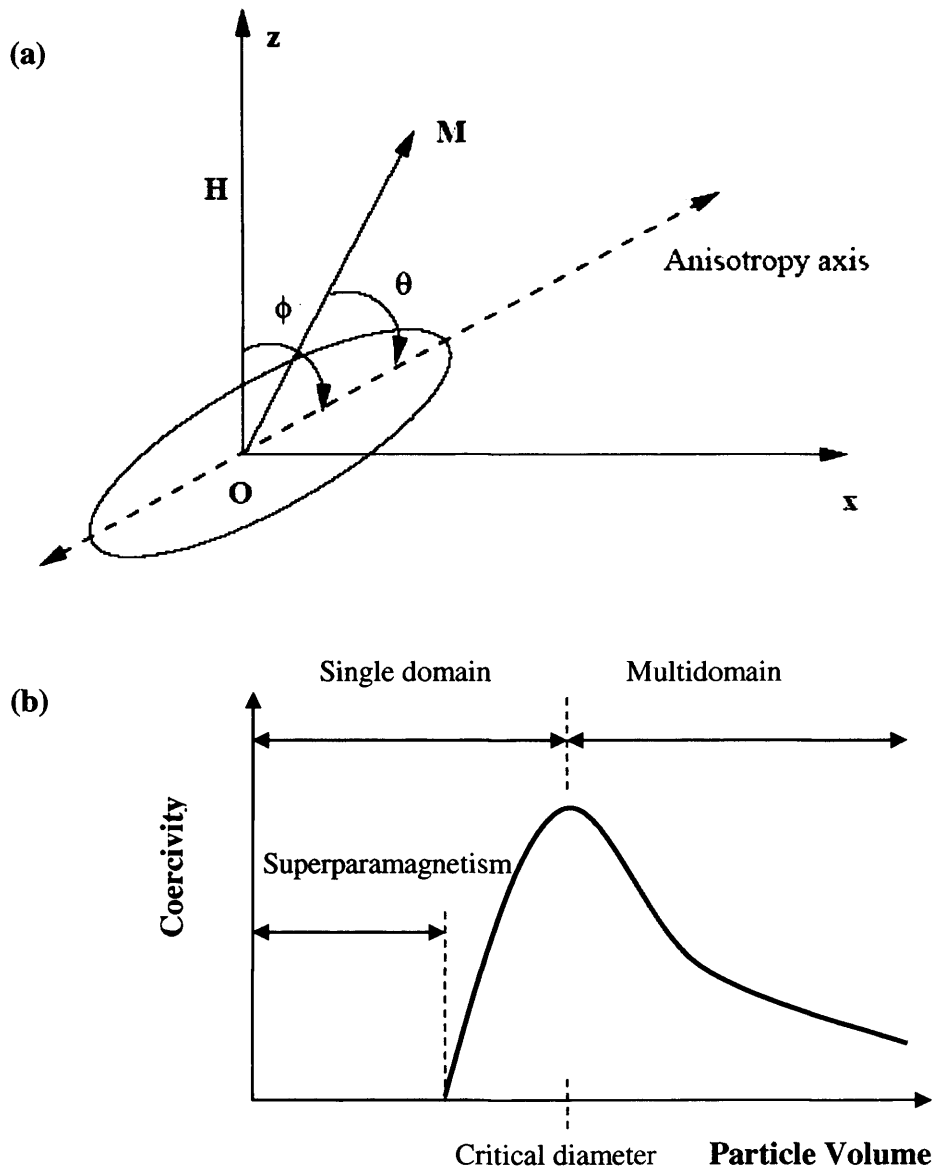
Coherent rotation of a single domain occurs when the anisotropy is much greater than the thermal energy (KV >> kT), where particles of a critical radius cannot thermodynamically support the formation of a domain wall. This requires magnetisation reversal via the rotation of the magnetisation, in the direction of the applied field. The preferred direction that the magnetic single domain grain takes, in the absence of an

applied field, is determined by the magnetic anisotropy (combination of all the anisotropies described earlier). This orientation is depicted in Figure 7 (a) as the anisotropy axis. [30]

As the particle size decreases below the single-domain value, the spins become increasingly affected by thermal fluctuations (KV << kT) and the system behaves superparamagnetically.[85]

Figure 8. Beating the superparamagnetic limit for small magnetic nanoparticles. (a) Magnetic anisotropy energy is comparable to the thermal energy (kT) (b) surface exchange bias between ferromagnetic material and antiferromagnetic material provides an additional anisotropy energy, which stabilises magnetisation in one direction and hence prevents superparamagnetism. [86]

(a)   **(b)**
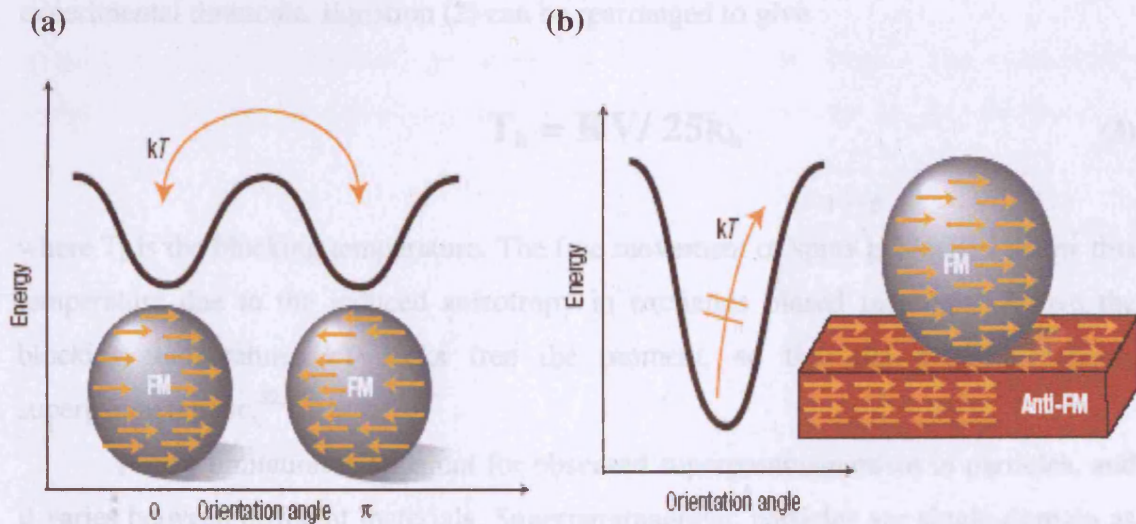
Superparamagnetism is a time-dependent phenomenon. The anisotropy energy, KV, may be thought of as the energy barrier required for keeping the magnetisation oriented in a certain direction. The probability for overcoming this energy barrier via thermal fluctuation is directly proportional to the Boltzmann factor exp(-KV/kT). When this occurs the particles are superparamagnetic, as thermal fluctuations cause the spins to randomly flip the magnetisation direction, between parallel and antiparallel orientations.[9, 86] By introducing an attempt timescale, τ_0, the probability for overcoming the fluctuation can be quantified. The timescale for a successful jump of the KV barrier is

$$\tau = \tau_0\, e^{-KV/kT} \tag{1}$$

The value for τ_0 is about 10^{-9} s. In a typical magnetic measurement, with a magnetometer, the experimental time, τ, would be between 10 to 100 s. If the saturation magnetisation reverses at times shorter than the experimental timescales, the system appears superparamagnetic. Therefore, using $\tau \sim 100$ s and $\tau_0 = 10^{-9}$ s to substitute into equation (1), we obtain for the critical volume,

$$V_{sp} = 25k_b T/K \tag{2}$$

A particle with a volume smaller than this behaves superparamagnetically on the 100 s experimental timescale. Equation (2) can be rearranged to give

$$T_b = KV/\,25k_b \tag{3}$$

where T_b is the blocking temperature. The free movement of spins is blocked below this temperature due to the induced anisotropy in exchange biased materials. Above the blocking temperature, kT kicks free the moment, so that the material appears superparamagnetic.[82, 85]

A size limitation is apparent for observed superparamagnetism in particles, and it varies between different materials. Superparamagnetic particles are single-domain as shown in Figure 7 (b), where the relationship between particle volume and coercivity is displayed. Superparamagnetic particles exhibit ferromagnetic behaviour below the blocking temperature. Above the blocking temperature, they behave as paramagnets with very large susceptibilities, because the thermal energy is sufficient to rotate the particle moment. Monodomain particles, on the other hand, can have blocking temperatures greater than room temperature e.g. typical sizes for single domain cobalt and nickel particles are 70 and 55 nm respectively.[85]

1.8   Hysteresis in magnetism

A key feature of magnetic materials is their ability to exhibit a complex change in

magnetisation upon the application of a magnetic field. This is best explained by a hysteresis loop. A great deal can be learnt about a magnetic material by analysing its hysteresis loop. The plot displays the relationship between applied field (H) and magnetisation (M). Hence, a loop is obtained by measuring the magnetic moment of a sample, as the applied field is cycled between large positive and negative values. An example of a hysteresis plot is shown in Figure 9.

Hysteresis is a widely recognised behaviour in ferromagnetic materials. When a magnetic field is externally applied to a ferromagnet, the material will become magnetised in the same direction as the applied field. When the field is removed, the ferromagnet will retain this magnetisation, due to the spin coupling energy. It needs to be driven back to zero by a field in the opposing direction. This irreversibility characterises magnetic hysteresis.[78, 81, 87]

Figure 9. The important features of a hysteresis loop. The saturation magnetisation, M_s, remanent magnetisation, M_r and coercivity, H_c, are shown. [87]

Domains are aligned in a positive direction to the field.

Saturation magnetisation

Remanence-No field (has been switched off). The magnetic effect remains as the domains are still aligned.

M/ emu/g

0.00

Key :-

⬤ No magnetisation

⬤ Saturation magnetisation, M_s

◀▶ Width of loop x ½ = coercivity, H_c

⬤ Remanent magnetisation, M_r

0.00

H (Oe)

Saturation in opposite direction

Domains are aligned in a negative direction to the field. The moments have flipped.

At high applied fields, the magnetisation approaches saturation point, or saturation magnetisation, M_s. Then if the magnetic field is decreased to zero, the M versus H curve does not follow the path of the initial curve but instead lags behind. Increasing the field in the opposite direction drives M to negative saturation. The magnetisation of a material is measured in emu/g. When H = 0, a residual magnetisation remains, this is called the remanence, M_r. If the field is applied in a reverse direction (a negative field), the magnetisation is forced to zero at a field magnitude known as the coercivity, H_c. The coercivity is the half-width of the hysteresis loop, where the magnetisation passes through zero in the positive and negative direction of field, and is measured in Oersted. Hence the cardinal points along the hysteresis plot are M_s, M_r and H_c.[78, 85] Materials with a $H_c \geq 100$ Oe are called hard magnets. Soft magnetic materials typically have a $H_c \leq 10$ Oe. However, the boundary between hard and soft is ambiguous and highly debated. [82]

1.9   Exchange anisotropy

Exchange anisotropy was first observed in fine cobalt nanoparticles enveloped with a cobaltous oxide shell, by Meiklejohn and Bean,[88] of the General Electric Research Laboratory in 1957. This new kind of magnetic anisotropy (K) was given the name "exchange anisotropy". The effect is also known as "exchange bias" or "exchange pinning" and also occurs in bilayers or multilayers of magnetic materials. [89-91] The discovery led to the development of the first commercially viable magnetic hard disk drive, produced in 1956, by IBM.

The phenomenon is attributed to the exchange interaction between adjacent ferromagnetic and antiferromagnetic materials. The Curie temperature (T_C) of the ferromagnet (FM) must be larger than the Néel temperature of the antiferromagnet (AFM). When a FM-AFM bilayer interface is cooled in an external magnetic field, through the Néel temperature (T_N) of the AFM, the AFM spins couple to the already aligned FM spins. The interfacial AFM-FM spin layers are subsequently pinned together, in parallel alignment, when a ferromagnet (FM)–antiferromagnetic (AFM) bilayer interface is cooled in an external magnetic field, through the Néel temperature (T_N) of the AFM. The Curie temperature (T_C) of the FM must be larger than the Néel temperature. As the AFM layer spins pass through their Néel temperature, they couple

to the already aligned FM spins. The interfacial AFM-FM spin layers are subsequently pinned together, in parallel alignment. The AFM spins are not reversed by the applied magnetic field.

Figure 10. Schematic displaying coercivity enhancement ($H_c \rightarrow 2H_c$) and loop shift (H_{ex}) due to FM-AFM exchange coupling, in a core-shell nanoparticle or bilayer, after field-cooling in an applied magnetic field.
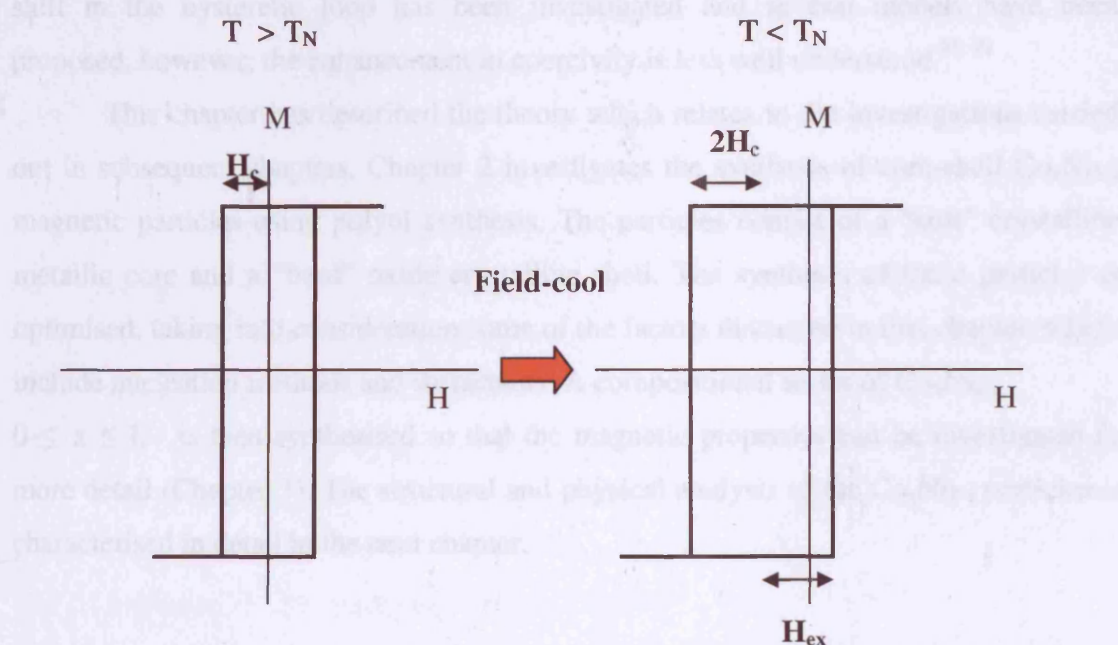
An indication of the existence of exchange bias is through an observed shift in the hysteretic loop, where the displacement occurs along the magnetic field axis. Figure 10 displays this phenomenon, where T is temperature and T_N is the Néel temperature.[92-94]

We can qualitatively explain this effect by assuming the exchange interaction occurs at the AFM-FM interface. The coupling between the AFM and FM spins at their boundary gives rise to an auxiliary torque on the FM spins. In the first half of the loop, this torque opposes the spin reversal, requiring a larger field magnitude to reverse the FM spins. In the second half of the loop, the torque promotes spin reversal, lowering the required field magnitude.[95, 96] It is important to differentiate cases where the AFM magnetic anisotropies are large or small. Instances where the AFM anisotropy (K_{AFM}) is large, would give rise to a shift in the hysteretic loop, whilst a smaller AFM anisotropy would result in coercivity enhancement (without a loop shift). Both effects are observed, however, where there are structural defects or particle size distributions, that

yields local differences in the AFM anisotropy.[97] Therefore the anisotropies, more specifically, the unidirectional anisotropy of a system can enable us to qualitatively explain interfacial interactions.

The coercivity, H_c, is greatly influenced by the exchange anisotropy in a system and this can be correlated with the anisotropy in the AFM layer of a particle or film. Coercivity enhancement is usually evident below the blocking temperature (T_B). Figure 10 displays a representation of coercivity enhancement due to exchange pinning. The shift in the hysteretic loop has been investigated and several models have been proposed, however, the enhancement in coercivity is less well understood.[98, 99]

This chapter has described the theory which relates to the investigations carried out in subsequent chapters. Chapter 2 investigates the synthesis of core-shell Co_xNi_{1-x} magnetic particles using polyol synthesis. The particles consist of a "soft" crystalline metallic core and a "hard" oxide crystalline shell. The synthesis of these particles is optimised, taking into consideration some of the factors discussed in this chapter, which include nucleation methods and surfactants. A compositional series of Co_xNi_{1-x}, $0 \leq x \leq 1$, is then synthesised so that the magnetic properties can be investigated in more detail (Chapter 3). The structural and physical analysis of the Co_xNi_{1-x} particles is characterised in detail in the next chapter.

1.10   References

1.   Lubbe, A. S.; Alexiou, C.; Bergemann, C., Clinical applications of magnetic drug targeting. *Journal of Surgical Research* **2001,** 95, (2), 200-206.

2.   Nethe, A.; Scholz, T.; Stahlmann, H. D., Improving the efficiency of electric machines using ferrofluids. *Journal of Physics-Condensed Matter* **2006,** 18, (38), S2985-S2998.

3.   Scherer, C.; Neto, A. M. F., Ferrofluids: Properties and applications. *Brazilian Journal of Physics* **2005,** 35, (3A), 718-727.

4.   Kim, E. H.; Lee, H. S.; Kwak, B. K.; Kim, B. K., Synthesis of ferrofluid with magnetic nanoparticles by sonochemical method for MRI contrast agent. *Journal of Magnetism and Magnetic Materials* **2005,** 289, 328-330.

5.   Li, K. B.; Wu, Y. H.; Guo, Z. B.; Zheng, Y. K.; Han, G. C.; Qiu, J. J.; Luo, P.; An, L. H.; Zhou, T. J., Exchange coupling and its applications in magnetic data storage. *Journal of Nanoscience and Nanotechnology* **2007,** 7, (1), 13-45.

6.   Sun, Y.; Salamon, M. B.; Garnier, K.; Averback, R. S., Memory effects in an interacting magnetic nanoparticle system. *Physical Review Letters* **2003,** 91, (16).

7.   Sugimoto, T., Monodispersed particles. **2001.**

8.   Murdock, E. S., ROADMAP FOR 10 GBIT/IN2 MEDIA - CHALLENGES. *IEEE transactions on magnetics* **1992,** 28, (5), 3078-3083.

9.   Skumryev, V., Stoyanov,S., Zhang,Y., Hadjipanayis, G.,Givord, D., Nogués, J.,, Beating the superparamagnetic limit with exchange bias. *Nature* **2003,** 423, 850-853

10.   Pankhurst, Q. A., Nanomagnetic medical sensors and treatment methodologies. *Bt Technology Journal* **2006,** 24, (3), 33-38.

11.   Pankhurst, Q. A.; Connolly, J.; Jones, S. K.; Dobson, J., Applications of magnetic nanoparticles in biomedicine. *Journal of Physics D-Applied Physics* **2003,** 36, (13), R167-R181.

12.   Tartaj, P., Nanomagnets-from fundamental physics to biomedicine. *Current Nanoscience* **2006,** 2, (1), 43-53.

13.   Sun, S. H.; Murray, C. B., Synthesis of monodisperse cobalt nanocrystals and their assembly into magnetic superlattices (invited). *Journal of Applied Physics* **1999**, 85, (8), 4325-4330.

14.   Puntes, V. F.; Krishnan, K. M.; Alivisatos, A. P., Colloidal nanocrystal shape and size control: The case of cobalt. *Science* **2001**, 291, (5511), 2115-2117.

15.   Hyeon, T., Chemical synthesis of magnetic nanoparticles. *Chemical Communications* **2003**, (8), 927-934.

16.   Shevchenko, E. V.; Talapin, D. V.; Schnablegger, H.; Kornowski, A.; Festin, O.; Svedlindh, P.; Haase, M.; Weller, H., Study of nucleation and growth in the organometallic synthesis of magnetic alloy nanocrystals: The role of nucleation rate in size control of CoPt3 nanocrystals. *Journal of the American Chemical Society* **2003**, 125, (30), 9090-9101.

17.   Lu, M. H.; Song, T.; Zhou, T. J.; Wang, J. P.; Piramanayagam, S. N.; Ma, W. W.; Gong, H., FePt and Fe nanocomposite by annealing self-assembled FePt nanoparticles. *Journal of Applied Physics* **2004**, 95, (11), 6735-6737.

18.   Mizuno, M.; Sasaki, Y.; Inoue, M.; Chinnasamy, C. N.; Jeyadevan, B.; Hasegawa, D.; Ogawa, T.; Takahashi, M.; Tohji, K.; Sato, K.; Hisano, S., Structural and magnetic properties of monolayer film of CoPt nanoparticles synthesized by polyol process. *Journal of Applied Physics* **2005**, 97, (10).

19.   Chantrell, R. W.; Weller, D.; Klemmer, T. J.; Sun, S.; Fullerton, E. E., Model of the magnetic properties of FePt granular media. *Journal of Applied Physics* **2002**, 91, (10), 6866-6868.

20.   Shevchenko, E.; Talapin, D.; Kornowski, A.; Wiekhorst, F.; Kotzler, J.; Haase, M.; Rogach, A.; Weller, H., Colloidal crystals of monodisperse FePt nanoparticles grown by a three-layer technique of controlled oversaturation. *Advanced Materials* **2002**, 14, (4), 287-290.

21.   Sun, S. H., Recent advances in chemical synthesis, self-assembly, and applications of FePt nanoparticles. *Advanced Materials* **2006**, 18, (4), 393-403.

22.   Tzitzios, V.; Niarchos, D.; Margariti, G.; Fidler, J.; Petridis, D., Synthesis of CoPt nanoparticles by a modified polyol method: characterization and magnetic properties. *Nanotechnology* **2005**, 16, (2), 287-291.

23.   Blackwood, D. J.; Li, Y. Y.; Chow, G. M., Polyol electroless and electrodeposition of nanostructured Ni-Co films and powders. *Journal of the Electrochemical Society* **2002**, 149, (3), D27-D34.

24.   Viau, G.; FievetVincent, F.; Fievet, F., Nucleation and growth of bimetallic CoNi and FeNi monodisperse particles prepared in polyols. *Solid State Ionics* **1996**, 84, (3-4), 259-270.

25.   Luna, C.; Morales, M. D.; Serna, C. J.; Vazquez, M., Exchange anisotropy in Co80Ni20/oxide nanoparticles. *Nanotechnology* **2004**, 15, (4), S293-S297.

26.   Faraday, M., Bakerian lecture- Experimental relations of gold (and other metals) to light. *Philosophical Transactions of the Royal Society of London* **1857**, 147, 145-181.

27.   Fredrickx, P.; Schryvers, D.; Janssens, K., Nanoscale morphology of a piece of ruby red Kunckel glass. *Physics and Chemistry of Glasses* **2002**, 43, (4), 176-183.

28.   Turkevich, J.; Stevenson, P. C.; Hillier, J., A Study of the Nucleation and Growth Processes in the Synthesis of Colloidal Gold. *Discussions of the Faraday Society* **1951**, (11), 55-75.

29.   Turkevich, J.; Stevenson, P. C.; Hillier, J., The Formation of Colloidal Gold. *Journal of Physical Chemistry* **1953**, 57, (7), 670-673.

30.   Willard, M. A.; Kurihara, L. K.; Carpenter, E. E.; Calvin, S.; Harris, V. G., Chemically prepared magnetic nanoparticles. *International Materials Reviews* **2004**, 49, (3-4), 125-170.

31.   Viau, G.; FievetVincent, F.; Fievet, F., Monodisperse iron-based particles: Precipitation in liquid polyols. *Journal of Materials Chemistry* **1996**, 6, (6), 1047-1053.

32.   Lamer, V. K.; Dinegar, R. H., Theory, Production and Mechanism of Formation of Monodispersed Hydrosols. *Journal of the American Chemical Society* **1950**, 72, (11), 4847-4854.

33.   Yamamuro, S. A., T.;Sumiyama, K.; Uchida, T., Kojima, I.,, Monodisperse metallic iron nanoparticles synthesized from noncarbonyl complexes. *Japanese Journal of Applied Physics* **2004**, 44, (No 7A), 4458-4459.

34.   Bonnemann, H.; Richards, R. M., Nanoscopic metal particles - Synthetic methods and potential applications. *European Journal of Inorganic Chemistry* **2001**, (10), 2455-2480.

35.   Viau, G.; Toneguzzo, P.; Pierrard, A.; Acher, O.; Fievet-Vincent, F.; Fievet, F., Heterogeneous nucleation and growth of metal nanoparticles in polyols. *Scripta Materialia* **2001**, 44, (8-9), 2263-2267.

36.   Jana, N. R.; Chen, Y. F.; Peng, X. G., Size- and shape-controlled magnetic (Cr, Mn, Fe, Co, Ni) oxide nanocrystals via a simple and general approach. *Chemistry of Materials* **2004,** 16, (20), 3931-3935.

37.   Yu, W. W.; Wang, Y. A.; Peng, X. G., Formation and stability of size-, shape-, and structure-controlled CdTe nanocrystals: Ligand effects on monomers and nanocrystals. *Chemistry of Materials* **2003,** 15, (22), 4300-4308.

38.   Battaglia, D.; Peng, X. G., Formation of high quality InP and InAs nanocrystals in a noncoordinating solvent. *Nano Letters* **2002,** 2, (9), 1027-1030.

39.   Peng, Z. A.; Peng, X. G., Nearly monodisperse and shape-controlled CdSe nanocrystals via alternative routes: Nucleation and growth. *Journal of the American Chemical Society* **2002,** 124, (13), 3343-3353.

40.   Yin, Y., Alivisatos A. P., , Colloidal nanocrystal synthesis and the organic-inorganic interface. *Nature* **2005,** 437, 664-670.

41.   Peng, X. G.; Thessing, J., Controlled synthesis of high quality semiconductor nanocrystals. In *Semiconductor Nanocrystals and Silicate Naoparticles*, 2005; Vol. 118, pp 79-119.

42.   Zhu, Y. C.; Yang, Q.; Zheng, H. G.; Yu, W. C.; Qian, Y. T., Flower-like cobalt nanocrystals by a complex precursor reaction route. *Materials Chemistry and Physics* **2005,** 91, (2-3), 293-297.

43.   Murray, C. B.; Kagan, C. R.; Bawendi, M. G., Synthesis and characterization of monodisperse nanocrystals and close-packed nanocrystal assemblies. *Annual Review of Materials Science* **2000,** 30, 545-610.

44.   Murray, C. B.; Sun, S. H.; Gaschler, W.; Doyle, H.; Betley, T. A.; Kagan, C. R., Colloidal synthesis of nanocrystals and nanocrystal superlattices. *Ibm Journal of Research and Development* **2001,** 45, (1), 47-56.

45.   Petit, C.; Taleb, A.; Pileni, M. P., Cobalt nanosized particles organized in a 2D superlattice: Synthesis, characterization, and magnetic properties. *Journal of Physical Chemistry B* **1999,** 103, (11), 1805-1810.

46.   Green, M., Organometallic based strategies for metal nanocrystal synthesis. *Chemical Communications* **2005,** (24), 3002-3011.

47.   Park, J.; An, K. J.; Hwang, Y. S.; Park, J. G.; Noh, H. J.; Kim, J. Y.; Park, J. H.; Hwang, N. M.; Hyeon, T., Ultra-large-scale syntheses of monodisperse nanocrystals. *Nature Materials* **2004,** 3, (12), 891-895.

48. Alivisatos, A. P., Semiconductor clusters, nanocrystals, and quantum dots. *Science* **1996**, 271, (5251), 933-937.

49. Puntes, V. F.; Krishnan, K. M., Synthesis, structural order and magnetic behavior of self-assembled epsilon-Co nanocrystal arrays. *Ieee Transactions on Magnetics* **2001**, 37, (4), 2210-2212.

50. Dinega, D. P.; Bawendi, M. G., A solution-phase chemical approach to a new crystal structure of cobalt. *Angewandte Chemie-International Edition* **1999**, 38, (12), 1788-1791.

51. Gao, Y. H.; Bao, Y. P.; Beerman, M.; Yasuhara, A.; Shindo, D.; Krishnan, K. M., Superstructures of self-assembled cobalt nanocrystals. *Applied Physics Letters* **2004**, 84, (17), 3361-3363.

52. Bao, Y. P.; Beerman, M.; Pakhomov, A. B.; Krishnan, K. M., Controlled crystalline structure and surface stability of cobalt nanocrystals. *Journal of Physical Chemistry B* **2005**, 109, (15), 7220-7222.

53. Kitakami, O.; Sato, H.; Shimada, Y.; Sato, F.; Tanaka, M., Size effect on the crystal phase of cobalt fine particles. *Physical Review B* **1997**, 56, (21), 13849-13854.

54. Puntes, V. F.; Krishnan, K. M.; Alivisatos, P., Synthesis, self-assembly, and magnetic behavior of a two-dimensional superlattice of single-crystal epsilon-Co nanoparticles. *Applied Physics Letters* **2001**, 78, (15), 2187-2189.

55. Puntes, V. F.; Zanchet, D.; Erdonmez, C. K.; Alivisatos, A. P., Synthesis of hcp-Co nanodisks. *Journal of the American Chemical Society* **2002**, 124, (43), 12874-12880.

56. Fievet, F.; Lagier, J. P.; Blin, B.; Beaudoin, B.; Figlarz, M., Homogeneous and Heterogeneous Nucleations in the Polyol Process for the Preparation of Micron and Sub-Micron Size Metal Particles. *Solid State Ionics* **1989**, 32-3, 198-205.

57. Yong, K. T.; Sahoo, Y.; Swihart, M. T.; Prasad, P. N., Growth of CdSe quantum rods and multipods seeded by noble-metal nanoparticles. *Advanced Materials* **2006**, 18, (15), 1978-1982.

58. Liu, X. Y., Heterogeneous nucleation or homogeneous nucleation? *Journal of Chemical Physics* **2000**, 112, (22), 9949-9955.

59. Auer, S.; Frenkel, D., Prediction of absolute crystal-nucleation rate in hard-sphere colloids. *Nature* **2001**, 409, (6823), 1020-1023.

60.   Shevchenko, E. V.; Talapin, D. V.; Murray, C. B.; O'Brien, S., Structural characterization of self-assembled multifunctional binary nanoparticle superlattices. *Journal of the American Chemical Society* **2006,** 128, (11), 3620-3637.

61.   Shafi, K.; Gedanken, A.; Prozorov, R., Surfactant-assisted self-organization of cobalt nanoparticles in a magnetic fluid. *Advanced Materials* **1998,** 10, (8), 590-593.

62.   Gelbart, W. M.; Sear, R. P.; Heath, J. R.; Chaney, S., Array formation in nano-colloids: Theory and experiment in 2D. *Faraday Discussions* **1999,** (112), 299-307.

63.   Chantrell, R. W.; Popplewell, J.; Charles, S. W., Measurements of Particle-Size Distribution Parameters in Ferrofluids. *Ieee Transactions on Magnetics* **1978,** 14, (5), 975-977.

64.   Farrell, D.; Cheng, Y.; McCallum, R. W.; Sachan, M.; Majetich, S. A., Magnetic interactions of iron nanoparticles in arrays and dilute dispersions. *Journal of Physical Chemistry B* **2005,** 109, (28), 13409-13419.

65.   Farrell, D.; Yamamuro, S.; Ijiri, Y.; Majetich, S. A., Magnetic interactions in Fe nanoparticle arrays. In *Nanopatterning-from Ultralarge-Scale Intergration to Biotechnology,* Merhari, L.; Gonsalves, K. E.; Dobisz, E. A.; Angelopoulos, M.; Herr, D., Eds. 2002; Vol. 705, pp 303-314.

66.   Giersig, M.; Hilgendorff, M., Magnetic nanoparticle superstructures. *European Journal of Inorganic Chemistry* **2005,** (18), 3571-3583.

67.   Milliron, D. J.; Alivisatos, A. P.; Pitois, C.; Edder, C.; Frechet, J. M. J., Electroactive surfactant designed to mediate electron transfer between CdSe nanocrystals and organic semiconductors. *Advanced Materials* **2003,** 15, (1), 58-61.

68.   Murray, C. B.; Norris, D. J.; Bawendi, M. G., Synthesis and Characterization of Nearly Monodisperse Cde (E = S, Se, Te) Semiconductor Nanocrystallites. *Journal of the American Chemical Society* **1993,** 115, (19), 8706-8715.

69.   Peng, X. G.; Manna, L.; Yang, W. D.; Wickham, J.; Scher, E.; Kadavanich, A.; Alivisatos, A. P., Shape control of CdSe nanocrystals. *Nature* **2000,** 404, (6773), 59-61.

70.   Manna, L.; Scher, E. C.; Alivisatos, A. P., Synthesis of soluble and processable rod-, arrow-, teardrop-, and tetrapod-shaped CdSe nanocrystals. *Journal of the American Chemical Society* **2000,** 122, (51), 12700-12706.

71.   Shukla, N.; Svedberg, E. B.; Ell, J.; Roy, A. J., Surfactant effects on the shapes of cobalt nanoparticles. *Materials Letters* **2006,** 60, (16), 1950-1955.

72.   Shevchenko, E. V.; Talapin, D. V.; Rogach, A. L.; Kornowski, A.; Haase, M.; Weller, H., Colloidal synthesis and self-assembly of COPt3 nanocrystals. *Journal of the American Chemical Society* **2002,** 124, (38), 11480-11485.

73.   Su, Y. K.; Shen, C. M.; Yang, T. Z.; Yang, H. T.; Gao, H. J.; Li, H. L., The dependence of Co nanoparticle sizes on the ratio of surfactants and the influence of different crystal sizes on magnetic properties. *Applied Physics a-Materials Science & Processing* **2005,** 81, (3), 569-572.

74.   Luna, C.; Morales, M. P.; Serna, C. J.; Vazquez, M., Effects of surfactants on the particle morphology and self-organization of Co nanocrystals. *Materials Science & Engineering C-Biomimetic and Supramolecular Systems* **2003,** 23, (6-8), 1129-1132.

75.   Park, J.; Kang, E.; Son, S. U.; Park, H. M.; Lee, M. K.; Kim, J.; Kim, K. W.; Noh, H. J.; Park, J. H.; Bae, C. J.; Park, J. G.; Hyeon, T., Monodisperse nanoparticles of Ni and NiO: Synthesis, characterization, self-assembled superlattices, and catalytic applications in the Suzuki coupling reaction. *Advanced Materials* **2005,** 17, (4), 429-434.

76.   Darling, S. B.; Bader, S. D., A materials chemistry perspective on nanomagnetism. *Journal of Materials Chemistry* **2005,** 15, (39), 4189-4195.

77.   Atkins, P., *Physical Chemistry*. Oxford: **1998.**

78.   Crangle, J., *Solid State Magnetism*. Van Nostrand Reinhold: **1991.**

79.   Ohanian, H., *Physics*. W. W. Norton & Company: **1989.**

80.   Chikazumi, S., *Physics of Ferromagnetism*. Oxford Science: **1997.**

81.   Chikazumi, S., *Physics of Magnetism*. Krieger: **1964.**

82.   Klabunde, K., *Nanoscale Materials in Chemistry*. Wiley: **2001.**

83.   Craik, D., J., Structure and properties of magnetic materials. Pion: **1971.**

84.   Stoner, E. C.; Wohlfarth, E. P., A Mechanism of Magnetic Hysteresis in Heterogeneous Alloys. *Philosophical Transactions of the Royal Society of London Series a-Mathematical and Physical Sciences* **1948,** 240, (826), 599-642.

85.   LesliePelecky, D. L.; Rieke, R. D., Magnetic properties of nanostructured materials. *Chemistry of Materials* **1996,** 8, (8), 1770-1783.

86.   Eisenmenger, J., Schuller, I. K.,, Magnetic nanostructures: overcoming thermal fluctuations. In *Nature*, 2003, 2, 437-438.

87.   Bertotti, G., *Hysteresis in magnetism: for physicists, material scientists and engineers*. Academic Press: 1998.

88.   Meiklejohn, W. H.; Bean, C. P., New Magnetic Anisotropy. *Physical Review* **1956,** 102, (5), 1413-1414.

89.   Kazakova, O.; Daly, B.; Holmes, J. D., Tunable magnetic properties of metal/metal oxide nanoscale coaxial cables. *Physical Review B* **2006,** 74, (18).

90.   Spray, J.; Nowak, U., Exchange bias in ferromagnetic/antiferromagnetic bilayers with imperfect interfaces. *Journal of Physics D-Applied Physics* **2006,** 39, (21), 4536-4539.

91.   van Belle, F.; Lew, W. S.; Vaz, C. A. F.; Bland, J. A. C., Coercivity and switching field - Engineered magnetic multilayers for 3-D patterned media. *Ieee Transactions on Magnetics* **2006,** 42, (10), 2957-2959.

92.   Nogues, J., Exchange bias in nanostructures. *Physics reports* **2005,** 422, (3), 65-117.

93.   Nogues, J.; Schuller, I. K., Exchange bias. *Journal of Magnetism and Magnetic Materials* **1999,** 192, (2), 203-232.

94.   Nowak, U.; Misra, A.; Usadel, K. D., Modeling exchange bias microscopically. *Journal of Magnetism and Magnetic Materials* **2002,** 240, (1-3), 243-247.

95.   Stamps, R. L., Mechanisms for exchange bias. *Journal of Physics D-Applied Physics* **2000,** 33, (23), R247-R268.

96.   Kiwi, M., Exchange bias theory. *Journal of Magnetism and Magnetic Materials* **2001,** 234, (3), 584-595.

97.   Stiles, M. D.; McMichael, R. D., Coercivity in exchange-bias bilayers. *Physical Review B* **2001,** 6305, (6).

98.   Takano, K.; Kodama, R. H.; Berkowitz, A. E.; Cao, W.; Thomas, G., Interfacial uncompensated antiferromagnetic spins: Role in unidirectional anisotropy in polycrystalline Ni81Fe19/CoO bilayers. *Physical Review Letters* **1997,** 79, (6), 1130-1133.

99.   Mauri, D.; Siegmann, H. C.; Bagus, P. S.; Kay, E., Simple-Model for Thin Ferromagnetic-Films Exchange Coupled to an Antiferromagnetic Substrate. *Journal of Applied Physics* **1987,** 62, (7), 3047-3049.

2. Polyol synthesis of Co_xNi_{1-x} magnetic nanoparticles

This chapter details the polyol synthesis of $Co_xNi_{1-x}/(CoNi)O$ magnetic alloy nanoparticles. The ideal structure of the particles is a metallic core (Co_xNi_{1-x}) surrounded by an oxide shell (CoO, NiO). The reaction conditions and post-synthesis treatment were studied in order to attain particles of the correct composition and size. All the particles synthesised in this chapter follow an approximate composition of $Co_{80}Ni_{20}$, apart from the section which investigates variations in alloy composition. This is to allow an effective comparison between the different synthetic variables that are tested.

A large number of synthetic procedures were studied-including homogeneous nucleation, heterogeneous nucleation, use of noble metal seeds, use of surfactants and heating rates in order to optimise the process. The ultimate aim being to make monodisperse ca~ 20 nm sized $Co_xNi_{1-x}/(CoNi)O$ core-shell nanoparticles, with an oxide shell thickness of 2-5 nm.

2.1 Introduction

Polyols are mild reducing agents that have the ability to reduce metallic salts to finely-divided metallic powders. Liquid diols are commonly used as a reducing agent. In this study, 1,2-hexadecanediol was used as the reducing agent. It is an α–diol that is analogous to traditional reducing agents used in polyol synthesis (ethylene glycol and propylene glycol).[1, 2] Polyol reduction is a chemical solution synthesis that has been used successfully to make magnetic nanoparticles with cobalt, nickel and iron as sole components. Binary alloy nanoparticles have also been made using the polyol technique and include FePt,[3-7] CoPt[8-10] and $CoPt_3$.[11] Further details about polyol synthesis and particle formation mechanisms are given in Chapter 1.

The polyol process described in this chapter, addresses the numerous variables that have an effect on the nature of the particle's produced. Endeavours are made to control the size and stability of particles by examining each of the factors in turn. The factors investigated include: (I) nucleation methods; (II) surfactants and (III) nanoparticle composition. Explanations are made for their specific effects on size and structure of the particles. Control of these numerous factors presents a complex and challenging task.

Although the syntheses of Co_xNi_{1-x} particles have been reported previously in the literature, in this work the polyol reaction has been modified further by using 1,2-hexadecanediol as the primary reducing agent, as opposed to ethylene glycol or 1,2-propanediol.[1, 2] The most significant change implemented here, is the absence of a base in the reaction to control pH, and the use of different metallic precursor salts (acetylacetonate and acetate salts). Several well-established methods, for the synthesis of metallic nanoparticles have been adapted and combined to create a novel route to magnetic nanoparticles.[12-14]

The particles discussed in this thesis vary from between 4 and 30 nm in mean diameter, and are close to monodisperse due to the presence of stabilising agents, with size distributions that are in the region of <30 %.

2.2 Overview of reaction

The polyol reaction was carried out using standard Schlenk line procedures, in an atmosphere of nitrogen. Full experimental details are given in Chapter 5. The precursors used are soluble metallic salts (cobalt and nickel acetate or acetylacetonate), a mild reducing agent (1,2-hexadecanediol), surfactant stabiliser (OA, OY, TOPO, TBP or mixtures of these), a high boiling point solvent and where appropriate nucleating seeds. The salts and surfactant are heated gradually to the nucleation temperature of the particles. This temperature is dependent upon a number of factors such as the surfactant, heat rate and nature of the starting material. Samples were analysed by a number of techniques, and these are also highlighted in Chapter 5. Isolation, storage and preparations of the particles for analysis are also explained in that chapter.

Overall reaction:

Metal salts + nucleating agent + 1, 2-hexadecanediol + surfactant $\xrightarrow[\Delta]{\text{Solvent} \atop N_2}$ Metal-metal oxide core-shell NP coated in surfactant.
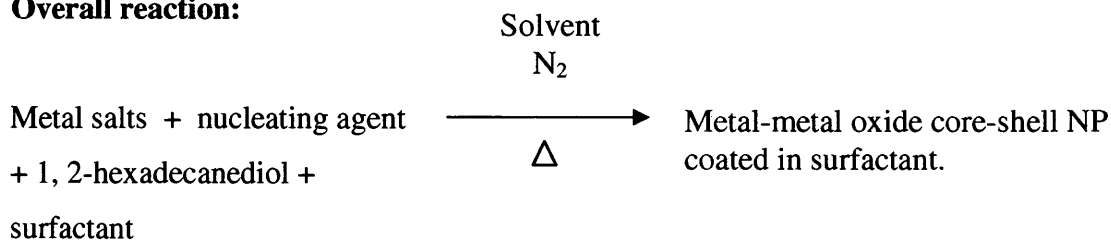
2.3 Reaction schematic

The following schematic (Figure 11) illustrates, in an integrated flow diagram, the experimental investigations that were made and their relationships to each other. Some of the investigations were more successful than others, and led to an evolution of the reaction conditions and enable synthetic optimisation. This is indicated by the thick lined black arrows that pass through the scheme. These arrows highlight the route that was taken to achieve an optimised synthesis, so a nanoparticle series with varied composition could be produced. The conditions necessary for effective nanoparticle synthesis are tested and their specific effects on particle size, shape and structure are evaluated throughout this chapter.

The schematic divides into three main investigatory paths. The principle variables that have been tested include; **(I) nucleation methods (II) surfactants** and **(III) composition**. These represent the three areas that were investigated in order to

optimise the nanoparticle synthesis. The reactions that were carried out, under the umbrella of these main variables are also shown in Figure 11.

The key explains the abbreviations that have been used throughout this chapter, for the surfactants employed in the syntheses. An indication of the size and shape of the particles synthesised in this study are also given in the schematic for certain samples. A scale bar, located at the bottom right-hand corner of the page, indicates approximately, the relative mean particle size of a particular sample.

Figure 11. Schematic diagram of the reactions discussed in this chapter (a) Key of abbreviations and codes used in diagram (b) reaction schematic linking the main themes in this chapter.

(a) Key:-

OA	Oleic acid
OY	Oleylamine
TOPO	Trioctylphosphine oxide
TBP	Tributylphosphine

Illustration of particles shapes and their approximate relative sizes.

Route taken to synthesise particles with varied composition.

(b)

Synthesis of Co_xNi_{1-x} particles

Homogeneous Nucleation
Sect 2.4

Heterogeneous nucleation
Sect 2.5

Platinum seeds
Sect 2.5.1.1

NP seeds
Sect 2.5.1.2

Other Noble metal seeds
Sect 2.5.1.3

OA
Sect 2.6.2

Surfactants
Sect 2.6

TBP
Sect 2.6.6

OA/OY
Sect 2.6.4

OY
Sect 2.6.3

TOPO
Sect 2.6.5

Co NP's
Sect 2.7.2

Composition
Sect 2.7

Ni NP's
Sect 2.7.8

$Co_{80}Ni_{20}$ NP's
Sect 2.7.3

$Co_{20}Ni_{80}$ NP's
Sect 2.7.7

$Co_{60}Ni_{40}$ NP's
Sect 2.7.4

$Co_{50}Ni_{50}$ NP's
Sect 2.7.5

$Co_{40}Ni_{60}$ NP's
Sect 2.7.6

Scale bar
20 nm

2.4 Homogeneous nucleation

2.4.1 Introduction

This section describes the homogeneous nucleation of $Co_{80}Ni_{20}$ particles using the polyol synthesis. Homogeneous nucleation involves the formation of nanoparticles without the use of foreign nuclei to seed particle growth. The nucleation occurs from the supersaturated solution, whereby the burst of nucleation relieves the saturation, and growth of particles subsequently occurs. The growth and nucleation stages are hence separated. Monodisperse particles are formed due to the temporally discrete nature of the nucleation process.[15, 16]

Metal atoms, made in homogeneous solutions are generally insoluble in the liquid solvent, and gradually coalesce to form clusters called "embryos". As additional metal atoms are generated, the embryos reach a critical size and grow into nuclei which separate themselves from the liquid and become solid particles. The number and size of nuclei is dependent upon factors such as temperature, in addition to nature and concentration of the surfactant. Further addition of metal atoms leads to growth of the nuclei and hence the formation of nanosize particles.[17]

The modified polyol method adopted in this study allows the formation of an oxide layer, and this is proven in similar works carried out by Jeyadevan et al.[18] The growth of an oxide layer was assisted by annealing the sample. Here, shell growth occurs by controlling the particle's exposure to oxygen in air, post-synthesis. This is described in Chapter 5 (Section 5.6).

2.4.2 Synthesis of $Co_{80}Ni_{20}$ particles by homogeneous nucleation

Synthesis of $Co_{80}Ni_{20}$ particles was carried out by heating cobalt and nickel tetrahydrate acetate salts, a mild reducing agent (1,2-hexadecanediol), and a surfactant stabiliser (oleic acid) in dioctyl ether solvent. The reactant mixture was magnetically stirred in an inert atmosphere (N_2) to prevent complete oxidation of particles during the synthesis. Further experimental detail is given in section 5.2 of chapter 5.

2.4.3 Results

TEM studies of the homogenously nucleated $Co_{80}Ni_{20}$ particles, made with oleic acid, indicated a single nucleation event that was evidenced by the sizes of nanoparticles

shown in Figure 12 (a) and (b). The TEM image displays contrast variations across the particles. This is due to differing orientations of the particles' with respect to the incident electron beam. The particles appear to be roughly spherical in shape. The existence of multi-grained particles cannot be ruled out or confirmed, due to the dark contrast of the particles making it difficult to elucidate individual grains.

Figure 12. (a) Image of a typical area on the TEM grid of 7.6 nm homogeneously $Co_{80}Ni_{20}$ particles (b) Lognormal size distribution curve of $Co_{80}Ni_{20}$ particles.

(a)   (b)
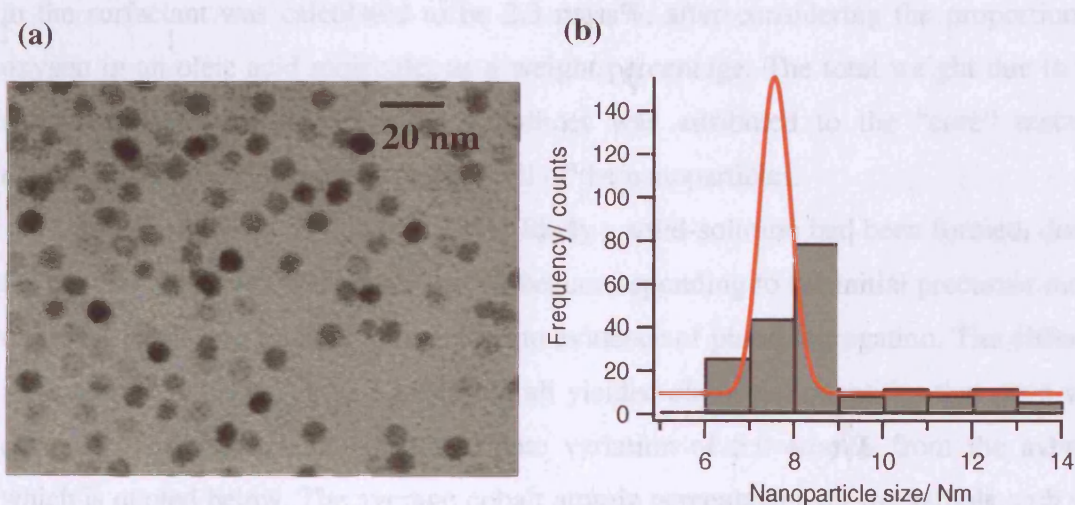
The particles in Figure 12 (a) appear close in size, with slight deviations in shape. However, size analysis of a large sample of particles indicates otherwise. The shape of the overall size distribution fits a log normal curve, so the mean fitted diameter was determined as 7.6 +/- 3.2 nm. By fitting the curve, the mean size of the particles was much more accurate than a calculation of the overall mean diameter. The standard deviation is large, due to the tail in the size distribution caused by the formation of larger particles. The size distribution curve also indicates a large population of particles with a mean diameter of between 7-9 nm. The tail in the graph could be eliminated with longer heating, as some smaller particles would coalesce to form larger particles.[19] The morphology of these particles is spherical-like, and this was confirmed by the majority of the particles having an aspect ratio of above 0.80. Aspect ratio is a measure of how circular a particle is, with a value of 1 indicating a perfect sphere.

The preparation of homogeneously nucleated bimetallic alloy particles can only occur if the precursor salts are soluble in the polyol, in this case, 1,2-hexadecanediol.

Previously, the size of nickel and cobalt particles produced using polyol methods with homogeneous nucleation, ranged from 1-5 μm.[2] However, the method used here has shown that particles with a much smaller mean diameter can be formed. TEM analysis has shown that with careful modifications to the reaction process, the particle size can be controlled and refined to nanometer regime.

Elemental analysis of the dried out $Co_{80}Ni_{20}$ particles, recovered by removal of solvent in the antechamber of a glovebox, revealed that ca~ 20.0 mass % was due to the carbon and hydrogen in the oleic acid surfactant coating. The carbon value was 17.3 mass% and the hydrogen proportion was 2.7 mass%. Therefore, the amount of oxygen in the surfactant was calculated to be 2.3 mass%, after considering the proportion of oxygen in an oleic acid molecule, as a weight percentage. The total weight due to the surfactant was 22.3 mass%. The remainder was attributed to the "core" metallic elements and the oxygen in the oxide shell of the nanoparticles.

EDX analysis showed that it was likely a solid-solution had been formed, due to the relative ratios between cobalt and nickel corresponding to the initial precursor molar ratios for the analogous salts. There was no evidence of phase segregation. The different areas across the stub that were analysed, all yielded elemental quantities that were very close in percentage, with an approximate variation of 5.0 atom% from the average which is quoted below. The average cobalt atomic percentage over the sample stub was determined as 45.6 atom%, whilst nickel was 12.1 atom%. The amount of oxygen present in the sample was calculated as being 42.3 atom%. The accuracy of EDX for oxygen measurements is not as good as with the electron energy-loss spectroscopy (EELS) technique, which has a better sensitivity for lighter elements. However, this measurement served as a good first approximation. The oxygen detected in the sample was due to the presence of CoO and NiO surrounding the metallic Co_xNi_{1-x} core of the particles. Due to the limitations of this EDX package, it was impossible to determine elemental composition of individual nanoparticles, but as was mentioned earlier, EELS was carried out on a select few samples to accurately quantify the presence of oxygen. These are described later, in the composition section of this chapter.

X-ray diffraction was tried, but no diffraction pattern from a crystalline component was observed, possibly due to the size of the particles. Although it is not clear from the image in Figure 12, it is possible that the particles were formed of multi-grains which had coalesced during the synthesis process. The multi-grain structure in

the particles could have meant that the individual grains which make up the nanocrystal, were not big enough to be detected by the diffractometer for these measurements.

The magnetic properties, are discussed in further detail, in chapter 3 (Section 3.2), and show this sample had a low magnetic moment. The larger particles in the sample may display core-shell morphology, however the smaller particles are probably completely oxidised. Therefore, any exchange bias effect that is seen, could be due to the larger particles (above 10 nm). It would be envisaged to be a small effect, due to the relatively low population of the larger particles, in comparison to the smaller particles (6-9 nm) as shown in Figure 12 (b). Increasing the size of the particles would lead to a more pronounced exchange bias effect. The oxide shell radius of the larger particles in this sample is also probably quite small and this could also cause minimal exchange bias in the sample.

In summary, the particles that have been synthesised using homogeneous nucleation methods have produced variable results. Particles with a mean diameter of 7.6 nm were formed but there was a tail in the particle's size distribution, at the larger end of the size scale. This has led to the large standard deviation cited for the particles. Heating for a longer period of time during the growth stage would possibly eliminate the tail in the size distribution.[19] Oleic acid was the sole surfactant used in the synthesis and did not seem to fully stabilise the particle against complete oxidation. Shape analysis of the particles showed that the majority were nearly spheres, with an aspect ratio of above 0.8. The particles did not remain stabilised in solution and responded very slightly to a magnet. The particles deviated from the solvent towards the magnet that was applied to the outside of the vial, housing the nanoparticulate solution.

Comparatively speaking, heterogeneous nucleation has been shown in the literature to allow better size control, and the presence of noble metal clusters in the centre of the particles also physically increases the overall mean diameter of the Co_xNi_{1-x} particle.[2, 20] The noble metal clusters themselves have a diameter of approximately 2-3 nm.[20] This method of synthesis is discussed in the next section of the chapter and could possibly improve upon what was observed for homogeneously nucleated $Co_{80}Ni_{20}$ particles described in this section.

2.5 Heterogeneous nucleation

2.5.1 Introduction to heterogeneous nucleation

Heterogeneous nucleation synthesis methods have been described in detail by Fievet and co-workers,[21] amongst others, as an excellent method of controlling particle size. Particle formation, using this method, is induced by the presence of seeds which act as nucleation sites for particle growth. The reactants then grow around the seed to form nanoparticles. It is believed that the addition of seeds, leads to a definite separation between the nucleation and growth steps. Control of the nucleation stage also means the final mean diameter of a synthesised particle can be tuned.[22] The presence of seed nuclei, lowers the energy barrier to particle formation and subsequently the nucleation rate. Therefore, heterogeneous nucleation can take place at lower supersaturation and precursor concentrations, whilst the opposite is true of homogeneous nucleation. Heterogeneous nucleation is kinetically, much more favourable, in comparison to homogenous nucleation.[16]

Following on from the studies carried out on homogeneous nucleation methods (Section 2.4), this section details the preparation of $Co_{80}Ni_{20}$ particles using a variety of nucleating seeds and heterogeneous methods.

2.5.1.1 Platinum seeds

2.5.1.1.1 Introduction

Noble metal salts such as Pt and Ag, have successfully acted as preferential growth sites for ferromagnetic nanoparticle formation, in previous works by Viau et al.[22] They have also contributed to helping achieve size control of the nanoparticles. A study has been carried out to establish the effect of the nature of a nucleating agent and concentration on the particle size and structure.[20] A linear relationship was established, between the mean diameter d_m and the inverse of the cubic root of the molar ratio of seeding agent over cobalt and nickel precursor concentration.

$$d_m = 3\sqrt{[Pt] / [Co + Ni]}$$

These types of seed are used due to their lower barrier to formation. Platinum salts are initially reduced to form clusters by the polyol.[23] These clusters act as seeds and hence, preferential growth sites for metallic nanoparticles.[20] They are much more effective in lower concentrations and at lower reaction temperatures, in comparison to transition metals. Pt colloidal particles were therefore, initially used to seed the reaction medium in this study.

2.5.1.1.2 Synthesis of $Co_{80}Ni_{20}$ particles with platinum seeds

The polyol method of synthesis was adapted to include the use of platinum seeds. Cobalt and nickel salts were heated with surfactant stabiliser (oleic acid) and seeding agent (platinum acetylacetonate salt) in dioctyl ether solvent. The ratio of the cobalt and nickel salts was adjusted to make particles. The reaction was carried out in an inert atmosphere. Further experimental details are given in section 5.3.1 of Chapter 5.

2.5.1.1.3 Results

TEM analysis was carried out on the $Co_{80}Ni_{20}$ particles, synthesised using platinum seeds. The image in Figure 13 depicts an area representative of observations made over the entire grid. The image on the left-hand side of the page (Figure 13 (a)) is a snapshot of typical areas on the TEM grid. The image on the right-hand side (Figure 13 (b)) has been enlarged so that particle morphology and details of structure can be seen much more easily. The larger particles appear to be imperfect spheres with elongated square-shaped particles also dispersed throughout the sample. Irregularity in the shape of particles, with a Co_xNi_{1-x} composition, has been reported previously and is consistent with what has been observed here in this study.[13] Another interesting feature to note in these images, are the changes in contrast across the profile of an individual particle. There are darker and lighter areas evident on some particles and in some instances, clear lines across the diameter of a particle. This provides evidence of a multi-grain structure within the nanocrystals.

Figure 13. (a) Low resolution TEM image of typical grid area for heterogeneously nucleated $Co_{80}Ni_{20}$ particles with a mean diameter of 12.6 nm (b) size distribution of the heterogeneously nucleated $Co_{80}Ni_{20}$ particles.
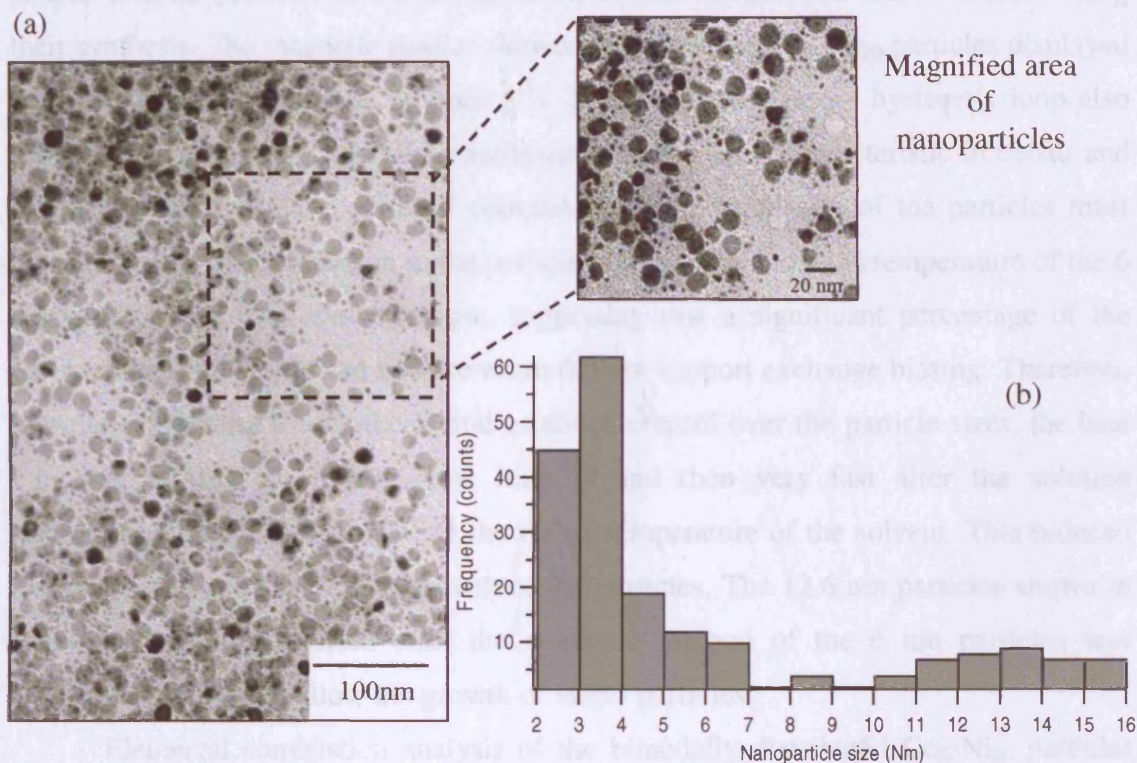
The images in Figure 13, shows small satellite particles surrounding the larger 12 nm particles. The satellite particles have not fully grown and are believed to be completely oxidised to their cores. The size distribution graph in Figure 13(b) displays clearly that two nucleation events have taken place, leading to the bimodality seen in this particular sample. This is evidenced by the two peaks seen in the graph. The peaks were fit to lognormal distributions, to obtain a mean diameter for each group of particles. The peak to the left of graph yielded a mean diameter of 2.6 +/- 0.9 nm. The deviation from the mean is large, at around 35%, but the accuracy of the TEM below 3 nm is not known. The peak to the right of graph gave a mean of 12.6 +/-1.1 nm, which is representative of what was observed across the TEM grid. The larger particles had a markedly narrower size distribution (~9%). If a mean diameter had been obtained for the sample overall, without taking into account the bimodality, a very large size distribution would be apparent. Both small and large particles were monodisperse and well separated from one another, due to the surfactant stabiliser.

Oxidation of the smaller satellite particles described above was confirmed due to magnetic studies, on 6 nm $Co_{80}Ni_{20}$ particles that had been synthesised using the heterogeneous nucleation method, earlier in this investigation. The particles were much smaller than the particles shown in Figure 13, as a slower heat rate had been used during their synthesis. The magnetic studies showed that the 6 nm $Co_{80}Ni_{20}$ particles displayed very low magnetic moments (6 emu g^{-1}). The room temperature hysteresis loop also resembled that of a polycrystalline antiferromagnet. This is characteristic in cobalt and nickel particles that have oxidised completely.[24] The small size of the particles must have led to complete oxidation to the particle's cores. The blocking temperature of the 6 nm $Co_{80}Ni_{20}$ particles was also low, suggesting that a significant percentage of the particles were fully oxidized and therefore did not support exchange biasing. Therefore, in order to optimise the synthesis and establish control over the particle sizes, the heat rate was adjusted so it was slow initially and then very fast after the solution temperature had reached 160 °C to the reflux temperature of the solvent. This induced fast nucleation and subsequent growth of the particles. The 12.6 nm particles shown in Figure 13 were synthesised after the synthetic method of the 6 nm particles was sufficiently adapted to allow the growth of larger particles.

Elemental combustion analysis of the bimodally distributed $Co_{80}Ni_{20}$ particles gave the percentage of sample weight that was due to surfactant stabiliser. Due to the multiple washings and addition of extra surfactant that took place post-synthesis, before the drying of the particles (section 5.6), this value varied from sample to sample by a few percent. The 12.6 nm particles showed that 16.9 mass% was due to the surfactant. Carbon corresponded to 13.6 mass% and hydrogen was 1.7 mass% respectively. Oxygen from the surfactant was determined as 1.6 mass%.

EDX analysis showed that the precursor had transferred into the final alloy in corresponding ratios. The five different spots that were examined showed consistency and indicated a solid solution had probably been formed. The atomic percentages for cobalt and nickel present were 51.2 atom% and 13.1 atom% respectively. This corresponded to a composition of $Co_{80}Ni_{20}$ for the particles. The oxygen component of the sample was 35.7 atom%.

X-ray diffraction was carried out, and the diffraction pattern displayed in Figure 14 was obtained, for the heterogeneously nucleated $Co_{80}Ni_{20}$ 12.6 nm particles. The crystalline phases cobalt (fcc) and nickel (fcc) were characterised, in addition to CoO (fcc) and NiO (fcc). The strongest reflection is due to the {111}planes of cobalt (fcc),

nickel (fcc) and cobalt (hcp) phases at 2θ ~44.0°. There was some evidence that Co_2O_3 crystallites may have been present, due to the peak at 2θ =51.8° possessing a shoulder. XPS results carried out on samples with a similar composition, which are described later (Section 2.7.2), also displayed peaks characteristic of Co_2O_3. However, this particular oxide has not been included in the peak assignments of the diffraction pattern (Figure 14) or in Table 1, as the peaks corresponding to Co_2O_3 are masked by the peaks due to Co(fcc)/ Ni (fcc) and the detector grid (2θ = 57.4°).

Figure 14. Diffraction pattern of heterogeneously nucleated, 12.6 nm $Co_{80}Ni_{20}$ nanoparticles.
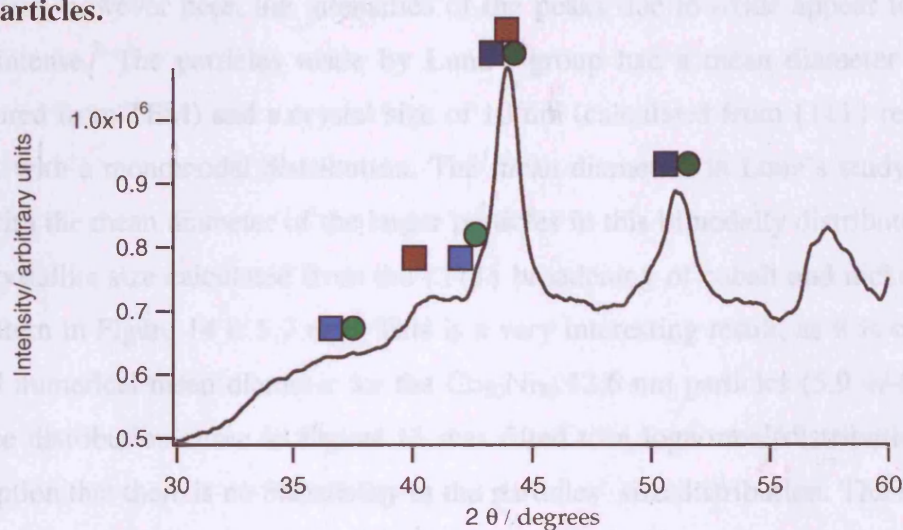
Table 1. XRD theoretical peak positions can be assigned to the diffraction pattern for the 12.6 nm $Co_{80}Ni_{20}$ nanoparticles.

Key	2θ/ degrees (Peak position)	Crystallographic Plane	Description
■	44.2	{111}	fcc Co
	51.8	{200}	
●	44.4	{111}	fcc Ni
	52	{200}	
■	36.4	{111}	fcc CoO
	42.4	{200}	
●	37.2	{111}	fcc NiO
	43.4	{200}	
■	41.5	{100}	hcp Co
	44.3	{002}	

The coloured boxes and spheres in Table 1 indicate the peak positions for the main crystallographic planes of cobalt, cobalt (II) oxide, nickel and nickel (II) oxide in Figure

14. The theoretical values in Table 1 correspond well to the peaks shown in the diffraction pattern in Figure 14. Due to background peaks from the substrate, only peaks between 30 ° and 60 ° have been shown. This has been maintained throughout this thesis, where it has been possible to obtain diffraction patterns.

The peaks for the {111} and {200} planes of cobalt (fcc) and nickel (fcc) correspond with what was found in a study carried out by Luna et al.[2] The peaks for the possible hcp phase of cobalt are also confirmed by the presence of {100} and {002} reflections, at $2\theta = 41.4°$ and 44.1° respectively. The reflections attributed to CoO and NiO are due to the partial oxidation of the particles. Luna reported broad peaks with low intensities, however here, the intensities of the peaks due to oxide appear to be much more intense.[2] The particles made by Luna's group had a mean diameter of 15 nm (measured from TEM) and a crystal size of 10 nm (calculated from {111} reflection of XRD), with a monomodal distribution. The mean diameters in Luna's study, correlate well with the mean diameter of the larger particles in this bimodally distributed sample. The crystallite size calculated from the {111} broadening of cobalt and nickel (fcc) for the pattern in Figure 14 is 5.7 nm.[2] This is a very interesting result, as it is close to the overall numerical mean diameter for the $Co_{80}Ni_{20}$ 12.6 nm particles (5.9 +/-0.9 nm), if the size distribution curve in Figure 13 was fitted to a lognormal distribution and the assumption that there is no bimodality in the particles' size distribution. The result from Scherrer analysis of the 12.6 nm $Co_{80}Ni_{20}$ particles, indicates one of two things; the particles are either multi-grained nanocrystals or the diameter obtained is due to an average over all the particles in the sample. The multi-grain structure in the particles is also evidenced by the TEM images shown in Figure 13. Therefore, it is most likely that the crystallite size obtained by Scherrer analysis is due to the multi-grain structure in the particles. It is however, important to remember that the Scherrer equation was not derived for samples with polydisperse crystallites. The equation does not take into account variations in size of nanoparticles as it was designed for particles that are approximately equal in diameter.[25]

In summary, $Co_{80}Ni_{20}$ particles have been synthesised using heterogeneous nucleation methods with platinum as the seed. The particles had a bimodal size distribution and exhibited multi-grain structure in TEM studies, characterised by lines across the surface of individual nanoparticles. The existence of multi-grains has been seen previously in studies carried out into the synthesis of $Co_{80}Ni_{20}$ particles, using a similar yet slightly different synthetic method.[2, 13] EDX showed that atomic ratios of

cobalt and nickel in the particles correlated well with the ratios of precursor materials initially used to make the particles. XRD identified the dominant phases in the sample and also indicated that the oxide shell of the particles could have been composed of a mixture of cobalt (II) and (III) oxide crystallites. Scherrer analysis correlated with the multi-grain theory determined by TEM analysis of the particles. The nanoparticle solution of these 12.6 nm $Co_{80}Ni_{20}$ particles was a stable ferrofluidic solution which responded to a magnet. The black nanoparticle solution deviated towards a magnet, although this response was much weaker in comparison to that of the dried nanoparticulate powder obtained from the solution.

The synthesis of $Co_{80}Ni_{20}$ particles has been carried out, prior to this investigation, but had required the use of a base solution (NaOH), to control the pH in the reactant solution.[2, 13, 18, 22] The base in that particular reaction, did not allow the precipitation of intermediate solid-phase alkoxides to occur, as these act as reservoirs for the metal ions species and inhibit their subsequent growth into particles.[22]

The 12.6 nm particles formed in this study displayed similar structure to those reported in the Luna study.[2] Luna *et al* found that larger particles were polycrystals, whilst smaller particles (<10 nm) were single crystals.[2, 13] TEM analysis of particles (Figure 13) in this investigation, have shown that the larger particles appeared to be polycrystals or multi-grains, due to the lines and contrast gradients across the particles. This confirms what was found in previous studies. Luna also reported a shoulder on the peak of the fcc{111} reflection for cobalt and nickel, attributed to a small fraction of hcp phase cobalt, in their 10 nm $Co_{80}Ni_{20}$ particles.[2] This was also observed in the 12.6 nm $Co_{80}Ni_{20}$ particles synthesised in this study. The particle fraction with hcp structure is said to become more significant as the particle size decreases, as Luna observed a progressive increase in the asymmetry of this fcc{111}reflection.[2]

If a comparison is made between the homogeneous and heterogeneous methods of synthesis, it is clear that the heterogeneous route appears to be more promising, as the mean size of the particles is larger than the homogeneously nucleated samples. The heterogeneously nucleated particles can therefore, support the growth of an oxide shell coating around the metallic alloy core. The key to continuing use of the heterogeneous method, is to manipulate the heat rate and other reaction variables to encourage a single nucleation event. Heterogeneous nucleation encourages a more definitive step between the nucleation and growth stages and therefore, the development of heterogeneous

synthesis methods could lead to monodisperse core-shell nanoparticles with a larger size and narrower size distribution than the Co_xNi_{1-x} particles made by other groups. [22]

2.5.1.2 Use of premade nanoparticles as nuclei for further growth

2.5.1.2.1 Introduction

An alternative heterogeneous synthetic approach was attempted in order to try and increase particle size further, and therefore improve exchange bias effects. Heterogeneous nucleation methods already employed in this investigation (section 2.5.1.1), were adapted so that premade nanoparticles were used as seed nuclei. This was a modification of a method adopted by Yamamuro *et al* for the synthesis of iron nanoparticles.[10]

The Yamamuro method involves the preparation of nanoparticles in a two-stage procedure, where the premade particles remain in the reaction vessel. Additional reagents are then introduced into the vessel, and the reagents are heated up with the nanoparticle seed solution. The monomers in the reactant solution grow around the pre-existing nanoparticle seeds and this leads to an increase in the size of the final particles. This two-stage method was implemented by calculating the extra amount of reactants required to increase the particle volume 8-fold, and hence double the particle diameter. The main aim of utilising this type of heterogeneous method was to double the particle size.

2.5.1.2.2 Synthesis of $Co_{80}Ni_{20}$ particles with premade nanoparticle seeds

Using the same methodology adopted by Yamamuro,[12] $Co_{80}Ni_{20}$ particles were also fabricated in a two stage process. In the first stage of the synthesis cobalt and nickel tetrahydrate acetate salts were dissolved in the solvent, with 1,2-hexadecanediol acting as a reducing agent. Two different surfactants (OA and TBP) were used as stabilisers and were introduced into the reaction flask at different stages of the reaction, due to their individual steric influences over the nanoparticles' rate of growth. OA was added to the reaction mixture with the other precursors at the beginning of the reaction, whilst TBP was injected into the flask at 160 °C when the nucleation and growth of the particles began to occur.[22] The solution was then heated rapidly to the reflux point. The nanoparticles that were formed in the first stage were the nanoparticle seeds. The

primary nanoparticles act as seed nuclei for the subsequent growth of secondary larger nanoparticles in the second stage. The two-stage process is pictorially depicted in Scheme 1.

Scheme 1. Schematic of particle growth in a two-step synthesis; [A] particles made in stage one of the reaction. [B] Particles grown from reaction of [A] with additional reactants which are heated to reflux in the second stage results in particles.
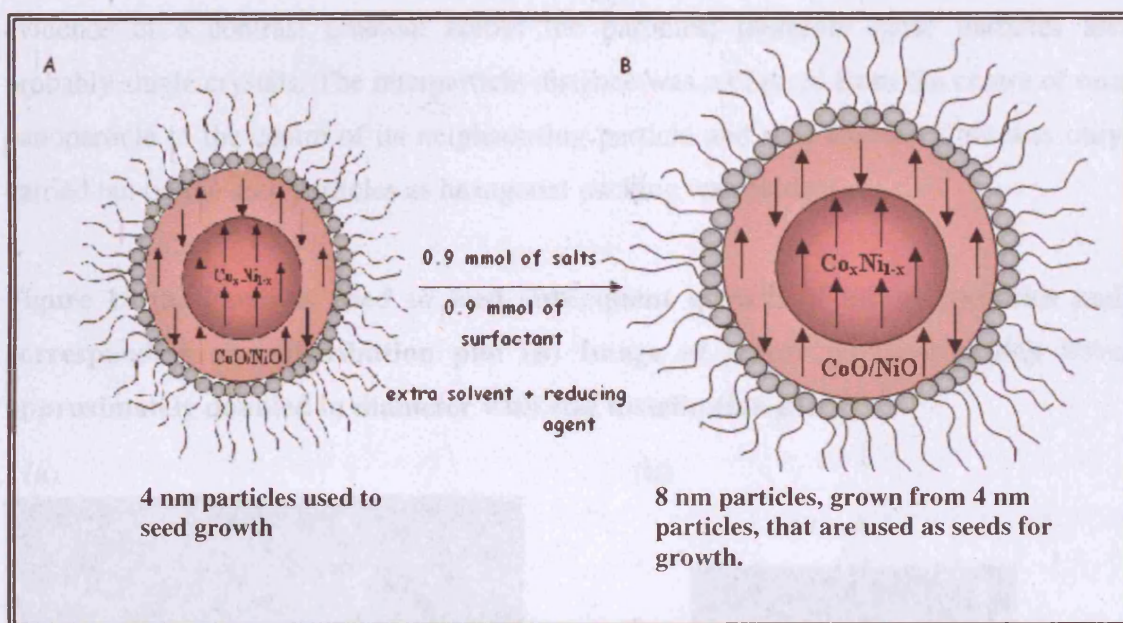
An appropriate volume of seed solution was then kept in the flask to be used as seed nuclei for the subsequent reaction, whilst the additional seed solution was extracted from the flask to be subsequently analysed. In the second step, additional cobalt and nickel salts, reducing agent, solvent and surfactant stabiliser were introduced to the flask that contained a few millilitres of the previously made nanoparticle seed solution.

The reaction to grow larger particles followed the same profile as that used to make seeds. The larger particles that were grown from the smaller nanoparticle seeds appeared to respond to a magnet. Whereas the smaller nanoparticle seed solution, which had been extracted from the flask prior to the second stage, did not show this magnetic response.

2.5.1.2.3 Results

A TEM image of the particles used to seed the subsequent reaction is shown in Figure 15(a). It can clearly be seen that these seed particles have partially ordered into an array-type formation. The packing seems to be hexagonal in the areas where the particles are mostly self-organised. The streaking, due the solvent edge drying, can also be seen on the right hand edge of the image. Detailed size distribution studies were carried out on the particles in this sample, and an average particle size of 4.4 +/- 2.0 nm was calculated. The size of seed particles was fit to a lognormal distribution. There was no evidence of a contrast gradient across the particles; therefore these particles are probably single crystals. The interparticle distance was measured from the centre of one nanoparticle to the centre of its neighbouring particle and was 6.6 nm. This was only carried out on the seed particles as hexagonal packing was evident.

Figure 15 (a) Particles used to seed subsequent growth of larger particles and corresponding size distribution plot (b) Image of larger particles which have approximately doubled in diameter with size distribution plot.

(a)   **(b)**
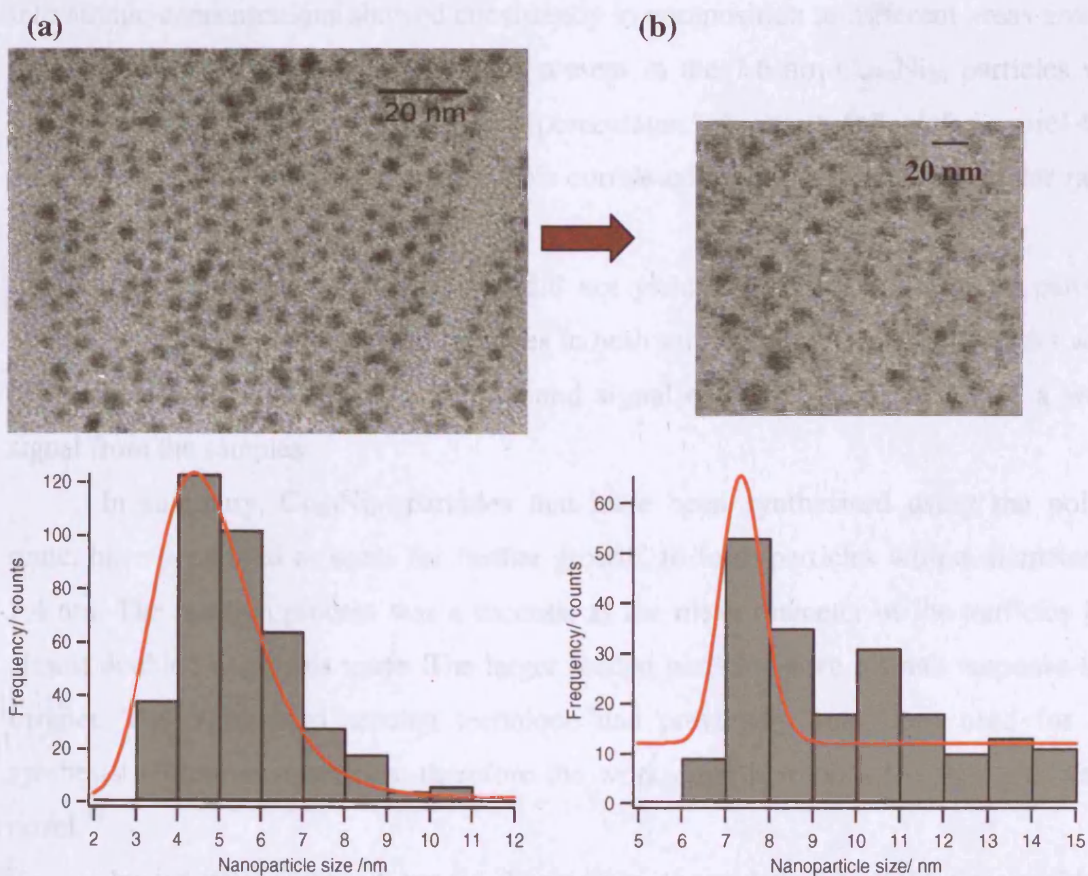
The particles that were grown from the nanoparticle seeds of Figure 15(a) appear to have almost doubled in size (Figure 15 (b)). The actual mean diameter obtained for them was 7.4 +/- 3.9 nm. The plot was fit to a lognormal distribution overall, although there appears to be slight bimodality with a reasonably large population of particles at around 10-11 nm. Although this method led to a significant increase in particle size, polydispersity was an issue. The size distribution of the initial seeds solution was quite large and this has followed through into the final seeded sample shown in 15(b).

Elemental analysis was carried out on the nanoparticle sample which had been grown from the initial seeds. The proportion of the nanoparticulate powder attributed to surfactant stabiliser, was found to be 23.8 weight%. The amount of carbon was found to be 18.9 weight% and hydrogen was 2.8 weight%. Oxygen in the oleic acid and tributylphosphine was 2.1 weight%. The remaining weight was assumed to be due to the metallic nanoparticle alloy.

EDX results suggested the larger 7.4 nm $Co_{80}Ni_{20}$ particles that were made after seeding with smaller 4.4 nm $Co_{80}Ni_{20}$ particles, had formed a solid solution as studies into atomic concentrations showed consistency in composition at different areas around the sample stub. The amount of oxygen present in the 7.6 nm $Co_{80}Ni_{20}$ particles was calculated as 47.2 atom%. The atomic percentages of cobalt and nickel were 40.9 atom% and 11.9 atom% respectively. This correlated with a 4:1 precursor molar ratio, between the cobalt and nickel salts.

XRD diffraction was tried and did not yield a crystalline diffraction pattern, possibly due the small sizes of the particles in both samples. The amorphous peaks were difficult to distinguish from the background signal of the instrument, due to a weak signal from the samples.

In summary, $Co_{80}Ni_{20}$ particles that have been synthesised using the polyol route, have been used as seeds for further growth, to form particles with a diameter of 7.4 nm. The reaction process was a success, as the mean diameter of the particles had almost doubled using this route. The larger seeded particles gave a small response to a magnet. The Yamamuro seeding technique had previously only been used for the synthesis of iron nanoparticles, therefore the work done here on a Co_xNi_{1-x} system is novel.[12]

Investigations carried out by Yamamuro showed that particle size could be tuned by controlling the reaction temperature, as this is a key parameter for the control

of supersaturation. [12, 26] His work showed an increase in particle size, from 5 nm seed particles to 8 nm and 12.5 nm nanometer particles depending on the heat rates used, in this two stage process. [10] The 4.4 nm $Co_{80}Ni_{20}$ seeds formed in this study were comparable in size to the 5 nm iron nanoparticle seeds used by Yamamuro.[12] After 75 minutes of heating the seed solution with additional reactants, 7.4 nm $Co_{80}Ni_{20}$ particles were formed. This compared well with the 8 nm iron particles, previously produced by Yamamuro with 145 minutes of heating. The key difference in both reactions was that Yamamuro had used a mixture of oleic acid and oleylamine as surfactant for the iron particles. In order to synthesise $Co_{80}Ni_{20}$ particles, a mixture of oleic acid and tributylphosphine surfactants was used.

The surfactant used plays a major role in the size control of particles. The steric bulk of the tributylphosphine inhibited the particle growth, and hence the mean particle diameter. Phosphine-based ligands are known to control nanoparticle sizes due to their steric bulk.[27] This was observed earlier in the investigation when TOPO and TBP were solely used to make Co_xNi_{1-x} particles. It is also possible that faster nucleation and therefore particle growth occurs with the OA/TBP combination of surfactants, due to the ease with which they complex to the metallic ion species. This could explain the faster reaction time over which the $Co_{80}Ni_{20}$ particles were formed, 75 minutes compared to 145 minutes, even though the reaction conditions were identical to those adopted by Yamamuro for iron particle synthesis.

The primary concern about this technique was indeed the small size of the particles formed after seeding, which was still quite small at around 8 nm and had led to the weak magnetic response. Polydispersity was also an issue as the size distributions that were determined were large. In order to solve this, careful manipulation of the heating rates and hence reaction temperatures could lead to better control of particle size and size distribution in the future. However, this would require intensive examination due to the complex nature of the Co_xNi_{1-x} system, in comparison to the iron nanoparticle synthesis, and so is beyond the scope of this project due to time constraints. This particular study of seeding particle growth with like-nanoparticle seeds, has indicated that a one step procedure better for the Co_xNi_{1-x} system. The Yamamuro technique was therefore, not pursued for the synthesis of Co_xNi_{1-x} particles, but had been successful in its' goal of increasing the mean particle size and in terms of being a novel method of increasing particle size for the Co_xNi_{1-x} system.

2.5.3 Other Noble metal seeds

Having investigated platinum seeds as nucleating agents for the synthesis, other possible seeds, gold and silver, were also examined to probe their effect on the synthesis of Co_xNi_{1-x} nanoparticles. The results would serve as a comparison between the noble metals, and their effectiveness as seeds. Previously, Viau *et al* [20, 22] had investigated silver as a seed in polyol synthesis, however gold has not been investigated prior to this. Investigations carried out where silver was a nucleating seed, showed that it was not as good a nucleating agent as platinum. The size range of particle diameter achieved by 200 nm< d_m <500 nm, even when the highest concentrations of silver nitrate concentrations were used. [20] Recently, Luna *et al* [13] investigated Ag and Pt seeds for the synthesis of $Co_{80}Ni_{20}$ particles. The platinum seeds produced fine nanosized particles of between 5 nm < d_m< 150 nm and the silver seeds, in their study ranged from between 100 nm < d_m< 540 nm.

In this study, the use of silver seeds yielded particles of 40 nm < d_m< 100 nm and gold seeds yielded 60 nm< d_m< 150 nm. However, the particles were extremely polydisperse with large size distributions. The particles had also aggregated, making it difficult to visualise them, as they had coalesced together in clumps. Therefore, this route was not pursued any further, due to the size and quality of particles that were obtained. These seeds were not deemed to be effective at controlling particle size.

Magnetic measurements were also not carried out, as the extremely large size and the aggregation put into question the magnetic properties of the particles, in terms of exchange bias. Platinum seeds offered better size control for the Co_xNi_{1-x} system and yielded crystalline particles with narrow size distributions. Therefore, platinum seeds were the most effective method of controlling particle sizes for this system.

2.6   Variations in stabilising surfactants

2.6.1 Introduction to variations in stabilising surfactant

A number of surfactants were tested to examine their effects on particle size, shape and stability to oxidation. These properties are affected by how tightly the surfactants bind to the metallic ions in the reactant solution and form a ligand-metallic ion complex. These complexes act as the reaction precursor and so are important for the eventual

formation of nanoparticles. Nucleating seeds were used in these syntheses, as the effect of using seeds was shown to help control particle size as reported in section 2.5 of this chapter. The only instance where this is not the case is for the tributylphosphine based reaction described in section   .

The use of a suitable surfactant was key to preventing oxidation of the particles to their cores. The stability of nanoparticles in their respective solvents is also affected by the surfactant, due to Van der Waals forces keeping the particles well separated to form a stable solution. A sufficiently coated nanoparticle will be repelled by similar particles, preventing coalescence and particle aggregation. This is due to the steric repulsion between neighbouring particles, caused by the presence of the organic surfactant ligand chain. The alkyl chains allow dispersion in non-polar solvents and prevent aggregation, by excluding other particles from their close environment.

Figure 16. Repulsion of neighbouring particles due to the steric bulk of the surfactant.
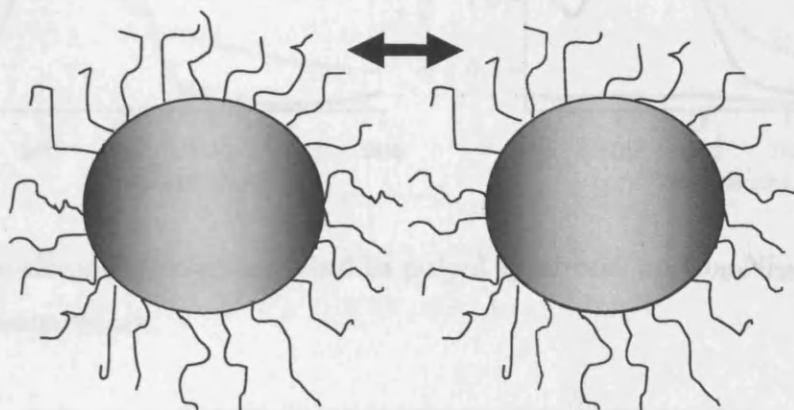
The experiments described in this subsection use tetrahydrated acetate salts for the syntheses. Initially reactions were mapped using UV-Vis to track the formation of complexes between the metal species and surfactant. During the course of the reaction, the colour of the solution changed through a variety of colours, indicating the reduction of the metallic ion species in solution. The change in colour was dependent upon the nature of the ions present in the reactant solution, during the heating process, at any given time. The characteristic black colour was common across the various surfactants, heat rates and seeds used. This indicated the onset of nanoparticle formation and

occurred at temperatures between 150 °C-232 °C, depending on the reaction conditions and precursors used for the synthesis.

In these reactions, nuclei formation is followed by the formation of metal-ion surfactant complexes. This is evident through the characteristic colour changes in the solution during synthesis. The bright coloured solutions result from the ions/complexes of Co^{2+}, Ni^{2+} and Co^{3+}. The solutions subsequently darken, to a brown/black colour upon the growth of particles, and hence the presence of absorption centres in the flask, characterised by a flat-line in the UV-Vis spectra.

Figure 17. UV-Vis spectra of synthesis of $Co_{80}Ni_{20}$ particles taken at (a) 120 °C (left) and (b) 150 °C (right) with different surfactants.
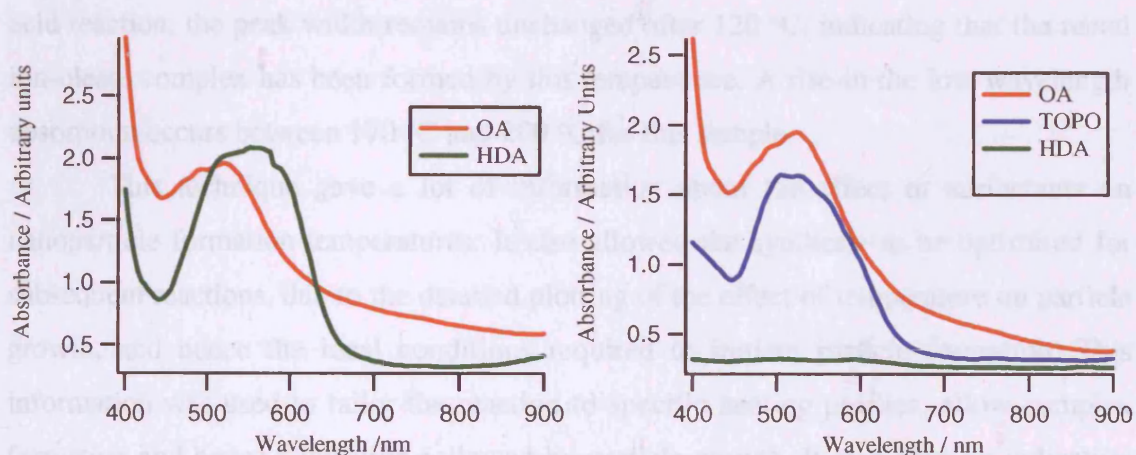
Table 2. The effect of surfactant used in polyol synthesis, on $Co_{80}Ni_{20}$ nanoparticle formation temperature.

Surfactant	NP formation temperature/ ° C
Oleic Acid	220
Oleylamine	218
OA/OY	232
Tributylphosphine	224
Trioctylphosphine	204
Hexadecylamine	150

Early investigations into the reaction profile were carried out using UV-Vis studies, where aliquots of reaction solution were taken at specific temperature points during the reaction, to track the formation of complexes and the subsequent growth of particles.

The point of nanoparticle formation was observed in each case, and is variable and dependent upon the reaction conditions and surfactant used (see Table 2).

The UV-Vis spectrum in Figure 17, on the left panel, displayed a shift in the largest peak when oleic acid (OA) was replaced with hexadecylamine (HDA). As the temperature rises, the peak intensity of the HDA reaction decreases, with the peak disappearing by 150 °C, as displayed in the right panel of Figure 17. This indicates particle formation as the particles absorb light across the visible spectrum. This effect is not seen until 220 °C in the samples made with OA. The spectrum on the right hand panel also shows an absorption produced by the formation of a TOPO-metal ion complex at around 150 °C. The peak position is similar to that of the OA reaction, however, the peak becomes characteristically sharp at this temperature. For the oleic acid reaction, the peak width remains unchanged after 120 °C, indicating that the metal ion-oleate complex has been formed by this temperature. A rise in the low wavelength absorption occurs between 170 °C and 200 °C for this sample.

This technique gave a lot of information about the effect of surfactants on nanoparticle formation temperatures. It also allowed the synthesis to be optimised for subsequent reactions, due to the detailed plotting of the effect of temperature on particle growth, and hence the ideal conditions required to initiate particle formation. This information was used to tailor the reaction to specific heating profiles, allow complex formation and hence nucleation followed by particle growth. It also gave an indication of the suitability of certain surfactants for nanoparticle growth and in particular, the type of surfactant that suits a particular composition of particle e.g. Ni- amine stabilised particles.

2.6.2 Oleic acid (OA)

2.6.2.1 Introduction

An investigation was carried out into the effect of using oleic acid as the sole surfactant stabiliser, to coat $Co_{80}Ni_{20}$ core-shell nanoparticles. The reaction was similar to that described in the platinum seeds section earlier (Section 2.5.1.1). The heating rate was different in this reaction, in order to try and control the bimodality that was evident before.

2.6.2.2 Synthesis of $Co_{80}Ni_{20}$ particles using oleic acid

The reaction was carried out in the same manner as reactions described earlier. Cobalt and nickel tetrahydrate acetate salts were combined in a flask with 1,2-hexadecanediol, platinum acetylacetonate, oleic acid and dioctyl ether. The reactants were heated to the boiling temperature of dioctyl ether and then refluxed. Further experimental detail is given in section 5.4.1 of Chapter 5. The particles that were formed from the synthesis were isolated and analysed. The results from this analysis are detailed in the next section.

2.6.2.3 Results

TEM analysis of $Co_{80}Ni_{20}$ particles synthesised in this study revealed that a polydisperse sample had been formed. The particles varied in size The particles appeared to be spherical-like in morphology. This could be due to the oleic acid inhibiting the particle growth to form spherical-shaped particles. The particles appeared to be multi-grained. Craters and lines were observed across individual particles, indicating the coalescence of crystal grains to form an individual particle. The size distribution curve in Figure 18 shows a mean particle diameter of 7.1 +/- 2.8 nm. The distribution was monomodal, indicating that it was likely a single-nucleation event had occurred. The distribution was fit to a lognormal shaped curve.

Figure 18. Size distribution of 7.1 nm $Co_{80}Ni_{20}$ particles made with oleic acid as sole surfactant displays single nucleation event.
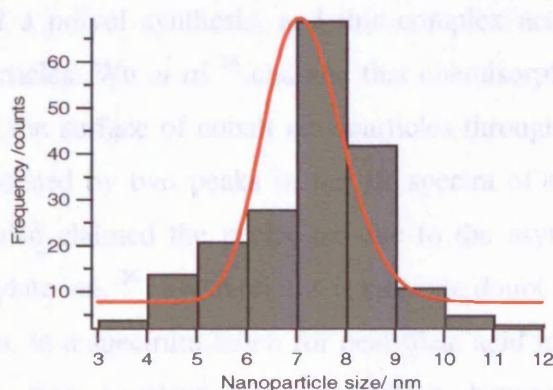
Elemental analysis of $Co_{80}Ni_{20}$ particles made with oleic acid, showed that 31.0 mass% of the sample was due to the surfactant weight. Carbon accounted for 24.9

mass%, whilst hydrogen was 3.2 mass% and oxygen was 3.0 mass%. EDX analysis of the particles showed that 38.7 atom% was due to oxygen, whilst 47.3 atom% was due to cobalt and 13.9 atom% due to nickel. The level of nickel was slightly high, however in general terms the relative cobalt: nickel ratios corresponded. The amount of oxygen observed was consistent with what has been seen with other samples in this study. Powder XRD studies revealed an amorphous material with no sharp crystalline peaks. The small size of the particles and hence the multigrain structure evident in TEM studies, could be a contributory factor to the difficulty in obtaining a strong signal from the sample, for the XRD technique. Fluorescence from the cobalt could have also contributed.

The particles formed using oleic acid as sole surfactant, with seeds, were small in size and displayed multi-grain structures. The amount of surfactant that remained adsorbed to the surface of the particles, determined by elemental analysis, was quite high. This is possibly due to oleic acid readily forming a complex with the metal ion species or excess surfactant that may have adsorbed onto the nanoparticle surface during the washing procedure. The mean size of the particles, and the distribution indicated a single nucleation event. However, the small size of the particles means that they have probably oxidised to their cores, and are primarily composed of antiferromagnetic cobalt-nickel oxide crystallites. This was further confirmed by a magnet being held up to the particles and producing no response. The complete oxidation of the $Co_{80}Ni_{20}$ particles, coated in oleic acid, indicates that it does not work well enough on its own to stabilise the particles.

Oleic acid forms a complex with Co and Ni ions very easily during the nucleation stages of a polyol synthesis, and this complex acts as a precursor to the formation of the particles. Wu et al [26] claimed that chemisorption occurs between the carboxylate ion and the surface of cobalt nanoparticles through the two oxygen atoms and this is characterised by two peaks in the IR spectra of oleic acid coated cobalt nanoparticles. Wu also claimed the peaks are due to the asymmetric and symmetric bands of the carboxylate ion. [26] However, this is cast into doubt as peaks have formed in those same positions, in a spectrum taken for neat oleic acid in this study (Figure 20). Thereby indicating that covalent bond formation between the surfactant and nanoparticle is unlikely. This theory has also proven to be inconclusive in this investigation, due to the oxidation of the Co_xNi_{1-x} particles described earlier.

Oleic acid could be used in conjunction with another surfactant such as oleylamine, for the synthesis of Co_xNi_{1-x} particles. Sun et al [7, 28] successfully used an oleic acid/oleylamine surfactant mixture to stabilise FePt nanoparticles. Therefore, the next logical step in this study was to examine the effects of oleylamine as a sole surfactant stabiliser for this system, followed by a study into the effects of using both OA and OY as surfactant stabiliser for the Co_xNi_{1-x} system.

2.6.3. Oleylamine (OY)

2.6.3.1. Introduction

Oleylamine has been used as a sole surfactant in the synthesis of CoO,[29] Ni and NiO[30] nanoparticles in previous studies. Therefore, the use of oleylamine as a stabiliser for $Co_{80}Ni_{20}$ alloy particles was attempted in this study. Oleylamine does not complex as tightly to the metallic ion species, as with some of the phosphine-based ligands or oleic acid. Therefore, oleylamine is generally used in conjunction with other surfactants, such as oleic acid, to allow control of particle shape and size.[14] However, this particular study is carried out in order to establish whether or not oleylamine can be used as a sole surfactant stabiliser for this particular system.

2.6.3.2 Synthesis of $Co_{80}Ni_{20}$ particles using oleylamine

Particles of expected composition, $Co_{80}Ni_{20}$, were synthesised using the modified polyol method which has been described earlier. Cobalt and nickel tetrahydrate acetates, platinum acetylacetonate, 1,2-hexadecanediol and oleylamine were dissolved in dioctyl ether, and heated in an atmosphere of nitrogen, in a round-bottomed flask. The solution was heated up to the reflux temperature of the solvent, and the resulting particles were extracted post-synthesis. Further experimental detail in given in section 5.4.2 of Chapter 5.

2.6.3.3 Results

The particles formed from the synthesis were small in size, but were clumped together in large aggregate superstructures, which made quantification of particle sizes difficult. The oleylamine surfactant did not appear to stabilise the particles from agglomeration. TEM determined the mean particle size as 6.0 +/- 4.0 nm, and the curve was fitted to a

Gaussian function, although it is slightly skewed at the higher end of the size scale. There were also large clumps of aggregates in the sample. This could be due to an excess of surfactant in this particular system. The particles formed here appeared to be much smaller than those made with oleic acid. They also appear to be much more irregular in shape. Particles of this size have in this investigation, been shown to oxidise to the core. This has been shown through the magnetic properties of the sample.

Figure 19. Size distribution of 6 nm $Co_{80}Ni_{20}$ particles made with oleylamine as sole surfactant stabiliser.
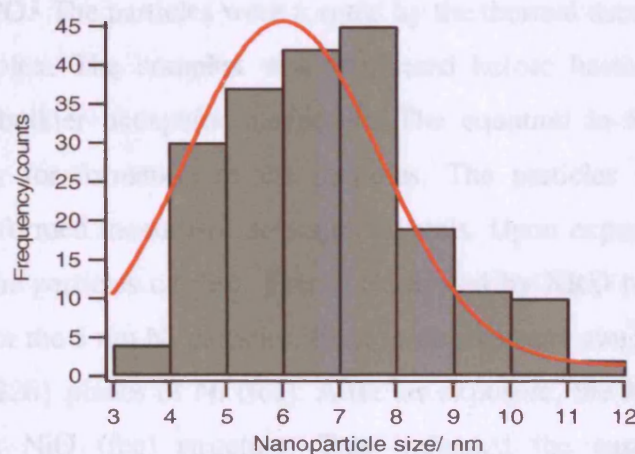
Elemental analysis revealed that 18.3 weight% of the $Co_{80}Ni_{20}$ particles, synthesised with an oleylamine coating, was due to carbon, hydrogen and nitrogen. The value is much lower than that shown for the sample with oleic acid as sole surfactant, indicating that it is possible oleylamine is easily washed off, and is therefore not very good at preventing oxidation. Studies carried out by Park et al [30] confirm this.

The particles also did not respond to a magnet at room temperature, therefore, detailed magnetic measurements were not carried out on the sample because of the likelihood of oxidation due to small size of the particles. Although, VSM indicated the particles had oxidised due to the low magnetic moment and the hysteresis loop resembling that of an antiferromagnet. EDX analysis also exhibited high oxygen levels in the particles, which indicated they had oxidised.

Previous works by Zhang et al [29] sought to produce CoO nanoparticles using oleylamine as a stabiliser and solvent, with cobalt (acetylacetonate)$_2$ as the precursor salt. Zhang found that particles of between 4 -23 nm could be synthesised using this

method.[29] Although, the oleylamine was degassed prior to the synthesis and a nitrogeneous atmosphere was kept during the synthesis. Zhang claimed that the oxidation arose from the decomposition of [Co(acac)$_2$], and was not due to the surfactant, or oxygen infiltration into the reaction flask as the reaction was carried out in an inert atmosphere.[29] However, during their post–reaction treatment of the synthesised particles, they exposed the sample to air, and dried the particles in a standard oven overnight. For particles of those sizes, particularly the smaller ones, it is likely that oxidation occurred post-synthesis, and not as they claim in the reaction vessel.

Park et al [30] investigated the synthesis of Ni and NiO particles using oleylamine followed by TOPO. The particles were formed by the thermal decomposition of the Ni-oleylamine complex. The complex was fabricated before heating the solution, and introducing the bulkier phosphine surfactant. The equation in Scheme 2 shows the reaction pathway for formation of the particles. The particles were protected from aggregation and formed monodisperse single crystals. Upon exposure to air, Park et al [30] claimed that the particles oxidise. This is evidenced by XRD taken before and after exposure to air for the 5 nm Ni particles. Prior to air exposure single peaks belonging to the {111} and {220} planes of Ni (fcc). After air exposure, the XRD pattern revealed peaks due to a NiO (fcc) structure. This indicated the susceptibility of nickel nanoparticles to oxidation.

Scheme 2. Synthesis of metallic nickel nanoparticles formed from a nickel-oleylamine complex.[30]
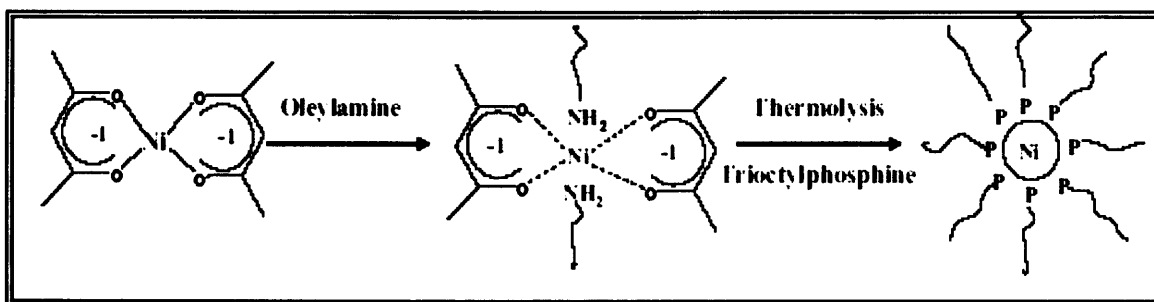
Oleylamine can complex with metallic ions at low temperatures. Park et al [30] claimed that this can occur at around 100 °C. This could explain the smaller mean diameters obtained, as oleylamine complexes easily with the metallic ions, and these complexes would also possibly decompose at lower temperatures to bring about the

formation of nanoparticles. The lower decomposition temperature would lead to smaller particles as the nucleation step would be very short in such reactions, and the growth step would not be sufficiently long enough to redress the balance of the short nucleation stage.

Similar results have been found in this investigation with Co_xNi_{1-x} particles of various compositions, where the particle size is predominantly below 10 nm. This total oxidation has been consistently observed in particles with a small mean diameter in this study. The variations in surfactant for a particular metallic nanoparticle synthesis should be specifically tailored, due to individual characteristics of each surfactant. Different surfactants can complex with metallic ions with ease or difficulty, depending on factors such as sterics and their individual affinity to a particular metallic ion species. Amine based stabilisers such as oleylamine and hexadecylamine have been generally used for Ni nanoparticle synthesis, however TOPO has also recently been used in conjunction with these to form Ni particles.[31-33]

The $Co_{80}Ni_{20}$ alloy particles coated with oleylamine, in this study, oxidised completely. This suggests that oleylamine is inefficient as a surfactant stabiliser, when used solely in particular. Other stabilisers used in this study thus far, such as oleic acid, have also to some extent shown they cannot sufficiently stabilise a particle from oxidation if the size of the particles formed is very small (approximately <10nm). In the case of oleylamine, for the Co_xNi_{1-x} system, it also could not prevent particle agglomeration.

Combinations of surfactant have recently been used in many investigations.[9, 34-36] As was mentioned earlier, mixtures of surfactants, such as oleylamine with other oleic acid have been investigated by other groups for the synthesis FePt nanoparticles.[14, 36] Therefore, the next plausible approach considered for this investigation was the combination of oleic acid and oleylamine to stabilise the Co_xNi_{1-x} particles much more effectively.

2.6.4. Oleic Acid/Oleylamine mixture

2.6.4.1. Introduction

Following work carried out with oleic acid and oleylamine as sole surfactants, attempts

were made to synthesise particles using $Co_{80}Ni_{20}$ particles with both stabilising agents together. Previous research on other metallic species, indicated that oleic acid and oleylamine could be used together, to synthesise metallic nanoparticles.[12] Sun *et al*[7] used an OA/OY mixture to produce monodisperse FePt colloids with a modified polyol method. However, the same principles have been applied to synthesise particles.

2.6.4.2 Synthesis of $Co_{80}Ni_{20}$ particles using oleic acid/ oleylamine

Cobalt and nickel acetylacetonate salts 1,2-hexadecanediol and a 1:1 mixture of OA/OY were combined in a flask and heated to the boiling temperature of dioctyl ether. Platinum seeds were not used in this particular reaction, as particles formed using oleic acid and oleylamine surfactants on their own with seeds, had yielded small particles (sections 2.6.2 and 2.6.3).Therefore, by removing seeds from the synthesis, larger particles were expected to be formed.

2.6.4.3 Results

TEM analysis of $Co_{80}Ni_{20}$ particles, coated with an OA/OY mixture showed that large spherical and round corner square-shaped particles were formed. The particles were well-separated from one another. However, the irregularity in shape and polydispersity meant the particles could not pack to form arrays. The large size of the particles was due to the lack of nucleating seeds. There were contrast differences across the particles and also areas on the grid with excess surfactant. This made it difficult to observe individual particles on occasion. The particles also appeared to be crystalline, and there were less occurrences of multi-grain structured particles. The mean particle diameter was determined to be 71.2 +/- 12.0 nm. A plot of the particle size versus frequency was fitted to a lognormal distribution to obtain an accurate mean diameter value.

Elemental combustion analysis (CHN analysis) determined the mass of the nanoparticulate sample, due to surfactant, was 12.7 weight%. This constituted 11.6 weight% carbon and 1.1 weight% hydrogen. Nitrogen was not picked up by the analysis, perhaps due to the trace amount associated with one atom of nitrogen, in the amide linkage.

EDX analysis of the $Co_{80}Ni_{20}$ particles coated with an OA/OY mixture, yielded an atomic percentage mass of 42.6 atom% for cobalt, whilst nickel was 11.7 atom%. The value for nickel indicates that the sample maybe slightly nickel-rich due to it nucleating before cobalt in the reaction solution. The amount of oxygen present, was

determined to be 45.7 atom%.

The $Co_{80}Ni_{20}$ particles coated with OA/OY, responded to magnet very strongly in solution, this was probably due to the size of the particles. Monodisperse particles of a smaller size are ideal due to the need to overcome the superparamagnetic limit of the particles and induce thermal switching.[37] It is possible that the $Co_{80}Ni_{20}$ particles made here are single domain, even though they are quite large, as the single-domain sizes for cobalt and nickel particles have previously been determined as 70 and 55 nm respectively.[38]

Both oleic acid and oleylamine surfactants were combined in 1:1 molar amounts before the reaction, as described in the experimental methods section. Evidence suggests that a weak acid and weak amine, when combined, react to release a molecule of water and form an amide through the head groups. The surfactant tail becomes double-sheathed which provides a stronger barrier to oxidation and agglomeration. Infra-red spectroscopy corroborates this theory, when compared to the spectra of neat oleic acid and oleylamine.

Figure 20. IR spectra of neat oleic acid (blue trace), neat oleylamine (green trace) and an OA/OY (red trace) 1:1 surfactant mixture.
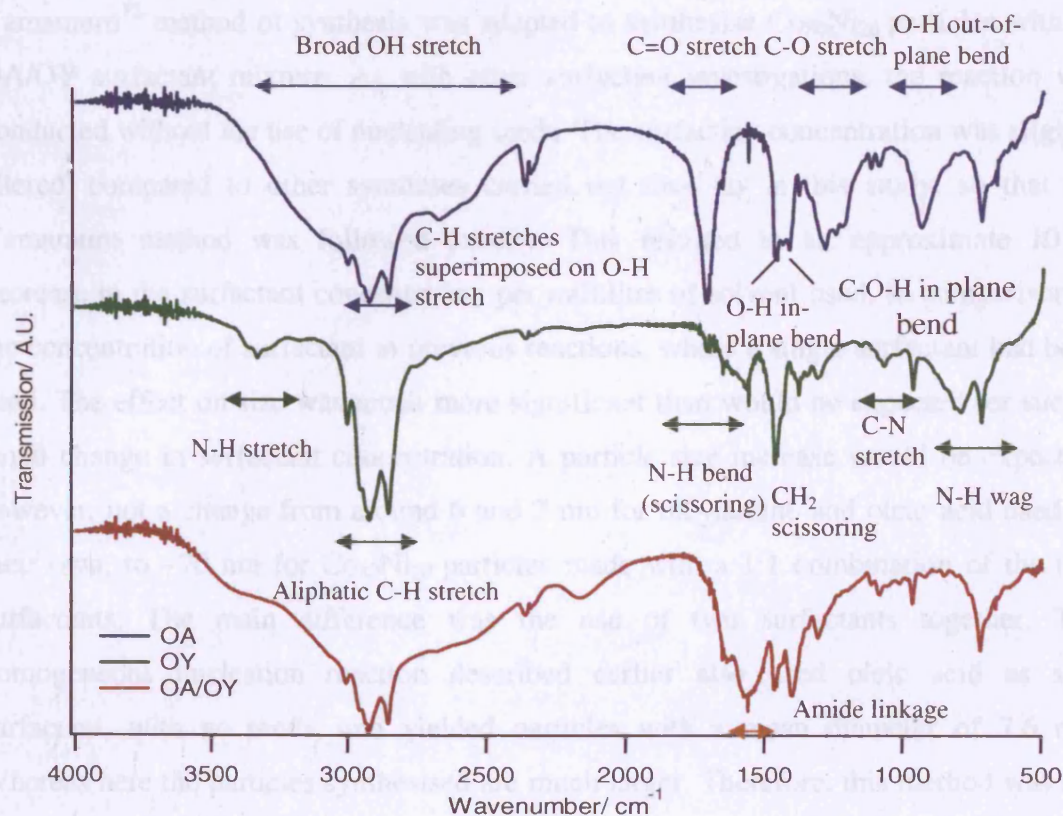
The amide group is proven by the existence of a peak at 1558 cm^{-1} in the red trace of Figure 20. Oleic acid inhibits growth when coupled with oleylamine. It works well as a stabiliser, as the amide that has formed complexes with the metal ions less tightly to the nanoparticle surface and allows particle growth. However, it is not as weak as oleylamine and therefore prevents oxidation somewhat compared to if both surfactants are used on a sole basis. This allowed the growth of the particles to occur and also their stability to oxidation.

In the literature, an OA/OY combination has previously been used to make FePt nanoparticles. Sun et al [28] carried out the thermal decomposition of $Fe(CO)_5$ in a high-temperature solution with 1,2-hexadecanediol as the reducing polyalcohol. Oleic acid and oleylamine were used to produce hexagonally close-packed 3-D arrays of $Fe_{50}Pt_{50}$ particles, with an interparticle distance of ~4nm maintained throughout the array due to the oleic acid/oleylamine mix. In that particular study, particle sizes were adjusted by controlling the molecular ratio of the iron carbonyl to the Pt salt. The OA/OY mixture also protected the particles from oxidation. Another similar procedure is described in the literature as a route to iron oxide nanoparticles, and involved the high-temperature reduction of iron (III) acetylacetonate in the presence of oleic acid and oleylamine. [39]

Cobalt and nickel carbonyls were not used in this study due to their toxicity. The Yamamuro[12] method of synthesis was adapted to synthesise $Co_{80}Ni_{20}$ particles with an OA/OY surfactant mixture. As with other surfactant investigations, the reaction was conducted without the use of nucleating seeds. The surfactant concentration was slightly altered, compared to other syntheses carried out thus far in this study, so that the Yamamuro method was followed exactly. This resulted in an approximate 10 % decrease in the surfactant concentration per millilitre of solvent used, in comparison to the concentration of surfactant in previous reactions, where a single surfactant had been used. The effect on size was much more significant than would be expected for such a small change in surfactant concentration. A particle size increase would be expected, however, not a change from around 6 and 7 nm for oleylamine and oleic acid used on their own, to ~70 nm for $Co_{80}Ni_{20}$ particles made with a 1:1 combination of the two surfactants. The main difference was the use of two surfactants together. The homogeneous nucleation reaction described earlier also used oleic acid as sole surfactant, with no seeds, and yielded particles with a mean diameter of 7.6 nm. Whereas here the particles synthesised are much larger. Therefore, this method was not pursued in its present form. The OA/OY seemed to stabilise and coat the particles well,

and it was felt that by adapting this method to include platinum seeds, which have also shown promising results in terms of size control (see section 2.5.1.1), it would be possible to make Co_xNi_{1-x} particles of a controlled size and stability to oxidation. Section 2.7 discusses the developments made to the synthesis in order to produce particles with varied composition, and build upon the methods and results described here.

2.6.5 Trioctylphosphine oxide

2.6.5.1 Introduction

TOPO has been used successfully for the synthesis of semiconductor nanocrystallites (CdE where E= S, Se, Te), in important works carried out by Bawendi and co-workers.[40] TOPO was presented to be an effective capping agent of nanoparticles, due to its selective binding characteristics. It has been found that TOPO selectively absorbs to preferred crystallographic planes and hence controls the growth of specific crystal faces.[41],[42]

The Bawendi group [43] also applied this to the synthesis of cobalt nanocrystals. Dicobalt octacarbonyl (DCOC) was subjected to thermolysis in toluene, yielding 20 nm spheroidal cobalt particles with a size distribution of approximately 15 %. An increase in the reaction temperature, together with a large increase in growth, indicated that the TOPO-metal complex was weak and could be easily removed. The particles would then be exposed to air and subsequently oxidise. In this investigation, several experiments have been carried out with trioctylphosphine oxide as the sole surfactant stabiliser. The effect of varying the concentration of TOPO and the use of heterogeneous and homogeneous nucleation was probed.

2.6.5.2 Synthesis of $Co_{80}Ni_{20}$ particles using trioctylphosphine

The particle synthesis proceeded in the same manner as other syntheses described in this chapter. The metal salts, surfactant, solvent and reducing agent were all heated to the boiling temperature of the solvent. The subsequently formed nanoparticle solutions were isolated and kept for analysis. Seeds were not used in the synthesis of sample A (see Table 3), whereas samples B-D were heterogeneously nucleated and hence were made with seeds. Table 3 details the range of experiments carried out with TOPO as

surface-active agent. However, experimental detail of how TOPO-coated particles were formed is given in Chapter 5 (section 5.4.4).

2.6.5.3 Results

The formation of TOPO-coated $Co_{80}Ni_{20}$ particles, without the presence of seeds was investigated. This yielded a stable solution, and particles with a mean diameter of 5.9 +/- 1.7 nm (sample A-Table 3). The particles formed a stable solution, but did not respond to a magnet, as they had probably oxidised.

The effect of platinum seeds on the nucleation of $Co_{80}Ni_{20}$ particles with TOPO was subsequently investigated. The concentration of the platinum seeds was varied, in addition to the surfactant concentration, to establish their effects on particle size. The molar amount of reactants was varied, over the series of experiments, yielding particles of different sizes.

Table 3. Reaction parameters of TOPO syntheses of $Co_{80}Ni_{20}$ nanoparticles, made with or without seeds. The amounts of each reactant with respect to one another are shown.

Sample	Seeds/ mmol	Surfactant/ mmol	Reactant salts /mmol	Particle size (notes)
Sample A	/	3.125	2	5.9 +/-1.7 nm particles formed
Sample B	0.0013	3.125	2	Particles are too small to get accurate size ~2-3 nm
Sample C	0.0013	6.25	2	Agglomerated particles mean an accurate size cannot be obtained
Sample D	0.0025	6.25	2	Polydisperse but with small particles - 4.1 +/-2.6 nm

The concentration of seeds was changed, therefore, in theory less seeds meant less nucleation sites, and so the particles would grow to a larger size when the reagents were all consumed. The same was true of the amount of surfactant. Less surfactant stabiliser can lead to larger particles, however, this depended upon the influence of steric factors on particle growth. Both the seed and surfactant concentration were low in Sample B and therefore, relatively large particles were expected. However, this was not

the case, and the particles that were formed were much smaller than particles made with oleic acid earlier. So much so, that an accurate size could not be determined as it was difficult to distinguish the particles from the noise generated by the carbon background, with the size analysis software.

The results for the TOPO did not follow the expected pattern, and polydispersity seemed to be intrinsic in any sample made with it as sole surfactant. It was thought that TOPO would stabilise the particles well from oxidation and control the growth. Sample D showed the best quality of particles. The particles sizes were fit to a Lorentzian distribution curve and this yielded a mean diameter of 4.1 nm +/- 2.6 nm. The size distribution of the particles was large at approximately 60 % and TEM analysis of the particles revealed polydispersity. Sample B was expected to have the largest particles due to the lower surfactant concentration. However, there was not enough surfactant to stabilise the $Co_{80}Ni_{20}$ particles, they had oxidised and did not respond to a magnet at room temperature. The same was true of samples B, C and D. Therefore, the particles were of a good shape and morphology, with an absence of multi-grains, but they were not the right size to support the growth of an oxide shell layer.

The small size of the particles meant that it was also not possible to resolve an XRD pattern. EDX measurements were not carried out as the size meant that the particles had almost certainly oxidised fully. The non-responsiveness of these particles to a magnet further confirmed this.

Figure 21. Size distribution of particles made with trioctylphosphine oxide as surfactant (sample C –see Table 3), with seeds.
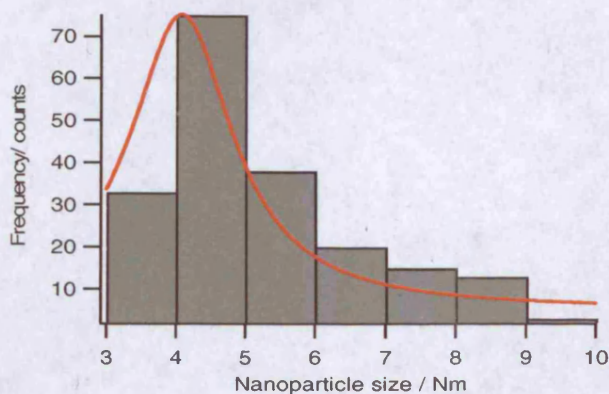
As Dinega [43] had observed in the synthesis of cobalt nanoparticles, TOPO does not sufficiently stabilise the particles from oxidation. However, it does stabilise the particles well enough to encourage separation and a spherical morphology.

The main drawback to using TOPO as sole surfactant was the small size of the particles produced. This led to full oxidation of nanoparticles and yielded a low magnetic moment. UV-Vis studies (Figure 17) had earlier indicated that the TOPO-metal ion complex, which precludes particle formation occurs at around 150 °C, with the point of nanoparticle formation at around 204 °C (Table 2). The metal ion-surfactant complex was formed much earlier, for particles that had a larger mean diameter, in comparison to TOPO (e.g oleic acid).

TOPO proved to be a slightly better stabilising agent than oleic acid or oleylamine in terms of ensuring a stable solution was formed and the particles did not precipitate out of their respective solvent. The TOPO-coated $Co_{80}Ni_{20}$ particles also redispersed well into non-polar solvents such as hexane and toluene. Samples made with just OA or OY as the primary stabiliser had sometimes remained stable, but the majority of the time precipitated out to the bottom of the sample vial. However, the main issue that appeared to affect this type of synthesis was the small size of the particles generated using TOPO. This led to the TOPO-coated particles oxidising readily and did not respond to a magnetic field. The TOPO-route of synthesising Co_xNi_{1-x} particles was therefore not pursued as it was unsuitable for this particular synthesis.

In order to improve upon these results, TBP was subsequently tested as a stabiliser for the synthesis of Co_xNi_{1-x} particles, as it is less bulky than TOPO. This would perhaps inhibit the particle growth less and lead to the formation of particles with a slightly larger mean diameter.[44]

2.6.6. Tributylphosphine

2.6.6.1 Introduction

When compared to TOPO, TBP provides less steric hindrance as it is less bulkier, and therefore promotes the growth of larger particles.[45] TOPO is much bulkier, and therefore slows the growth of the nanocrystal, which should result in smaller nanoparticles overall. In order to improve upon the results shown in previous studies

with TOPO as a stabiliser, the surfactant concentration was doubled in order to prevent oxidation of the particles and to take into account the fact that TBP is less bulky.

2.6.6.2 Synthesis of $Co_{80}Ni_{20}$ particles using tributylphosphine

Synthesis of $Co_{80}Ni_{20}$ particles proceeded in the same manner as with other reactions described in Section 2.6. The cobalt and nickel acetate salts were mixed with the reducing agent and tributylphosphine surfactant and heated to the reflux temperature of the solvent, diphenyl ether. Nucleating seeds were not used in the reaction in order to try and enhance the particle size, from what was observed with the TOPO particles formed. The resulting nanoparticles were isolated, washed and stored for analysis. Full experimental detail in given in section 5.4.5 of the experimental chapter.

2.6.6.3 Results

TEM results of the $Co_{80}Ni_{20}$ particles coated with TBP were interesting. The particle's mean diameter was determined as 3.0 +/-1.1 nm. This was smaller than expected for TBP-coated particles, in comparison to the TOPO-coated particles that were synthesised earlier. The particle size distribution was fitted to a Lorentzian curve, as shown in Figure 22. The $Co_{80}Ni_{20}$ particles made using TBP were spherical in shape, however, their small size again meant they had oxidised completely. This was confirmed by the lack of response, of the TBP-coated $Co_{80}Ni_{20}$ particles, when a magnet was placed alongside the vial which contained the nanoparticulate solution.

Figure 22. Size distribution of 3 nm $Co_{80}Ni_{20}$ particles made with tributylphosphine.
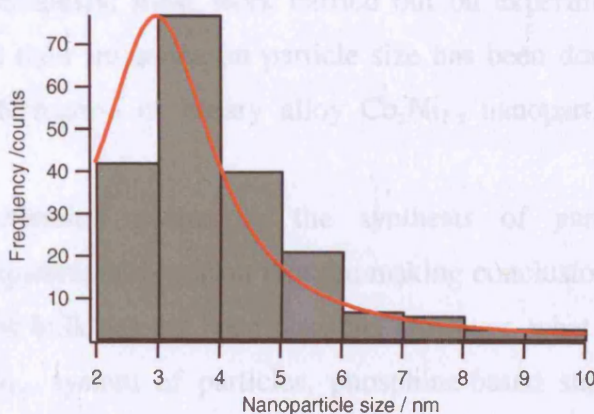
Elemental analysis showed that 18.9 mass% of the sample weight was due to surfactant. This is similar to the value obtained for other surfactants used in the investigation. EDX analysis was again not carried out as the particles had completely oxidised, as illustrated by the powder's non-response to the magnet. XRD was also not possible on particles of this size, as the crystallites were too small to be picked up and also due to fluorescence from the cobalt yielding a large background.

The size of the particles produced using tributylphosphine, were an obvious indicator that this method could not be used for the synthesis of Co_xNi_{1-x} alloy nanoparticles. This method had yielded very small particles which oxidised and were therefore non-magnetic. The absence of seeds in the reaction should have led to larger particles forming, however this was evidently not the case. What this particular micro-study, within this investigation, has shown is that TBP is an excellent surfactant to use in terms of particle size control. It offers great stability to nanoparticles at their surface in terms of shape and also the size. This is good for this particular type of synthesis, as it limits the additional anisotropy due to deviations in shape, and any exchange bias that did occur in larger core-shell particles that could be made in the future, would be due to exchange anisotropy. If the concentration of TBP was adjusted in future studies or if the TBP was added post-synthesis to the nanoparticle solutions and used with another surfactant, such as oleic acid for example, this could lead to good shape and stability for this particular Co_xNi_{1-x} system.

Hyeon[44] has reported on the effect of the steric bulk, of phosphine stabilisers, on particle size and how the use of phosphine-based ligands can be controlled to achieve particles of a particular size. This generalisation holds true to some extent, but this study shows that for different systems, such as the Co_xNi_{1-x} particles made here, this is not always the case. Previously, most work carried out on experimenting with different surfactant types and their influence on particle size has been done with a pure cobalt system. Here, the formation of binary alloy Co_xNi_{1-x} nanoparticles yielded slightly different results.

Multiple nucleation events in the synthesis of particles, and bimodal distributions in the systems have meant that the making conclusions relating to the size of particles and steric bulk has not been possible. However, what this study has shown is that for a Co_xNi_{1-x} system of particles, phosphine-based stabilisers used as sole surfactants are probably not the best to use. The phosphine stabilisers yield smaller particles as they tend to complex to the metallic ions in solution much earlier than oleic

acid for example, and this has led to inhibited particle growth and particle formation at lower temperatures.

2.6.7 Summary of samples made with different surfactant stabilisers

The investigations carried out using the different surfactant stabilisers were very useful in determining the optimum reaction conditions for this system. The synthesis of Co_xNi_{1-x} alloy nanoparticles has proven to be difficult, due to the varying relationships of Co and Ni ions, with respect to the surfactants that have been studied. Oleic acid on its own, did not seem to provide particle stability to both oxidation and nucleation. This led in many instances, to bimodal distributions of particles. However, in some instances where the growth of the particles was controlled and the particles that were formed were large, oleic acid did stabilise the particles from oxidation (heterogeneous nucleation with platinum seeds-section 2.5.1.1). The particles made with oleic acid were generally polycrystalline, with multiple grains fusing together during the growth stage of particle formation.

Oleylamine did not seem to stabilise Co_xNi_{1-x} particles well and yielded multi-grain nanocrystals, which did not respond to a magnet due their complete oxidation. Trioctylphosphine and tributylphosphine, used as sole-surfactants for the synthesis of $Co_{80}Ni_{20}$ particles, had spherical morphology and were single crystals. However, the nanocrystals were very small (between 3-5.9 nm) and oxidation of such small particles to their cores could not be prevented. Therefore, the use of these particular surfactants, for this alloy system, was not pursued as they did not sufficiently stabilise the particles from oxidation due to the small size of the particles formed using them.

A mixture of oleic acid and oleylamine was tested and this produced well-formed spherical particles which responded to a magnet. A 1:1 mixture of both components was used in the syntheses. The particles formed were very large at 70 nm in mean diameter. Due to the size of the particles produced using this method, the need to decrease the size was evident, as was the need to retain the quality and shape of particles produced. The size needed to be decreased as exchange bias is an interfacial effect, and with such large particles the effect was not evident.

It was hypothesised that by introducing heterogeneous nucleation methods, which had proven successful in the initial stages of this synthetic optimisation study, it

would be possible to tune the size of the 70 nm Co_xNi_{1-x} particles to ca~10-15 nm. Platinum seeds had given the best results out of the various seeds and seeding techniques that had been trialled (Section 2.5). Therefore, the synthetic route that was deemed appropriate for synthesising Co_xNi_{1-x} particles, which would display exchange bias properties, were those that were heterogeneously nucleated with an OA/OY surfactant mixture and were made of acetylacetonate precursor salts. This optimised method was adopted for subsequent investigations into the synthesis of Co_xNi_{1-x} alloy magnetic particles, where x was varied to produce particles with different compositions.

2.7 Composition

2.7.1 Introduction to composition series

A series of synthetic experiments were carried out, where the composition of the magnetic nanoparticles was varied. The aim of this study was to synthesise a compositional series of Co_xNi_{1-x} nanoparticles that had tuned magnetic properties. Following investigations into the effects of an OA/OY mixture as a stabilising agent, an effective method of making the particles was established (Section 2.6.4). Subtle modifications were made to the design of the OA/OY synthesis described in section 2.6.4.2, in order to obtain nanoparticles of a smaller size (~10-15 nm), compared to what was generated previously by using that particular surfactant mix (~70 nm). In these studies, nucleating Pt seeds were also used to control the particle size.

2.7.2 Cobalt nanoparticles

2.7.2.1 Introduction

Cobalt nanoparticle synthesis has been famously documented in the literature, and has been the basis of many magnetic studies.[42, 46-49] Here, several methods were employed to try and synthesise cobalt nanoparticles. Different reactant salts and surfactants were used in order to try and optimise the synthesis. The use of metal tetrahydrate acetate salts yielded particles that were too small and hence unstable to oxidation. Therefore, acetylacetonate salts were used as precursors for the synthesis of Co_xNi_{1-x} particles. Cobalt particles were synthesised using methods that were highlighted earlier[12] (Section 2.6.4).

2.7.2.2 Synthesis of cobalt nanoparticles

Cobalt particles were synthesised by heating the acetylacetonate salt, reducing agent and platinum seeds in dioctyl ether. The solution was heated and the particles that were formed were isolated and kept for analysis. Further experimental detail is given in Chapter 5. Acetylacetonate precursor salts were deemed to be better than acetate salts due to there being less water molecules within the salt structure. Water molecules from the salts had been found to affect the efficiency of the heating, during particle synthesis. This had contributed to the lack of reproducibility and problems with reducing the salts in reactions with tetrahydrate salt precursors.

2.7.2.3 Results

The cobalt particles made using the acetylacetonate salts were better in terms of size, in comparison to cobalt particles made with acetate salts, as they were large enough to support the growth of an oxide shell. TEM analysis of the pure cobalt nanoparticles showed they had clumped together in some areas, due to excess surfactant. In the image of the cobalt nanoparticles (Figure 23 (a), it is easy to distinguish between the carbon background (light grey) and the darker spherical particles laid on top. The wispy darker objects, encasing some of the particles, are due to excess surfactant. The particles are spherical-like but exhibit contrast differences across their surfaces indicating facets and multigrain crystals are present. The mean particle size that was determined has been split into two values, due to the bimodality in the size distribution. If an overall average was taken, this would be skewed, and not representative of the sizes of particles that have been seen.

Figure 23(a) Image of heterogeneously synthesised 8.8 nm cobalt nanoparticles made with OA/OY and Pt seeds (b) overall size distribution of the 8.8 nm cobalt particles.
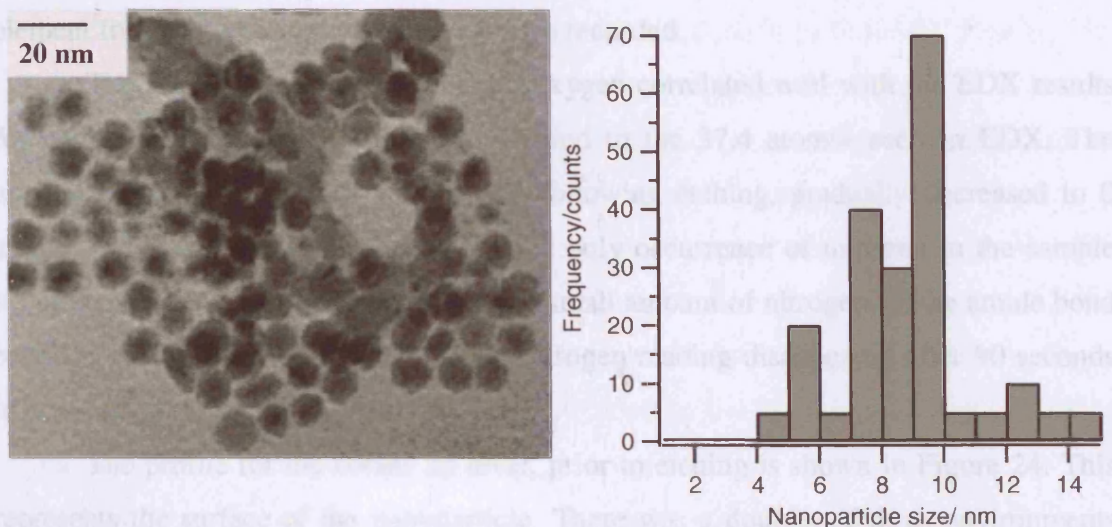
If slight bimodality in the sample was considered, the mean diameter of the smaller particles, measuring those between 4 -7 nm, was 5.5 +/- 0.7 nm. This gave a standard deviation of 12.8 %. The average diameter for the larger particles was 9.4 +/- 1.8 nm, and measured for particles between 8-15 nm. This yielded a deviation of 19.2%. The overall mean diameter for the particles, which was fit to a Lorentzian distribution, was 8.8 +/- 2.2 nm. Repeat syntheses gave mean diameters, within the standard deviation results, for this sample.

Elemental analysis showed that 20.8 mass% of the sample's weight was due to surfactant. The amount of carbon calculated was 18.8 mass% and hydrogen was 2.0 mass%. The nitrogen from the amide bond due to the oleylamine was not detected by this analytical technique.

EDX analysis of the cobalt nanoparticles showed that the atomic percentage of cobalt in the sample was 61.7 atom%, whilst oxygen was found to be 37.4 atom%. The remainder was expected to be due to platinum or carbon contamination. No contamination from other impurities was observed. The amount of oxygen observed was consistent with what had been seen other samples made in this study, in a similar fashion.

X-ray photoelectron spectroscopy was also carried out on the cobalt nanoparticles, in order to try and prove the existence of an oxide shell, in a qualitative

manner. The sample was bombarded with argon ions and was surface etched, followed by five etching cycles at preset intervals. The final etch took place at 390 seconds. For this particular sample, cobalt, oxygen, nitrogen and carbon atomic percentages were calculated, during the different etch cycles. The local environment of each particular element following the etch process, was also recorded.

The atomic percentage of surface oxygen correlated well with the EDX results for surface oxygen at 36.7 atom% compared to the 37.4 atom% seen in EDX. The amount of nitrogen was 0.8 atom% and following etching, gradually decreased to 0 atom%. This was an expected result as the only occurrence of nitrogen in the sample should have been at the surface, due to the small amount of nitrogen, in the amide bond between oleic acid and oleylamine. The nitrogen reading disappeared after 90 seconds of etching.

The profile for the cobalt 2p level, prior to etching is shown in Figure 24. This represents the surface of the nanoparticle. There was a doublet of three environments detected. The triplet on the right-hand side is due to the $2p_{3/2}$ level orbital splitting, and the triplet of the left-hand side is caused by the 2p 1/2 level orbital splitting.

Figure 24. Co 2p level surface etch for 8.8 nm cobalt nanoparticles.
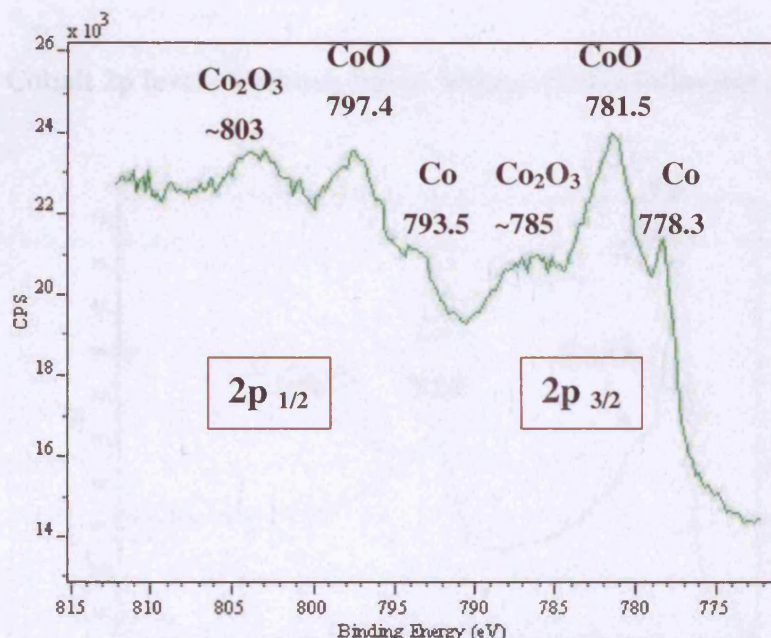
The peak at 778.3 eV is due to the 2p 3/2 level of elemental cobalt, and the peak at 793.5 eV is due to the 2p 1/2 of elemental cobalt.[50, 51] In comparison to the other peaks, these are less intense. The peaks at 781.5 eV and 797.4 eV may be attributed to the

cobalt (II) oxide (CoO) 2p 3/2 and 2p 1/2 levels respectively.[52, 53] Assignment of the peaks that occur at around 785 eV and 803 eV is a little more difficult. The peaks are broad and so the binding energies which are encompassed in this particular range could be either of two possibilities. The peaks could be due to the 2p 3/2 or 2p 1/2 levels of either Co_2O_3 or Co_3O_4. The values correspond most closely to those for Co_2O_3, with cobalt in an oxidation state of +3.[53] The results for the oxygen 1s level after 0 seconds of etching, show that they could have corresponded to oxygen bound to cobalt (II) oxide or cobalt (III) oxide. Therefore, this cannot be conclusively assigned.

Following the various etch cycles, ranging between the surface etch and 390 seconds, the peaks attributable to oxygen bound to cobalt had almost disappeared, with only a slight shoulder remaining. The shoulders are indicated by the arrows in Figure 25. The position of the shoulder peaks correspond to the 2p 1/2 and 2p 3/2 levels of cobalt (II) oxide.

The intensity of the peak due to elemental cobalt increased significantly as monolayers were etched away, as did the atomic percentage of cobalt. The atomic percentage rose from 21.1 % to 62.0 %, from the nanoparticle surface to its' respective core. Bearing in mind, the value for cobalt atom% is predominantly due to cobalt attached to oxygen, which forms the oxides in the nanoparticle.

Figure 25. Cobalt 2p level of 8.8 nm cobalt nanoparticles following 390 seconds of etching.
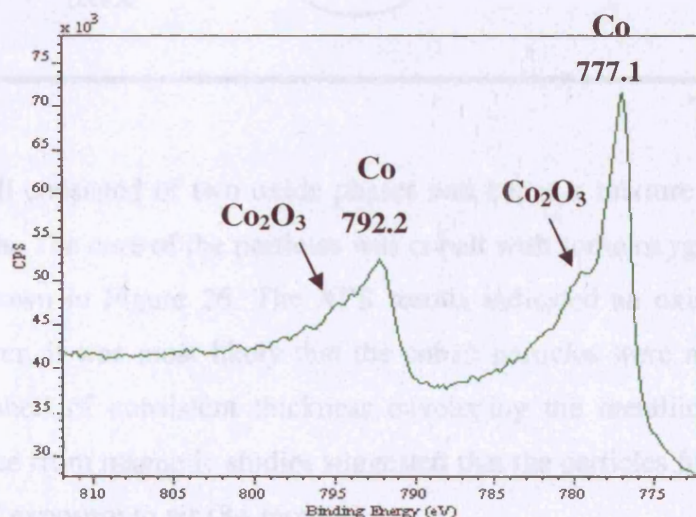
If a comparison is made between Figure 24 and 25, the changes in the plot as etching into the particle occurs, are evident. There is clearly one dominant environment due to

elemental cobalt. In terms of particle structure, Figure 25 represents the core of the core-shell nanoparticle, which has been uncovered following 390 seconds of etching. This confirms that there is some sort of oxide shell formation, when compared to Figure 24, which displays the snapshot of the environments, at surface of the nanoparticle. The consistent presence of oxygen as etching progresses into the core of the particle is explained in Figure 26. This particular schematic illustrates the oxygen, due to the oxide shell of the nanoparticle, will always be evident in the measurements as etching progresses over time. Initially, the surface oxygen would be detected, followed by the oxide layers at either edge of the particle after the "slicing" of monolayers, by argon ions that are bombarded on the nanoparticle surface.

Figure 26. Top-down etching of a core-shell cobalt, or Co_xNi_{1-x} nanoparticle, via x-ray photoelectron spectroscopy. Argon ions bombard the surface of the nanoparticle and etch away monolayers over time.
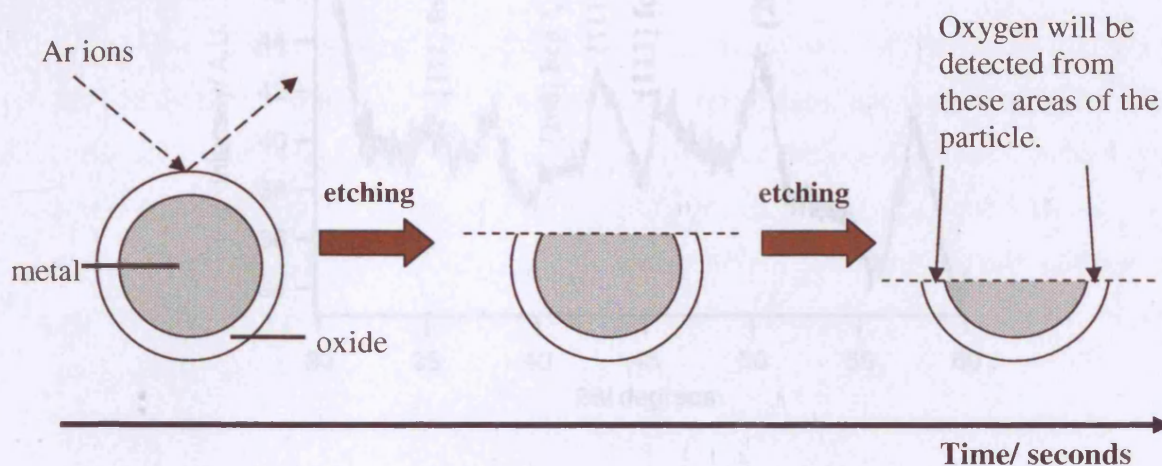
The shell consisted of two oxide phases and hence a mixture of the crystallites of both materials. The core of the particles was cobalt with some oxygen detected due to the shell, as shown in Figure 26. The XPS results indicated an oxide shell had been formed. However, it was most likely that the cobalt particles were not passivated, but had an oxide shell of consistent thickness enveloping the metallic particle. This is because evidence from magnetic studies suggested that the particles fully oxidised, after a long period of exposure to air (8+ months).

XRD studies were carried out on the cobalt particles. It was difficult to obtain any well resolved diffraction patterns due to the size of the particles made. However, a pattern was obtained and is depicted in Figure 27. TEM had indicated that the sample

appeared to be polycrystalline and that single crystal grains had not been formed. As mentioned earlier, the contrast gradients across the particle were indicative of the multi-grain structure within particles. The smaller grains within an overall multi-grain particle mean that it was very difficult for the XRD instrument to detect anything due to the sample. The mean diameter of the particle was on the border for what the instrument was able to resolve. The peaks that are believed to be due to the sample, are labelled in the diffractogram in Figure 27. The unassigned peaks in Figure 26 are due to the background substrate or signal from the detector gridlines.

Figure 27. X-ray powder diffraction pattern of platinum seeded cobalt nanoparticles coated with OA/OY, between 40 and 60 2θ degrees.
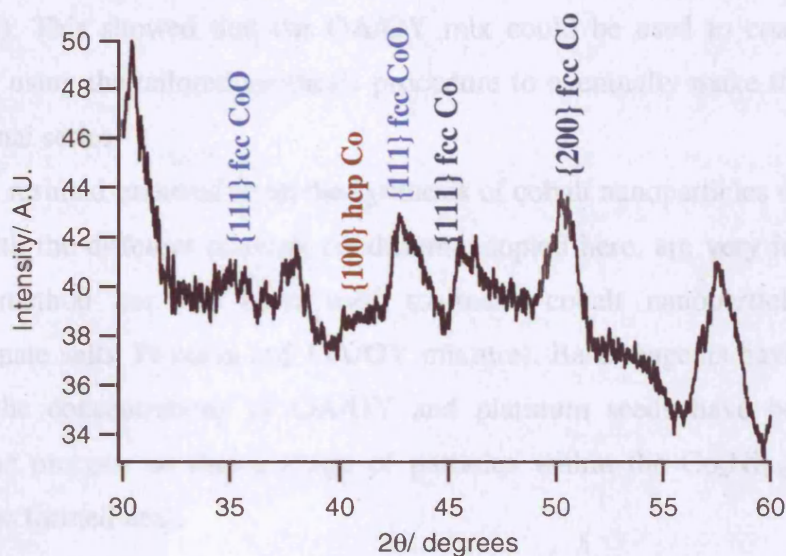
TGA analysis was carried out on the pure cobalt nanoparticle sample. The TGA analysis was adapted so that the nanoparticulate powders were heated in a magnetic field. Therefore, a magnet which wrapped around the furnace, within which the particles were heated in an atmosphere of nitrogen, was attached to the set-up. The point at which the curie transition occurs in such measurements is characterised by a sudden increase in the weight of the sample, as detected by the highly sensitive balance in the instrument.[54] It was not possible to obtain an accurate measure, of Curie temperature, on this occasion. Although, the literature value for Curie temperature of pure cobalt is 1131 °C.[54]

In comparison to other groups who have also made cobalt nanoparticles by a variety of methods, this study has shown that it is possible to make magnetic cobalt nanoparticles of a controlled size with an OA/OY coating. Luna *et al* reported the synthesis of 8 nm cobalt nanocrystals using only oleic acid as surfactant.[48] They also reported that the individual cobalt particles that were formed coalesced into large superstructures of around 100 nm in magnitude. This was not apparent in this study and the amount of surfactant added to the nanoparticles meant they were well separated and did not form these large superstructures of particles. The fact that the particles did not coalesce so readily was good, as this meant that characterisation of the particles via TEM was much easier. The mean size and size distribution of the particles made by Luna using OA surfactant coating (8 +/- 2 nm) was very similar to the overall mean determined for the cobalt particles synthesised in our study, using an OA/OY mix (8.8 +/- 2.2 nm). This showed that the OA/OY mix could be used to coat nanoparticles effectively, using the tailored synthesis procedure to eventually make the full Co_xNi_{1-x} compositional series.

The resulted garnered from the synthesis of cobalt nanoparticles using the polyol method, with the different reaction conditions adopted here, are very interesting. This particular method has not been used to make cobalt nanoparticles before (i.e acetylacetonate salts, Pt seeds and OA/OY mixture). Base reagents have also not been used and the concentrations of OA/OY and platinum seeds have been tailored to optimise the process, so that a range of particles within the Co_xNi_{1-x} compositional series can be formed next.

Synthesis of the cobalt nanoparticles using OA/OY and Pt seeds was successful in yielding particles that were larger than those produced earlier in this investigation using other surfactants, such as TBP and TOPO. The use of Pt nucleating seeds helped control the size of the cobalt nanoparticles. When an equivalent of 0.0063 mmol of Pt seed was added to the 10 mL of solvent and the other reactants, this produced particles of 8.8 nm in mean diameter, although a large population of particles were around 9-10 nm in size. The platinum seeds are thought to be around 1-2 nm in size and the cobalt nanoparticle growth occured around the seed.[48] The cobalt particles were almost spherical in shape and were polycrystalline (Figure 23 (a)). The particles also responded to a magnet on the day of synthesis and several days afterwards. This indicated that the particles were large enough to support oxide shell growth and maintain a core-shell structure, as the material still responded to a magnet. As has been shown in this study so

far, where particles have been too small, they are fully oxidised and have not responded to a magnet. The actual synthesis reaction was scaled up, to allow for the production of more nanoparticles for analysis (chapter 5). Repeat syntheses were carried out so the magnetic properties could be compared to those obtained from the cobalt nanoparticles described in this section. The magnetic properties of these cobalt samples are discussed in detail in chapter 3.

2.7.3 $Co_{80}Ni_{20}$ nanoparticles

2.7.3.1 Introduction

The synthesis of $Co_{80}Ni_{20}$ particles has been carried out in similar studies where the preparation of bimetallic alloy nanoparticles via the polyol synthesis has been examined. Luna et al [2, 13] succeeded in making $Co_{80}Ni_{20}$ particles with diameters ranging from between 18 and 540 nm in mean diameter. They investigated the use of silver and platinum, as seeds for growth, and determined that platinum seeds yielded better size control. The particles made with this platinum nucleating seeds were at the lower end of the size range described above. The size of the particles made in that particular study, was dependent upon the concentration of the seeds in the reactant medium. The higher the concentration of seeds, the more nucleating sites for the reactants to grow around and therefore the smaller the nanoparticle mean diameters.[2]

The $Co_{80}Ni_{20}$ particles made in this study were relatively small in comparison to those made by Luna et al.[2] The precursor salts used to make particles with a particular composition, in that study were acetate salts. This was in comparison to the acetylacetonate salts utilised in this investigation.

2.7.3.2 Synthesis of $Co_{80}Ni_{20}$ nanoparticles

Particles of the expected composition, $Co_{80}Ni_{20}$, were made using the polyol procedure. The ratios of cobalt and nickel salts were adjusted to produce alloy particles of a particular composition (Co_xNi_{1-x}). The metallic salts, nucleating seeds (Pt), reducing agent, surfactant and solvent were all heated together in an atmosphere of nitrogen. The particles that were formed were isolated and removed for analysis.

2.7.3.3 Results

TEM analysis of the heterogeneously nucleated $Co_{80}Ni_{20}$ nanoparticles, coated with OA/OY, showed they had grown in a variety of shapes. There were particles that were triangular, hexagonal and rhomboidal in shape, with apparent size variations. The mean particle size was calculated as 12.0 +/-3.4 nm, and the distribution fitted well to a lognormal curve. This can be seen in Figure 28, as can the range of shapes of particle formed within this sample. The image also shows that the particles that have been laid down onto the carbon film for TEM analysis have clumped together slightly, due to excess surfactant. The particles have different contrasts across their surface indicated the existence of multi-grains in the sample. A repeat synthesis of the $Co_{80}Ni_{20}$ particles yielded a mean diameter of 10.9 +/- 3.1 nm. The magnetic properties of both sets of the 12.0 nm and 10.9 nm particles are described in section 3.5.2 of Chapter 3. In this chapter, the structural and physical properties of the 12.0 nm particles are described in detail.

Figure 28. Image of 12.0 nm mean diameter $Co_{80}Ni_{20}$ particles made with platinum seeds and oleic acid/oleylamine surfactant, shows particles of a variety of shapes. Particles are polydisperse but fit well to a lognormal distribution.

30 nm
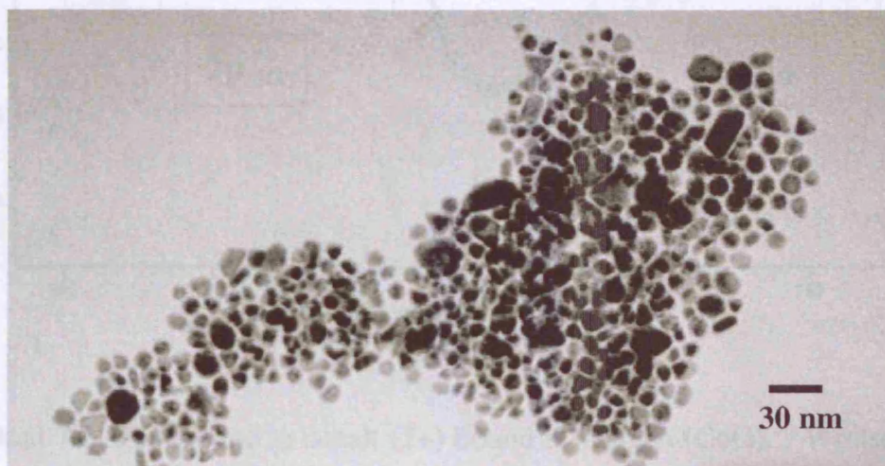
Elemental analysis of the 12.0 nm $Co_{80}Ni_{20}$ particles showed that 16.2 % of the sample's mass was due to surfactant weight. Carbon was 13.0 mass % whilst hydrogen was 3.18 mass% of the sample's weight. EDX analysis showed that the atomic percentage shown by cobalt was 48.6 atom%. The amount due to nickel was 11.5 atom% and oxygen was 39.9 atom%.

XPS analysis gave interesting results and indicated the formation of a bimetallic alloy. Figure 29 displays a doublet of triplets, therefore, cobalt has three predominant environments. The surface layer shows a high concentration of oxygen, which would be expected in a metal/metal oxide core-shell structure. The peak at 777.2 eV is due to the Co 2p 3/2 level of cobalt bound to nickel (CoNi), as this occurs in this particular region.[55] This peak increases in intensity as the particle is etched into, as the atomic concentration of CoNi increases and the metallic core of the core-shell particle is progressively reached.

Figure 29. XPS spectrum-surface etch of Co 2p core level at 0 seconds for $Co_{80}Ni_{20}$ nanoparticles.
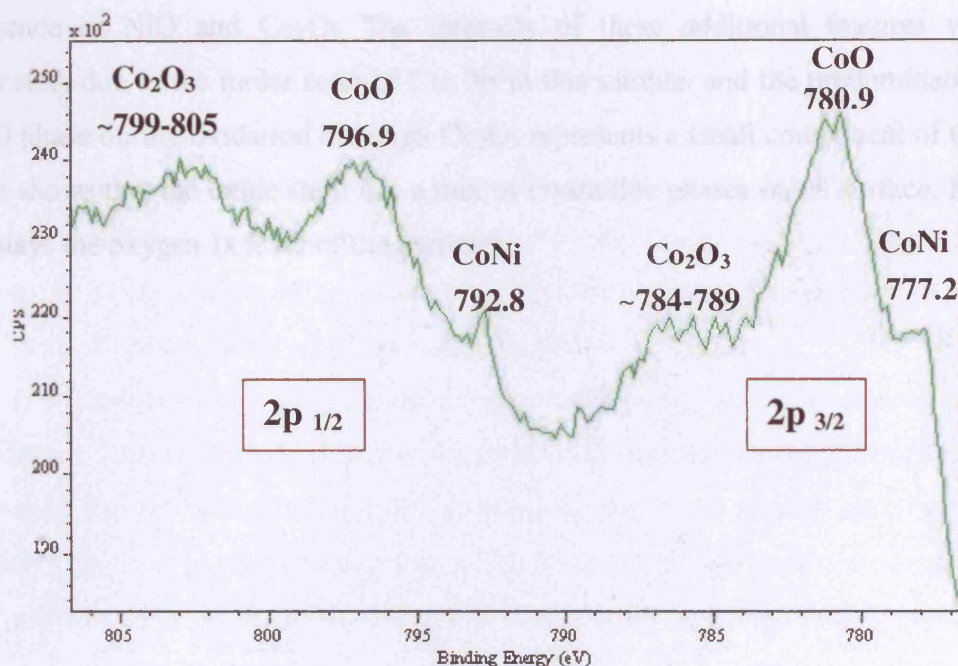
The peak at 780.9 eV is due to cobalt (2+) bound to oxygen (CoO).[56] Whilst the peaks between 784-789 eV were more difficult to characterise, due to their broad range. These particular values were closest to those cited in the literature, for the 2p 3/2 level of cobalt (3+) bound to oxygen (Co_2O_3).[53] This indicated the oxidation processes occurring at the shell was not uniform. The peak due to Co_2O_3 decreases in intensity and disappears after the 90 second etch. The corresponding 2p 1/2 level peaks are present on the left-hand side of Figure 29. Therefore, the peak at 792.8 eV is caused by cobalt (2p ½) alloyed to nickel (CoNi) and the peak at 796.9 eV is due to the cobalt (2p ½) bound

to oxygen (CoO). The peak range between 799 -805 eV is the 2p 1/2 level of Co_2O_3.[53, 55, 56]

The bimetallic nature of these particles is confirmed by the results obtained for the Ni 2p levels. Before etching, there are two peaks at each energy level (2p 3/2 and 2p 1/2), or a doublet of doublets, which both correlate with literature values for nickel bound to cobalt (852.0 and 870.0 eV) and nickel (2+) bound to oxygen (856.1 and 872.0 eV) respectively.[55, 57] As the sample is etched further, the peak for NiO significantly reduces in intensity, whilst the peak due to CoNi increases. This again gives strong evidence for the structure of the particle as being formed of a metallic alloy core with an oxide shell uniformly coating the particle.

The Oxygen 1s level of the particles at the surface shows a large concentration of CoO, with some shoulder features on the side of the main peak, that indicate the presence of NiO and Co_2O_3. The intensity of these additional features would be expected, due to the molar ratio of Co: Ni in this sample, and the predominance of the CoO phase during oxidation although Co_2O_3 represents a small component of this shell. This shows that the oxide shell has a mix of crystalline phases on its surface. Figure 30 displays the oxygen 1s level of the particles.

Figure 30.   Oxygen 1s level, of $Co_{80}Ni_{20}$ particles, after surface etch.

CoO
531.6
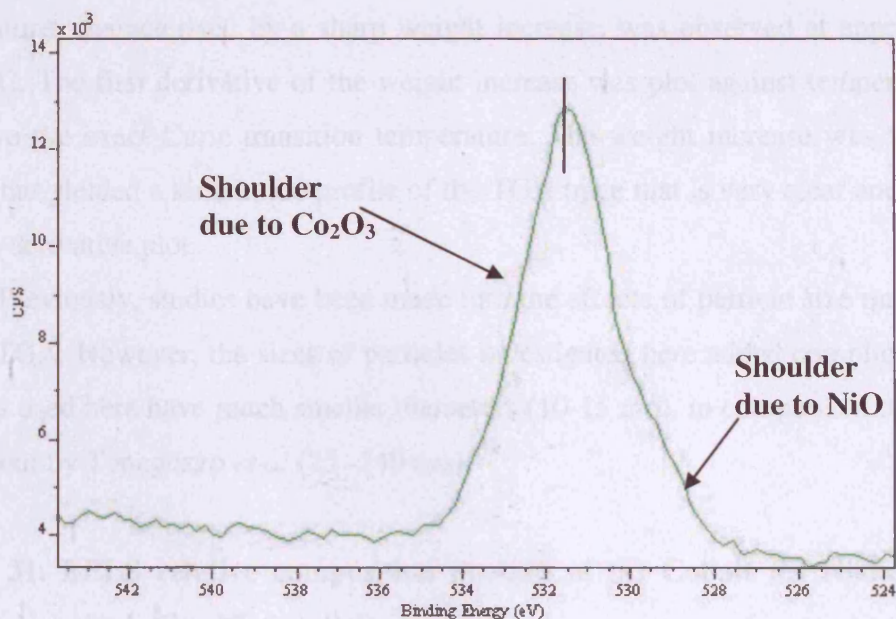
The quantitative measure of atomic concentration, showed oxygen levels depleted with etching. The amount of cobalt and nickel, conversely increased. The ratio between cobalt and nickel was consistent throughout the etching cycles. The relative amount of nickel to cobalt was slightly elevated, as the metallic core of the particle was penetrated. This was possibly due to the nucleation of nickel occurring before slightly that of cobalt in the synthesis of the $Co_{80}Ni_{20}$ particles.

In comparison to the XPS data of the cobalt particles described in section 2.7.2, the doping 20% nickel into these particles seems to have shifted the peaks slightly. This indicates the probability of a solid solution having been formed and therefore the particles are well mixed with each other. XRD measurements were also carried out but the peaks from the diffraction pattern could not be distinguished from the background signal from the detector and the substrate. This was due to the weak signal and broadness of the peaks in the diffraction pattern.

TGA in a magnetic field was carried out to confirm the presence of surfactant and determine the Curie transition (θ_c) temperature of the alloy sample. The sample was heated in an alumina crucible over the temperature range of 0 °C- 1400 °C. The boiling temperatures of oleic acid and oleylamine would lead to the expectation that all organic surfactant would be volatilised by 360 °C. The mass loss at approximately 100°C was due to the removal of adsorbed water. Any mass loss between 100-360 °C was due to the decomposition of the surfactant. This resulted in a 17.4 % mass loss, which correlates nicely with the results from elemental combustion analysis. A Curie transition

temperature, characterised by a sharp weight increase, was observed at approximately 995.3 °C. The first derivative of the weight increase was plot against temperature, and this gave the exact Curie transition temperature. The weight increase was very small (<1%), but yielded a kink in the profile of the TGA trace that is very clear and a peak in the first derivative plot.

Previously, studies have been made into the effects of particle size on mass loss during TGA. However, the sizes of particles investigated here added complication. The particles used here have much smaller diameters (10-15 nm), in comparison to the work carried out by Toneguzzo *et al* (25 -240 nm). [58]

Figure 31. EELS relative composition profiles of (a) Cobalt (b) Nickel and (c) Oxygen in a single $Co_{80}Ni_{20}$ particle.

(a) Cobalt

(b) Nickel

(c) Oxygen
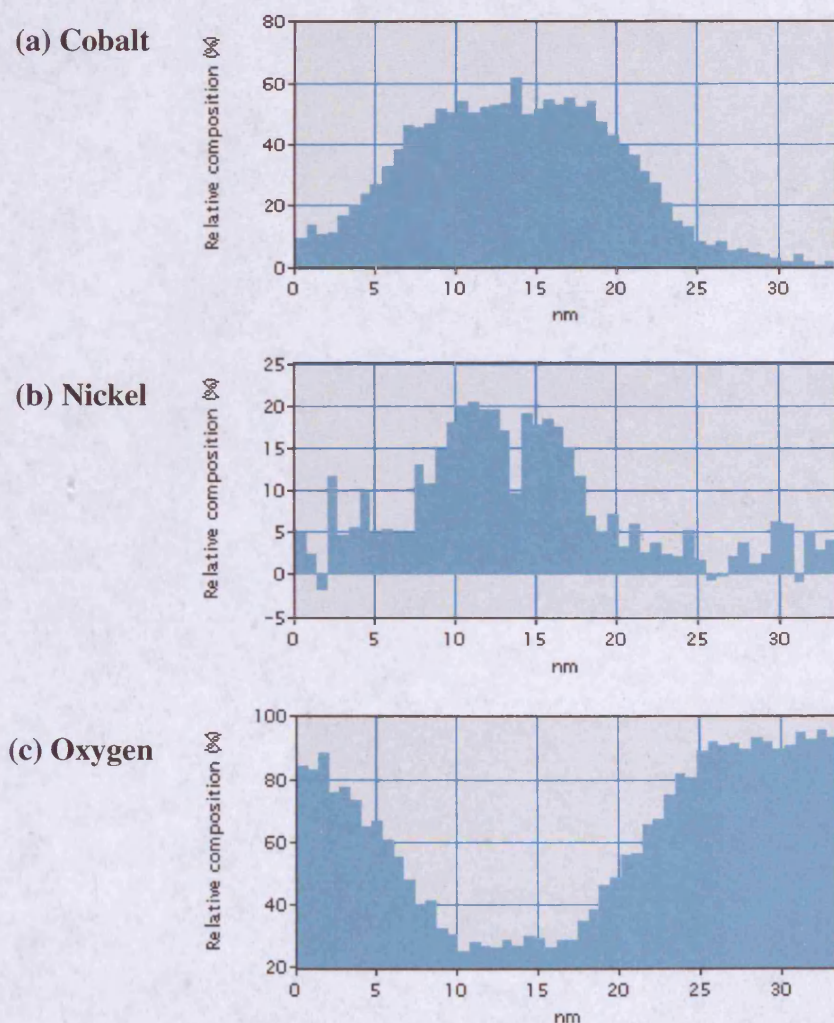
Energy electron-loss spectroscopy (EELS) analysis was carried out on the $Co_{80}Ni_{20}$ particles to verify the nature of alloying that had occurred and also to confirm a core-shell structure had been formed. Further detail about this technique is given in Chapter 5. The instrument measured the relative compositions of each element simultaneously at 0.2 nm intervals across the diameter of a particle. A single line profile, across an individual particle was analysed to ascertain the relative compositions of the elements, as well as their distribution throughout a particle. The relative compositions of the three main elemental components (Co, Ni and O) was mapped and showed that the particles in this sample had nickel rich cores, and a mix of cobalt and nickel in the proposed location of the oxide shells. The profiles are displayed in Figure 31. The relative ratios were approximately proportional to the precursor molar ratios, employed at the start of a reaction. However, there were slight variations across the particle for the core and shell. The oxygen levels spiked towards the outer edges of the particle diameter indicating oxide shell formation. The oxygen levels shown in Figure 31 (c) display a huge trough, with the majority of oxygen located on the outer rims of the particle. There is some oxygen detected when the beam passes through the centre of a particle. Depending on where the electron beam transmits through the core-shell particle, different counts are observed for each of the elements (Figure 31). If the beam passes through the central region of the particle, contributions from the oxide of the top and bottom surfaces of the particle are observed. The beam therefore, passes through oxide as it enters and leaves the particle. At the edge of a core-shell particle, as the beam transmits through the shell, oxygen counts would be expected to be quite large as it would pass through more oxygen at that point. This is proven by the spikes, at either edge of the particle, shown in Figure 31 (c).   The core-shell structure of the particles is very well supported by this data.

The relative proportions of cobalt to nickel are indicative of an approximate $Co_{80}Ni_{20}$ composition. However if oxygen is excluded from calculations and a relative ratio between cobalt and nickel is measured, the ratio between both elements is approximately 7.5:2.5 which indicates a nickel-rich core, perhaps due to the nickel nucleating first. The levels of cobalt are consistently slightly lower in comparison to nickel, throughout the sample.

In summary, these results have shown that $Co_{80}Ni_{20}$ alloy core-shell nanoparticles have been successfully synthesised. The particles are core-shell in structure with an oxide layer coating, composed of CoO, NiO and possibly some Co_2O_3

crystallites, enveloping the crystalline $Co_{80}Ni_{20}$ metallic core. The alloying in the particles has been proven by EELS analysis, XPS and magnetic TGA, which all confirmed the formation of a solid solution.

The solid solution is proven in the EELS data shown in Figure 31. The technique measured the composition across the particle at 0.2 nm intervals and therefore gives a definitive picture of the intrinsic particle composition. XPS of the $Co_{80}Ni_{20}$ particles showed a solid solution had formed, as when compared to the XPS results for the cobalt particles (section 2.7.2.3), the peaks had shifted slightly and corresponded to the Co 2p 3/2 and ½ levels of cobalt bound to nickel instead of elemental cobalt. TGA confirmed a solid solution had been formed as one Curie transition temperature was obtained. If individual nickel and cobalt particles had been formed, then two Curie transition temperatures for each of the elements would have been observed at their respective transition points. A comparison was also made with theoretical work carried out by P. K. Gallagher et al [54] They examined magnetic transition temperatures for cobalt, nickel and three Co_xNi_{1-x} alloys using a similar instrument set-up, to the one used in this investigation. Although a comparative measurement was not made for the exact composition investigated in this section, the curve in the figure below shows that if the point at which the composition has 20% nickel is extrapolated to the curve, an approximate expected Curie transition for this alloy may be determined.

Figure 32. Curie temperature as a function of composition in the Co-Ni system in a study by Gallagher et al. [54]
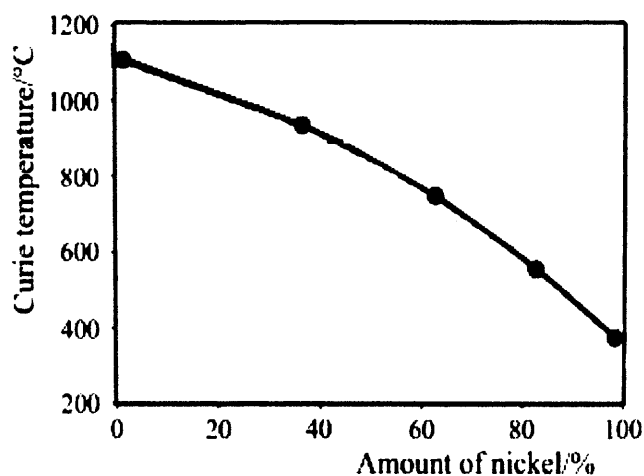
The value determined from the graph above, by extrapolating the corresponding point for a 20 % nickel alloy from the trend line, is approximately 1010 °C. There is a difference of about 15 °C, in comparison the literature values described by Gallagher *et al*.[54] This is due to the calibration of the instrument at high temperatures. The accuracy of the curve above approximately 1100 °C cannot be guaranteed, as there are no calibration standards that can be melted at such a high temperature, with this particular instrument. The value obtained for the $Co_{80}Ni_{20}$ sample, lies within the errors determined for the calibration curve of the instrument. It is also important to consider that the study carried out by Gallagher *et al*,[54] used sheet form alloys and not powders, that have been used in this study. The measurement conditions of that particular study were mimicked for the purpose of these measurements. Differences in the set-up, as well as those between the samples measured can cause variations in the Curie temperature obtained.

The particles that were formed were relatively monodisperse and of a good size. Multi-grains were evident in the structure of the particles due to polycrystallinity and the particles were also non-spherical in shape. However, due to their size and the choice of surfactant stabiliser, the particles remained stable to oxidation for several months and responded well to a magnet at room temperature. The results from magnetic measurements, of particles made with a $Co_{80}Ni_{20}$ composition, are shown in Chapter 3.

2.7.4 $Co_{60}Ni_{40}$ nanoparticles

2.7.4.1 Introduction

The synthesis of a compositional series of Co_xNi_{1-x} alloy nanoparticles was continued, with the fabrication of $Co_{60}Ni_{40}$ particles. The results obtained are described in the following sections.

2.7.4.2 Synthesis of $Co_{60}Ni_{40}$ nanoparticles

Particles of expected composition, $Co_{60}Ni_{40}$, were synthesised using methods described in detail in the experimental section. The cobalt, nickel and platinum salts were mixed with OA/OY surfactant in dioctyl ether. These reactants were magnetically stirred and heated until particle formation occurred. The synthesis of particles with this composition was repeated once, as with all other samples where compositions have

been varied. The particle formation profile followed a similar path to other reactions, (Section 2.7.2 and 2.7.3).

2.7.4.3 Results

TEM analysis showed that the $Co_{60}Ni_{40}$ particles had a slight bimodality in their distribution. Figure 33 shows the size distribution for the $Co_{60}Ni_{40}$ particles and the curve if the overall distribution was fit to a lognormal curve, which was entirely feasible if the general shape of the distribution was considered. The larger particles had the greater frequency count overall. Particle separation was also good in the sample, and in cases where agglomeration did occur, it was due to the presence of excess surfactant stabiliser. However, in order to make representative assumptions of the particles in terms of the magnetic properties, calculations were made on the basis of a bimodal distribution with two sets of particles of different sizes representing a bimodal nucleation event. The mean particle size for the larger particles was fit to a Gaussian distribution and was 10.8 +/-1.9 nm which represents a standard deviation of 17.5%. The distribution of the smaller particles was also fit to a Gaussian curve and was 6.4 +/- 0.9 nm, giving a standard deviation of 14.1 % which may also be classified as narrow. The particles are visibly much more spherical in shape, with less faceting being apparent due to the lack of contrast or line features in some cases, across a particle. The repeat synthesis showed a similar size and distribution for the particles. The presence of excess surfactant contributed to the lack of self assembly and has caused localised agglomeration.

Figure 33. Overall size distribution of the $Co_{60}Ni_{40}$ nanoparticles shows a lognormal distribution, although the calculations of mean particle size were made using the two peaks which represented bimodal nucleation events.
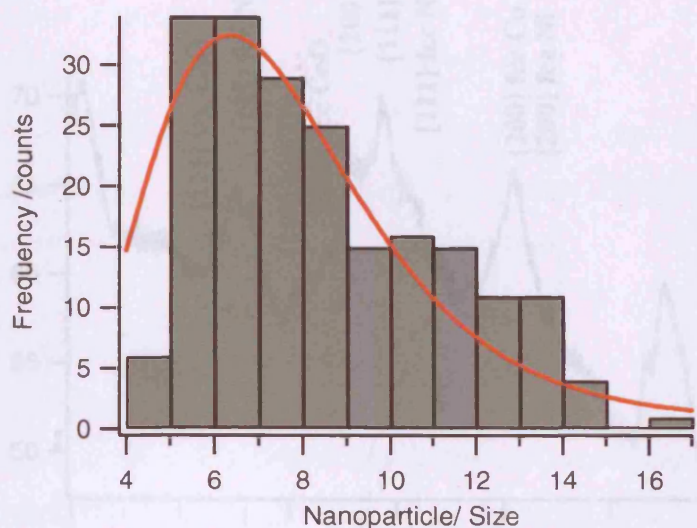
Elemental analysis of the particles showed that 14.2 mass% was due to surfactant stabiliser coating the particles, after the washing and cleaning procedures had taken place. EDX analysis showed that the cobalt to nickel ratio was determined as approximately 3:2, whilst oxygen was 36.4 atom%. If the results for cobalt and nickel are normalised to 1, and a relative percentage taken between these two elements, then it is clear that the particles appear to be slightly nickel rich. This was consistent throughout all the samples. XPS studies were not performed on this particular sample due to information gained from analysing other alloys in this series.

XRD studies were carried on the $Co_{60}Ni_{40}$ particles and the diffraction pattern that was obtained is displayed in Figure 34. The reflections for this sample are much stronger and therefore clearer, in comparison to those for $Co_{80}Ni_{20}$ particles. The structure on the peaks was indicative of the presence of a number of different phases, with some reflections being masked by others. The peaks positions also corresponded well to those reported by previous authors, and the traces that have been captured in this investigation.[13, 22] The fcc phases of Co, Ni, CoO and NiO were apparent. The peaks at approximately 31° and 57° are due to the substrate.

Figure 34. XRD pattern of 10.8 nm $Co_{60}Ni_{40}$ particles made with Pt seeds and coated in an OA/OY surfactant mixture.
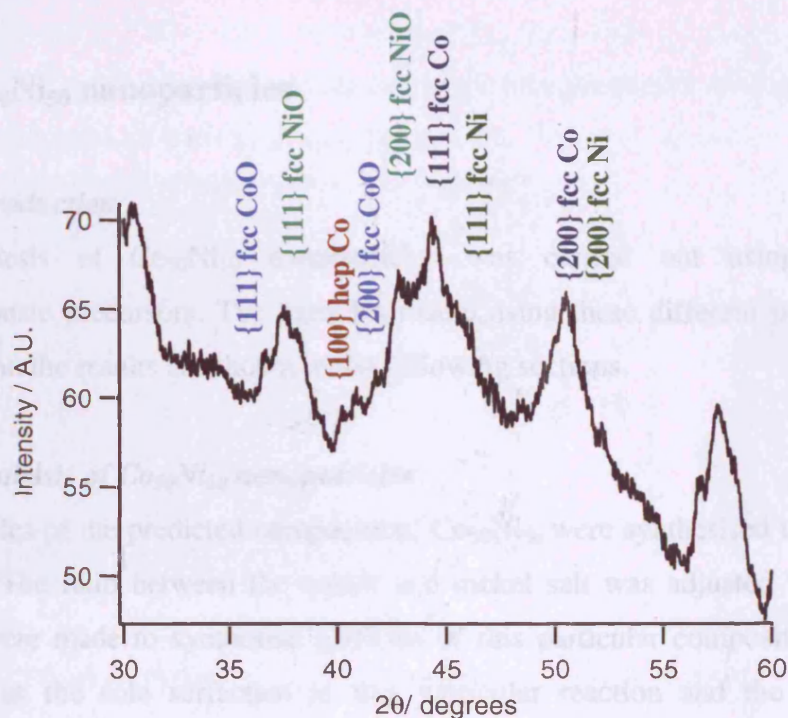
The fcc Ni and Co peaks appeared to have shifted peaks appeared to have slightly shifted from the expected positions shown in Appendix A. This indicates a solid solution rather than individual nickel and cobalt particles having been formed. Therefore, the fact that the particles are alloys is proven.

TGA of the sample in an applied field showed a mass change due to surfactant of 13.7 mass%. This correlated well with the value determined by elemental analysis. The first derivative of the weight increase was plotted and revealed that there was a magnetic transition at 828.8 °C. This value followed the curve of best fit, for Curie transition temperatures of Co_xNi_{1-x} alloys. It was not possible to carry out EELS analysis on this sample due to time constraints.

The particles that were formed with this composition were large, and correlated well in size to the mean diameter of the $Co_{80}Ni_{20}$ particles described in section 2.7.3. The magnetic transition temperature found by TGA indicated that a solid solution had been formed as two separate Curie transitions were not observed and therefore the particles appeared to exist as a soft "Co_xNi_{1-x}" core with an outer oxide layer. The particles were crystalline, and responded exceptionally well to a magnet at room

temperature. This magnetic effect was observed a few months later, therefore, the particles had not fully oxidised.

2.7.5 $Co_{50}Ni_{50}$ nanoparticles

2.7.5.1 Introduction

The synthesis of $Co_{50}Ni_{50}$ nanoparticles was carried out using acetate and acetylacetonate precursors. The particles made, using these different precursors, were analysed and the results are shown in the following sections.

2.7.5.2 Synthesis of $Co_{50}Ni_{50}$ nanoparticles

Nanoparticles of the predicted composition, $Co_{50}Ni_{50}$ were synthesised using an acetate precursor. The ratio between the cobalt and nickel salt was adjusted to 1:1. Various attempts were made to synthesise particles of this particular composition. Oleic acid was used as the sole surfactant in this particular reaction and the particles were nucleated using platinum seeds.

For the synthesis of $Co_{50}Ni_{50}$ particles using an acetylacetonate precursor, the cobalt, nickel and platinum salts were mixed with the reducing agent, OA/OY surfactant and solvent. The mixture was magnetically stirred and heated until particle formation occurred.

2.7.5.3 Results

The particles shown Figure 35 are those made using the acetate precursor. The particle's size distribution was fit to a Lorentzian function and the mean particle size was 15.6 +/- 2.7 nm, yielding a standard deviation of 17.3 %. The particles appear to be multi-grain, indicated by the contrast and lines across the particles. There is also shape variation, with some triangular and rhomboid shaped particles dispersed throughout the sample grid. The size of the larger particles however, was an improvement in terms of what had been observed previously. Smaller particles were observed (ca~3 nm), but overall the occurrence of the larger particles dominated. The particles were deposited onto the TEM grid using hexane and had begun to order in a hexagonally close-packed pattern. The narrow size distribution has aided the packing of these particles, although the

anomalies in shape of the particles have led to imperfections in array formation due to defects.

Figure 35(a) $Co_{50}Ni_{50}$ particles made using acetate precursor with platinum seeds (b) size distribution of the $Co_{50}Ni_{50}$ particles.
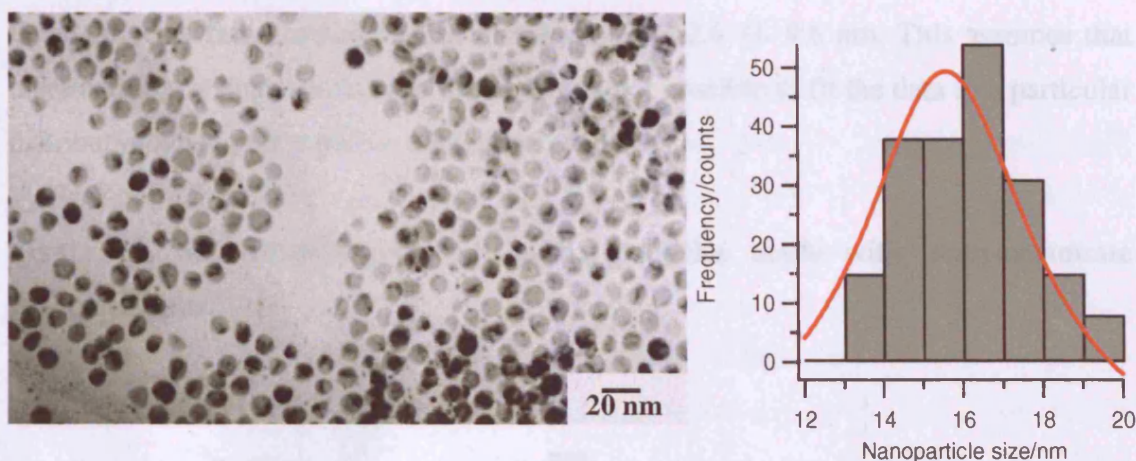
Elemental analysis confirmed that 18.32 mass% of the sample was due to the surfactant, oleic acid. This is consistent with surfactant mass loss displayed by TGA. Whilst EDX analysis showed that the particles were slightly nickel rich, but primarily maintained the approximate 1:1 atomic ratio between cobalt (31.1 atom%) and nickel (33.7 atom%), in terms of atomic ratio percentage. Oxygen content was found to be 35.2 atom%. The amount of oxygen present is consistent with oxygen levels in other alloy samples, made in the same way.

XRD of this sample showed that the sample was crystalline. However, the small size of the particles meant the peaks were broad. The peak positions between 30 and 60° on the 2θ scale matched those seen by Luna *et al*,[2] in similar particles of approximately 10 nm mean diameter. Scherrer analysis to determine particle crystallite size, gave a mean particle diameter of 12.5 nm, which is comparable with the value determined by TEM analysis.

TGA showed the decomposition of the organic material from the surface of the particles, however, a magnetic transition was absent from the profile of the spectrum. These particles, did not respond to a magnet as well, and this is discussed further in section 3.5.4 of this thesis.

An alternative approach to synthesising $Co_{50}Ni_{50}$ particles was attempted using acetylacetonate salts. This is the same method that has been used to synthesise the other alloy particles described in sections 2.7.2-2.7.4. The sample made using the

acetylacetonate salts was also analysed by TEM. Images showed that particles had more shape variations in comparison to the sample made with acetate salts. The size distribution curve in Figure 36 shows that multiple nucleation events have occurred and the particles mean diameter is therefore difficult to determine. The distribution from the mean is great, due to the breadth in size of particles. The mean diameter for this sample, if the curve is fitted to a Gaussian distribution is 12.6 +/- 9.6 nm. This assumes that there was just a single nucleation event. It was not possible to fit the data to a particular distribution due to the multiple nucleation events.

Figure 36. Size distribution of $Co_{50}Ni_{50}$ particles made with acetylacetonate precursor salts.
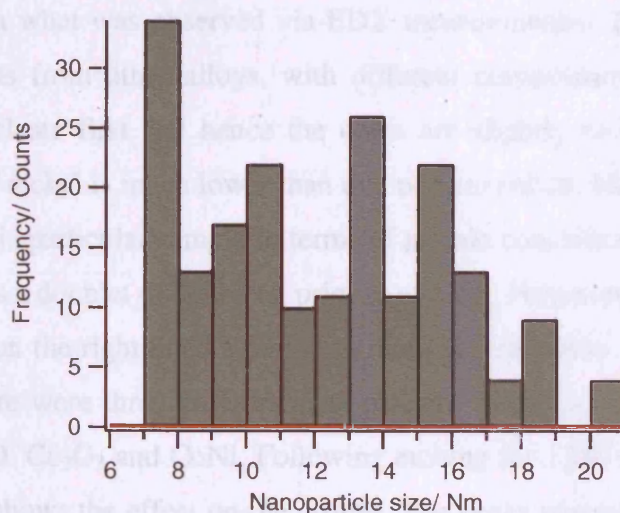
The shape of the distribution could also be described as being multimodal, and therefore the mean diameter for each of these modes should be calculated from the numerous peaks. However, the general distribution of the curve overall will be used as nothing meaningful can be gathered from splitting the data into several plots to obtain accurate means for each of the nucleation events that have occurred.

Elemental analysis of these particles showed that 10.7 mass% was due to surfactant stabiliser. This is a quite low compared to other samples that have had EA carried out. This could possibly explain the poor magnetic properties of the particles, which are discussed in Chapter 3. Due to poor coverage over the nanoparticle surface, it is possible that these particles have oxidised, even though their size is large compared other oxidised samples in this investigation.

EDX studies determined that 25.4 atom% was due to cobalt in the sample, whilst 30.8 atom% was due to nickel. The amount of oxygen present was determined to be

43.8 atom% of the sample. The sample was therefore, slightly nickel rich and this is consistent with what has been seen elsewhere with the other alloy particles discussed in this chapter.

XPS results differ slightly to those discussed earlier for $Co_{80}Ni_{20}$ in section 2.7.3, when the relative atomic percentages of each element were measured during the etching process. The quantitative elemental values for each of the main components are different, due to change in relative ratio between Co and Ni. The surface layer of the particles, displayed a lower level of nickel than cobalt, however, as etching proceeded the nickel content superseded that of cobalt. After 90 seconds of etching, the levels of cobalt: nickel, were approximately equal. The core of the particle, after 1330 seconds of etching, showed cobalt content of 23.2 atom% versus 28.6 atom% for nickel. This is consistent with what was observed via EDX measurements. These results corroborate with the results from other alloys, with different compositions in this series. Nickel appears to nucleate first and hence the cores are slightly nickel-rich. The nucleation temperature of nickel is much lower than that of pure cobalt. However, the oxide phases dominate in this particular sample in terms of atomic concentration. The plot in Figure 37 (a), displays a doublet of doublets, prior to etching. However, there was an indication of a shoulder on the right-hand side of the main central peaks, of each of the doublets. Therefore, there were three environments present. These are consistent with literature values for CoO, Co_2O_3 and CoNi. Following etching for 1330 seconds, the spectrum in Figure 37 (b) shows the effect on the profile. The peaks corresponding to the 2p $_{3/2}$ and 2p $_{1/2}$ levels of CoO decrease significantly in intensity. Whilst the equivalent peaks for Co_2O_3 have disappeared. The peak indicating that cobalt and nickel have alloyed becomes dominant in the spectrum. This proves that oxygen content decreases as the particles are infiltrated by etching and the core is predominantly composed of a Co_xNi_{1-x} alloy, with some CoO inclusions.

Figure 37. $Co_{50}Ni_{50}$ particles made with acetylacetonate precursor, OA/OY surfactant mixture and platinum seeds in dioctyl ether (a) Co 2p level at 0 seconds of etching (b) Co 2p level at 1330 seconds of etching.
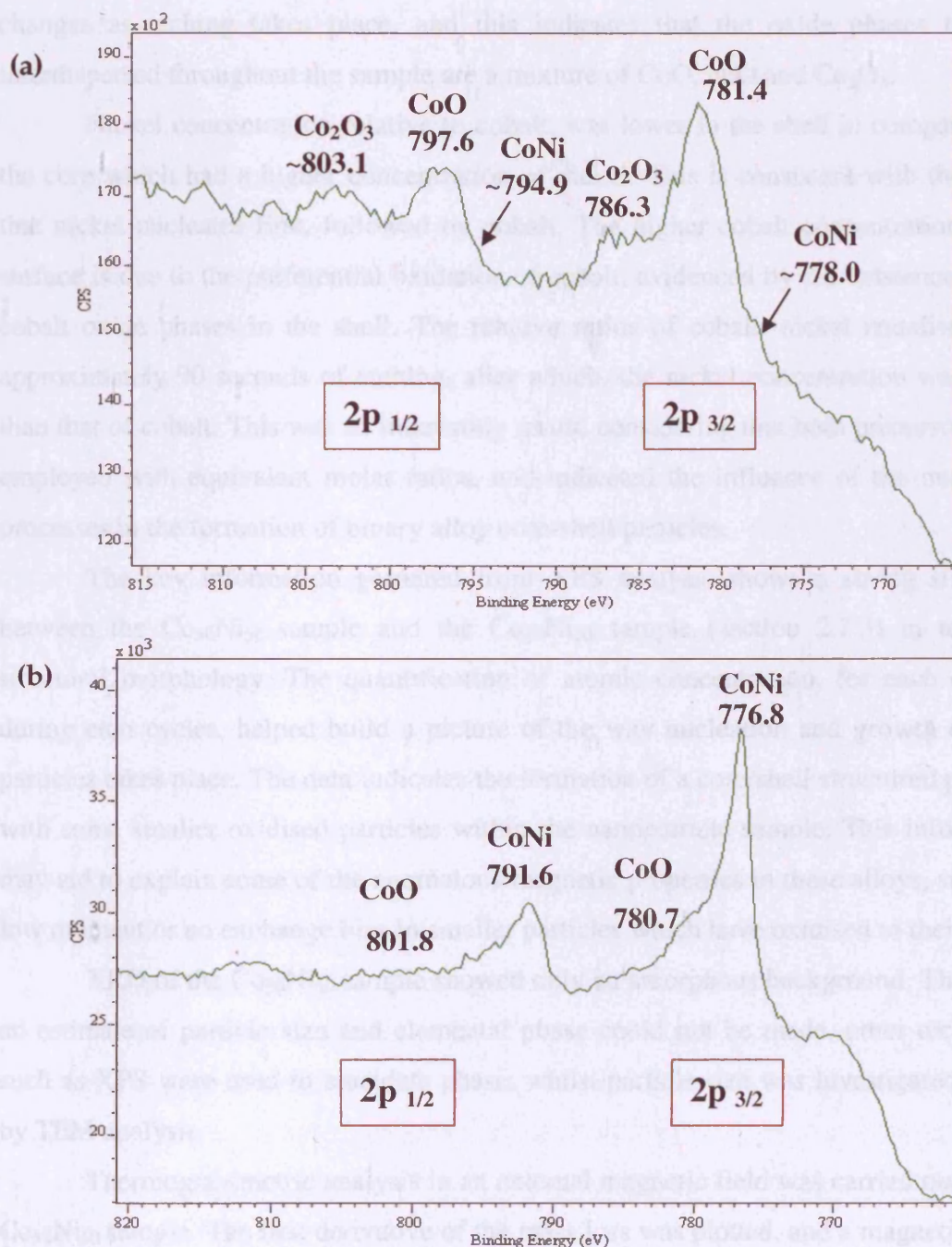
Quantitative analysis of the sample by XPS, showed that oxygen concentration decreased from 37.7 atom% to 14.9 atom% during etching. This shows that there are slight inclusions of oxygen in the core. The value for surface oxygen, correlates approximately with that determined by EDX analysis. The oxygen peak at the surface showed a predominant peak at 531.5 eV, consistent with a CoO 1s level peak. The peak

displayed two shoulders on either side of the peak's incline profile. These were due to NiO at approximately 529 eV and Co_2O_3 at around 534 eV. The oxygen atomic concentration significantly decreases during etching. The shape of the peak due to CoO changes as etching takes place, and this indicates that the oxide phases that are interdispersed throughout the sample are a mixture of CoO, NiO and Co_2O_3.

Nickel concentration relative to cobalt, was lower in the shell in comparison to the core which had a higher concentration of nickel. This is consistent with the belief that nickel nucleates first, followed by cobalt. The higher cobalt concentration at the surface is due to the preferential oxidation of cobalt, evidenced by the existence of two cobalt oxide phases in the shell. The relative ratios of cobalt: nickel equalised after approximately 90 seconds of etching, after which, the nickel concentration was larger than that of cobalt. This was an interesting result, considering that both precursors were employed with equivalent molar ratios, and indicated the influence of the nucleation processes in the formation of binary alloy core-shell particles.

The key information garnered from XPS analysis shows a strong similarity between the $Co_{50}Ni_{50}$ sample and the $Co_{80}Ni_{20}$ sample (section 2.7.3) in terms of structural morphology. The quantification of atomic concentration, for each element during etch cycles, helped build a picture of the way nucleation and growth of these particles takes place. The data indicates the formation of a core/shell structured particles with some smaller oxidised particles within the nanoparticle sample. This information may aid to explain some of the anomalous magnetic properties in these alloys, such as a low moment or no exchange bias in smaller particles which have oxidised to their cores.

XRD of the $Co_{50}Ni_{50}$ sample showed only an amorphous background. Therefore, an estimate of particle size and elemental phase could not be made, other techniques such as XPS were used to elucidate phase, whilst particle size was investigated earlier by TEM analysis.

Thermogravimetric analysis in an external magnetic field was carried out on the $Co_{50}Ni_{50}$ sample. The first derivative of the mass loss was plotted, and a magnetic Curie transition (T_c) was determined as 786.1 °C. The value determined for this alloy is consistent with the study carried out by Gallagher et al, which was discussed earlier (see Figure 32). It is also within the error boundaries found by this investigation.

EELS analysis was also conducted on the $Co_{50}Ni_{50}$ sample, in order to clarify the expected core-shell structure of particles and monitor the pattern of oxidation across an individual particle.

The profiles of each element showed a distinct anomaly between the relative concentrations of cobalt and nickel. As was seen in the XPS quantitative results, the nickel concentration was lower than that of cobalt at the surface or shell. However, here the nickel concentration remains low throughout the sample. The amount of nickel atoms is skewed so there are more present on the left-hand side of the particle than the right. The average composition of the particle, as determined by EDX, shows that the ratio between cobalt and nickel remains as approximately 1:1, with the sample being slightly nickel rich. However, here the results show that in this particular particle, the amount of nickel is slightly lower than anticipated. If comparisons are made with other particles, which have been analysed on this grid, then a different conclusion could be drawn. This shows that there can be major differences in the composition between individual particles at an atomic level. The oxygen level displays peaks at either end of the particle, and a trough represents the metallic core of the particle. The fact that oxygen remains throughout the particle has been proven earlier by XPS (section 2.7.3). This technique may help to explain the problems with reproducibility experienced with particles of different compositions, in terms of their physical and functional properties.

Particle sizes are slightly different between samples made following an identical method. However, the reactions reported in this thesis have attained a certain level of reproducibility, which allows assumptions to be made. This means that the particles that have been formed, as repeats to an earlier synthesis, have maintained sizes within the distribution of the initial sample. Although the actual mean particle sizes are different due to the different nucleation processes.

In summary, the properties of $Co_{50}Ni_{50}$ particles, made with acetate and acetylacetonate salts has been discussed. The acetate salt method yielded well formed particles of a good shape and size, however, the particles had fully oxidised and did not respond well to an external magnetic field. Multi-grains were also evident in the particles made in this manner. The acetylacetonate salts method, which has been adopted for other alloys in this compositional series, displayed interesting results. Although the particles were smaller in mean diameter compared to the acetate salt sample, they responded well to a magnet and therefore had not oxidised. The various analytical techniques employed to characterise these particles, displayed strong evidence for the existence of core-shell morphology and crystallinity in these particles. XPS and EELS analysis, in particular showed that there was a high concentration of oxide at the surface of the particles, with a marked increase in Co_xNi_{1-x} alloy

concentration with etching into the particle. This was also observed in the $Co_{80}Ni_{20}$ sample discussed earlier. Magnetic TGA analysis proved that the particles were formed from a solid solution, however, EELS analysis showed that there are variations in composition across individual particles and this should also be considered. The information gained from analysis of this sample helped in the understanding of the Co_xNi_{1-x} system in general.

2.7.6 $Co_{40}Ni_{60}$ nanoparticles

2.7.6.1 Introduction

Particles of predicted composition, $Co_{40}Ni_{60}$ were synthesised via the polyol process. The method used to synthesise the particles was identical to that used to make other alloy particles in this compositional series.

2.7.6.2 Synthesis of $Co_{40}Ni_{60}$ nanoparticles

Cobalt and nickel precursor salts were used in a 2:3 ratio, respectively. These salts, along with a platinum salt (nucleating agent), 1,2-hexadecanediol (reducing agent) and the OA/OY surfactant mixture were stirred and heated to the reflux temperature of the solvent, dioctyl ether.

2.7.6.3 Results

TEM analysis of the particles showed that the particles were of a similar size to those synthesised in this compositional series. The mean particle diameter for the larger particles was determined to be 13.6 +/- 2.5 nm which is equivalent to a standard deviation of 18.4 %. These particles can be described as having a narrow size distribution. The bimodality of the overall size distribution of the particles in the $Co_{40}Ni_{60}$ sample cannot be neglected, therefore the size distribution of the smaller set of particles was also determined. The mean diameter was found to be 6.7 +/- 1.4 nm, which corresponds to a deviation of 19.4 %, therefore the distribution of these particles may also be described as narrow.

The nucleation of the Co_xNi_{1-x} particles has led to the bimodality that has been seen throughout this compositional series. The largest particles formed in this sample (13.6 nm) appeared to be large enough to support oxide shell growth. The smaller

particles had possibly oxidised to their cores. Sangregorio *et al* [59] have described the synthesis of Co_xNi_{1-x} particles, via a sol-gel technique, which were embedded within a silica matrix and were subsequently tested for their magnetic properties. The particle synthesised in this particular compositional series increased in size as cobalt content increased. Therefore, the blocking temperature for pure nickel particles (7 K) was much lower than that for the pure cobalt particles (70 K). [59] In comparison, the synthesis of particles using polyol methods in this study have shown that as nickel content increases, the general particle size has also increased.

Elemental analysis of the sample showed that the percentage mass due to surfactant was 13.8 mass%. This was correlated with the TGA data. EDX analysis of samples showed that the composition of the particles was nickel rich, as has been seen with some of the other alloys in this series. Cobalt was determined at 18.3 atom%, with the amount of nickel found to be 45.7 atom%. Therefore, the Co/Ni ratio was 1: 2.5, which corresponds to the composition that had slightly higher nickel levels, than had been predicted prior to synthesis. This has been attributed to the nickel nucleating first in the reaction process. Oxygen levels in the sample, at 36.0 atom%, were consistent with what has been seen in other alloys samples.

XRD analysis of the sample yielded an amorphous background. The trace that was obtained was a very weak pattern and could not be clearly distinguished against the background signal. This was due to the multi-grain structure of the particles, as the small particles within a whole particle were not large enough to be detected. Therefore, assignment of the crystallographic planes was not possible.

TGA analysis of the $Co_{40}Ni_{60}$ particles, in an applied magnetic field, revealed that approximately 13.2 mass% decrease could be assigned to the surfactant decomposition from the surface of the nanoparticle. This corroborated well with the mass loss determined via elemental analysis. The Curie transition of the particles was found to be 719.9 °C. The transition was characterised by a small peak, in the profile of the first derivative, from the weight loss measured by the instrument.

The results from studies carried out this sample, indicated that there were clear trends in terms of the particle nucleation becoming apparent. The elevated levels of nickel (+ 5-8 %) in the samples prove this. The size of the particles formed using this adapted polyol method seem to be pretty consistent, although the multi-grain structure in the particles, has led to problems in characterising them with XRD. The size distribution in the particles indicates that some more work could be done on

investigating the nucleation process in further details, so that monomodal distributions could be consistently achieved.

2.7.7 Co$_{20}$Ni$_{80}$ nanoparticles

2.7.7.1 Introduction

Particles of the composition Co$_{20}$Ni$_{80}$, have been synthesised before in works by Viau *et al*, [22] using the polyol method. However, the particles made by Viau and co-workers were larger. This section describes the controlled synthesis of Co$_{20}$Ni$_{80}$ nanoparticles using a synthetic process that has evolved, so that core-shell particles can be formed.

2.7.7.2 Synthesis of Co$_{20}$Ni$_{80}$ nanoparticles

Particles were prepared by polyol synthesis methods. Cobalt and nickel salts were used in a proportional molar ratio of 1:4 respectively. The metallic precursor salts, platinum acetylacetonate (nucleating agent), 1,2-hexadecanediol (reducing agent) and OA/OY surfactant mixture were all dissolved in dioctyl ether and heated under nitrogen and stirring until particle formation occurred. A more detailed description of the synthesis is given in section 5.5.6 of chapter 5.

2.7.7.3 Results

Initially, acetate salts were used as the starting material and resulted in large particles, as with the Co$_{50}$Ni$_{50}$ particles described in section 2.7.4. TEM analysis showed that the particles, made with acetate salts, appeared to attempt to self-assemble due to better uniformity in shape.

Figure 38 (a) Particles made using acetate salts, with no exchange bias interactions (b) size distribution of the particles shown in (a).
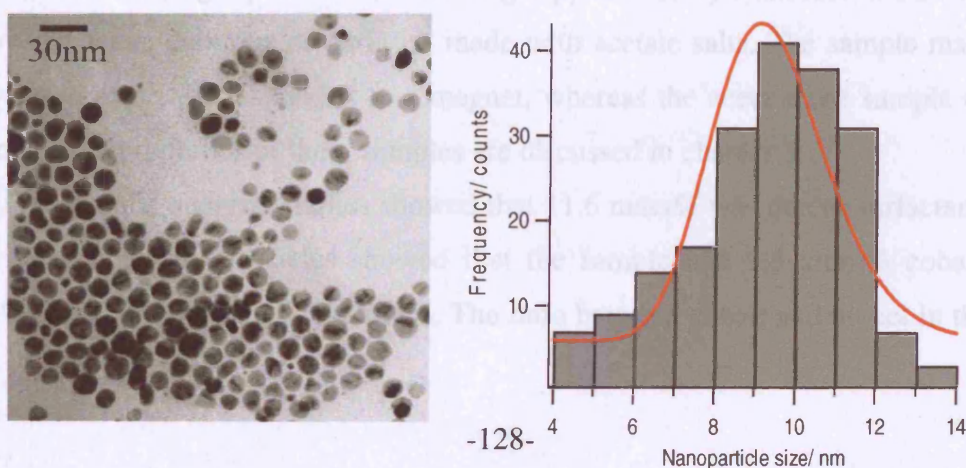
The $Co_{20}Ni_{80}$ particles are shown in Figure 38 (a) and indicated a mean particle diameter of 9.1 +/- 3.1 nm which translates to a standard deviation of 34 %. The particle sizes were fit to a lognormal curve and had a broad distribution. The particles clearly exhibit multi-grain structure, due to the contrast and clear lines across the particles. There are also more occurrences of spherical-like particles than the triangular and rhomboidal shapes, in comparison to what has been seen in particles made using acetylacetonate salts.

TEM analysis of the particles made using acetylacetonate salts, indicated a slight bimodal distribution, as shown in Figure 38 (b). Due to the bimodality, in order to accurately calculate the distribution of the particles, the dataset was split into two groups of smaller and larger particles. The calculated mean for the larger particles was 13.0 +/- 3.0 nm (standard deviation 23 %), whilst the average particle diameter for the smaller particles was 7.9 +/- 0.7 nm (standard deviation 8.9 %). The particle distribution displayed two peaks with a large tail at the higher end of the particle size scale, and hence was difficult to fit to a specific distribution. The two peaks for each set of particle, were fitted to Lorentzian distributions.

Figure 39. Size distribution of $Co_{20}Ni_{80}$ sample made with acetylacetonate salts.
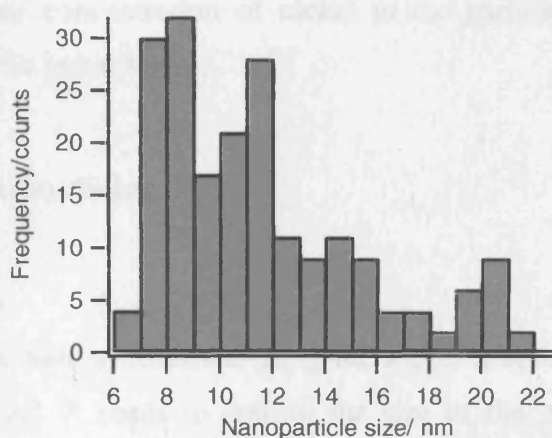
The mean for the larger particles is on average approximately 3 nm less in diameter than the overall mean diameter of particles made with acetate salts. The sample made with acetyalacetonate salts responded to a magnet, whereas the acetate salt sample did not. The magnetic properties of these samples are discussed in chapter 3.

Elemental analysis studies showed that 11.6 mass% was due to surfactant mass. EDX analysis of the particles showed that the sample had 9.5 atom% cobalt, 68.1 atom% nickel and oxygen 22.4 atom%. The ratio between cobalt and nickel in this case

is interesting as these results show that the nickel precursor has transferred better into the final particle. The atomic percentages of Co/Ni correlate with a 12% and 88% Co: Ni ratio. Therefore the particles in this case have clearly shown the dominance of nickel in the nucleation process. The oxygen value determined is lower than what has previously been observed with the other alloys. This could be due to the way in which nickel oxidises, as this will have the dominant oxide phase in the shell due to the higher molar ratio of nickel precursor to its analogous cobalt precursor.

The particles appeared be crystalline in the TEM microscope. It was also not possible to obtain TGA results for this particular sample, following several attempts. The particles however, did respond to a magnet and warranted magnetic property investigations due to their size. This is interesting, as it was the first particular composition, in the series to display non-magnetic behaviour. The results from the physical characterisation of the $Co_{20}Ni_{80}$ particles could contribute to a predicted lack of exchange anisotropy in the particles. The particle size displayed in this sample is quite large, however, there is evidence of multiple nucleation events during the synthesis, provided by the size distribution plot in Figure 39. A multi-grain structure is evident in the samples as nanocrystal grains have coalesced to form these particles. The properties of the nickel particles, discussed in the following section are interesting, as it will confirm if the higher concentration of nickel in the particles has an effect on their structure and magnetic properties.

2.7.8 Nickel nanoparticles

2.7.8.1 Introduction

Nickel nanoparticles were synthesised using the nickel acetylacetonate salt, an OA/OY surfactant mixture and Pt seeds to control the size of the particles. Nickel has been shown to bind well to oleylamine, and other amine based surfactants, in similar polyol reactions. [30, 31, 60, 61] Earlier investigations into a suitable surfactants showed that nickel salts formed complexes with hexadecylamine and oleylamine at low temperatures. However, upon reaching the reflux temperature the particles "crashed out" of solution and became aggregated. By using oleic acid with oleylamine, in this study, the stability of the nickel particles in terms of aggregation has been improved.

2.7.8.2 Synthesis of nickel nanoparticles

Nickel nanoparticles were synthesised by heating nickel acetylacetonate, platinum seeds, 1,2-hexadecanediol, OA/OY surfactant mixture in dioctyl ether. The solution was heated and magnetically stirred in reflux conditions until particle formation occurred. The resultant particles were isolated and stored for analysis using various characterisation techniques.

2.7.8.3 Results

TEM analysis showed a mean particle diameter of 16.0 nm +/- 5.6 nm, which is a standard deviation of 35 %. The distribution was fitted to a monomodal Lorentzian function to obtain mean particle size. The particles had a broad size distribution, and excess surfactant caused spherical superstructures of particles to form. The shape of the individual particles, as can be seen in Figure 40(a), was highly irregular with triangular and square shaped particles being formed. The particles were well separated apart from in areas where there is excess surfactant. A repeat of this reaction led to particles with mean diameters that were within the size distribution determined above.

Figure 40(a) Image of nickel nanoparticles made with platinum seeds and OA/OY surfactant coating (b) Size distribution of the nickel nanoparticles.
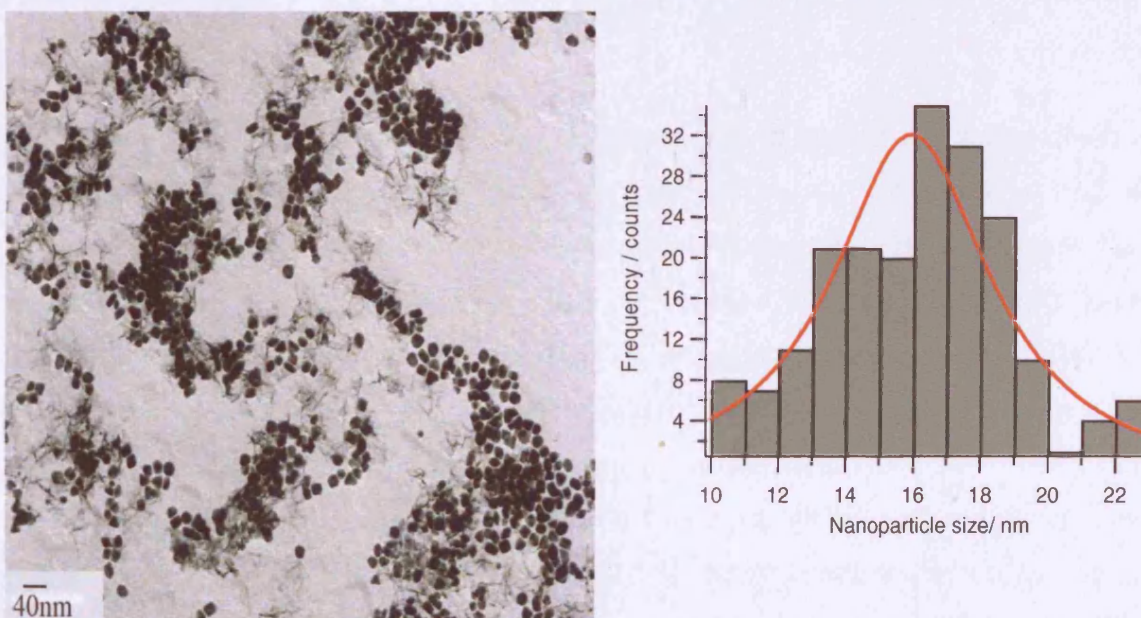
Elemental analysis of these particles showed that 10.3 mass% was due to the surfactant weight. This is less than what has been seen previously for particles in this

series. EDX showed that 76.3 atom% was due to nickel, whilst 23.7 atom% was due to oxygen. The oxygen is quite low in comparison to samples which have some cobalt in them. XRD showed only an amorphous background.

TGA analysis of the sample showed a Curie transition temperature of 348 °C. This was consistent with the intrinsic error within the particular instrument and is close to the Curie transition expressed by Gallagher et al, of 357.2 °C, for nickel.

Figure 41 displays the Curie transition of a nickel calibration standard and is characterised by a weight increase in the TGA profile. The plot shows the very small percentage change exhibited. This graph is indicative of the results obtained using the TGA with an applied magnetic field. The first derivative of each sample's TGA profile was measured and the Curie temperature obtained from that particular plot. For alloy samples measured over the large temperature range (0- 1400 °C), this effect was characterised by a small deviation in the profile of the TGA trace, and a peak in the first derivative plot. Figure 41 highlights the small weight increase that is observed. Therefore, over this temperature range, the Curie transition for the Co_xNi_{1-x} alloy particles was just as small.

Figure 41. TGA with an applied magnetic field of a nickel calibration standard shows a Curie transition, characterised by a small percentage weight increase (red trace). The blue trace shows the DSC measurement for the nickel calibration standard and yields the melting point.
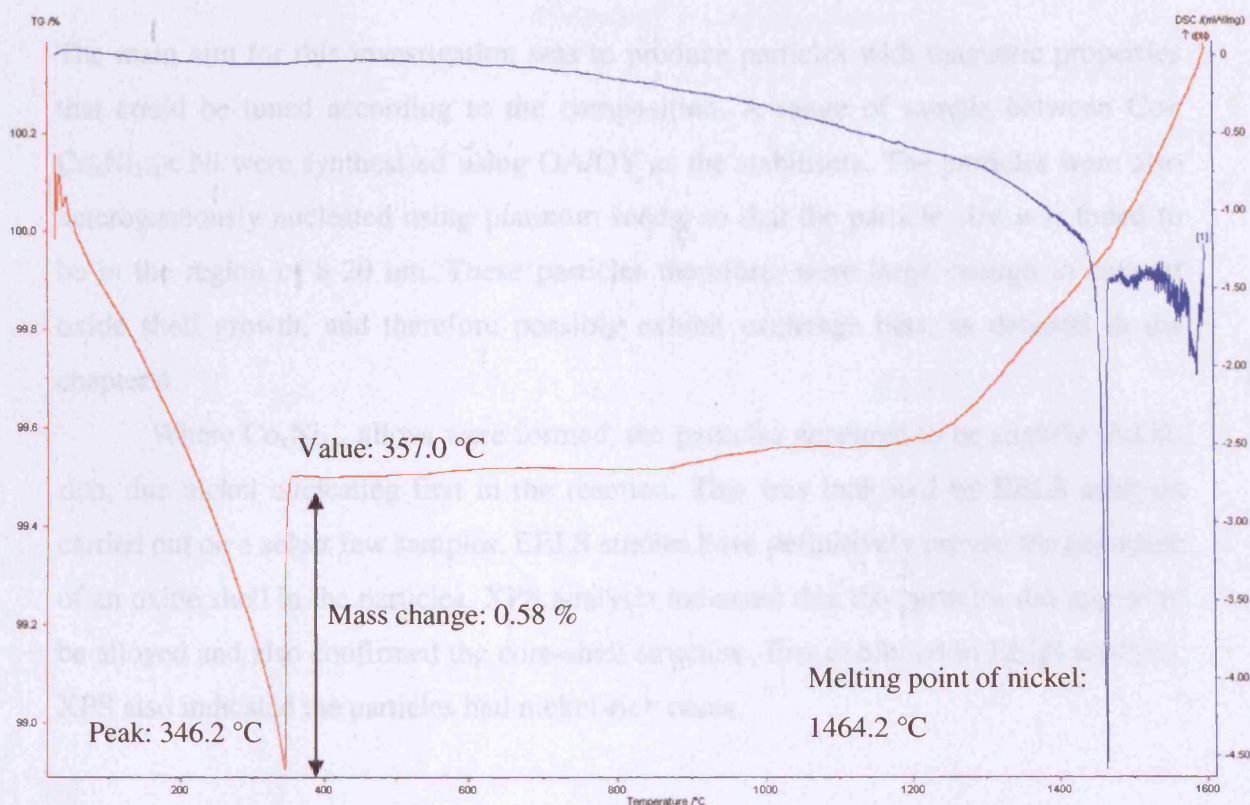
The nickel particles in this compositional series displayed interesting results. They did not seem to respond to a magnet, as with the $Co_{20}Ni_{80}$ particles described in 2.7.7. This begins to indicate that as nickel content is increased through the series, the magnetic effect of the particles at room temperature is lost. This could have implications on the exchange bias properties of the particles, which are discussed in Chapter 3. The size of the nickel particles was also, on average, larger than those with some cobalt doped into them. They also seem to have nucleated much more easily and this is indicated by the lower temperature at which the nickel particles form. The solution turned instantaneously black at 220 °C, whereas, the particles with some cobalt doped in have consistently shown higher formation temperatures of between 230-240°C, with the OA/OY combination of surfactant. The XPS results of other alloys within this compositional series have also indicated that the nucleation of nickel progresses much more easily than that of alloy particles. This has been evidenced by the

elevated levels of nickel in the core of the particles (following etching), which have shown that nickel tends to nucleate first.

2.7.9 Summary of samples made with variations in composition

The main aim for this investigation was to produce particles with magnetic properties that could be tuned according to the composition. A range of sample between Co< Co_xNi_{1-x}< Ni were synthesised using OA/OY as the stabilisers. The particles were also heterogeneously nucleated using platinum seeds, so that the particle size was tuned to be in the region of 8-20 nm. These particles therefore, were large enough to support oxide shell growth, and therefore possibly exhibit exchange bias, as detailed in the chapter 4.

Where Co_xNi_{1-x} alloys were formed, the particles appeared to be slightly nickel-rich, due nickel nucleating first in the reaction. This was indicated by EELS analysis carried out on a select few samples. EELS studies have definitively proven the existence of an oxide shell in the particles. XPS analysis indicated that the particles did appear to be alloyed and also confirmed the core-shell structure, first exhibited in EELS analysis. XPS also indicated the particles had nickel-rich cores.

Figure 42. Magnetic TGA study of particles with varied composition shows a close correlation between the curie transition found by Gallagher et al (blue) versus the results for particles with different compositions, measured in this study (pink).

TGA study of Co_xNi_{1-x} alloys
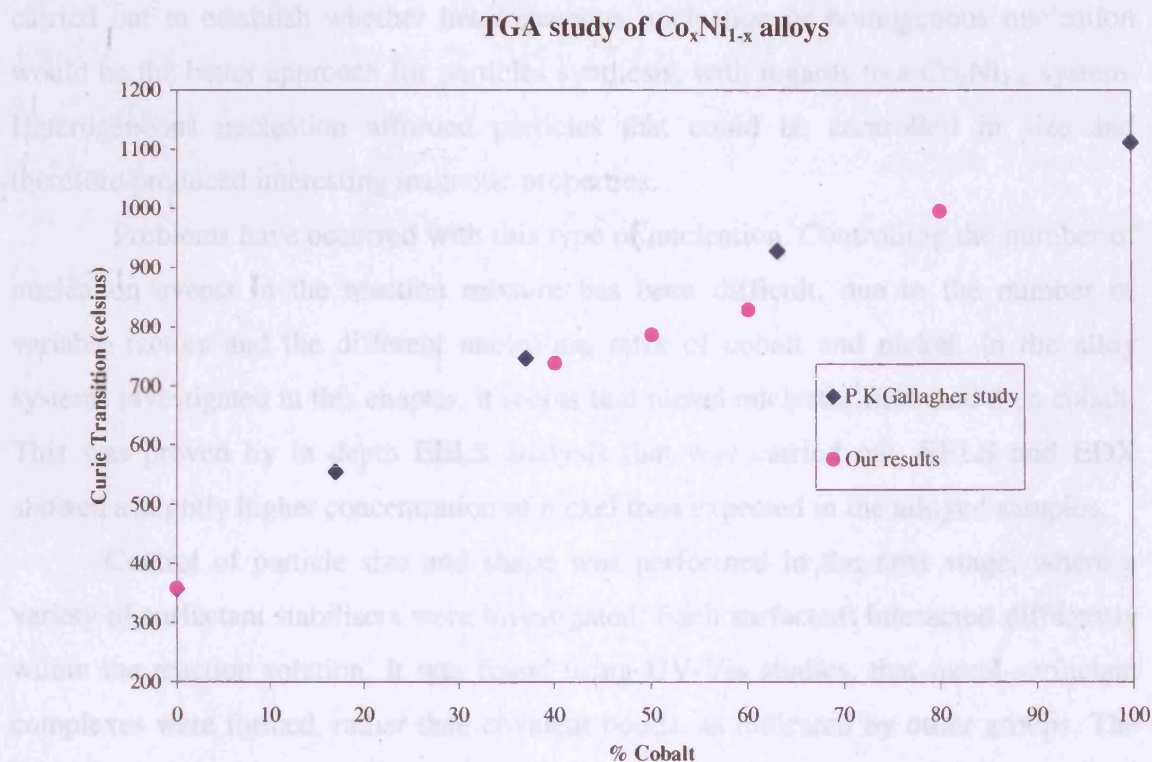
Thermogravimetric magnetic analysis was carried out on these samples, and this technique showed that the Curie temperature of the particles could be altered by varying the composition. This proved that the particles were a solid-solution, and had formed alloys. The technique showed that by increasing the nickel concentration, the Curie temperature of the materials decreased. The magnetic properties of the particles synthesised in this chapter are investigated in detail in chapter 3. The structural characterisation of particles in this chapter has provided a wealth of information, and given detailed evidence of specific properties, which could impact upon the magnetic properties observed in the particles.

2.8 Conclusions

Particles of various sizes and compositions have been synthesised by altering the reaction conditions and variables in this polyol-based synthesis. Initially, studies were carried out to establish whether heterogeneous nucleation or homogenous nucleation would be the better approach for particles synthesis, with regards to a Co_xNi_{1-x} system. Heterogeneous nucleation afforded particles that could be controlled in size and therefore produced interesting magnetic properties.

Problems have occurred with this type of nucleation. Controlling the number of nucleation events in the reaction mixture has been difficult, due to the number of variable factors and the different nucleation rates of cobalt and nickel. In the alloy systems investigated in this chapter, it seems that nickel nucleates first, and then cobalt. This was proven by in depth EELS analysis that was carried out. EELS and EDX showed a slightly higher concentration of nickel than expected in the alloyed samples.

Control of particle size and shape was performed in the next stage, where a variety of surfactant stabilisers were investigated. Each surfactant interacted differently within the reaction solution. It was found using UV-Vis studies, that metal-surfactant complexes were formed, rather than covalent bonds, as indicated by other groups. The overall best stabilising agent was proven to be a mixture of OA and OY. This was used in subsequent reactions for particle synthesised with a varied composition.

A solid solution was formed when Co_xNi_{1-x} particle synthesis was attempted. This was evidenced by results from XPS analysis and magnetic TGA. The growth of an oxide shell surrounding the metallic alloy core was proven by EELS analysis of a select few samples. The particles were exposed to air in a controlled manner, and therefore, oxide shell growth was permitted after the reaction had taken place. For the duration of the synthesis, the particles were held in an inert atmosphere, so that controlled shell growth would occur post-synthesis.

Various other synthetic techniques have been implemented to characterise the particles, however size-effects have led to the problems with characterising some of the particles via techniques such as XRD. Where it has been successful, particles have shown that they were predominantly composed from the fcc phase of cobalt and nickel, with corresponding CoO and NiO fcc crystallites, surrounding the metallic alloy core. There have been indications of other oxide phases, such as Co_2O_3 being formed, by

XRD and XPS. However, these have been dominated by other signals, and so have been difficult to definitively assign.

The polyol method of synthesis has been effectively used to synthesise a variety of particles with different sizes, shapes, nucleation methods and surfactant coatings. The synthetic process was optimised so that a compositional series of Co_xNi_{1-x} particles could be made and the magnetic functional properties could be investigated in further detail. Chapter 3 details the way in which the Co_xNi_{1-x} particles were characterised magnetically. The particles are examined to see if the exchange bias effect is apparent and how this relates to the nucleation and growth of the particles, which were described in Chapter 2.

2.9   References

1.   Larcher, D.; Patrice, R., Preparation of metallic powders and alloys in polyol media: A thermodynamic approach. *Journal of Solid State Chemistry* **2000**, 154, (2), 405-411.

2.   Luna, C.; Morales, M. D.; Serna, C. J.; Vazquez, M., Exchange anisotropy in Co80Ni20/oxide nanoparticles. *Nanotechnology* **2004**, 15, (4), S293-S297.

3.   Shevchenko, E.; Talapin, D.; Kornowski, A.; Wiekhorst, F.; Kotzler, J.; Haase, M.; Rogach, A.; Weller, H., Colloidal crystals of monodisperse FePt nanoparticles grown by a three-layer technique of controlled oversaturation. *Advanced Materials* **2002**, 14, (4), 287-290.

4.   Jeyadevan, B.; Hobo, A.; Urakawa, K.; Chinnasamy, C. N.; Shinoda, K.; Tohji, K., Towards direct synthesis of fct-FePt nanoparticles by chemical route. *Journal of Applied Physics* **2003**, 93, (10), 7574-7576.

5.   Jeyadevan, B.; Urakawa, K.; Hobo, A.; Chinnasamy, N.; Shinoda, K.; Tohji, K.; Djayaprawira, D. D. J.; Tsunoda, M.; Takahashi, M., Direct synthesis of fct-FePt nanoparticles by chemical route. *Japanese Journal of Applied Physics Part 2-Letters* **2003**, 42, (4A), L350-L352.

6.   Lu, M. H.; Song, T.; Zhou, T. J.; Wang, J. P.; Piramanayagam, S. N.; Ma, W. W.; Gong, H., FePt and Fe nanocomposite by annealing self-assembled FePt nanoparticles. *Journal of Applied Physics* **2004**, 95, (11), 6735-6737.

7.   Sun, S. H.; Murray, C. B.; Weller, D.; Folks, L.; Moser, A., Monodisperse FePt nanoparticles and ferromagnetic FePt nanocrystal superlattices. *Science* **2000**, 287, (5460), 1989-1992.

8.   Mizuno, M.; Sasaki, Y.; Inoue, M.; Chinnasamy, C. N.; Jeyadevan, B.; Hasegawa, D.; Ogawa, T.; Takahashi, M.; Tohji, K.; Sato, K.; Hisano, S., Structural and magnetic properties of monolayer film of CoPt nanoparticles synthesized by polyol process. *Journal of Applied Physics* **2005**, 97, (10).

9.   Tzitzios, V.; Niarchos, D.; Margariti, G.; Fidler, J.; Petridis, D., Synthesis of CoPt nanoparticles by a modified polyol method: characterization and magnetic properties. *Nanotechnology* **2005**, 16, (2), 287-291.

10.	Tzitzios, V.; Niarchos, D.; Gjoka, M.; Boukos, N.; Petridis, D., Synthesis and characterization of 3D CoPt nanostructures. *Journal of the American Chemical Society* **2005**, 127, (40), 13756-13757.

11.	Shevchenko, E. V.; Talapin, D. V.; Rogach, A. L.; Kornowski, A.; Haase, M.; Weller, H., Colloidal synthesis and self-assembly of COPt3 nanocrystals. *Journal of the American Chemical Society* **2002**, 124, (38), 11480-11485.

12.	Yamamuro, S. A., T.;Sumiyama, K.; Uchida, T., Kojima, I.,, Monodisperse metallic iron nanoparticles synthesized from noncarbonyl complexes. *Japanese Journal of Applied Physics* **2004**, 44, (No 7A), 4458-4459.

13.	Luna, C.; Morales, M. D.; Serna, C. J.; Vazquez, M., Multidomain to single-domain transition for uniform Co80Ni20 nanoparticles. *Nanotechnology* **2003**, 14, (2), 268-272.

14.	Sun, S. H., Compositionally controlled FePt nanoparticle materials. *IEEE transactions on magnetics* **2001**, 37, (4), 1239-1243.

15.	Lamer, V. K.; Dinegar, R. H., Theory, Production and Mechanism of Formation of Monodispersed Hydrosols. *Journal of the American Chemical Society* **1950**, 72, (11), 4847-4854.

16.	Liu, X. Y., Heterogeneous nucleation or homogeneous nucleation? *Journal of Chemical Physics* **2000**, 112, (22), 9949-9955.

17.	Goia, D. V.; Matijevic, E., Preparation of monodispersed metal particles. *New Journal of Chemistry* **1998**, 22, (11), 1203-1215.

18.	Jeyadevan, B.; Chinnasamy, C. N.; Perales-Perez, O.; Iwasaki, Y.; Hobo, A.; Shinoda, K.; Tohji, K.; Kasuya, A., Synthesis and magnetic properties of core-shell structured (NiCo)O(AFM)-NiCo(FM) magnetic nanoparticles. *Ieee Transactions on Magnetics* **2002**, 38, (5), 2595-2597.

19.	Buhrman, R. A.; Granqvist, C. G., Size Distributions of Ultrafine Particles. *Bulletin of the American Physical Society* **1976**, 21, (3), 229-229.

20.	Viau, G.; Toneguzzo, P.; Pierrard, A.; Acher, O.; Fievet-Vincent, F.; Fievet, F., Heterogeneous nucleation and growth of metal nanoparticles in polyols. *Scripta Materialia* **2001**, 44, (8-9), 2263-2267.

21.	Fievet, F.; Lagier, J. P.; Blin, B.; Beaudoin, B.; Figlarz, M., Homogeneous and Heterogeneous Nucleations in the Polyol Process for the Preparation of Micron and Sub-Micron Size Metal Particles. *Solid State Ionics* **1989**, 32-3, 198-205.

22.   Viau, G.; FievetVincent, F.; Fievet, F., Nucleation and growth of bimetallic CoNi and FeNi monodisperse particles prepared in polyols. *Solid State Ionics* **1996,** 84, (3-4), 259-270.

23.   Toneguzzo, P.; Viau, G.; Acher, O.; Fievet-Vincent, F.; Fievet, F., Monodisperse ferromagnetic particles for microwave applications. *Advanced Materials* **1998,** 10, (13), 1032-1035.

24.   Patel, J., Farrell, D., Pankhurst, Q.A.;Parkin, I. P.,, Particle size and oxidation in CoNi nanoparticles. *Mater Res Soc Symp Proc* **2005,** 877E S5 8 1-6.

25.   Calvin, S. R., C. J.; Carpenter, E. E. ;Morrison, S. A., Stroud, R. M. ;Harris, V. G.;, Estimating crystallite size in polydispersed samples using EXAFS. *Physica Scripta* **2005,** T115, 744.

26.   Wu, R.; Fu, F.; Su, M.; Aslam, M.; Wong, K. C.; Dravid, V. P., Interaction of fatty acid monolayers with cobalt nanoparticles. *Nano Letters* **2004,** 4, (2), 383-386.

27.   Su, Y. K.; Shen, C. M.; Yang, T. Z.; Yang, H. T.; Gao, H. J.; Li, H. L., The dependence of Co nanoparticle sizes on the ratio of surfactants and the influence of different crystal sizes on magnetic properties. *Applied Physics a-Materials Science & Processing* **2005,** 81, (3), 569-572.

28.   Sun, S. H., Recent advances in chemical synthesis, self-assembly, and applications of FePt nanoparticles. *Advanced Materials* **2006,** 18, (4), 393-403.

29.   Zhang, H. T.; Chen, X. H., Controlled synthesis and anomalous magnetic properties of relatively monodisperse CoO nanocrystals. *Nanotechnology* **2005,** 16, (10), 2288-2294.

30.   Park, J.; Kang, E.; Son, S. U.; Park, H. M.; Lee, M. K.; Kim, J.; Kim, K. W.; Noh, H. J.; Park, J. H.; Bae, C. J.; Park, J. G.; Hyeon, T., Monodisperse nanoparticles of Ni and NiO: Synthesis, characterization, self-assembled superlattices, and catalytic applications in the Suzuki coupling reaction. *Advanced Materials* **2005,** 17, (4), 429-434.

31.   Cordente, N.; Respaud, M.; Senocq, F.; Casanove, M. J.; Amiens, C.; Chaudret, B., Synthesis and magnetic properties of nickel nanorods. *Nano Letters* **2001,** 1, (10), 565-568.

32.   Hou, Y. L.; Gao, S., Monodisperse nickel nanoparticles prepared from a monosurfactant system and their magnetic properties. *Journal of Materials Chemistry* **2003,** 13, (7), 1510-1512.

33.   Hou, Y.; Kondoh, H.; Ohta, T.; Gao, S., Size-controlled synthesis of nickel nanoparticles. *Applied Surface Science* **2005**, 241, (1-2), 218-222.

34.   Sun, S. H.; Murray, C. B., Synthesis of monodisperse cobalt nanocrystals and their assembly into magnetic superlattices (invited). *Journal of Applied Physics* **1999**, 85, (8), 4325-4330.

35.   Zeng, H.; Sun, S. H.; Sandstrom, R. L.; Murray, C. B., Chemical ordering of FePt nanoparticle self-assemblies by rapid thermal annealing. *Journal of Magnetism and Magnetic Materials* **2003**, 266, (1-2), 227-232.

36.   Chen, M.; Nikles, D. E.; Yin, H.; Wang, S.; Harrell, J. W.; Majetich, S. A., Patterning self-assembled FePt nanoparticles. *Journal of Magnetism and Magnetic Materials* **2003**, 266, (1-2), 8-11.

37.   Willard, M. A.; Kurihara, L. K.; Carpenter, E. E.; Calvin, S.; Harris, V. G., Chemically prepared magnetic nanoparticles. *International Materials Reviews* **2004**, 49, (3-4), 125-170.

38.   LesliePelecky, D. L.; Rieke, R. D., Magnetic properties of nanostructured materials. *Chemistry of Materials* **1996**, 8, (8), 1770-1783.

39.   Vargas, J. M., Zysler, R.D., Tailoring the size in colloidal iron oxide magnetic nanoparticles. *Nanotechnology* **2005**,16, 1474-1476

40.   Murray, C. B.; Norris, D. J.; Bawendi, M. G., Synthesis and Characterization of Nearly Monodisperse Cde (E = S, Se, Te) Semiconductor Nanocrystallites. *Journal of the American Chemical Society* **1993**, 115, (19), 8706-8715.

41.   Green, M., Organometallic based strategies for metal nanocrystal synthesis. *Chemical Communications* **2005**, (24), 3002-3011.

42.   Puntes, V. F.; Zanchet, D.; Erdonmez, C. K.; Alivisatos, A. P., Synthesis of hcp-Co nanodisks. *Journal of the American Chemical Society* **2002**, 124, (43), 12874-12880.

43.   Dinega, D. P.; Bawendi, M. G., A solution-phase chemical approach to a new crystal structure of cobalt. *Angewandte Chemie-International Edition* **1999**, 38, (12), 1788-1791.

44.   Hyeon, T., Chemical synthesis of magnetic nanoparticles. *Chemical Communications* **2003**, (8), 927-934.

45.   Murray, C. B.; Sun, S. H.; Gaschler, W.; Doyle, H.; Betley, T. A.; Kagan, C. R., Colloidal synthesis of nanocrystals and nanocrystal superlattices. *Ibm Journal of Research and Development* **2001**, 45, (1), 47-56.

46.   Chakroune, N.; Viau, G.; Ricolleau, C.; Fievet-Vincent, F.; Fievet, F., Cobalt-based anisotropic particles prepared by the polyol process. *Journal of Materials Chemistry* **2003**, 13, (2), 312-318.

47.   Gao, Y. H.; Bao, Y. P.; Beerman, M.; Yasuhara, A.; Shindo, D.; Krishnan, K. M., Superstructures of self-assembled cobalt nanocrystals. *Applied Physics Letters* **2004**, 84, (17), 3361-3363.

48.   Luna, C.; Morales, M. P.; Serna, C. J.; Vazquez, M., Effects of surfactants on the particle morphology and self-organization of Co nanocrystals. *Materials Science & Engineering C-Biomimetic and Supramolecular Systems* **2003**, 23, (6-8), 1129-1132.

49.   Murray, C. B.; Sun, S. H.; Doyle, H.; Betley, T., Monodisperse 3d transition-metal (Co, Ni, Fe) nanoparticles and their assembly into nanoparticle superlattices. *Mrs Bulletin* **2001**, 26, (12), 985-991.

50.   Andersson, S. L. T., Howe, R.F. , *Journal of Physical Chemistry* **1989**, 93, 4913.

51.   Bonnelle, J. P., Grimblot J., D'huysser A., *J. Electron Spectrosc. Relat. Phenom.* **1975**, 7, 151.

52.   Oku, M., Hirokawa, K. , *J. Electron Spectrosc. Relat. Phenom.* **1976**, 8, 475.

53.   Tan, B. J., Klabunde, K.J., Sherwood. P.M.A., *Journal of American Chemical Society* **1991**, 113, 855.

54.   Gallagher, P. K.; Blaine, R.; Charsley, E. L.; Koga, N.; Ozao, R.; Sato, H.; Sauerbrunn, S.; Schultze, D.; Yoshida, H., Magnetic temperature standards for TG. *Journal of Thermal Analysis and Calorimetry* **2003**, 72, (3), 1109-1116.

55.   Turner, N. H., Single, A.M. , *Surf. Interface Anal.* **1990**, 15, 215.

56.   Okomoto, Y., Imanaka, T., Teranishi, S., *J. Catal.* **1980**, 65, 448.

57.   Khawaja, E. E., Salim, M.A., Khan, M.A., Al-Adel, F.F., Khattak, G.D., and Hussain, Z, *J. Non-cryst. Solids* **1989**, 110, 33.

58.   Toneguzzo, P.; Viau, G.; Acher, O.; Guillet, F.; Bruneton, E.; Fievet-Vincent, F.; Fievet, F., CoNi and FeCoNi fine particles prepared by the polyol process: Physico-chemical characterization and dynamic magnetic properties. *Journal of Materials Science* **2000**, 35, (15), 3767-3784.

59.   Sangregorio, C.; Fernandez, C. d. J.; Battaglin, G.; De, G.; Gatteschi, D.; Mattei, G.; Mazzoldi, P., Magnetic properties of Co-Ni alloy nanoparticles prepared by

the sol-gel technique. *Journal of Magnetism and Magnetic Materials* **2004,** 272-276, (Supplement 1), E1251-E1252.

60.   Kodama, R. H.; Makhlouf, S. A.; Berkowitz, A. E., Finite size effects in antiferromagnetic NiO nanoparticles. *Physical Review Letters* **1997,** 79, (7), 1393-1396.

61.   Seto, T.; Akinaga, H.; Takano, F.; Koga, K.; Orii, T.; Hirasawa, M., Magnetic properties of monodispersed Ni/NiO core-shell nanoparticles. *Journal of Physical Chemistry B* **2005,** 109, (28), 13403-13405.

3. Magnetic properties of Co$_x$Ni$_{1-x}$ nanoparticles

This chapter describes the magnetic characterisation of the core-shell Co$_x$Ni$_{1-x}$/CoNiO magnetic nanoparticles whose synthesis and structural characterisation, has been described in Chapter 2. The aim was to produce particles with a large magnetic moment and exchange bias effect, which arises in particles with core-shell morphology, where the metallic core is ferromagnetic and the oxide shell is antiferromagnetic. Exchange bias manifests itself with a pronounced shift in the hysteresis loop at low temperatures, coupled with an enhancement in coercivity. Relationships between the physical properties of the Co$_x$Ni$_{1-x}$ nanoparticles, established in Chapter 2, and their magnetic properties are discussed in this chapter.

3.1 Introduction

The magnetic properties of Co_xNi_{1-x}/CoNiO nanoparticles synthesised using the polyol reduction technique are described in this chapter. The magnetic measurements were carried out using the SQUID technique. Hysteresis loops gave key information about the nature of the materials, including the saturation magnetisation (M_s), the remanence (M_r) and the coercivity (H_c). When particles were cooled in a magnetic field, any shift or enhancement in coercivity was measured as an indication of exchange bias. Zero-field cooled/field cooled magnetisation versus temperature measurements were also made and used to measure the blocking temperature (T_b) of the materials. The intersection point of the ZFC and FC curves is known as the "bifurcation point". The temperature at which a peak forms in the ZFC curve is indicative of the superparamagnetic blocking temperature of the material (T_b). Below the blocking temperature, materials behave as ferri- or ferromagnets, as there is insufficient energy to randomize the magnetic dipoles. Above the blocking temperature, the inverse is true, and materials behave as paramagnets due to there being enough energy to randomize the magnetic dipoles. [1]

Figure 43. Typical ZFC and FC behaviour in fine magnetic nanoparticles, in this case illustrating a blocking temperature (T_b) of approximately 135 K, due to the peak in the ZFC curve.
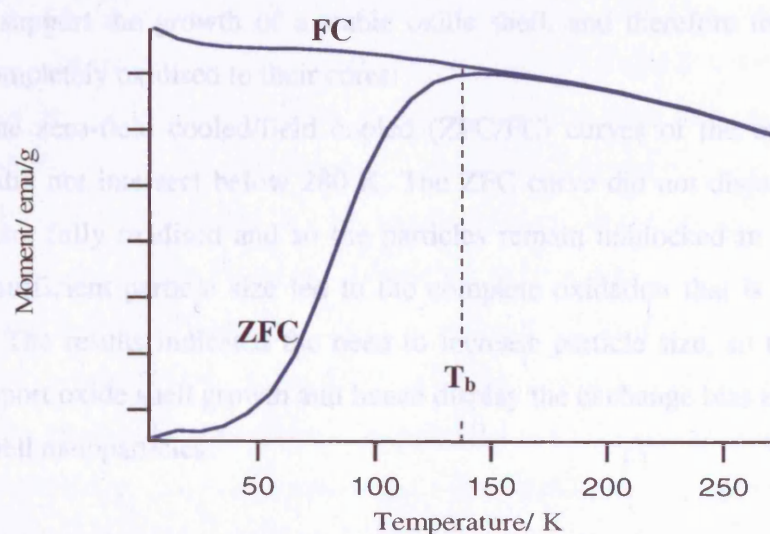
3.2 Homogeneously nucleated particles

Experiments were carried out to synthesise $Co_{80}Ni_{20}$ nanoparticles that were homogeneously nucleated. However, what was in fact initially made using the homogeneous nucleation method, were oxidised $Co_{80}Ni_{20}$ nanoparticles, which had a mean particle diameter of 7.6 nm (Section 2.4). The magnetic properties of the oxidised form of these particles were measured, as it was important to characterise the antiferromagnetic phase in the particles for future reference. The measurements also served as an indicator of the typical properties of the oxidised form of these particles. The low moment and slope of the curve indicate AFM behaviour due to the oxidation of the said particles.

Figure 44 displays the two measured hysteresis loops for the homogeneously nucleated oxidised $Co_{80}Ni_{20}$ particles, field-cooled to 10 K in 0 kOe and 60 kOe fields. The hysteresis loop that was measured at 10 K and in a zero-applied field gave a coercivity of 920 Oe. The coercivity of the material after cooling in a 60 kOe field, at the same temperature, was found to be 930 Oe. The shift of 110 Oe during the field-cooling process indicated a minimal exchange bias. The moment was also correspondingly small at 1.7 emu/g. The slight enhancement in coercivity and the small loop shift indicated that some exchange-biasing had occurred, however the effect was very small. Exchange-pinning in this instance was due to pinning in the antiferromagnetic oxide within the particle. This was due to the particles being too small to support the growth of a stable oxide shell, and therefore the particles were almost completely oxidised to their cores.

The zero-field cooled/field cooled (ZFC/FC) curves of the oxidised $Co_{80}Ni_{20}$ particles did not intersect below 280 K. The ZFC curve did not display a peak as the particles are fully oxidised and so the particles remain unblocked in this temperature range. Insufficient particle size led to the complete oxidation that is evident in these particles. The results indicated the need to increase particle size, so that the particles could support oxide shell growth and hence display the exchange bias effect that is seen in core-shell nanoparticles.[2]

Figure 44. Hysteresis loops of oxidised homogeneously nucleated $Co_{80}Ni_{20}$ nanoparticles, with a 7.6 nm mean diameter, in 0 kOe and 60 kOe fields. The small shift in the loops between the zero-field and field-cooled condition indicates a minimal exchange bias effect in the antiferromagnetic material.
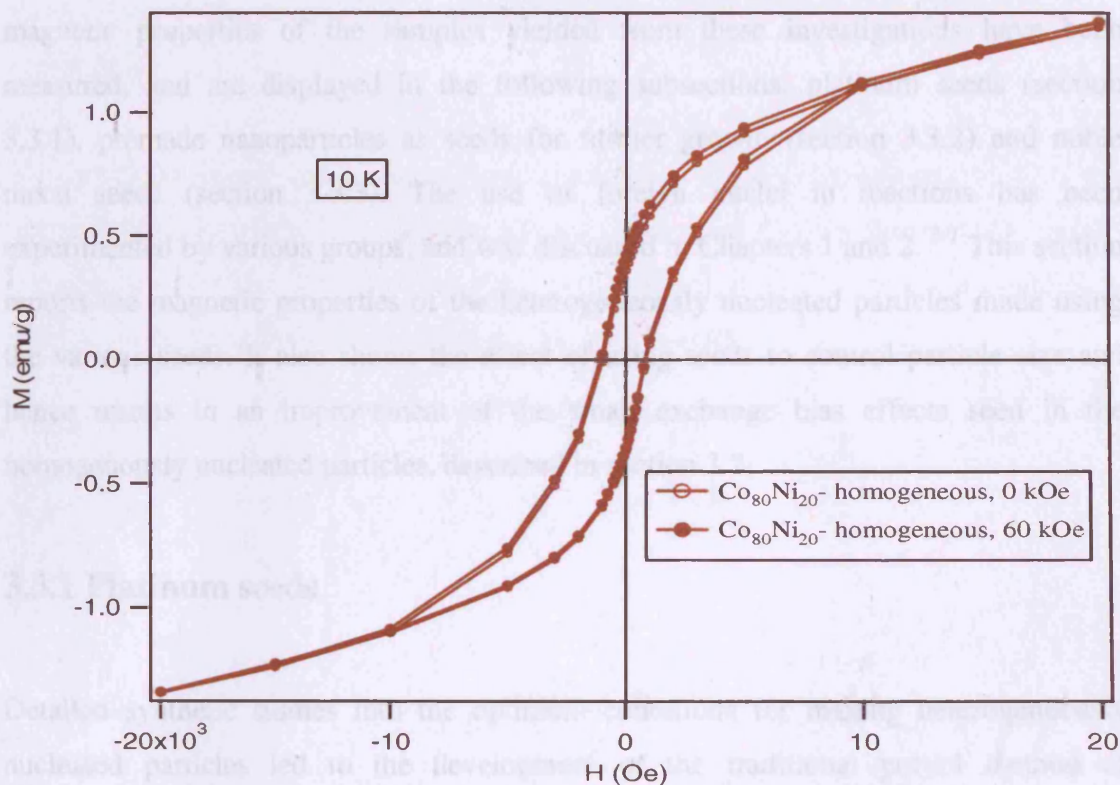
In order to step up particle size, it was essential to look at the growth of the particles and the key factors that affected particle size in particular. Therefore, investigations were subsequently carried out into the effects of introducing foreign nuclei (Section 2.5) and the addition of stabilising surfactants (Section 2.6), to control the size of the particles. The nucleation of particles heterogeneously has been adopted by previous authors, as a means to controlling the particle size and hence their respective magnetic properties.

In this particular instance, enhancing the particle size would result in an improvement in the exchange bias effect as the particles would then be large enough to support the growth of an oxide shell, without complete oxidation of their cores. Therefore, a number of experiments were carried out to determine the best method of producing particles using a suitable surfactant stabiliser and nucleating seed. The magnetic properties of the particles yielded from these investigations are documented in the following subsections.

3.3 Heterogeneously nucleated particles

The nucleation of $Co_{80}Ni_{20}$ particles was investigated using different types of nucleating seed and seeding techniques, as described in detail in Chapter 2 (Section 2.5). The magnetic properties of the samples yielded from these investigations have been measured, and are displayed in the following subsections; platinum seeds (section 3.3.1), premade nanoparticles as seeds for further growth (section 3.3.2) and noble metal seeds (section 3.3.3). The use of foreign nuclei in reactions has been experimented by various groups, and was discussed in Chapters 1 and 2. [3-7] This section reports the magnetic properties of the heterogeneously nucleated particles made using the various seeds. It also shows the effect of using seeds to control particle size and hence results in an improvement of the small exchange bias effects seen in the homogenously nucleated particles, described in section 3.2.

3.3.1 Platinum seeds

Detailed synthetic studies into the optimum conditions for making heterogeneously nucleated particles led to the development of the traditional polyol method of synthesis. [3, 4, 8-10] The heterogeneously nucleated $Co_{80}Ni_{20}$ particles described in section 2.5. of the previous chapter, were characterised magnetically as they had responded strongly to a magnet upon drying, and had formed a stable solution. TEM analysis showed that the particles displayed bimodality in their distribution. The larger particles were 12.6 nm in mean diameter and were surrounded by satellite particles with a mean of 2.6 nm, which had not completely grown (Figure 13(b)), or had been created by a secondary nucleation event.

Magnetic studies showed that these particles were superparamagnetic, characterised by the distinctive shape of the hysteresis loop recorded at room temperature (Figure 45(a)). The coercivity of the $Co_{80}Ni_{20}$ Pt nucleated particles was very small and could not be distinguished from 0 Oe, which confirmed the superparamagnetic nature of the particles. The saturation magnetisation of the particles at room temperature was approximately 11 emu g^{-1} as seen in then curve shown in Figure 45(a). However, when measurements were carried out at lower temperatures, the saturation magnetisation increased significantly. This is evidenced by the exponential

relationship displayed in Figure 45(b) between magnetisation and temperature. The saturation magnetisation increases, as the temperature decreases, to a maximum of 25 emu g^{-1} at 2 K. The ZFC curve of the Co$_{80}$Ni$_{20}$ platinum-seeded particles showed a peak developing at approximately 130 K which indicates the superparamagnetic blocking temperature of the Co$_{80}$Ni$_{20}$ Pt nucleated particles. The ZFC and FC curves meet at approximately 150 K.

Figure 45(a) Room temperature hysteresis loop of superparamagnetic 12.6 nm heterogeneously nucleated Co$_{80}$Ni$_{20}$ particles (bimodal distribution) (b) M$_s$ versus temperature for the 12.6 nm Co$_{80}$Ni$_{20}$ particles (c) ZFC/FC curves measured at 100 Oe for heterogeneously nucleated Co$_{80}$Ni$_{20}$ particles.
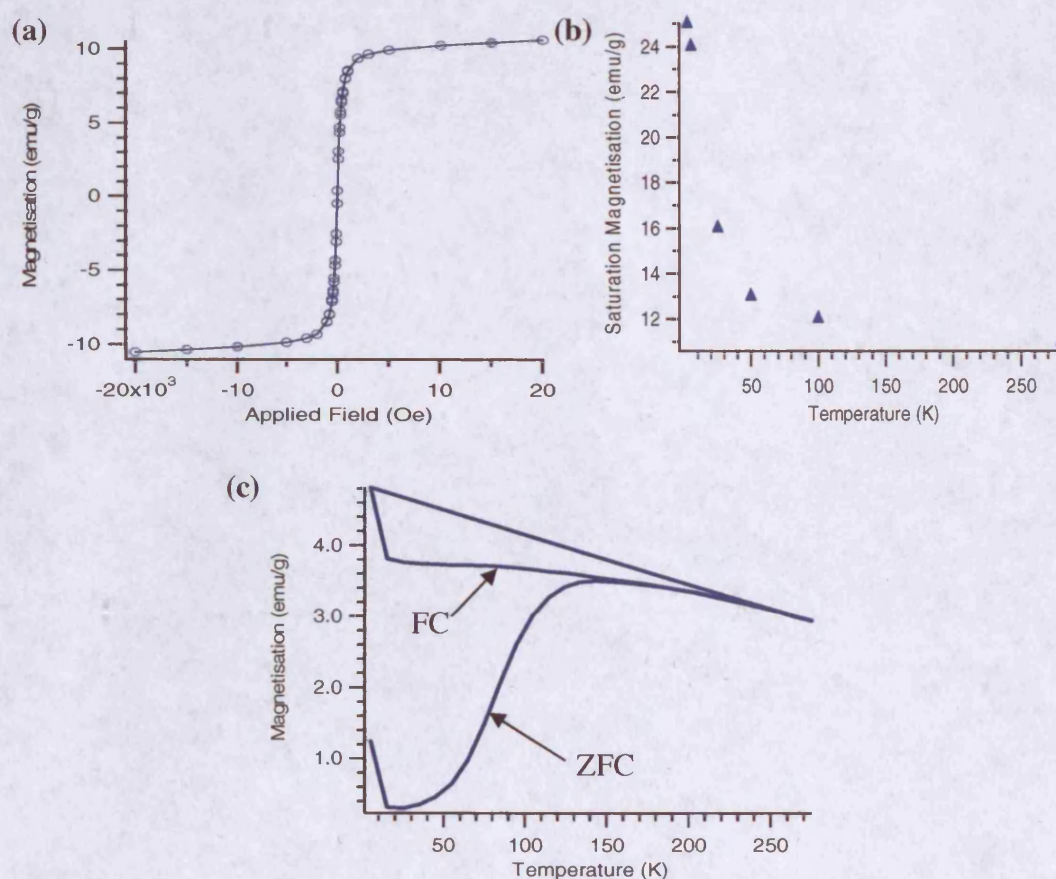
The low temperature measurements carried out on the sample, indicated that these heterogeneously nucleated Co$_{80}$Ni$_{20}$ particles displayed exchange bias properties below 100 K, but above 50 K (Figure 46). This is evidenced by the enhanced coercivity in the loop measured at 50 K. The measurements carried out at 100 K and 280 K respectively, both displayed loops that were characteristic of superparamagnetic behaviour. This is also displayed in Figure 46 where the 100 K and 280 K loops have small coercivities

that cannot be accurately distinguished from 0 Oe.

Figure 46. The M-H loops of the heterogeneously nucleated, $Co_{80}Ni_{20}$ nanoparticles with a mean diameter of 12.6 nm (bimodal distribution), measured after field cooling from 280 K to the labelled temperature.
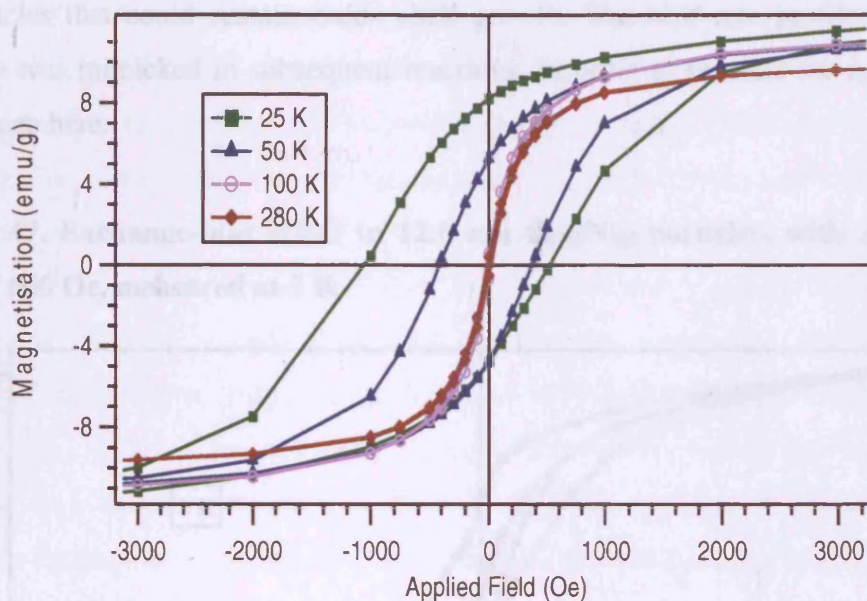
The 12.6 nm $Co_{80}Ni_{20}$ nanoparticles were cooled from 280 K, well above the blocking temperatures, to 2 K in both 0 and 60 kOe fields. These particles had interesting magnetic properties. The saturation magnetization of the sample at 2 K was 25 emu/g, and the particles cooled in a 60 kOe field from 280 K to 5 K had a coercivity increase from 220 Oe to 780 Oe, in the zero-field cooled condition. The exchange field of the sample at this temperature was 670 Oe.[11]   The corresponding hysteresis loops displaying this exchange bias are shown in Figure 47.

The size of the exchange and coercive fields are smaller than those previously reported for 10 nm $Co_{80}Ni_{20}$ particles, most likely due to the 2.6 nm particles dispersed throughout this sample, which were completely oxidized before the measurements were made.[6] This probably also explains the strange penguin-shapes in the hysteresis loops in Figure 43. The loops measured in a 0 kOe field after field-cooling is wasp-waisted and so has a constricted central waist. Whereas the loop measured in a 60 kOe applied field, after-cooling is pot-bellied i.e the loop is fatter at the bottom than at the top. The larger 12.6 nm particles have a ferromagnetic core and are enveloped by an antiferromagnetic

shell. However, the prevalence of the much smaller 2.6 nm fully oxidised antiferromagnetic-phase particles, dispersed throughout the sample, had a profound effect upon the shape of the hysteresis loops, as the coercivities in both sets of different sized particles are so varied.

The results obtained and the particles produced, indicated that the reaction condition employed in these syntheses were effective in allowing nucleation and growth of particles that could sustain oxide shell growth. The heat rate profile used in this reaction was mimicked in subsequent reactions, in order to emulate the exchange bias effect seen here.

Figure 47. Exchange-bias effect in 12.6 nm $Co_{80}Ni_{20}$ particles, with an exchange field of 650 Oe, measured at 5 K.
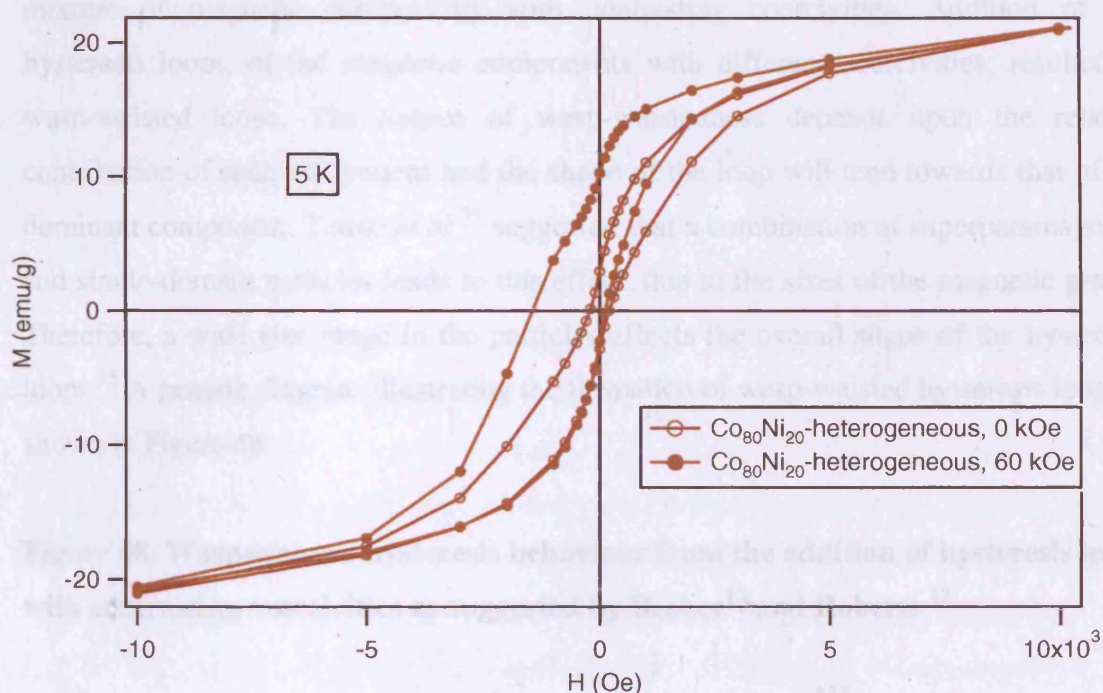
Earlier attempts at synthesising particles using a slower initial heat rate had yielded much smaller particles which were around 6 nm in size. Magnetic studies of the 6 nm $Co_{80}Ni_{20}$ particles showed that they had completely oxidised to their cores due to their small size. Particles with a smaller diameter provide a larger surface area over which oxidation could occur. The 6 nm particles had a small coercivity of 100 Oe at 5 K, and the hysteresis loops taken after cooling in 0 and 60 kOe fields were identical, with no evidence of a shift due to exchange anisotropy. The low saturation magnetization (6 emu/g) of the particles also indicated that a significant amount of

oxide phase was present. Combined with the low blocking temperature of the sample, this confirmed a significant percentage of the particles were fully oxidized and thus did not support exchange biasing. The room temperature hysteresis loop of the 6 nm particles resembled that of a polycrystalline antiferromagnet, indicating formation of a mixture of CoO and NiO crystallites.

The wasp-waisted and pot-bellied hysteresis loops that have been described in these results, have also been described in works carried out by Becker,[12] Roberts[13] and Tauxe[14] et al in previous research into the magnetic properties of geological materials. They have all cited possible causes for the strange penguin-shaped and wasp-waisted hysteresis loops found in paleomagnetic studies of such materials, and these causes can also be applied to studies carried out here into the properties of metallic core-shell magnetic nanoparticles. Becker attributed the wasp-waisted hysteretic behaviour due to mixture of magnetic components with contrasting coercivities. Addition of the hysteresis loops, of the magnetic components with different coercivities, resulted in wasp-waisted loops. The degree of wasp-waistedness depends upon the relative contribution of each component and the shape of the loop will tend towards that of the dominant component. Tauxe et al [14] suggested that a combination of superparamagnetic and single-domain particles leads to this effect, due to the sizes of the magnetic grains. Therefore, a wide size range in the particles affects the overall shape of the hysteresis loops.[15] A generic diagram illustrating the formation of wasp-waisted hysteresis loops is shown in Figure 48.

Figure 48. Wasp-waisted hysteresis behaviour from the addition of hysteresis loops with contrasting coercivities as suggested by Becker[12] and Roberts.[13]
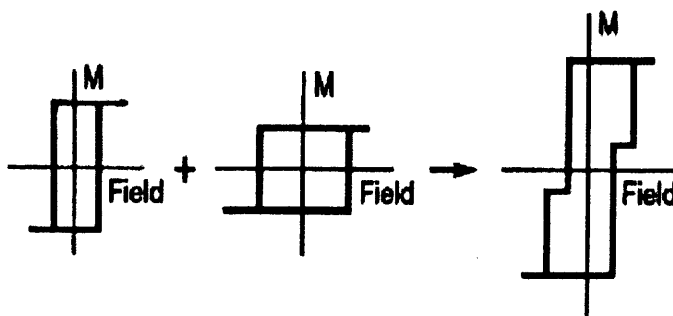
In summary, the heterogeneous method produced particles that displayed exchange bias after the synthesis conditions were varied to promote fast nucleation followed by slower growth. The bimodality in the 12.6 nm $Co_{80}Ni_{20}$ sample, which

displayed exchange bias, affected the shape of the hysteresis loop as the smaller particles oxidised and this caused a penguin-shaped loop. This was due to a mixture of superparamagnetic and single-domain particles within the sample.

Initial magnetic studies indicated that heterogeneous nucleation of nanoparticles was a better route to synthesising particles with exchange bias, due to the control in particle size that could be implemented, during synthesis. The use of oleic acid as a sole surfactant has been shown to be successful where large particle growth has occurred. However, the results shown by the 6 nm $Co_{80}Ni_{20}$ particles have shown that oleic acid did not sufficiently stabilise the smaller particles. The washing procedure post-synthesis, if not replaced with sufficient stabiliser, can induce premature oxidation of the particles. The heterogeneous route of synthesis was therefore developed further in this investigation, through the use of different seeding techniques and different types of seeds (Section 2.5.1.2 and 2.5.1.3). The magnetic studies of these particular samples are detailed in the following subsections.

3.3.2 Premade particles as nuclei for further growth

It had been previously shown by Yamamuro *et al* [16] that particle size could be increased using premade particles, that were reintroduced into the reaction set-up with additional reactants, to improve particle size. The seed particles described in subsection 2.5.1.2 were small at around 4.4 nm in diameter, and displayed partial self assembly when initially made and when additional reactants were added to promote the growth of larger particles, the mean diameter of the resultant nanoparticles almost doubled. The particles that were grown from these seeds were 7.4 nm in mean diameter. The hysteresis loop of the 7.4 nm particles is shown in Figure 49. Low temperature measurements of this sample were carried out at 5 K. The loop's saturation point was 10 emu/g at 5 K. The coercivity of the particles was 440 Oe in zero-field, whereas in a 60 kOe field this increased to 520 Oe. This increase was not much greater than that determined for the homogeneously nucleated particles described earlier (section 3.2), and therefore did not improve upon the results garnered from heterogeneously nucleating the particle's grown with platinum seeds.

Figure 49. M vs H loops measured at 5 K in 0 kOe and 60 kOe fields, for 7.4 nm $Co_{80}Ni_{20}$ particles seeded with 4.4 nm $Co_{80}Ni_{20}$ particles, in a two-step synthetic process.
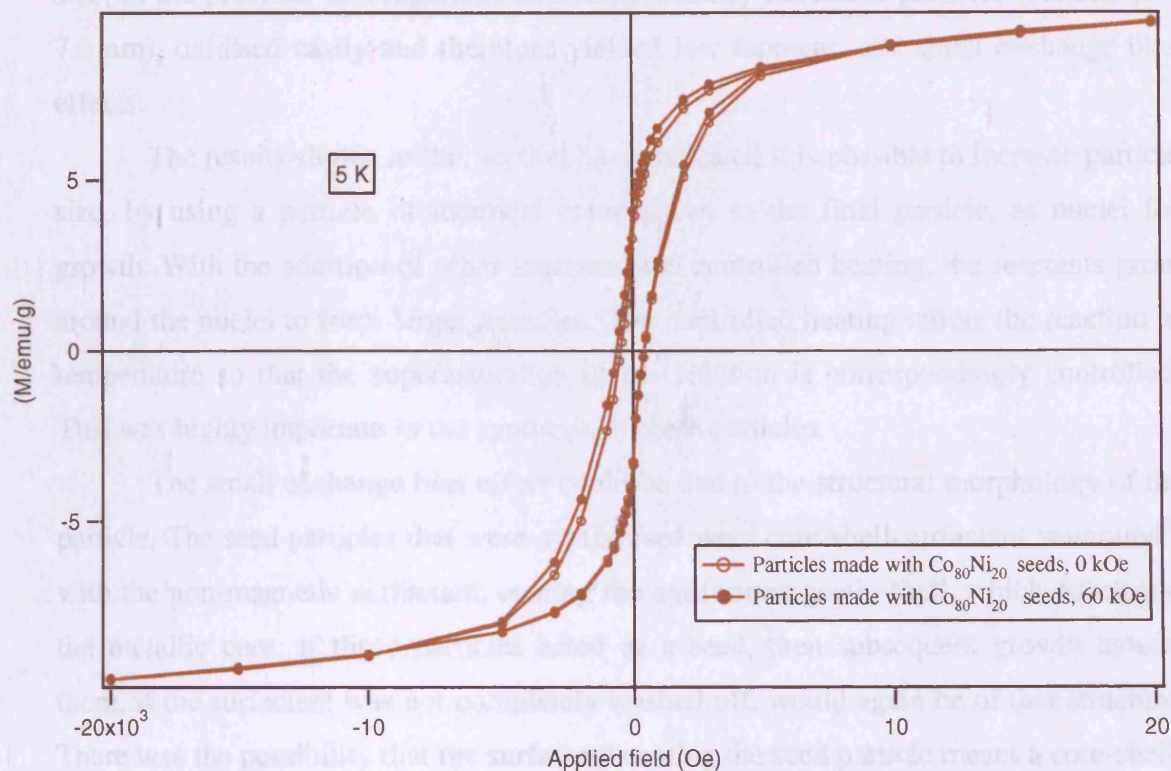
The ZFC/FC curves did not overlap below 280 K when the particles were measured at 100 Oe. The ZFC curve displayed a plateau at approximately 40 K and then rose to 130 K, however, there was no evidence of a peak. This line of investigation was not pursued, in terms of the synthesis, as the particles made using this method had almost oxidised completely to their cores. This resulted in the low moment that is seen in Figure 49 and hence the minimal exchange bias effect that can also be seen due to the domination of the antiferromagnetic phase.

The polyol method of synthesis had been used in the synthesis of iron nanoparticles by Yamamuro[16] whereas here, the Co_xNi_{1-x} system was experimented with. These results are therefore novel, as this particular seeding technique had not been used before to synthesise this type of particle. The particles did show evidence of exchange bias, however, the reaction conditions would require further investigation to eliminate oxidation of the smaller preformed seed particles, as this translated through into the final 7.4 nm particles. Although nitrogen flow was maintained, the small seed particles (4.4 nm) may have oxidised quickly when the additional reactants were

introduced to the vessel, as the flask was opened up to the atmosphere. Although the subsequent heating of the reaction, to grow larger particles occurred in a nitrogen atmosphere, the seed particles could have partially oxidised. Particles of around this size, in the previous investigations of homogeneously nucleated particles (section 2.4-7.6 nm), oxidised easily and therefore yielded low moment, and small exchange bias effects.

The results shown in this section have indicated it is possible to increase particle size, by using a particle of identical composition to the final particle, as nuclei for growth. With the addition of other reactants and controlled heating, the reactants grow around the nuclei to form larger particles. The controlled heating tailors the reaction to temperature so that the supersaturation of the solution is correspondingly controlled. This was highly important in the synthesis of these particles.

The small exchange bias effect could be due to the structural morphology of the particle. The seed particles that were synthesised were core-shell-surfactant structured[17] with the non-magnetic surfactant, coating the antiferromagnetic shell, which enveloped the metallic core. If these particles acted as a seed, then subsequent growth around them, if the surfactant was not completely washed off, would again be of that structure. There was the possibility that the surfactant coating the seed particle meant a core-shell--core[1]-shell[1]-surfactant[1] structure was present. Exchange bias is an interfacial effect which occurs across the antiferromagnet shell and ferromagnetic core interface.[1, 2, 18-20] Therefore, it is possible that the small effect seen in Figure 49, is due to the interaction between core[1] and shell[1] seen in Figure 50.

Figure 50. Possible structure of $Co_{80}Ni_{20}$ 7.4 nm particles seeded with 4.4 nm $Co_{80}Ni_{20}$ particles, made via the Yamamuro method [16]
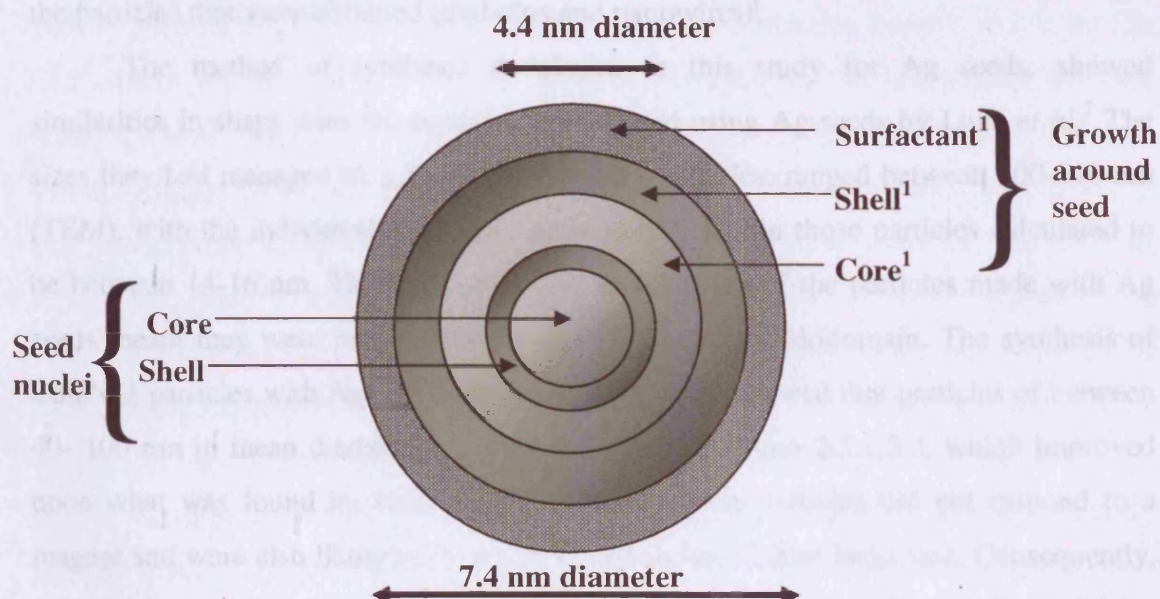
These ambiguities, in terms of structure meant that this synthetic method was not pursued, as it was difficult to definitively attribute the magnetic phenomena to one specific reason. However, in terms of synthesis the investigation was successful as it succeeded in increasing the particle size to almost double that of the original seed particle. The partial oxidation at the surface of the particle led to minimal exchange bias. However, this effect was not as large as had been hoped, and so alternative methods of increasing the particle's mean diameter were pursued.

3.3.3 Noble metal seeds

Following studies into heterogeneous nucleation of $Co_{80}Ni_{20}$ nanoparticles with platinum seeds (section 2.5.1.1), investigations were also carried out into the nucleation of these particles with other types of noble metal seed, such as gold and silver. Luna *et al* [7] had already investigated seeding of Co_xNi_{1-x} particles with silver, whilst Ung *et al* [21, 22] had investigated ruthenium to synthesise Co_xNi_{1-x} nanowires and dumbbell-shaped particles. Chakroune *et al* [9] also produced diabolo-shaped particles, with ruthenium seeds, that were between 25-100 nm in size. The shape of particles made with ruthenium seeds was not ideal for the core-shell structure that was required in order for exchange bias to be evident, in the Co_xNi_{1-x} particles. Therefore, further investigations

into ruthenium seeds were not carried out for the purpose of this investigation. Ung *et al* [21, 22] had clearly displayed the limitations of using ruthenium, in terms of the shape of the particles that were obtained (diabolos and nanowires).

The method of synthesis developed in this study for Ag seeds, showed similarities in shape with the particles synthesised using Ag seeds by Luna *et al.*[7] The sizes they had managed to achieve for $Co_{80}Ni_{20}$ particles, ranged between 200-540 nm (TEM), with the individual crystallite sizes (XRD) within those particles calculated to be between 14-16 nm. Therefore, the large overall size of the particles made with Ag seeds meant they were polycrystalline and likely to be multidomain. The synthesis of $Co_{80}Ni_{20}$ particles with Ag seeds, in our investigation, showed that particles of between 40- 100 nm in mean diameter could be fabricated (section 2.5.1.3), which improved upon what was found by Luna *et al.* [7] However, the particles did not respond to a magnet and were also likely to be polycrystalline due to their large size. Consequently, they did not warrant a detailed investigation into the magnetic properties. The particles made with Au seeds were also polycrystals due to their size of between 60-150 nm, and did not respond to a magnet. Therefore, the use of Ag and Au seeds in the synthesis of Co_xNi_{1-x} was not developed any further and Pt seeds were subsequently used, as they had controlled the size of the particles in this particular system, much better in comparison to the other noble metals that were tested.

3.4 Surfactant stabilisers

The investigations carried out into the most effective nucleation process to use for the synthesis of Co_xNi_{1-x} particles, indicated that heterogeneous nucleation was the best route to follow. The seed that was found to be the best for this system was platinum. The heterogeneously nucleated particles displayed the strongest exchange bias effects in this study, when compared to the homogeneously nucleated particles described in section 3.2. Another method of controlling particle size that has been investigated by various groups, and in this study, was the use of stabilising surfactants to arrest or promote particle growth. [17, 23, 24] The binding of the surfactant to form a complex with the metallic ions and steric effects that led to the ability to tune the size of particles.

Particles formed using oleic acid displayed variable results. The homogeneously nucleated particles coated with oleic acid, almost completely oxidised due to their small size. Whereas the particles that had heterogeneously nucleated were much larger and were therefore able to support oxide shell growth. This had a significant impact on the magnetic properties, as the almost completely oxidised homogeneously nucleated $Co_{80}Ni_{20}$ particles had a low moment, and therefore did not display exchange bias effect due to the absence of a core-shell structure. The larger $Co_{80}Ni_{20}$ particles that were heterogeneously nucleated, did support oxide shell growth, and hence exchange bias was observed. What this did show was the importance of balancing the nucleation, with the appropriate type of surfactant for a particular sample.

When amine-based surfactants were used, the nickel particles were stabilised well from agglomeration. However, this was not the case for samples with cobalt-doped into them. The particles formed by oleylamine as sole surfactant were too small and had completely oxidised, as they did not respond to a magnet. Therefore, they did not warrant any further magnetic investigation. The same was true for TOPO and TBP. The particles formed using these particular surfactants, on a sole-basis, were too small to warrant detailed magnetic studies as they are predominantly oxidised to their cores. The exception to this was oleic acid, which had shown evidence of core-shell textured particles being formed. Therefore, some investigations were carried out on particles made with oleic acid as sole surfactant due to the promising results achieved where larger particles had been grown.

The use of an oleic acid/ oleylamine mixture had previously been developed for

the stabilisation of iron nanoparticles by Sun *et al.*[25] Studies into the suitability of surfactants in this investigation, also indicated the possibility that the OA/OY combination could successfully mediate particle growth and stabilise the particles from oxidation. This was due to the strong interaction between the metallic ion species in solution with OA, and the weaker interaction with OY. The use of these surfactants, in addition to heterogeneously nucleating the particles, led to successful results. These are described in detail within the compositional study subsection (section 3.5). The OA/OY mixture was believed to have formed an amide, and hence a double-sheathed surfactant, which protected the particles from agglomeration and full-oxidation. The particles were also sufficiently large to warrant detailed magnetic investigations. The OA/OY synthesised particles were partially oxidised and this gave rise to the interesting properties described in the following sections.

3.5 Composition study

Attempts to make cobalt particles via the polyol process have been well documented over recent years.[23, 26] The magnetic properties of these particles have been of great interest, with specific regard to their applications in high-density memory storage devices.[27-32] Previously, studies have been carried out by Toneguzzo et al,[5, 33] Fievet et al[34], Jeyadevan et al[35] and Luna et al,[6, 7] into Co_xNi_{1-x} alloy nanoparticles with a presumed oxide shell composed of CoO and NiO crystallites. However, only a select few compositions were investigated, here a complete compositional range has been fully characterised magnetically. This investigation looks in detail, at the effect of compositional change on the magnetic properties of Co_xNi_{1-x} nanoparticles, where x has been varied. Specifically, an investigation has been made into the manner by which the magnetic properties of the particles may be tuned, by correspondingly altering the composition. The effect that this has on the exchange bias properties of the particles is an important aspect of this work.

3.5.1 Cobalt nanoparticles

Following the detailed investigations carried out, in order to optimise the synthesis, cobalt particles were fabricated using the process highlighted in Chapter 5. This included the use of platinum seeds so that the particles were heterogeneously nucleated with a mixture of OA/OY as surfactant and acetylacetonate precursor salts. A systematic method of drying the materials was adopted, therefore any changes in the magnetic properties of the samples were due to size variations between particles. This led to either partial or full oxidation of the particles. The smaller particles fully oxidised, whilst the larger ones could support oxide shell growth and hence displayed partial oxidation. The partially oxidised particles were more likely to show exchange bias and a high magnetic moment.

      Preliminary investigations with just oleic acid as surfactant, platinum seeds and acetate salts yielded mixed results. Some good samples were produced in terms of the exchange bias effects exhibited, however, most of the syntheses were difficult to reproduce. One of the samples that displayed good moment and exchange bias was made in a similar fashion to the sample described in section 5.3.1. The M vs H loop of

the cobalt sample, made with an acetate salt is shown in Figure 51. These cobalt particles gave a saturation magnetisation of 53 emu/g, although the loop did not completely saturate. The shape of the loop was slightly penguin-shaped with a wider and narrower portion. This variation in shape was again due to the different sizes of particle within the sample, which yielded different coercivities and caused the penguin-shape.

Figure 51. M vs H curve of cobalt nanoparticles made with platinum seeds, oleic acid surfactant and acetate salt. Slight penguin shape to the loops indicates the different sizes of particle within the sample.
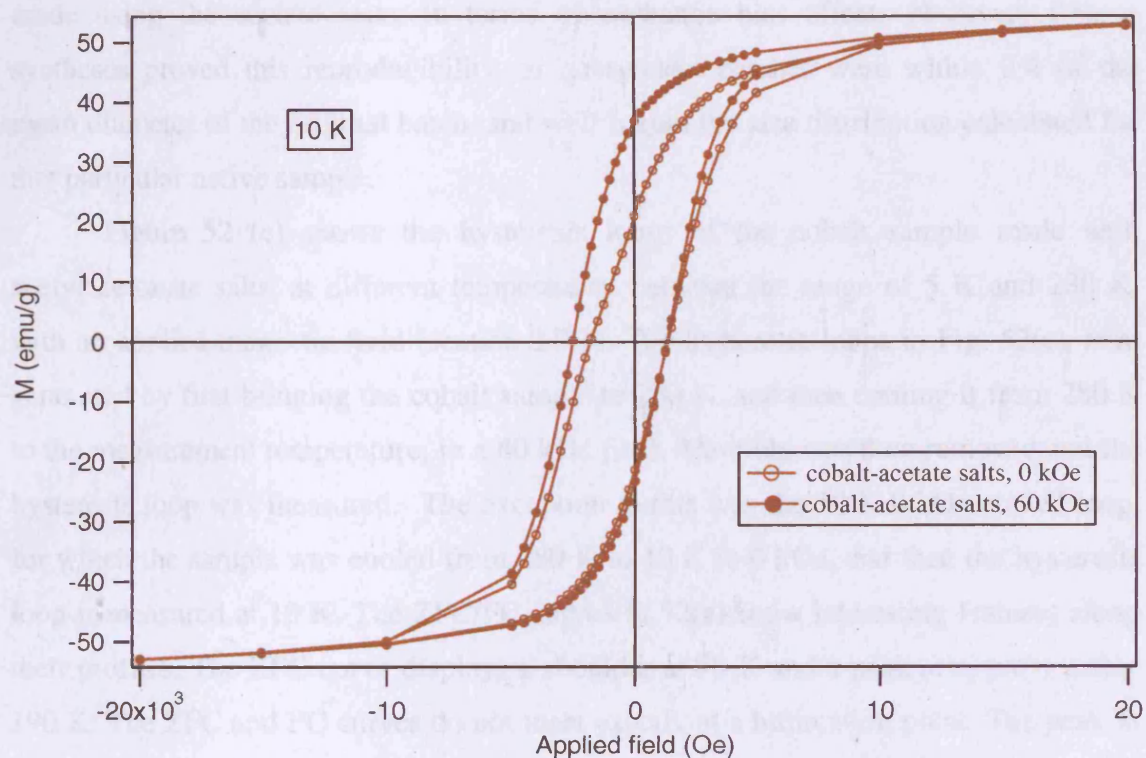
The hysteresis loops were measured after cooling in 0 kOe or 60 kOe. The coercivity of the cobalt nanoparticles made with acetate salts, measured in zero field was 1570 Oe, and in a 60 kOe field was 1910 Oe. An enhancement in coercivity of 340 Oe was therefore observed. The exchange field of the sample, once the field had been applied, was 600 Oe. The cobalt particles had a blocking temperature above 280 K. If this result is compared to that of the homogeneously nucleated particles described in section 3.2, the difference in blocking temperatures is due to the size of the particles, and hence the

oxidation which has occurred. The cobalt particles described in this section have more ferromagnetic character compared to the $Co_{80}Ni_{20}$ particles which had almost completely oxidised, and therefore would have little ferromagnetic character. The exchange-bias effect seen in Figure 51, of cobalt nanoparticles, is characterised by the shift in the hysteresis loop. This shift has arisen because of the interfacial effect between the cobalt metallic core and the cobalt oxide shell, within the core-shell particle.

Due to the difficulty in reproducing these results, subsequent reactions were carried out with cobalt and nickel acetylacetonate salts, platinum seeds and an OA/OY surfactant mixture. This was an adaptation of the Yamamuro[16] and Sun[25] methods for synthesis of iron nanoparticles and ensured a better level of reproducibility. The size of particles produced, using the OA/OY method was a distinct improvement upon those made using the acetate salts, in terms of exchange bias effects observed. Repeat syntheses proved this reproducibility, as subsequent batches were within 2% of the mean diameter of the original batch, and well within the size distribution calculated for that particular native sample.

Figure 52 (c) shows the hysteresis loops of the cobalt sample made with acetylacetonate salts, at different temperatures between the range of 5 K and 280 K, with an applied magnetic field (section 2.7.2). The hysteresis loops in Fig. 52(c) were generated by first bringing the cobalt sample to 280 K, and then cooling it from 280 K to the measurement temperature, in a 60 kOe field. The field was then removed and the hysteresis loop was measured. The exception to this was the 10 K 0 kOe cooled loop, for which the sample was cooled from 280 K to 10 K in 0 kOe, and then the hysteresis loop is measured at 10 K. The ZFC/FC curves in 52(a) show interesting features along their profiles. The ZFC curve displays a shoulder at 70 K and a peak at approximately 190 K. The ZFC and FC curves do not meet exactly at a bifurcation point. The peak in the ZFC curve could represent the sample's core blocking temperature, whilst the shoulder feature at around 70 K could possibly be due to the blocking temperature of the shell. The gradual rise of the ZFC curve, and the lack of definition in the peaks, indicates the broad nature of the size distributions of particles in the sample. The size of particles and its relation to blocking temperature has been investigated in detail by several groups and should be considered when evaluating the blocking temperatures in this study.[36] The bimodality in some of the sample, however, does make it difficult to make generalisations about size and blocking temperature.

The measurement carried out to determine the exchange bias in the particles

took place at 10 K (Figure 52 (b)). The sample was measured in zero-field and then in a 6 kOe field. This generated a loop shift of 2000 Oe, a very large exchange bias and comparable with results seen for cobalt particles of this size.[37] The characteristic loop shift and enhancement in coercivity indicates the likelihood of core-shell particles having been formed.

The hysteresis plot (Figure 52 (c)) shows a superparamagnetic curve at 280 K. The measurement cycle begins at low temperatures, and the particles are slowly heated to room temperature whilst the moment is measured in an applied field of 60 kOe. At 5 K the loop shows some asymmetry and the loop's waist was constricted at low fields. The coercivity of the loop is extremely large at 5 K and gradually decreases with an increase in temperature. The saturation magnetisation determined at 5 K was 37 emu/g.

Figure 52 (a) ZFC/FC curve measured at 100 Oe (b) M-H plot of bimodal cobalt nanoparticles at 10 K, with 0 kOe and 60 kOe fields (c) M vs H curves at a range of temperatures

(a)

(b)

(c)
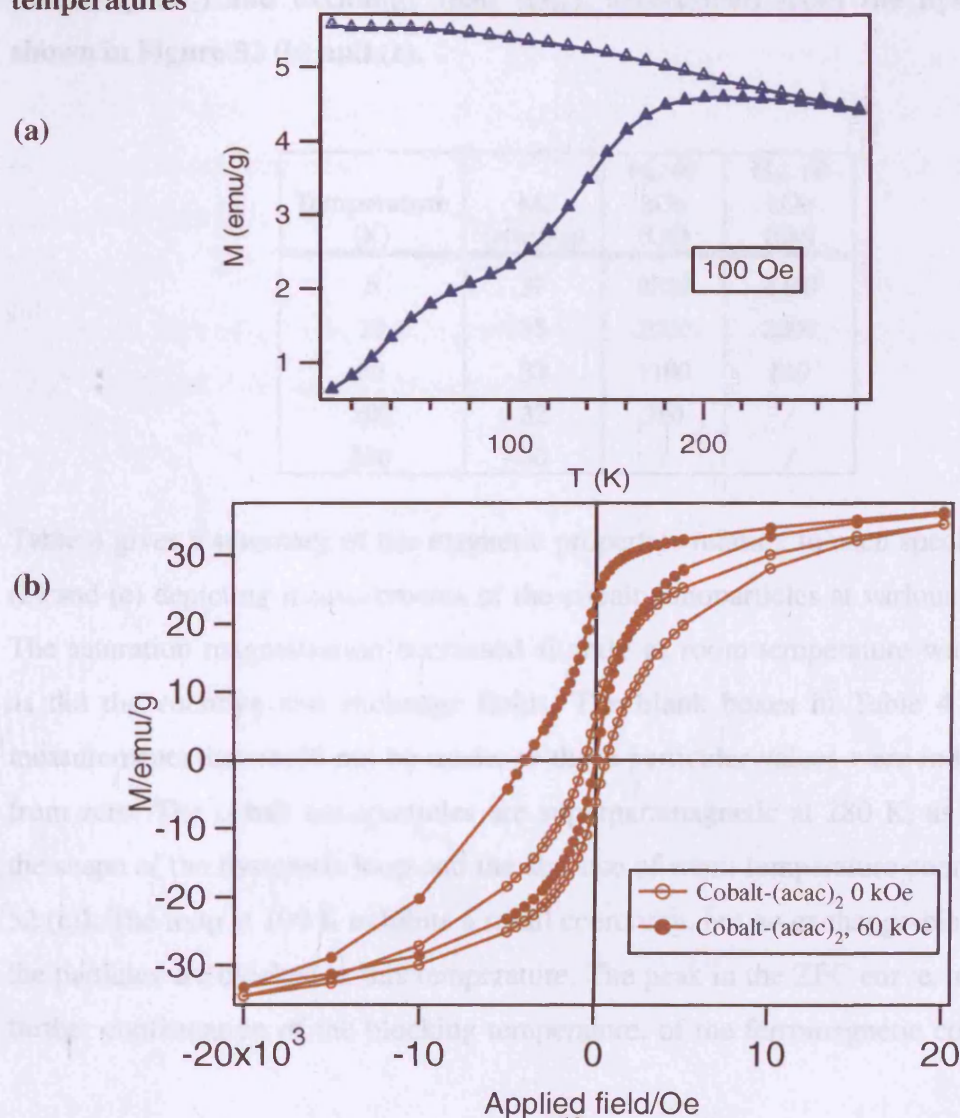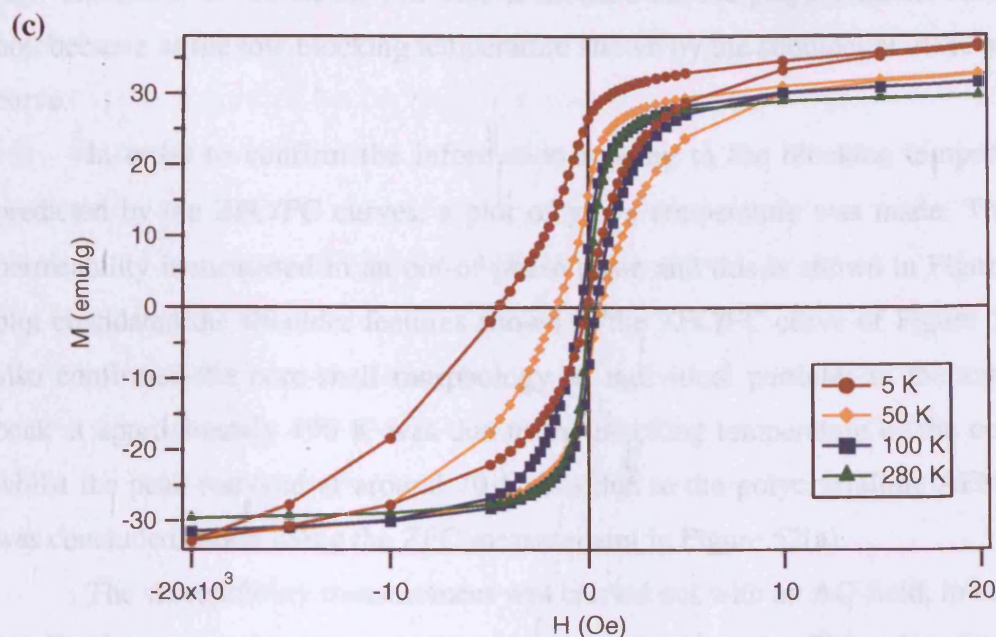
Table 4. Key magnetic properties such as; saturation magnetisation (M_s), coercivity (H_c) and exchange field (H_{ex}), ascertained from the hysteresis loops shown in Figure 52 (b) and (c).

Temperature (K)	M_s (emu/g)	H_c- 60 kOe (Oe)	H_{ex}- 60 kOe (Oe)
5	37	2320	2240
10	35	2020	2000
50	33	1100	510
100	32	380	/
280	30	/	/

Table 4 gives a summary of the magnetic properties relating to each specific loop in 52 (b) and (c) depicting measurements of the cobalt nanoparticles at various temperatures. The saturation magnetisation decreased slightly as room temperature was approached, as did the coercive and exchange fields. The blank boxes in Table 4 represent the measurements that could not be made, as those particular values were indistinguishable from zero. The cobalt nanoparticles are superparamagnetic at 280 K, as evidenced by the shape of the hysteresis loop and the absence of room-temperature coercivity (Figure 52 (c)). The loop at 100 K exhibits a small coercivity, but no exchange-bias. This means the particles are blocked at this temperature. The peak in the ZFC curve, at 190 K gives further confirmation of the blocking temperature, of the ferromagnetic core (Figure 52

(a)). Therefore, at 100 K, the FM core is blocked but the polycrystalline AFM shell is not, because of the low blocking temperature shown by the shoulder at 70 K in the ZFC curve.

In order to confirm the information relating to the blocking temperatures, as predicted by the ZFC/FC curves, a plot of χ'' vs temperature was made. The relative permeability is measured in an out-of-phase plane and this is shown in Figure 53. The plot elucidated the shoulder features shown in the ZFC/FC curve of Figure 52(a), and also confirmed the core-shell morphology of individual particles in the sample. The peak at approximately 190 K was due to the blocking temperature of the cobalt core, whilst the peak resolved at around 70 K was due to the polycrystalline AFM shell, as was concluded earlier using the ZFC measurement in Figure 52(a).

The susceptibility measurement was carried out with an AC-field, in comparison to all other magnetic measurements, that have been made. This takes into account measurement of an applied field in addition to internal magnetic field generated within the particles themselves. These AC measurements have provided a new type of information in the investigation. Whilst it was not possible to measure all of the samples made, the information yielded from this meant that it should definitely be used in the future to characterise core-shell particles, and gain a greater understanding of the structure of particles made using these methods.

Figure 53. Plot of χ'' versus temperature, to obtain the blocking temperatures (T_b) of the core and shell, of cobalt nanoparticles.
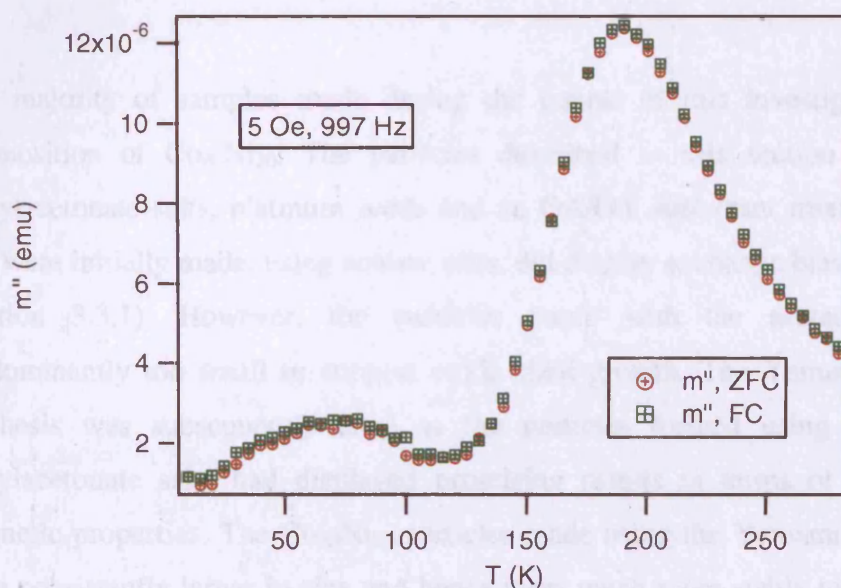
Work carried out by Tracy *et al* [38] has shown distinct similarities with the research carried out here. The Tracy group [38] investigated cobalt particles that had been oxidised in a controlled atmosphere. The results that are referred to, for comparisons sake, are the partially oxidised samples. It is expected that the particles made in this investigation possess a similar morphology, although the drying methods and experimental detail are slightly different in this case. Tracy *et al* [38] measured the blocking temperature of cobalt, by looking for a peak in the ZFC temperature-dependent magnetisation for DC measurements. They reported a blocking temperature of 195 K for the cobalt core.[38] This correlates nicely with what was found in this investigation using AC measurements shown in Figure 53 alongside the ZFC/FC curves for the sample in Figure 52 (a).

The CoO grains also have a blocking temperature above which they behave superparamagnetically. The random orientation of the crystal axes and their antiferromagnetic nature means that the grains cannot be directly measured for magnetic moment. Hence, a peak in the in-phase susceptibility was determined via AC measurements. The blocking temperature of the shell, which consists of CoO grains, was found to be approximately 70 K. The broadness of the peaks is also due to the size distribution, which although is not completely uncharacteristic in materials of this type, is particularly wide. The synthesis was repeated, and deemed to be reproducible, as the following the magnetic measurements tallied.

3.5.2 $Co_{80}Ni_{20}$ nanoparticles

The majority of samples made during the course of this investigation have had a composition of $Co_{80}Ni_{20}$. The particles described in this section were made with acetylacetonate salts, platinum seeds and an OA/OY surfactant mixture. The particles that were initially made, using acetate salts, did display exchange bias in some instances (section 3.3.1). However, the particles made with the acetates method were predominantly too small to support oxide shell growth. The Yamamuro[16] method of synthesis was subsequently used as the particles formed using this method and acetylacetonate salts had displayed promising results in terms of particle size and magnetic properties. The $Co_{80}Ni_{20}$ particles made using the Yamamuro polyol process were consistently larger in size and hence were much more stable to oxidation. Figure

54 displays the M vs H loop for $Co_{80}Ni_{20}$ particles after cooling from 280 K to 10 K, in 0 kOe and 60 kOe fields.

Figure 54. M vs H plot of 12.0 nm $Co_{80}Ni_{20}$ nanoparticles made with acetylacetonate salts, OA/OY surfactant mixture and platinum seeds after field cooling, at 10 K in a 0 kOe and 60 kOe applied field.
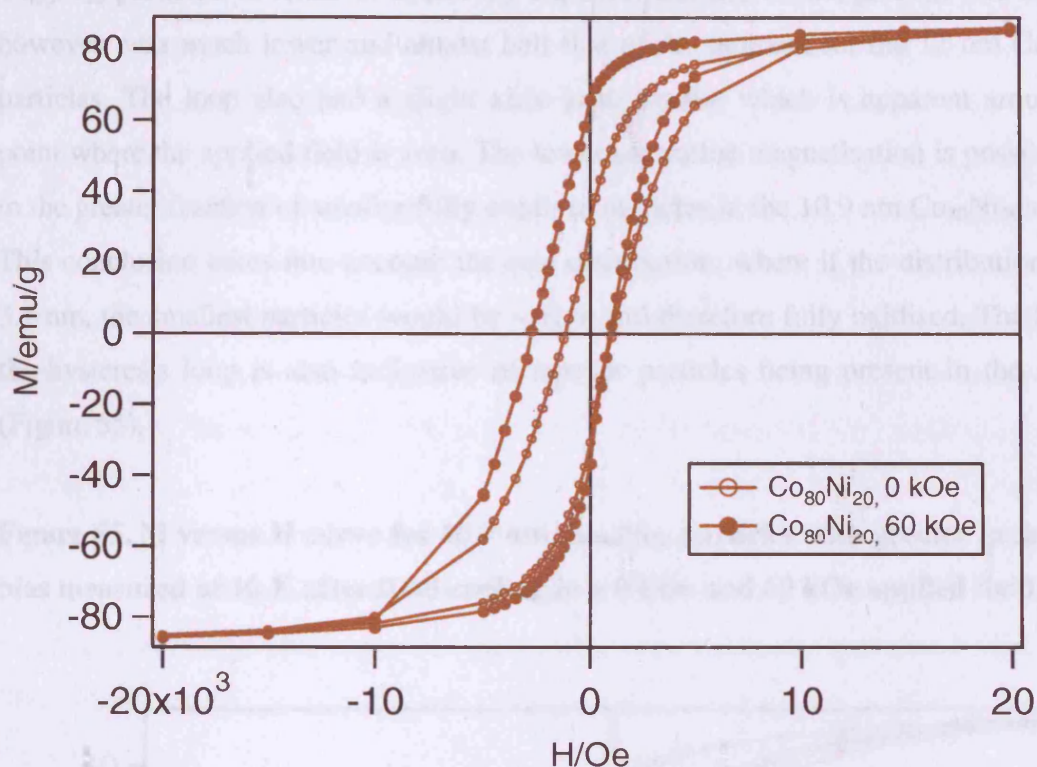
The key magnetic properties of the hysteresis loops in Figure 54 were determined and the coercivity was measured as 1110 Oe, after cooling in 0 kOe. The coercivity increased to 1840 Oe once the particles were field-cooled in a 60 kOe field. This represented an increase of 730 Oe. The enhancement in coercivity was an indicator of additional anisotropy being present in the particles. The exchange anisotropy was confirmed when the exchange field of the $Co_{80}Ni_{20}$ nanoparticles was measured, and found to be 910 Oe. The exchange field is a measure of the shift in the hysteresis loop from 0 kOe to 60 kOe. This was a promising breakthrough in terms of establishing a synthetic procedure, that yielded particles of good size and which exhibited exchange bias properties. The ZFC curve for these $Co_{80}Ni_{20}$ nanoparticles, measured at 100 Oe, displayed a steady monotonic increase and did not meet with the FC curve which followed a similar profile. Therefore, the particles did not seem to block within this range. The hysteresis loop of the $Co_{80}Ni_{20}$ nanoparticles indicates a ferromagnetic

material, at low temperatures. Therefore, the divergent ZFC and FC curves confirm the blocking temperature is >280 K. The ZFC/FC curves for the 12 nm $Co_{80}Ni_{20}$ particles can be seen in Figure 56 alongside the ZFC/FC curves for 10.9 nm $Co_{80}Ni_{20}$ particles.

A repeat of the synthesis, for the 12 nm particles described earlier, led to the production of $Co_{80}Ni_{20}$ particles that were 10.9 +/-3.1 nm in mean diameter. The particles in this sample exhibited even better magnetic properties than the 12.0 nm $Co_{80}Ni_{20}$ particles, in terms of coercivity enhancement and exchange bias. The moment however, was much lower and almost half that of the moment for the 12 nm $Co_{80}Ni_{20}$ particles. The loop also had a slight kink in its profile which is apparent around the point where the applied field is zero. The lower saturation magnetisation is possibly due to the greater fraction of smaller fully oxidised particles in the 10.9 nm $Co_{80}Ni_{20}$ sample. This conclusion takes into account the size distribution, where if the distribution is +/- 3.1 nm, the smallest particles would be ~ 7nm and therefore fully oxidised. The kink in the hysteresis loop is also indicative of smaller particles being present in the sample (Figure 55).

Figure 55. M versus H curve for 10.9 nm $Co_{80}Ni_{20}$ particles with greater exchange bias measured at 10 K after field cooling in a 0 kOe and 60 kOe applied field.
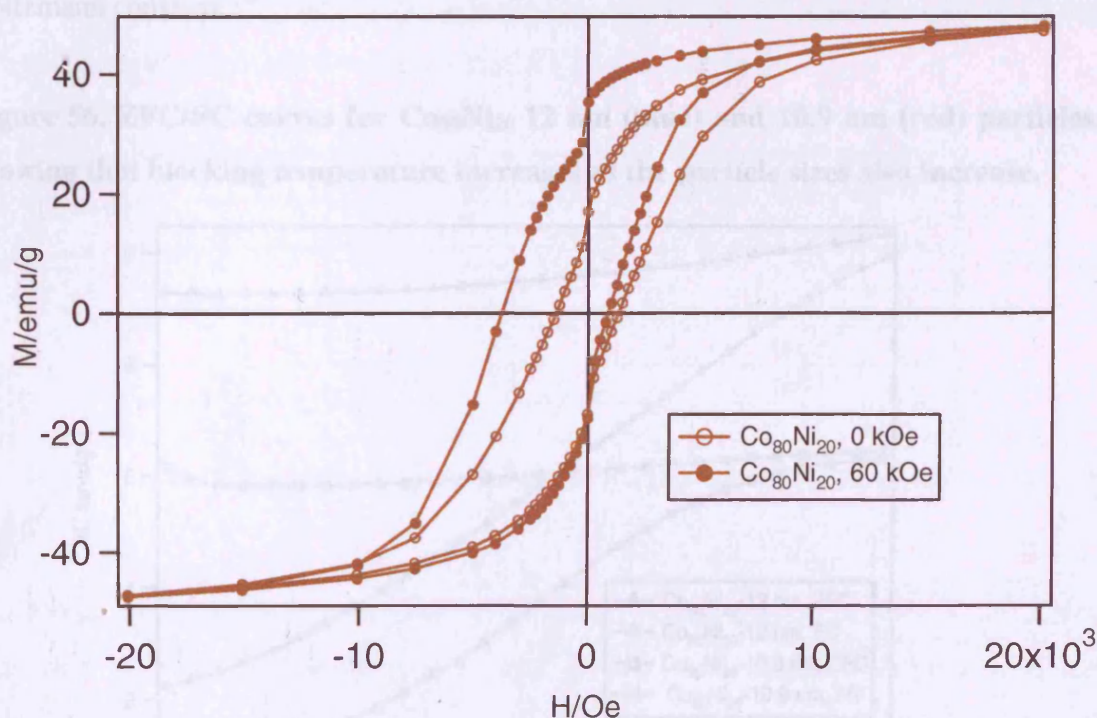
The saturation magnetisation of the 10.9 nm particles was 48 emu/g compared to 85 emu/g for the 12 nm particles described earlier. When the particles were field-cooled in a 60 kOe applied field, this resulted in an enhanced coercivity. The coercivity changed from 1390 Oe to 2340 Oe, a significant increase in the width of the loop, representing an approximate 70 % change. Compared to the 12 nm particles with a coercivity enhancement of 730 Oe, these particles displayed a 950 Oe enhancement. The overall value of 2340 Oe coercivity in a 60 kOe field is in the region of coercivity cited by Murdock et al,[39] to encode data on magnetic grains, as is the size of the particles produced. The exchange field exhibited by the particles was around 1440 Oe, showing a 60 % increase in the effect in comparison to the 12 nm $Co_{80}Ni_{20}$ particles.

The ZFC/FC curves displayed in Figure 56 show different characteristics, due to the variation in size of particles. The blue ZFC and FC traces (Figure 56) show that the curves do not meet by 280 K. However, as stated earlier, due to the ferromagnetic nature of the sample at low temperature, the particles would probably become blocked above 280 K. The red ZFC and FC curves, for the 10.9 nm $Co_{80}Ni_{20}$ particles, show the curves are about to meet at around 270 K. This correlates with previous studies that have suggested that the blocking temperature (T_b) of particles increases as particle size increases. This is because of the T_b following the relationship of $T_b = KV/30\ k_b$, where K is the anisotropy constant, V is the average volume of the particles and k_b is the Boltzmann constant. [38]

Figure 56. ZFC/FC curves for $Co_{80}Ni_{20}$ 12 nm (blue) and 10.9 nm (red) particles, showing that blocking temperature increases as the particle sizes also increase.
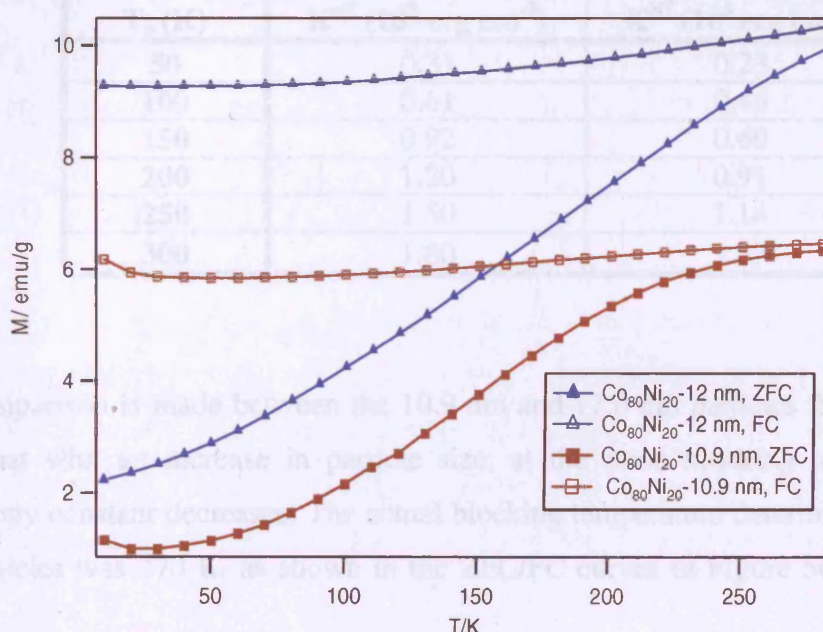
The relationship between blocking temperature and particle size has been investigated in detail, and the correlation between the two is evident. This helps to explain the relationship between the two $Co_{80}Ni_{20}$ samples with particles of different mean diameters and the convergence in the 12 nm $Co_{80}Ni_{20}$ particle's ZFC/ FC curves occurring after that of the 10.9 nm $Co_{80}Ni_{20}$ particles.

A comparison can be made between the 10.9 nm and 12.0 nm $Co_{80}Ni_{20}$ particles by looking at their anisotropy constants at estimated blocking temperatures. Table 3 shows the change in anisotropy constant (K^{eff}) with respect to a change in blocking temperature for particles with a constant volume. Table 5 shows that as the blocking temperature increases, the anisotropy constant for a particle with constant volume, also increases. This is shown for both the 10.9 nm and 12.0 nm $Co_{80}Ni_{20}$ particles. The anisotropy values quoted in Table 5 and 6 are actually effective anisotropies. This must be stipulated before any conclusions are made on the basis of these values, as the total anisotropy of nanoparticles is a component of the magnetocrystalline anisotropy (from Co_xNi_{1-x}), exchange anisotropy (from alloy/oxide interface and shape anisotropy (particle shapes). However, this exercise serves to model the expected values for particles of these particular volumes.

Table 5. Effective anisotropy constants of 10.9 nm and 12.0 nm, $Co_{80}Ni_{20}$ nanoparticles at estimated blocking temperatures (T_b). The equation for blocking temperature is rearranged to determine K ($T_b = KV/30\ k_b$).

T_b (K)	$Co_{80}Ni_{20}$ 10.9 nm K^{eff} (10^5 erg cm^{-3})	$Co_{80}Ni_{20}$ 12.0 nm K^{eff} (10^5 erg cm^{-3})
50	0.31	0.23
100	0.61	0.46
150	0.92	0.69
200	1.20	0.91
250	1.50	1.14
300	1.80	1.37

If a comparison is made between the 10.9 nm and 12.0 nm particles from Table 5 it is clear that with an increase in particle size, at the same blocking temperatures, the anisotropy constant decreases. The actual blocking temperature determined for the 10.9 nm particles was 270 K, as shown in the ZFC/FC curves in Figure 56. Therefore, the

anisotropy constant determined for the 10.9 nm $Co_{80}Ni_{20}$ particles, using the method used for calculating K in Table 5 was 1.65×10^5 erg cm^{-3}. The blocking temperature for the 12.0 nm particles cannot be given definitively, as the ZFC and FC curves for these particles do not meet. However, an estimate of the blocking temperature can be made, as it is known that it is definitely greater than 280 K. If the blocking temperature of these particles is taken as 310 K, this would yield anisotropy of 1.42×10^5 erg cm^{-3}.

The moment of the particles also increases as particle volume increases.[40] Effective anisotropy of the sample made in this study are calculated and shown in Table 4. Coercivity and saturation magnetisation are used to estimate K^{eff} using the relationship, $(H_c M_s)/2 = K^{eff}$ in this particular table.

Table 6. Effective anisotropy calculated using the coercivity and saturation magnetisations of the $Co_{80}Ni_{20}$ nanoparticles $((H_c M_s)/2 = K^{eff})$. The exchange field of the 10.9 nm and 12.0 nm particles are also shown.

	$Co_{80}Ni_{20}$ 10.9 nm		$Co_{80}Ni_{20}$ 12.0 nm	
	0 kOe field	60 kOe field	0 kOe field	60 kOe field
H_c/ Oe	1390	2340	1110	1840
M_s/emu/g	48	48	85	85
K^{eff}/ 10^5 erg cm^{-3}	0.33	0.56	0.47	0.78
H_{ex}/ Oe	/	1440	/	910

The effective anisotropies calculated in Table 6 yielded interesting results. Table 6 shows the effects of oxidation of the smaller particles on the anisotropy and gives a measure of the strength of the exchange anisotropy in the particles. This is shown by comparing the effective anisotropies of the particles are field-cooling in 0 kOe or 60 kOe.

The smaller particles in the 10.9 +/-3.1 nm sample, as mentioned earlier, were probably fully oxidised as they would have had a mean diameter of ~7 nm. If the size distribution in the 12.0 +/- 3.4 nm sample is taken into consideration, it is likely that some of the smaller particles will have oxidised, however less so than with the 10.9 nm particles. This is reflected in the difference in effective anisotropies, between the values in Table 5 and the values determined in Table 6, from the coercivities and saturation magnetisations of both sets of particle. The 270 K blocking temperature elucidated from

the ZFC/FC plots is quite high. Partial oxidation of metallic nanoparticles significantly increases the blocking temperature as shown in the study by Tracy *et al* [38] into cobalt nanoparticles. The blocking temperature is also linearly proportional to the volume, therefore the standard deviation obtained from TEM in terms of particle size can be translated into a standard deviation of 65 K, in the blocking temperature. These factors would have all contributed to the variations in blocking temperature.

The exchange fields cited in Table 6 are for the particles measured at 10 K after field-cooling in a 60 kOe field. The exchange coupling in the 10.9 nm and 12.0 nm $Co_{80}Ni_{20}$ particles becomes much stronger as particle diameter decreases. This was also observed in $Co_{80}Ni_{20}$ particles of different sizes made by Luna *et al* [6] using a different version of the polyol method.

Previous work carried out by Luna *et al* [6, 7] and Viau *et al* [3, 4] had also focussed upon the $Co_{80}Ni_{20}$ composition. However, the objectives in those particular studies were different to those expressed in this investigation. Luna *et al* [6, 7] reported a saturation magnetisation for 10 nm $Co_{80}Ni_{20}$ particles of approximately 45 emu/g. By comparison the 10.9 nm particles made in this study yielded a 48 emu/g saturation point. This compared well with the literature.[6] The mean diameter for another $Co_{80}Ni_{20}$ sample of particles, made in this study, was 12.0 +/- 3.4 nm. The magnetic moment for those particles was determined to be 85 emu/g at 10 K. Therefore, the results achieved here proved to be promising. This significantly larger moment was probably due to good crystallinity of the particles. Uniformity of alloying in the $Co_{80}Ni_{20}$ nanoparticles may have also contributed to the good magnetic moment exhibited. EELS studies carried out on the sample also evidenced the relative compositions between cobalt and nickel being approximately 4:1 in an individual core-shell nanoparticle. The larger particle diameter could have also contributed to the greater moment, as this has been shown in the literature to occur with various other metallic nanoparticles as particle size increases.

Metallic nanoparticle crystallinity has been investigated previously, and some research groups have induced greater crystallinity in nanoparticles by annealing them, so that the moment increases. The theoretical saturation magnetisation values for bulk cobalt and bulk nickel are 161 emu/g [38] and 55 emu/g [41] respectively. Therefore, by mixing the two elements, a magnetic moment between these values is likely. The size and hence oxidation of the particles is critical to the properties which have been described thus far, especially properties such as the moment. The broad size distribution of the particles, formed in this particular study has contributed to the variations in

moment, between samples of identical composition. Fractions of small oxidised superparamagnetic particles dispersed throughout a sample of core-shell ferromagnetic nanoparticles leads to a lower moment. This phenomenon also gives rise to the penguin-shaped hysteresis loops that have been observed. These arise due to the smaller particles being superparamagnetic at 10 K.

A model proposing the ideal conditions, for future ultra-high-density recording media was detailed in 1992, by Murdock *et al* [39] from the Hewlett Packard research laboratories in California. At that time, they had offered an insight into routes towards achieving 10 Gb/in^2 in media. They had discussed the need for uniform particles with a mean diameter of 8-10 nm or less, and a high H_c of approximately 2500 Oe was needed, to be able to encode data in individual magnetic grains. More recently, authors have sought to synthesise particles that self-organise into arrays and deliver an increase in magnetic recording densities, of between 100 Gb/in^2 and 1 Tb/in^2. [25, 42] A coercivity, in this particular region, was attained by the $Co_{80}Ni_{20}$ nanoparticles with a diameter of 10.9 nm in this study by comparison.

Generally speaking, the majority of particles synthesised in this study have been of the $Co_{80}Ni_{20}$ composition. Partly due to the fact that any similar work carried out in this area, has usually incorporated the study of this particular composition. Therefore, comparisons could be made between work carried out here, with other research work undertaken in this field. The size of particles does have a major influence on the magnetic properties, as has been seen in this study. It impacts upon the overall structure of the particles in terms of whether or not they form an oxide shell or completely oxidise, in addition to affecting properties such as the blocking temperature.

Composition can also affect the blocking temperature of particles, as shown in a study by Sangregorio *et al.*[43] They used the sol-gel technique to make Co_xNi_{1-x} particles and showed that increasing the nickel content in particles lowers the blocking temperature significantly. They had found that by adding just 20 % nickel to the composition of pure cobalt particles, the blocking temperature would be reduced to approximately 90 K from around 225 K for pure cobalt. Although this has thus far not been the case if a comparison is made between the cobalt particles described in section 3.5.1, when compared to the $Co_{80}Ni_{20}$ described in this section, these variations can be attributed to the inconsistencies in particle size between the different compositions. If the sizes were identical, it would much easier to build a picture of such properties, in a conclusive manner. This can be achieved by controlling the nucleation of the particles

better, and would form the basis of any future investigations.

3.5.3 $Co_{60}Ni_{40}$ nanoparticles

$Co_{60}Ni_{40}$ particles, made using the polyol method of synthesis, also exhibited interesting properties. There was slight bimodality exhibited in the distribution of the particles made of this composition. The mean diameter determined for the larger particles was 10.8 +/-1.9 nm, with the smaller particles yielding a mean of 6.4 +/- 0.9 nm. These particles yielded a saturation magnetisation of 38 emu/g.

Figure 57 (a) M-H loops in 0 kOe and 60 kOe after 10 K field-cooling from 280 K, for $Co_{60}Ni_{40}$ nanoparticles made with platinum seeds, OA/OY mixture and acetylacetonate salts (b) ZFC/FC curves for $Co_{60}Ni_{40}$ particles with $T_b> 280$ K.
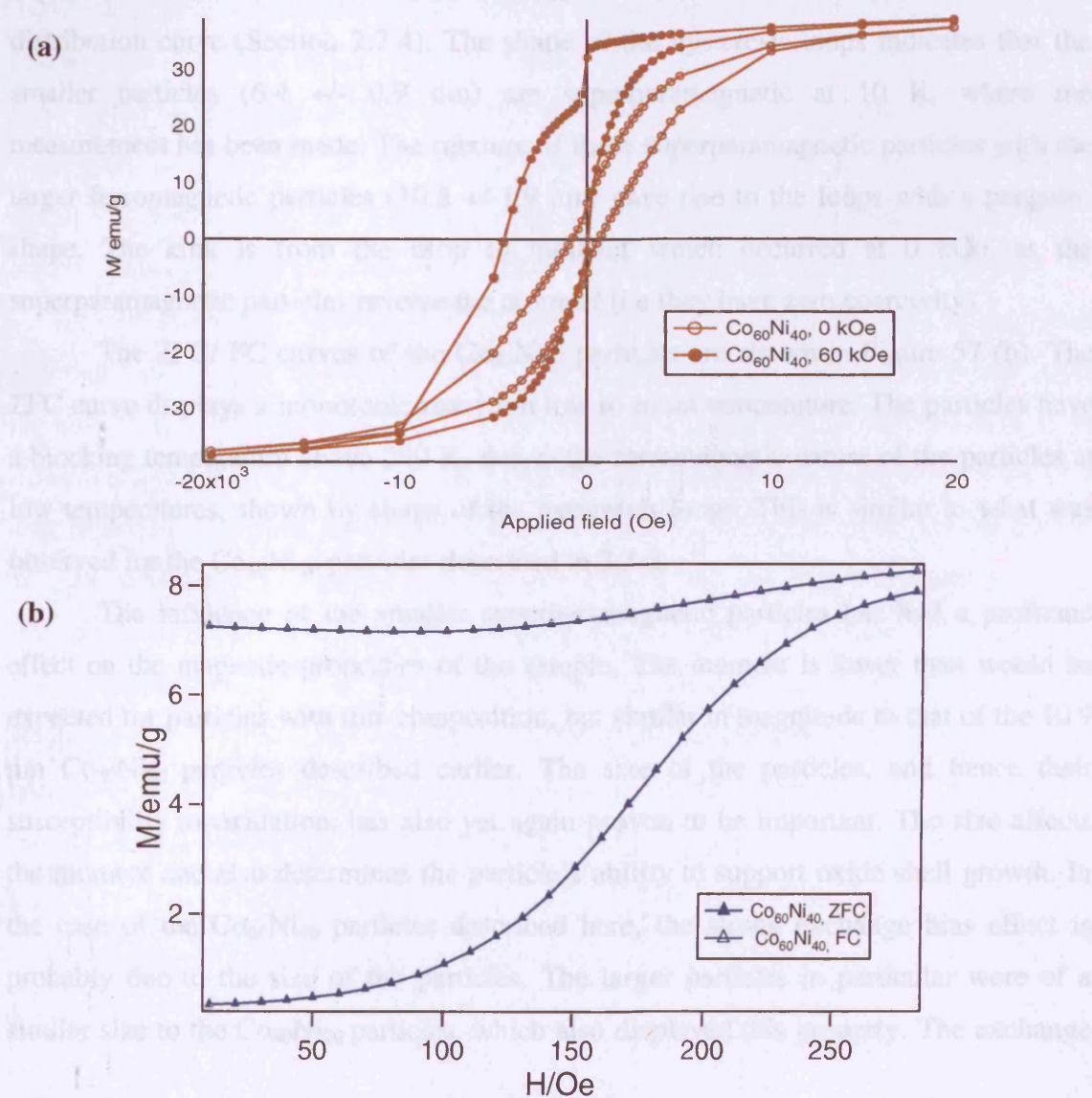
The M versus H curves after cooling in 0 kOe and 60 kOe fields, showed the interesting nature of these particles. Figure 57(a) displays the corresponding hysteresis loops. The zero-field curve yielded a coercivity of 405 Oe, and when a 60 kOe field was applied, this increased to 2250 Oe. The enhanced coercivity indicated an additional anisotropy in sample, namely exchange anisotropy. There was also a large exchange field of 2200 Oe, characterised by a shift in the hysteresis loop, when the particles were field-cooled.

The shape of the loop also changed considerably when the sample was field-cooled in 60 kOe. The loop was considerably "fatter" at the bottom, in comparison to the top. This may have been due to the phases present in the particles. The penguin-shape in the hysteresis loops has been characteristic in many of the particles described in this thesis. The size distributions in the samples are very important, as are the nucleation processes. The $Co_{60}Ni_{40}$ particles which have been described clearly experienced multi-modality in their nucleation, which led to two peaks in the size distribution curve (Section 2.7.4). The shape of the hysteresis loops indicates that the smaller particles (6.4 +/- 0.9 nm) are superparamagnetic at 10 K, where the measurement has been made. The mixture of these superparamagnetic particles with the larger ferromagnetic particles (10.8 +/-1.9 nm) gave rise to the loops with a penguin-shape. The kink is from the drop in moment which occurred at 0 kOe, as the superparamagnetic particles reverse the moment (i.e they have zero coercivity).

The ZFC/ FC curves of the $Co_{60}Ni_{40}$ particles are shown in Figure 57 (b). The ZFC curve displays a monotonic rise from low to room temperature. The particles have a blocking temperature above 280 K, due to the ferromagnetic nature of the particles at low temperatures, shown by shape of the hysteresis loops. This is similar to what was observed for the $Co_{80}Ni_{20}$ particles described in 3.5.2.

The influence of the smaller superparamagnetic particles has had a profound effect on the magnetic properties of the sample. The moment is lower than would be expected for particles with this composition, but similar in magnitude to that of the 10.9 nm $Co_{80}Ni_{20}$ particles described earlier. The size of the particles, and hence their susceptibility to oxidation, has also yet again proven to be important. The size affects the moment and also determines the particle's ability to support oxide shell growth. In the case of the $Co_{60}Ni_{40}$ particles described here, the strong exchange bias effect is probably due to the size of the particles. The larger particles in particular were of a similar size to the $Co_{80}Ni_{20}$ particles, which also displayed this property. The exchange

bias effect shown by the $Co_{60}Ni_{40}$ particles was stronger than that of the larger and similar sized 12.0 nm and 10.9 nm $Co_{80}Ni_{20}$ particles. Although 40 % nickel had been doped in, the particles showed an exchange bias that was comparable to the exchange field of the pure cobalt nanoparticles, made by similar methods and described in section 5.5.1 of Chapter 5. This was due to the size of the cobalt nanoparticles, overall, being smaller than that of the $Co_{60}Ni_{40}$ particles described here. The probability of the larger $Co_{60}Ni_{40}$ particles sample supporting oxide shell growth was greater. Although some of the larger particles in the cobalt sample could support the core-shell model, the majority were susceptible to oxidation. These slight variations in size can influence a particle's oxidation, due to the amount of surface area exposed to air.

3.5.4 $Co_{50}Ni_{50}$ nanoparticles

The results from this particular composition of particles proved to be very interesting, due to the 1: 1 mix of nickel and cobalt precursors, and hence the supposed effect this would have on the magnetic effects of the particles. The bimodal distribution of particle sizes had an influence on the moment due to the presence of smaller particles throughout the sample. The slightly elevated levels of oxygen, as evidenced by EDX, also indicate that smaller particles may have oxidised more so than in other samples.

The saturation magnetisation of the $Co_{50}Ni_{50}$ particles synthesised in our study was determined to be 57 emu/g using SQUID measurements. If compared to the curve of best fit that was experimentally determined by Toneguzzo et al[33] for saturation magnetisation of $Co_{50}Ni_{50}$ particles (Figure 58), this value correlated with that determined by their research group. The value obtained by carrying out this calculation was approximately 58 emu/g. The curve of best fit for the $Co_{50}Ni_{50}$ (white squares trace) was extrapolated to a reciprocal radius value of 0.159 nm^{-1}. This value represented an average diameter of 12.6 nm (radius = 6.3 nm) for the particles, which was calculated through TEM analysis. The calculation served as an excellent first approximation, as the values for moment were almost identical, despite the multimodality in size distribution of the particles made in our study (section 2.7.5).

Figure 58. Saturation magnetisation, M_s, of $Co_{80}Ni_{20}$, $Co_{50}Ni_{50}$, $Co_{20}Ni_{80}$ and $Fe_{0.13}[Co_{50}Ni_{50}]_{0.87}$ versus the reciprocal of particles mean radius.[33]
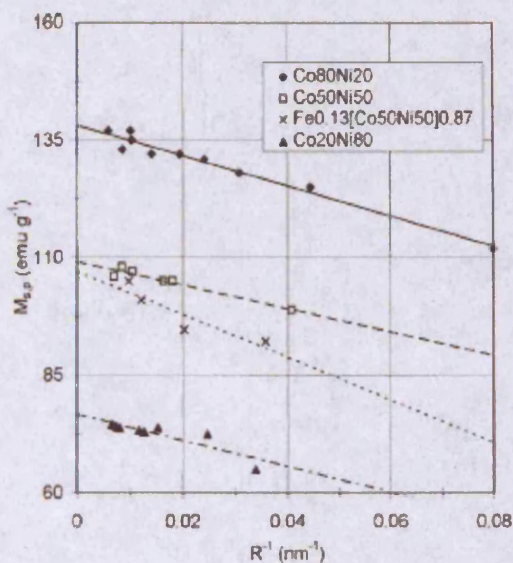
Figure 59 displays the exchange bias that is evident in the $Co_{50}Ni_{50}$ particles. Exchange bias had not been investigated prior to this, in $Co_{50}Ni_{50}$ particles made using the method adopted here and in particles of this small size. The coercivity of the particles with no applied field was 1240 Oe. This was quite a large value due to the large size of these particles, compared to the other particles described in this compositional series so far.

Figure 59. Hysteresis loops of $Co_{50}Ni_{50}$ after cooling from room temperature in 0 kOe (or 60 kOe) to 10 K.
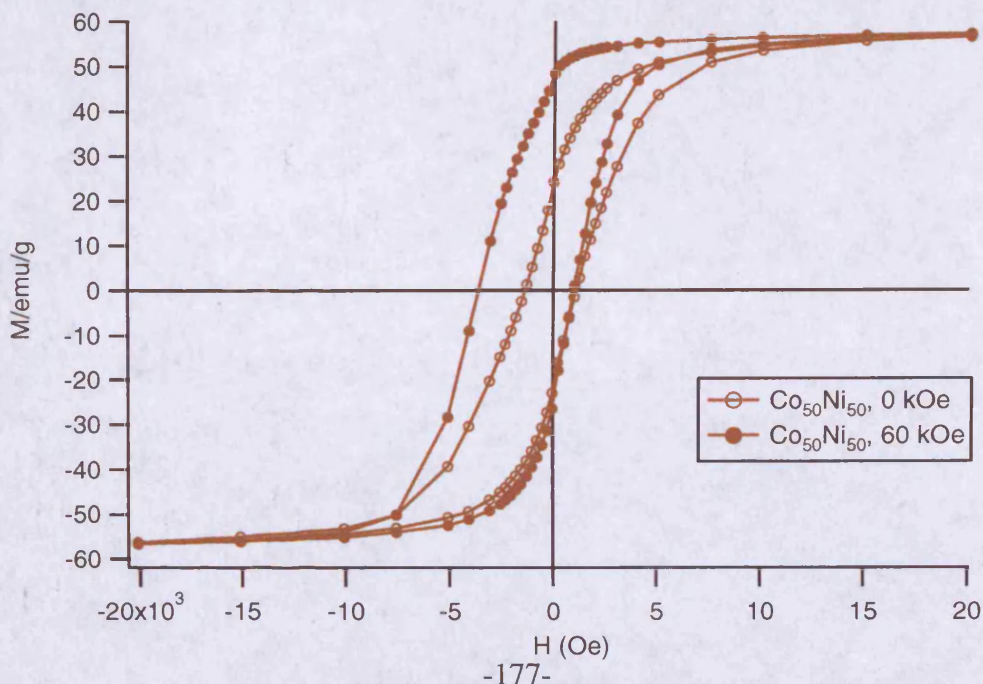
In the literature, single domain ferromagnetic particles exhibit an increase in coercivity as particle volume increases. This relationship continues to a maximum, after which the coercive force decreases due to the particle volume being too great for it to be single-domain, and multidomain particles become apparent. The coercivity decreases as the particle volume is reduced, until the particle becomes superparamagnetic (H_c).[40, 44] These particles therefore exhibit single-domain behaviour.

The coercivity of the $Co_{50}Ni_{50}$ particles increased to 2280 Oe, when they were field-cooled to 10 K in a 60 kOe field. The exchange field for these particles was 1290 Oe. The shift in the hysteresis loop, due to exchange bias, was slightly smaller than what has been seen for other alloys in this series with a higher abundance of cobalt in their compositions. This was a significant result, as the $Co_{40}Ni_{60}$ alloy particles that are discussed in section 3.5.5, displayed a larger exchange bias. However, this may be again due to the sizes of the particles formed. The particles formed with a composition of $Co_{40}Ni_{60}$ are marginally larger, 13.6 nm compared with the 12.6 nm determined here, for the $Co_{50}Ni_{50}$ particles.

The ZFC and FC curves for the $Co_{50}Ni_{50}$ particles, displayed a monotonic rise up to 280 K, where a peak appeared to form. The ZFC and FC curves also began to converge although a clear bifurcation point was not evident. The particles again showed evidence of blocking around room temperature, due to the characteristic ferromagnetic hysteresis loops at low temperature.

Toneguzzo and co-workers [5, 33] have investigated the magnetic properties of these $Co_{50}Ni_{50}$ particles in the past. Jeyadevan et al[35] reported the synthesis of 40 and 100 nm $Co_{50}Ni_{50}$ particles which were supposedly core-shell in structure. The particles made by the Jeyadevan group were annealed to induce oxidation and hence a core-shell structure.

3.5.5 $Co_{40}Ni_{60}$ nanoparticles

$Co_{40}Ni_{60}$ nanoparticles were made using methods described in Chapter 5 and displayed a bimodal distribution. The particle's mean diameters were 13.6 nm and 6.7 nm, respectively, for each set of particles across the bimodally distributed sample. The magnetic saturation point determined for these particles was 42 emu/g. A repeat synthesis of the $Co_{40}Ni_{60}$ particles yielded a saturation magnetisation of 30 emu/g. The second $Co_{40}Ni_{60}$ sample was much larger in size, with a mean diameter of 17.4 nm.

The 13.6 nm particles displayed a larger moment, but were much smaller in size. This conflicts with the results that have been observed thus far. It is normally the case that the larger the particles, the greater the saturation magnetisation will be.[33] However, in the scheme of things the difference between the saturations points is relatively small. The difference could have arisen due to the contribution made by the oxide shell.

The shape of the loop was again penguin-shaped, with a thinner top portion and a fatter bottom portion. The 13.6 nm particles displayed exchange bias and an enhanced coercivity. The loop's exchange field was 1590 Oe after field-cooling in a 60 kOe field at 10 K. The coercivity increased from 1080 Oe in a 0 kOe field, to 2220 Oe in a 60 kOe field, after field-cooling. The second sample, with 17.4 nm sized particles also exhibited exchange bias with an exchange field of 1760 Oe. This was an improvement upon the exchange field shown by the 13.6 nm particles. The enhanced coercivity, after the application of a magnetic field, for the 17.4 nm particles was an increase of 560 Oe (0 kOe) to 1840 Oe (60 kOe).

The ZFC and FC curves, for the samples with different 13.6 and 17.4 nm mean diameters respectively, were very similar. Both did not display blocking temperatures, as the convergence of the ZFC and FC curves did not occur. The plots also both illustrated the beginnings of peak formation in the ZFC curve, at around 280 K. These results showed that exchange bias effect has slightly increased as the nickel concentration in the particles has been increased. This result showed that the exchange field of the particles were following a general trend of decreasing over the whole series, although the results are variable and would need further tests to confirm this relationship if the particles were all of the same size, and followed a monomodal distribution.

3.5.6 $Co_{20}Ni_{80}$ nanoparticles

As has been discussed in chapter 2, $Co_{20}Ni_{80}$ particles were made with both acetate and acetylacetonate salts. The particles that were synthesised using the acetate salts, were large in size and hence it was believed they would be large enough to support a passivating oxide layer. However, subsequent magnetic measurements that were carried out, painted another picture altogether. Figure 60 displays the hysteresis measurement for $Co_{20}Ni_{80}$ particles made with acetate salts, oleic acid and platinum seeds.

Figure 60. Hysteresis loop of $Co_{20}Ni_{80}$ particles, with a mean diameter of 16.2 nm, made using acetate salts, oleic acid and platinum seeds after field-cooling to 10 K in a 60 kOe field.
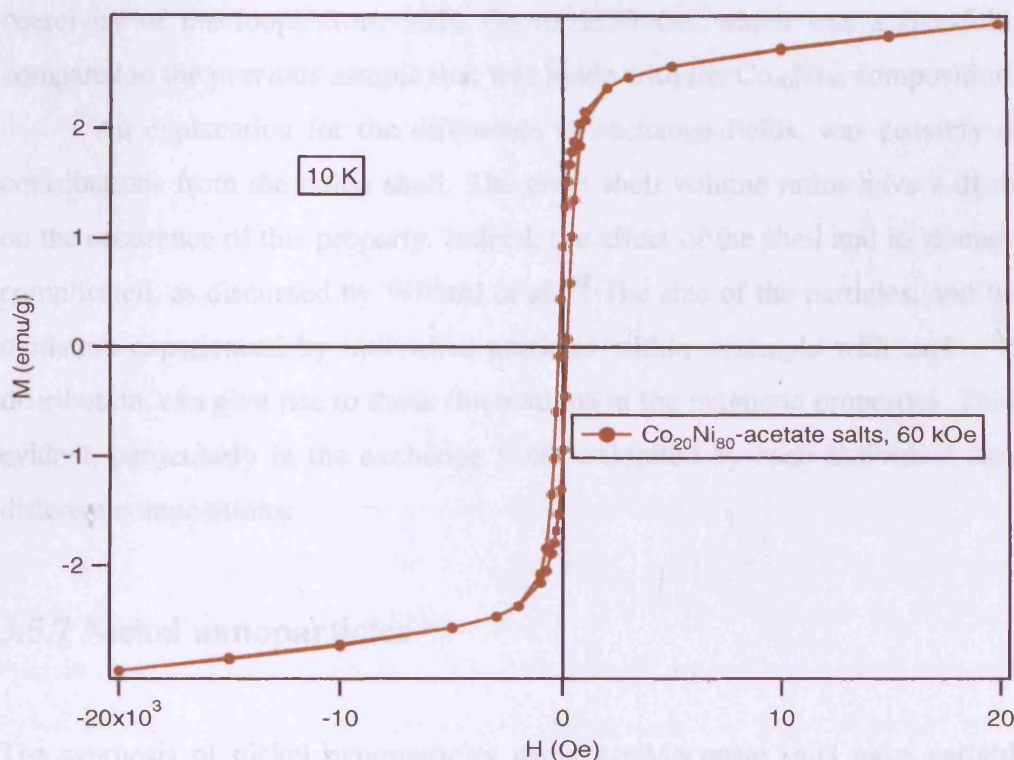
The magnetic moment of the particles was extremely low (3 emu/g). The multi-grain structure that was evident, in the particles, meant that it was highly possible that smaller particles coalesced to form the larger particle, resulting in a polycrystal. This could have contributed to the low moment and lack of exchange bias. The acetate salts method was deemed to be ineffective, as was the sole use of oleic acid as a surfactant, early on during this investigation. Therefore, later syntheses of the $Co_{20}Ni_{80}$ particles, using acetylacetonate salts, OA/OY surfactant mixture and platinum seeds, were implemented

to synthesise larger, single crystal particles. This method yielded larger particles and has been much more reproducible in comparison to the acetate salts method. The particles formed with this approach displayed a bimodal distribution however, between a range of 6-22 nm, 59 % of the population was above 10 nm. The mean diameter for the sample overall was 13 nm. The results here, in terms of particle size showed that as the nickel loading in the particles increased, the average size of particles also increased somewhat.

The first sample that was made using the acetylacetonate salts had a saturation magnetisation of 29 emu/g. The coercivity increased by 80 Oe, from 570 Oe to 650 Oe, when a 60 kOe field was applied. The exchange field was determined as 140 Oe. The second sample that was made with this composition, using the same synthetic methods, had a larger exchange field of 760 Oe. This coincided with an enhancement in the coercivity of the loops from 1050 Oe to 1530 Oe, which was a five-fold increase compared to the previous sample that was made with the $Co_{20}Ni_{80}$ composition.

An explanation for the difference in exchange fields, was possibly due to the contributions from the oxide shell. The core: shell volume ratios have a distinct effect on the occurence of this property. Indeed, the effect of the shell and its diameter is very complicated, as discussed by Willard et al. [32] The size of the particles, and the level of oxidation experienced by individual particles within a sample with such a broad size distribution, can give rise to these fluctuations in the magnetic properties. This has been evident, particularly in the exchange fields exhibited by each individual sample, with different compositions.

3.5.7 Nickel nanoparticles

The synthesis of nickel nanoparticles using acetylacenate salts gave variable results. This may have been due to the use of oleic acid and oleylamine as surfactant stabilisers. Previous attempts to make nickel nanoparticles, of a similar size to the Co_xNi_{1-x} alloy particles which had displayed exchange bias, yielded varied results and were heavily dependent on the specific reaction conditions. Conducting the experiment without seeds led to particles of between 60-150 nm in mean diameter and hence a large magnetic moment. Exchange bias is an interfacial effect, and the absence of this effect in the nickel nanoparticles was probably due to the large size of the particles leading to a

relatively small percentage of atoms at the interface.

The nickel particles that were synthesised, following modifications to the synthesis, displayed the largest mean diameter of all the particles that were made throughout the study. The particles had a mean diameter of 16.1 +/2.8 nm. The structure of the nickel particles varied somewhat in comparison to the pure cobalt and Co_xNi_{1-x} alloy particles that have been synthesised throughout this study. The particles appeared to be single crystal and of a larger size (section 2.7.8). However, they did not respond to a magnet at room temperature and this indicated they were likely to be fully oxidised,

The nickel nanoparticles made here, displayed very small coercivities in 0 kOe and 60 kOe fields which could not be distinguished from zero, and did not display exchange bias. This was also the case with the repeat syntheses that were carried out. The saturation magnetisation was extremely low at 1.7 emu/g. The particles behave as paramagnets, because the magnetic moment exhibited a linear change with respect to the applied magnetic field in a hysteresis loop measured at 10 K. The form of the ZFC and FC curves was a monotonic decrease. The nickel particles, therefore appeared to be fully oxidised, maybe as a consequence of poor surface coating with the OA/OY surfactant, in comparison to the cobalt containing samples.

The magnetic properties found in this study, correlated very well with results from a similar study of Ni and NiO nanoparticles, carried out by Park et al.[45] Thermal decomposition of a nickel-oleylamine complex had previously been used by Park[45], as a method of synthesising Ni and NiO particles, with trioctylphosphine introduced in a further surfactant addition, after nucleation has occurred. The laser ablation technique has also been employed in the past, to make core-shell Ni/NiO nanoparticles from between 5-20 nm in mean diameter, by Seto et al.[46] Low moment in NiO nanoparticles was observed in an investigation by Park et al,[45] where particles of between 2-7 nm exhibited moments of approximately the same order as those observed in this study.

In Park's study, magnetic measurements carried out below 10 K yielded blocking temperatures of 2 K and 5 K, for the respective 2 nm and 7 nm NiO particles. In comparison, the ZFC/FC curves for the Ni particles made using polyol methods did not display any signs of features such as a peak, although the measurements began at 10 K and so it would be interesting to measure hysteresis loops at 2 and 5 K to eliminate the existence of any hysteresis.

3.6 Summary

The magnetic properties of samples made in a variety of compositions were measured in detail. Comparisons were made between properties such as coercivity (H$_c$), saturation magnetisation (M$_s$) and exchange field (H$_e$) to the composition of the particles (Co$_x$Ni$_{1-x}$). It was therefore possible to gain an understanding of, and map the effects of compositional change on the intrinsic properties of the nanoparticles.

If the highest values, for the respective magnetic properties, are plotted against the size or composition of the nanoparticles, some general patterns can be unearthed. For instance, Figure 61(a) displays the changes in coercivity as a consequence of increasing the cobalt loading within the nanoparticles. The general trend of the plot evidences the positive correlation between increasing cobalt loading and hence the coercivity in a 60 kOe applied magnetic field. The nickel particles are denoted by 0 molar % of cobalt content, shown on the graph, and have a small coercivity. The change in composition by doping 20 molar% of cobalt, improved the coercivity of the particles by 80 times the original value. The effect of cobalt doping between 40-60 % of the total composition causes the coercivity to plateau, before increasing when cobalt forms approximately 80 % of the particles composition. The pure cobalt nanoparticles displayed the highest coercivity, however, the results show that by varying composition it is possible to control the magnetic properties of a core-shell nanoparticle. The same was true of the exchange field exhibited by each of the samples.

Figure 61 (a) Cobalt content versus coercivity and (b) Cobalt content versus exchange field, of Co$_x$Ni$_{1-x}$ nanoparticles, after field-cooling in a 60 kOe field at 10 K
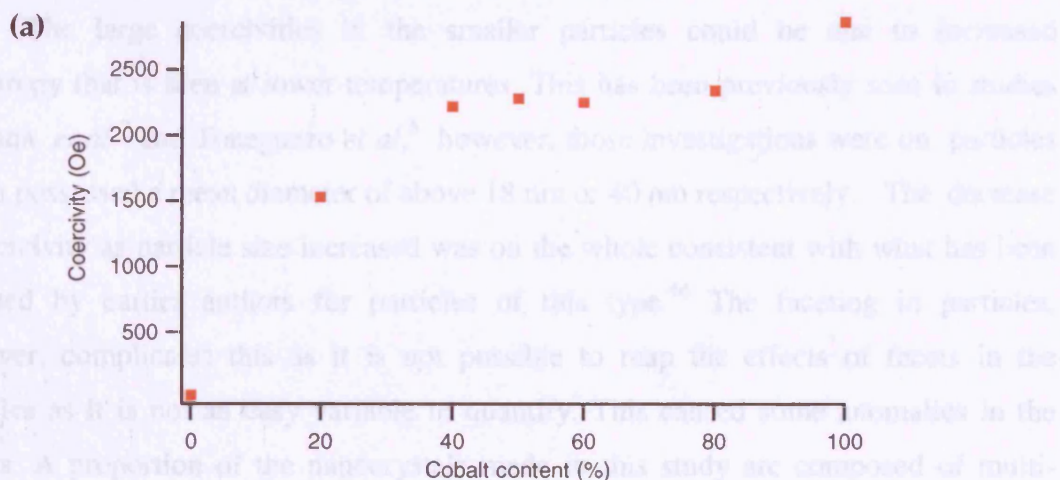
(b)
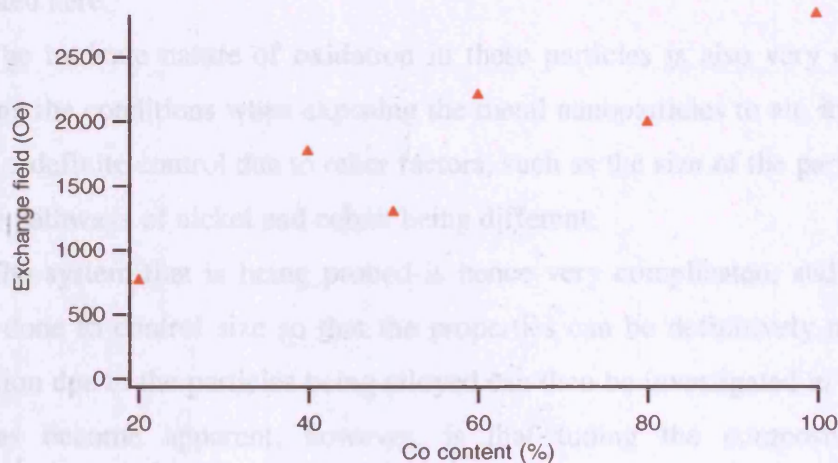
In general terms, the magnitude of the loop shift, due to exchange bias, increases with cobalt concentration. The changes in exchange bias with increased cobalt content are however, slightly erratic, and the correlation between the two should be investigated further. The fluctuations in the exchange bias, which is evident in Figure 61 (b), are probably due to the size distributions of the particles and the occurrence of multiple nucleation events during the syntheses. Plotting the same magnetic data versus mean diameter of the particles shows that as the particle size increases, the exchange field and coercivity both decrease. The smaller particles seemed to have, in general, larger coercivities when field cooled and correspondingly larger exchange bias. The largest particles, which incidentally happened to be particles with a higher proportion of nickel: cobalt in their make-up, were those which had the smallest exchange bias effects and lowest coercivity in the 60 kOe applied field. Those particles also seemed to have the least concentration of atomic oxygen measured by EDX.

The large coercivities in the smaller particles could be due to increased anisotropy that is seen at lower temperatures. This has been previously seen in studies by Luna *et al* [7] and Toneguzzo *et al*,[5] however, those investigations were on particles which possessed a mean diameter of above 18 nm or 40 nm respectively. The decrease in coercivity as particle size increased was on the whole consistent with what has been reported by earlier authors for particles of this type.[44] The faceting in particles, however, complicates this as it is not possible to map the effects of facets in the particles as it is not an easy variable to quantify. This caused some anomalies in the results. A proportion of the nanocrystals made in this study are composed of multi-

grains, hence the problems in obtaining meaningful XRD data. This must have also contributed to the irregularities in some of the magnetic properties of samples investigated here.

The intricate nature of oxidation in these particles is also very clear. Despite controlling the conditions when exposing the metal nanoparticles to air, it is difficult to maintain a definite control due to other factors, such as the size of the particles, and the oxidative pathways of nickel and cobalt being different.

The system that is being probed is hence very complicated, and further work must be done to control size so that the properties can be definitively modelled. The contribution due to the particles being alloyed can then be investigated in further detail. What has become apparent, however, is that tuning the composition of alloy nanoparticles can control their magnetic properties. These investigations have highlighted the various factors which contribute to creating nanoparticles with good magnetic properties.

3.6.1 Summary table

Composition	Salt	M_s/emu/g	H_c/ 0 kOe	H_c/ 60 kOe	H_{ex}/ Oe	$K^{eff}/10^5$ erg cm^{-3}	T_b/ K	Description (ZFC/FC curves)	Size/ Nm	Comments
Co	Acet	53	1570	1910	600	0.51	>280 K		/	/
Co	Acac	35	620	2020	2000	0.35	~280 K	shoulder in ZFC around 70K, broad peak from ~190K	9.4 +/- 1.8 and 5.5 +/- 0.7	8.8 +/- 2.2 (overall) SB
Co	Acac	23	1170	2860	2830	0.33	~270 K	shoulder in ZFC at ~40K, and broad peak at ~240K	8.6 +/- 2.4	SB
Co$_{80}$Ni$_{20}$	Acac	85	1110	1840	910	0.78	>280 K	monotonic increase, peak not visible at 280K	12.0 +/- 3.4	M
Co$_{80}$Ni$_{20}$	Acac	48	1390	2340	1440	0.56	>280 K	decrease between 10-20K in ZFC. Curves haven't met by 280K, but looks like beginning of peak	10.9 +/- 3.1	M
Co$_{60}$Ni$_{40}$	Acac	38	720	2250	2200	0.43	>280 K	monotonic increase, curves have not met by 280 K.	10.8 +/-1.9 and 6.4 +/- 0.9	BM
Co$_{50}$Ni$_{50}$	Acac	57	1240	2280	1290	0.65	>280 K	monotonic increase, curves have not met by 280K, looks like ZFC peak just beginning	12.6 +/-9.6	MM
Co$_{40}$Ni$_{60}$	Acac	42	1080	2220	1590	0.47	>280 K	ZFC is maybe beginning to reach peak at 280 K; ZFC/FC haven't met by 280 K	13.6 +/- 2.5 and 6.7 +/- 1.4	BM

Composition	Salt	M_s/emu/g	H_c/ 0 T	H_c/ 6 T	H_{ex}/ Oe	$K^{eff}/10^5$ erg cm^{-3}	T_b/ K	Description (ZFC/FC curves)	Size/ Nm	Comments
$Co_{40}Ni_{60}$	Acac	30	560	1850	1760	0.28	>280 K	ZFC and FC haven't met at 280 K; ZFC is begun to reach peak	13.6+/- 2.5 and 6.7 +/-1.4	BM
$Co_{20}Ni_{80}$	Acac	29	570	650	140	0.09	~250 K	shoulder in ZFC around 70K, broad peak from ~190K	13.0 +/- 3.0 and 7.9 +/- 0.7	BM
$Co_{20}Ni_{80}$	Acac	11	1050	1530	760	0.08	~250 K	ZFC peak ~180 K, meets FC around 250 K	/	/
Ni	Acac	2	20	20	0	0.00	/	monotonic decrease	16.0 +/- 5.6	M

Key:-

Acac- Acetylacetonate salt

Acet- Acetate salt

SB-Slightly bimodal

M- Monomodal

BM- Bimodal

MM- Multimodal

M-Monomodal

/-TEM analysis failed

3.7 Conclusions

This chapter has described detailed investigations into the magnetic properties of Co_xNi_{1-x}, fully and partially oxidised nanoparticles. The partially oxidised particles have indicated core-shell texture due to the evidence of an additional anisotropy which has been induced in the particles. This anisotropy gave rise to shifts in the hysteresis plots of many of the particles, when they were field-cooled in an applied magnetic field. Hence, exchange bias was evident in particles that had been synthesised in a manner of different ways. Exchange bias also caused an enhancement in the coercivity (half-width) of the respective hysteresis loops, when the sample in question was placed in a magnetic field and cooled. These effects occur in metallic particles which are enveloped in an oxide shell coating, and were evident in many of the samples that have been discussed in this chapter.

The investigations showed that in general terms, the exchange bias effect seemed to decrease as more nickel was doped into the particles. The coercivity of the particles, with a low concentration of nickel, was also likely to be low in a 60 kOe field, at 10 K. However, this effect showed evidence of a plateau between cobalt concentrations of 40-80%. Further investigations would be required to verify this as size effects seemed to play a major role in magnetic properties of the particles.

Size seemed to affect the blocking temperatures of the particles, where it was possible to obtain them at all. With increases in particle size, the blocking temperature also seemed to increase. The size of particles seemed to affect their susceptibility to oxidation. Smaller particles seemed to tend towards full oxidation, whereas larger particles could support oxide shell growth. The oxide shell cannot be definitively claimed to be a "passivating oxide shell" as over time the samples lost their response to a magnet. This effect was dependent on the sample, however, the particles that displayed the largest magnitude exchange fields, tended to retain their responsiveness to a magnet at room temperature for several months. The samples that displayed a weak exchange bias effect, had oxidised much more quickly. Oxide inclusions within the shell and gradual oxidation of the core, due to degradation or loss of the surfactant could be the cause of this.

Interesting results were obtained through the use of AC susceptibility measurements, and this method enabled the characterisation of the core and shell's

respective blocking temperatures. This technique also helped to clarify ambiguous structural features in the ZFC and FC curves of the cobalt sample. This would be an interesting method of analysis to develop in the future, and use on similar particles to elucidate the structural profiles that are evident on occasions, in ZFC and FC plots.

These results have shown improvements, in terms of the exchange bias effects, previously reported for particles of this size and composition. Limitations with the nucleation of the particles have presented difficulties in terms of modelling the particles due to size. However, generic conclusions can be drawn in terms of the size effects. The great advancement that has been made, through this investigation, is that it has been proven that the magnetic properties can be tuned by varying the composition of the particles. This was the key objective that was set out at the beginning of this thesis, and the studies in this chapter have presented evidence that this can be achieved. Investigations carried out in Chapter 2, resulted in an optimisation of this process. This resulted in the advancements that have been documented in this chapter. More work must be done to improve the synthesis, so that the magnetic properties of the particles can be modelled, alongside the results achieved from the structural characterisation of the particles described in Chapter 2. Processes and investigations that could be carried out to achieve this in the future are highlighted in the next chapter.

3.8 References

1.   Nogues, J., Exchange bias in nanostructures. *Physics reports* **2005**, 422, (3), 65-117.

2.   Meiklejohn, W. H.; Bean, C. P., New Magnetic Anisotropy. *Physical Review* **1956**, 102, (5), 1413-1414.

3.   Viau, G.; Toneguzzo, P.; Pierrard, A.; Acher, O.; Fievet-Vincent, F.; Fievet, F., Heterogeneous nucleation and growth of metal nanoparticles in polyols. *Scripta Materialia* **2001**, 44, (8-9), 2263-2267.

4.   Viau, G.; FievetVincent, F.; Fievet, F., Nucleation and growth of bimetallic CoNi and FeNi monodisperse particles prepared in polyols. *Solid State Ionics* **1996**, 84, (3-4), 259-270.

5.   Toneguzzo, P.; Acher, O.; Viau, G.; Pierrard, A.; Fievet-Vincent, F.; Fievet, F.; Rosenman, I., Static and dynamic magnetic properties of fine CoNi and FeCoNi particles synthesized by the polyol process. *Ieee Transactions on Magnetics* **1999**, 35, (5), 3469-3471.

6.   Luna, C.; Morales, M. D.; Serna, C. J.; Vazquez, M., Exchange anisotropy in Co80Ni20/oxide nanoparticles. *Nanotechnology* **2004**, 15, (4), S293-S297.

7.   Luna, C.; Morales, M. D.; Serna, C. J.; Vazquez, M., Multidomain to single-domain transition for uniform Co80Ni20 nanoparticles. *Nanotechnology* **2003**, 14, (2), 268-272.

8.   Viau, G.; FievetVincent, F.; Fievet, F., Monodisperse iron-based particles: Precipitation in liquid polyols. *Journal of Materials Chemistry* **1996**, 6, (6), 1047-1053.

9.   Chakroune, N.; Viau, G.; Ricolleau, C.; Fievet-Vincent, F.; Fievet, F., Cobalt-based anisotropic particles prepared by the polyol process. *Journal of Materials Chemistry* **2003**, 13, (2), 312-318.

10.   Toneguzzo, P.; Viau, G.; Acher, O.; Fievet-Vincent, F.; Fievet, F., Monodisperse ferromagnetic particles for microwave applications. *Advanced Materials* **1998**, 10, (13), 1032-1035.

11.   Patel, J., Farrell, D., Pankhurst, Q.A.;Parkin, I. P.,, Particle size and oxidation in CoNi nanoparticles. *Mater Res Soc Symp Proc* **2005**, 877E S5 8 1-6.

12.   Becker, J. J., Surface Effects on Hysteresis Loop Shapes in High-Coercive-Force Crystallized Amorphous-Alloys. *Ieee Transactions on Magnetics* **1982**, 18, (6), 1451-1453.

13.   Roberts, A. P.; Cui, Y. L.; Verosub, K. L., Wasp-Waisted Hysteresis Loops - Mineral Magnetic Characteristics and Discrimination of Components in Mixed Magnetic Systems. *Journal of Geophysical Research-Solid Earth* **1995**, 100, (B9), 17909-17924.

14.   Tauxe, L.; Mullender, T. A. T.; Pick, T., Potbellies, wasp-waists, and superparamagnetism in magnetic hysteresis. *Journal of Geophysical Research-Solid Earth* **1996**, 101, (B1), 571-583.

15.   Linford, N., Archaeological applications of naturally occurring nanomagnets. In *Fifth International Conference on Fine Particle Magnetism*, Pankhurst, Q., Ed. 2005; Vol. 17, pp 127-144.

16.   Yamamuro, S. A., T.;Sumiyama, K.; Uchida, T., Kojima, I.,, Monodisperse metallic iron nanoparticles synthesized from noncarbonyl complexes. *Japanese Journal of Applied Physics* **2004**, 44, (No 7A), 4458-4459.

17.   Giersig, M.; Hilgendorff, M., Magnetic nanoparticle superstructures. *European Journal of Inorganic Chemistry* **2005**, (18), 3571-3583.

18.   Stamps, R. L., Mechanisms for exchange bias. *Journal of Physics D-Applied Physics* **2000**, 33, (23), R247-R268.   .

19.   Nogues, J.; Schuller, I. K., Exchange bias. *Journal of Magnetism and Magnetic Materials* **1999**, 192, (2), 203-232.

20.   Nogues, J., Exchange bias in ferromagnetic nanoparticies embedded in an antiferromagnetic matrix. *International journal of nanotechnology* **2005**, 2, (1-2), 23-42.

21.   Ung, D.; Viau, G.; Ricolleau, C.; Warmont, F.; Gredin, P.; Fievet, F. F., CoNi nanowires synthesized by heterogeneous nucleation in liquid polyol. *Advanced Materials* **2005**, 17, (3), 338-344.

22.   Ung, D.; Viau, G.; Fievet-Vincent, F.; Herbst, F.; Richard, V.; Fievet, F., Magnetic nanoparticles with hybrid shape. *Progress in Solid State Chemistry* **2005**, 33, (2-4), 137-145.

23.   Luna, C.; Morales, M. P.; Serna, C. J.; Vazquez, M., Effects of surfactants on the particle morphology and self-organization of Co nanocrystals. *Materials*

Science & Engineering C-Biomimetic and Supramolecular Systems **2003**, 23, (6-8), 1129-1132.

24.   Bao, Y. P.; Beerman, M.; Pakhomov, A. B.; Krishnan, K. M., Controlled crystalline structure and surface stability of cobalt nanocrystals. *Journal of Physical Chemistry B* **2005**, 109, (15), 7220-7222.

25.   Sun, S. H.; Murray, C. B.; Weller, D.; Folks, L.; Moser, A., Monodisperse FePt nanoparticles and ferromagnetic FePt nanocrystal superlattices. *Science* **2000**, 287, (5460), 1989-1992.

26.   Lu, A. H.; Li, W. C.; Matoussevitch, N.; Spliethoff, B.; Bonnemann, H.; Schuth, F., Highly stable carbon-protected cobalt nanoparticles and graphite shells. *Chemical Communications* **2005**, (1), 98-100.

27.   Bertotti, G., *Hysteresis in magnetism: for physicists, material scientists and engineers*. 1998.

28.   Chantrell, R. W.; Weller, D.; Klemmer, T. J.; Sun, S.; Fullerton, E. E., Model of the magnetic properties of FePt granular media. *Journal of Applied Physics* **2002**, 91, (10), 6866-6868.

29.   Darling, S. B.; Bader, S. D., A materials chemistry perspective on nanomagnetism. *Journal of Materials Chemistry* **2005**, 15, (39), 4189-4195.

30.   Murray, C. B.; Sun, S. H.; Gaschler, W.; Doyle, H.; Betley, T. A.; Kagan, C. R., Colloidal synthesis of nanocrystals and nanocrystal superlattices. *Ibm Journal of Research and Development* **2001**, 45, (1), 47-56.

31.   Skumryev, V., Stoyanov,S., Zhang,Y., Hadjipanayis, G.,Givord, D., Nogués, J.,, Beating the superparamagnetic limit with exchange bias. *Nature* **2003**, 423, 850-853

32.   Willard, M. A.; Kurihara, L. K.; Carpenter, E. E.; Calvin, S.; Harris, V. G., Chemically prepared magnetic nanoparticles. *International Materials Reviews* **2004**, 49, (3-4), 125-170.

33.   Toneguzzo, P.; Viau, G.; Acher, O.; Guillet, F.; Bruneton, E.; Fievet-Vincent, F.; Fievet, F., CoNi and FeCoNi fine particles prepared by the polyol process: Physico-chemical characterization and dynamic magnetic properties. *Journal of Materials Science* **2000**, 35, (15), 3767-3784.

34.   Fievet, F.; Lagier, J. P.; Blin, B.; Beaudoin, B.; Figlarz, M., Homogeneous and Heterogeneous Nucleations in the Polyol Process for the Preparation of Micron and Sub-Micron Size Metal Particles. *Solid State Ionics* **1989**, 32-3, 198-205.

35.   Jeyadevan, B.; Chinnasamy, C. N.; Perales-Perez, O.; Iwasaki, Y.; Hobo, A.; Shinoda, K.; Tohji, K.; Kasuya, A., Synthesis and magnetic properties of core-shell structured (NiCo)O(AFM)-NiCo(FM) magnetic nanoparticles. *Ieee Transactions on Magnetics* **2002**, 38, (5), 2595-2597.

36.   Park, J.; An, K. J.; Hwang, Y. S.; Park, J. G.; Noh, H. J.; Kim, J. Y.; Park, J. H.; Hwang, N. M.; Hyeon, T., Ultra-large-scale syntheses of monodisperse nanocrystals. *Nature Materials* **2004**, 3, (12), 891-895.

37.   Spasova, M.; Wiedwald, U.; Farle, M.; Radetic, T.; Dahmen, U.; Hilgendorff, M.; Giersig, M., Temperature dependence of exchange anisotropy in monodisperse cobalt nanoparticles with a cobalt oxide shell. *Journal of Magnetism and Magnetic Materials* **2004**, 272-276, (Part 2), 1508-1509.

38.   Tracy, J. B.; Weiss, D. N.; Dinega, D. P.; Bawendi, M. G., Exchange biasing and magnetic properties of partially and fully oxidized colloidal cobalt nanoparticles. *Physical Review B* **2005**, 72, (6).

39.   Murdock, E. S., Roadmap for 10 $GBit/in^2$ media- Challenges. *IEEE transactions on magnetics* **1992**, 28, (5), 3078-3083.

40.   Klabunde, K., *Nanoscale Materials in Chemistry*. Wiley: 2001.

41.   Nayak, B. B.; Vitta, S.; Nigam, A. K.; Bahadur, D., Ni and Ni-nickel oxide nanoparticles with different shapes and a core-shell structure. *Thin Solid Films* **2006**, 505, (1-2), 109-112.

42.   Sun, S. H.; Murray, C. B., Synthesis of monodisperse cobalt nanocrystals and their assembly into magnetic superlattices (invited). *Journal of Applied Physics* **1999**, 85, (8), 4325-4330.

43.   Sangregorio, C.; Fernandez, C. d. J.; Battaglin, G.; De, G.; Gatteschi, D.; Mattei, G.; Mazzoldi, P., Magnetic properties of Co-Ni alloy nanoparticles prepared by the sol-gel technique. *Journal of Magnetism and Magnetic Materials* **2004**, 272-276, (Supplement 1), E1251-E1252.

44.   Sugimoto, T., *Monodispersed particles*. Elsevier: **2001**.

45.   Park, J.; Kang, E.; Son, S. U.; Park, H. M.; Lee, M. K.; Kim, J.; Kim, K. W.; Noh, H. J.; Park, J. H.; Bae, C. J.; Park, J. G.; Hyeon, T., Monodisperse nanoparticles of Ni and NiO: Synthesis, characterization, self-assembled superlattices, and catalytic applications in the Suzuki coupling reaction. *Advanced Materials* **2005**, 17, (4), 429-434.

46.   Sakiyama, K.; Koga, K.; Seto, T.; Hirasawa, M.; Orii, T., Formation of size-selected Ni/NiO core-shell particles by pulsed laser ablation. *Journal of Physical Chemistry B* **2004**, 108, (2), 523-529.

4. Conclusions and Future Work

4.1 Conclusions

4.1.1 Synthesis of Co_xNi_{1-x} nanoparticles

Co_xNi_{1-x}/CoNiO core-shell nanoparticles have been synthesised using a modified version of the polyol method. The particles varied in mean diameter from between 6-22 nm. A number of parameters were varied in order to optimise the synthesis, so that it was possible to fabricate a compositional series of Co_xNi_{1-x}/CoNiO alloy core-shell nanoparticles.

The three reaction parameters that were investigated in detail were nucleation methods, surfactants and composition. The particles were homogeneously nucleated, and heterogeneously nucleated with platinum seeds, preformed nanoparticles and noble metal seeds. The heterogeneous nucleation of particles using platinum seeds was the most effective for controlling particle size in this system. A number of surfactants were trialled, to test their ability to prevent agglomeration during particle growth, control

particle size and act as a barrier to prevent oxidation. Investigations into the binding of the surfactant with the metallic ion species in solution was carried out using UV-Vis studies. This indicated that the surfactants formed complexes with the metallic ion species, and it was these complexes that acted as nuclei for subsequent particle growth. The formation of these complexes was tracked and approximate nucleation and particle formation temperatures were determined for a range of particles that were synthesised.

The surfactant, which best provided these elements of control and contributed to the optimisation of the synthesis, was the 1:1 mixture of oleic acid and oleylamine. This particular mix enabled the formation of particles that were pre-dominantly air-stable and of a suitable size to warrant oxide shell growth, without oxidation occurring to the core of the particles. The unusual feature of using this surfactant mixture was the shape of the particles formed. Some were spherical, however, a large proportional of the particles produced were triangular, square and rhomboidal in shape. The optimisation of the synthetic process, in terms of nucleation and surfactant type was then completed, and it was subsequently possible to vary the composition of the particles.

Characterisation of the particles, and therefore the effectiveness of the synthetic process, was carried out using a number of techniques. Elemental analysis of the particles indicated that between 10-25% of the particle's mass was due to surfactant. This value was dependent upon how well the surfactant coated the nanoparticle surface and the ease with which it was washed away. EDX analysis showed that the molar ratios of precursor material, translated through to the relative atomic ratios of elements in the nanoparticulate powders.

The particles that were formed were characterised as being core-shell using the EELS and XPS techniques. EELS displayed a high concentration of oxygen atoms at the edges of individual particles that were measured. EELS also showed that the relative ratios between cobalt and nickel varied across a single particle, with the cores being slightly nickel-rich. This indicated that the nucleation of nickel occurred first during the synthesis of the particles. There was also oxygen present across the diameter of the particle, as an oxygen count was measured. The electron beam penetrated through the top and bottom of the particle and yielded a summed measure of the oxide shell. UV-Vis studies had also shown that the nucleation of nickel occurs slightly before that of cobalt.

XPS studies revealed a higher concentration of oxygen atoms bounds to cobalt and nickel at the surface of the nanoparticles. After a few etch cycles, the concentration of oxygen dramatically decreased and the concentration of cobalt bound to nickel, in a binary alloy was a dominant feature. The profiles of each of the samples that were measured all indicated core-shell morphology to the particles. This analysis also indicated evidence of nickel-rich cores, due to the marginally elevated concentration of nickel atoms, following a few etch cycles. The ratio between the nickel and cobalt atoms at various etching stages showed that this was more pronounced as the core of the particle was approached. The core-shell texture in particles was a prerequisite for the occurrence of exchange bias which is discussed in section 4.1.2.

XPS and XRD indicated that there could have been another oxide phase of cobalt present at the surface of the particles (Co_2O_3). XRD confirmed the dominant fcc phased for the cobalt, nickel, cobalt (II) oxide and nickel (II) oxide. In some samples, it was also possible to calculate crystallite size using Scherrer analysis. This indicated that in some samples, particles were composed of multigrains. TEM studies gave further evidence for this, as the multigrain structure in the individual particles could be seen. Finally, magnetic TGA studies showed that a solid solution and hence alloyed particles had been formed, as it was also possible to tune the Curie temperature of the particles.

4.1.2 Magnetic properties of Co_xNi_{1-x} nanoparticles

The magnetic properties of the Co_xNi_{1-x}/CoNiO core-shell nanoparticles have also been investigated in this thesis. Initially, room temperature hysteresis loops were measured of the samples, and if a large moment was evident and the particles responded to a magnet, then measurements were made at low temperatures using SQUID magnetometry. Only the most promising samples had measurements taken to determine whether or not they displayed the characteristic traits of exchange bias. Exchange anisotropy is characterised by an enhancement in the coercivity from 0 kOe to 6 kOe at low temperatures e.g 10 K. The measured hysteresis loop also shifts if exchange anisotropy is induced from the particles.

Particles that were not sufficiently stabilised, displayed hysteresis loops characteristic of polycrystalline antiferromagnets, as they oxidised fully to their cores. This was the case with many of the particles synthesised using oleic acid, oleylamine,

trioctylphosphine and tributylphosphine as sole surfactants. The particles synthesised using these surfactants were very small in mean diameter and so became fully oxidised upon exposure to air. However, the use of oleic acid and oleylamine in tandem, produced particles that were stabilised to oxidation and aggregation over prolonged periods of time. The oleic acid and oleylamine formed an amide when heated together, and this yielded a double-sheathed surfactant stabiliser. The use of this surfactant mixture allowed the growth of larger particles, in comparison to what had been obtained using the other sole surfactants. The particles formed using this method, were large enough to support oxide shell growth. Hence, when magnetic measurements were made of these particular particles they tended to display exchange bias effects.

When chemical composition of the Co_xNi_{1-x} particles was varied, it was possible to correlate some of the magnetic properties of the particles, with the composition. Measurements made of the exchange fields in samples where the composition was varied showed that as nickel-loading increased the exchange bias effect was dampened. The largest exchange field determined for any sample in this study was for the pure cobalt sample at around 2800 Oe. The addition of 20 % nickel decreases this slightly to around 2000 Oe. However, the exchange field increases again, slightly for the sample with 40 % nickel content. Therefore, detailed investigations into this particular range would be interesting to carry out in the future. Large enhancements in coercivity were also evident in these samples, which was characteristic of exchange anisotropy in the particles.

Studies carried out into the blocking temperatures of the particles were less conclusive. However, there were some encouraging results which suggested a correlation between particle diameter and blocking temperature. Measurements on two sets of $Co_{80}Ni_{20}$ particles, with different mean diameters, showed that the smaller particles blocked at a lower temperature than the larger particles. This suggests a positive correlation between particle size and blocking temperature.

These results coupled with the physical and structural characterisation described earlier, indicated the highly interesting properties of particles within the Co_xNi_{1-x} system. This study has shown that it is possible to tune the magnetic properties, and in particular control the exchange bias in a systematic fashion, by altering the composition.

4.2 Future work

The key to any future work, which follows on from what has been achieved in this study, is to establish more control over the size of the particles by establishing rigid control over their nucleation. The process that was adopted for the synthesis of these particles has presented many problems, and by possibly adapting the synthesis a little further, the benefits could be immense. For example, if the heating of the reactant solutions were controlled by using a temperature programmable heating mantle, the effect of the heat rate on nucleation could be much more definitive.

Another improvement which could be made to the synthetic process is the implementation of all reactions in a glove-box under an atmosphere of argon. This would severely limit the possibility of oxidation to the core of the smaller particles. It would also allow particles to be oxidised in a more controlled manner, so that experiments could be carried out on the native, partially oxidised and fully oxidised particles. This would enable a detailed picture to be built of the composite alloy particles and their physical and functional magnetic properties at the various stages of oxidation. Furthermore, the particles could be stored in their native solutions, in an inert atmosphere to prolong their life and lengthen the time over which analysis can occur. If reactions were carried out in such an atmosphere, it may even be possible to experiment with nickel and cobalt carbonyls to synthesise alloy particles. The thermal decomposition of carbonyls has been extensively researched, and the nucleation of particles using this method could be investigated to compare with the polyol reduction process reported in this thesis.

Studies into the local environment of the particles that have been produced, using EXAFS would be very interesting, and would provide a great deal of valuable information about the structure of the particles. HRTEM would also be beneficial for routine observation work, as it would prove the presence of a core-shell structure. The ability to resolve lattice planes using this technique could be correlated with XRD studies, to characterise the phases present across an individual particle.

XPS studies gave very interesting results in this study and it would be illuminating to build upon the work carried out here, and be able to quantify the depth of the penetrating beam during the etching process. By determining this, it may be possible to use this information, along with the particles' mean diameter to determine

the oxide shell diameter, in addition to the information already garnered from this technique.

The magnetic studies carried out in this investigation have yielded useful information, and helped characterise the functional properties of core-shell Co_xNi_{1-x}/CoNiO nanoparticles. Preliminary AC susceptibility studies were carried out, and given more time, it would have been interesting to analyse some of the other samples using this technique. This technique helped to shed light on the profile of the ZFC and FC curves of a specific sample, and could be used in the future to elucidate the structure in such plots and in turn, characterise core-shell blocking temperatures in the particles.

The work described in this thesis has shown that the magnetic properties of Co_xNi_{1-x}/CoNiO nanoparticles can be tuned. This system has been interesting to characterise, however, if some of the issues discussed in this section are addressed, then the synthesis and hence the magnetic properties could be further refined in the future.

5. Experimental

5.1 Introduction

This chapter gives an outline of each of the individual synthetic processes developed during the course of this investigation, in order to achieve the aims set out at the beginning of this thesis. An overview of each of the various analytical techniques used to characterise the particles is given in section 5.7 of this chapter.

Chapter 1 introduced the nucleation theory which forms the basis of polyol synthesis, in addition to describing the significance of making magnetic nanoparticles and their various properties. Chapter 2 discussed in great detail the main lines of investigation that were probed during this study, which included homogenous nucleation, heterogeneous nucleation, surfactants and compositional variation. The evolution and developments of the reaction conditions are also described in detail in Chapter 2. The main objective of the project was to synthesise magnetic nanoparticles

which displayed the exchange bias functional property. The characterisation of magnetic properties, and the results obtained from these processes, is documented in Chapter 3.

5.1.1 Reactant materials

The syntheses were carried out using standard airless Schlenk line techniques under N_2. Absolute ethanol (GPR), toluene (GPR) and hexane (Analar) were used as received, for the cleaning and washing of nanoparticle solutions before the particles were isolated and dried for analysis. Dioctyl ether (99.9%), dodecane, decalin, diphenyl ether, 1,2-hexadecanediol, oleic acid (~90% technical grade), oleylamine (~70% technical grade), trioctylphosphine oxide, tributylphosphine, cobalt (II) tetrahydrate acetate, nickel (II) tetrahydrate acetate, cobalt (III) acetylacetonate, nickel (II) acetylacetonate and platinum (II) acetylacetonate were purchased from Aldrich Chemical Company. These commercially available reagents were also used as received and no further purification was carried out to any of the reagents.

5.1.2 Reaction set-up

The synthesis of Co_xNi_{1-x} particles was carried out using the polyol method. The particles were made using Schlenk line techniques in an atmosphere of nitrogen, so that oxygen was excluded during the synthesis and particle oxidation was limited. The metallic salts, reducing agent, nucleating agent (if used), surfactants and solvent were all added to a 250 mL two- or three-necked round-bottomed flask prior to the reaction beginning. The flask and its contents were subsequently evacuated and flushed with nitrogen in three cycles. The reactant solution was then heated using a heating mantle with a magnetic stirring function. The particles were stirred, and the temperature of the reactant solution was measured throughout the synthetic process, with a thermometer attached to the set-up. A diagram of the apparatus required for a typical polyol synthesis in this study is shown in Figure 62.

Figure 62. Polyol reduction synthesis-typical set-up for synthesis of Co$_x$Ni$_{1-x}$ core-shell nanoparticles

N$_2$ flow from Schlenk Line

Water out

Water in

Heat and Stirring
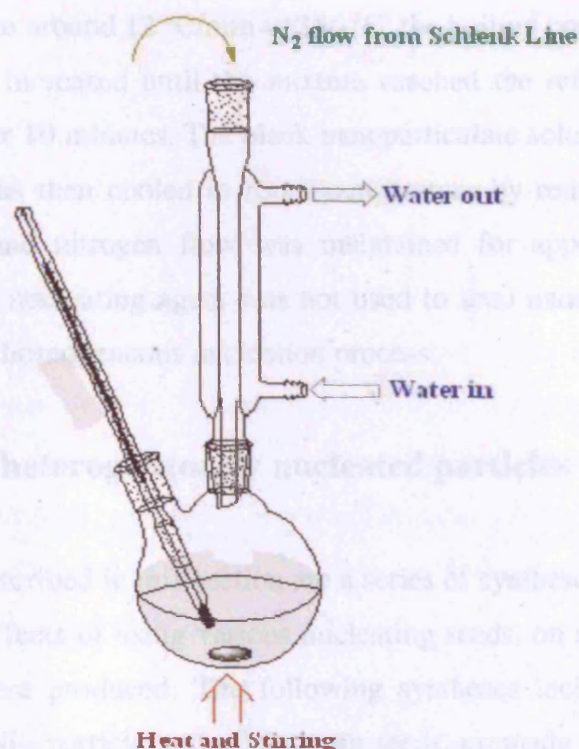
The changes in colour of the solution were noted throughout the heating process. Once particle formation had occurred, the nanoparticle solution was isolated and stored in its respective solvent. The nanoparticle solution was stored in this manner, prior to the washing and drying procedures described in section 5.6 of this chapter, which were required before any characterisation and analysis could take place. The methods of characterising the nanoparticles in solution, or in dried powder form, are detailed in section 5.7 of this chapter.

5.2 Synthesis of homogeneously nucleated Co$_{80}$Ni$_{20}$ particles

A 250 mL three-necked round bottomed vessel was initially charged with all the reactants. Cobalt tetrahydrate acetate (0.3992 g, 1.603 mmol) and nickel tetrahydrate acetate (0.0992 g, 0.3986 mmol), oleic acid (3.5600 g, 12.6036 mmol), 1,2-hexadecanediol (0.9994 g, 3.8670 mmol) and dioctyl ether (30 mL) were then mixed and magnetically stirred. The flask and reactants were evacuated to remove any air,

subsequently purged with nitrogen three times and left under nitrogen flow for the duration of the reaction. The salts, surfactant stabiliser and solvent were heated gradually at a rate of approximately 2 °C/min to 160 °C over 75 minutes, and then heated at a faster rate around 12 °C/min to 286 °C, the boiling point of dioctyl ether. The heat rate was then increased until the mixture reached the reflux temperature of the solvent, and kept for 10 minutes. The black nanoparticulate solution was formed at 227 °C. The mixture was then cooled to room temperature by removing the heat source. Magnetic stirring and nitrogen flow was maintained for approximately 30 minutes during this time. A nucleating agent was not used to seed nanoparticle growth in this reaction to ensure a homogeneous nucleation process.

5.3 Synthesis of heterogeneously nucleated particles

The experiments described in this section are a series of syntheses that were carried out, to investigate the effects of using various nucleating seeds, on the size of the $Co_{80}Ni_{20}$ particles, which were produced. The following syntheses include the heterogeneous nucleation of $Co_{80}Ni_{20}$ particles using platinum seeds, premade $Co_{80}Ni_{20}$ nanoparticles, gold and silver seeds.

5.3.1 Synthesis of $Co_{80}Ni_{20}$ particles using platinum seeds

In this experiment, a platinum salt was used to seed the growth of $Co_{80}Ni_{20}$ nanoparticles. The 250 mL three-necked round-bottomed flask was charged with cobalt tetrahydrate acetate (0.4009g, 1.6095 mmol), nickel tetrahydrate acetate (0.1026g, 0.4123 mmol), oleic acid (3.5000g, 12.3911 mmol), platinum acetylacetonate (0.0051g, 0.01297 mmol), 1,2-hexadecanediol (1.0010g, 3.8773 mmol) and dioctyl ether (30 mL). All of the reagents were placed in the flask, at the start of the reaction in this one-pot synthesis. The reactant mixture was heated to 160 °C, gradually over a 75 minute period, and magnetically stirred under a flow of nitrogen during this time. The water supply to the reflux condenser, was switched on when the reactant solution was at 160 °C, prior to the heat rate being ramped. The heat rate was then increased so the nanoparticle solution reached the solvent boiling temperature (286 °C). The solution was refluxed for 10 minutes, and then removed from the heat source whilst the

dispersion was cooled to room temperature under nitrogen flow, with magnetic stirring. The flask was then opened to air and the particles were washed with ethanol and then toluene in 3 cycles (1 x 30 mL ethanol followed by 1 X 10 mL toluene). Finally, the particles were redispersed in 20 mL hexane or toluene and the solutions stored in glass screw cap vials.

The colour of the reaction solution changed from red to mauve, bright purple to deep purple and then to a blackcurrant colour before particle formation was observed. The solution changed from red to blackcurrant over a period of 25 minutes, from between 38 °C and 120 °C. Prior to the solution turning red, the salts and reducing agent remained undissolved between room temperature and 38°C. Nanoparticle formation occurred at approximately 230 °C in this instance, and the solution was completely black at around 242 °C. The observed colour changes were similar to those in the homogeneously nucleated sample. This solution was stable upon application of a magnet, and a few days later, the particles had not fallen out of solution. The black liquid remained stable for a several months in air.

5.3.2 Synthesis of $Co_{80}Ni_{20}$ particles using premade particles as seeds.

In the first step of this two-stage synthesis, cobalt tetrahydrate acetate (0.4021g, 1.6143 mmol), nickel tetrahydrate acetate (0.1016g, 0.4083 mmol), 1,2-hexadecanediol (1.0030g, 3.8809mmol) and oleic acid (0.4494g, 1.5911 mmol) were dissolved in diphenyl ether (30 mL). The entire reaction was carried out in an atmosphere of nitrogen with magnetic stirring. The resulting solution was heated from room temperature to approximately 150°C over 20 minutes. At this point tributylphosphine (0.3048g, 1.5070 mmol) was injected into the hot solvent solution. The heat rate was then increased and the solution's temperature rapidly rose to the reflux point of diphenyl ether (260 °C). The black nanoparticle seed solution was formed at approximately 228 °C. The temperature of the solution was maintained at this 260 °C for 90 minutes to allow for the full crystallisation of the particles during reflux. The resulting black colloidal solution was then cooled to room temperature. $Co_{80}Ni_{20}$ particles were synthesised and used as a seed solution to grow larger $Co_{80}Ni_{20}$ particles.

The second step of the growth process was then implemented. A calculated volume, of the black nanoparticle solution was kept in the reaction flask (3 mL), whilst

the rest of the solution was removed for storage. This 3 mL aliquot of solution was used to seed the growth of larger nanoparticles. Further reactants including cobalt tetrahydrate acetate (0.1777g, 0.7134 mmol), nickel tetrahydrate acetate (0.0447g, 0.1796 mmol), 1,2-hexadecanediol (0.4600g, 1.9050 mmol), and oleic acid (0.1685g, 0.5965 mmol) were directly added to the 3 mL aliquot of solution that had remained in the reaction flask with diphenyl ether (30 mL). The solution with the additional reactants was then heated to about 150°C. At this point tributylphosphine (0.1464g, 0.7236 mmol) was injected into the flask. The solution was then heated to the reflux temperature of the diphenyl ether (260 °C), and kept at that temperature for 30 minutes. The formation of the larger particles in the second reaction occurred at approximately 238 °C.

5.3.3 Synthesis of $Co_{80}Ni_{20}$ particles using other noble metal seeds

Particles were synthesised using noble metal seeds, as described in section 5.3.1. However, silver chloride (AgCl) and auric acid ($HAuCl_4$) were used as a replacement for platinum acetylacetonate. The same synthetic procedure and molar ratios between reactants were adopted, as with the platinum seeds experiments. The effect of these seeds on the size of the $Co_{80}Ni_{20}$ particles that were synthesised is described in Section 2.2.2. These experiments were not developed any further, as there was no improvement to the size control of the $Co_{80}Ni_{20}$ from this method.

5.4 Surfactant variations

The following sections detail syntheses of $Co_{80}Ni_{20}$ nanoparticles, using a number of surfactant stabilisers to control particle growth, prevent oxidation and also limit aggregation.

5.4.1 Synthesis of $Co_{80}Ni_{20}$ particles with oleic acid

Cobalt tetrahydrate acetate (0.4003g, 1.6071 mmol), nickel tetrahydrate acetate (0.1013g, 0.4071 mmol), 1,2-hexadecanediol (1.0009g, 3.8729 mmol), oleic acid

(3.5308g, 12.5002 mmol), platinum acetylacetonate (0.0048g, 0.02204 mmol) and dioctyl ether (30 mL) were added to the flask. The reactants were heated with magnetic stirring in an atmosphere of nitrogen. The heat rate was initially slow, and the reactants were heated to 160°C, over a period of 75 minutes. The solution's colour changed from red to deep purple during this period. The heat rate was then increased so that the solution reached the reflux point of 286°C in 15 minutes. The black nanoparticulate solution was recovered from the flask and stored in glass sample vials until the cleaning procedure was implemented for analysis of the particles. Particle formation occurred at 220°C, the liquid was stable and particles were not drawn out of solution upon application of a magnet, or over time due to gravity. The reaction proceeded in a similar manner to that described earlier for platinum seeds (section 5.3.1). These reactions are essentially the same in terms of molar quantities of salts and reactant used.

5.4.2 Synthesis of $Co_{80}Ni_{20}$ particles with oleylamine

$Co_{80}Ni_{20}$ nanoparticles were synthesised using cobalt tetrahydrate acetate (0.4007 g, 1.6087 mmol), nickel tetrahydrate acetate (0.1003 g, 0.4031 mmol), 1,2-hexadecanediol (1.0005 g, 3.8713 mmol), oleylamine (3.3436 g, 12.4999 mmol), platinum acetylacetonate (0.0053 g, 0.0135 mmol) and dioctyl ether (30 mL) were stirred and heated in an atmosphere of nitrogen. The solution was initially heated to 160°C over a 75 minute period, and then rapidly heated to 286°C, the boiling temperature of dioctyl ether. Particle formation occurred at 218 °C and was characterised by the sudden appearance of black particles around rim of the flask. The nanoparticle solution was recovered and subsequently analysed using a variety of techniques.

5.4.3 Synthesis of $Co_{80}Ni_{20}$ particles with oleic acid/oleylamine mixture (OA/OY)

The method adopted for the OA/OY synthesis was different to other reactions where surfactant has been altered. Reasons for adopting this new method are given in Chapter 2. Cobalt (acetylacetonate)$_3$ (0.2850 g, 0.8000 mmol), nickel (acetylacetonate)$_2$ (0.0518 g, 0.2016 mmol), 1,2-hexadecanediol (1.2923 g, 5.0004 mmol), oleic acid (0.8474 g, 3.0001 mmol), oleylamine (0.8025 g, 3.0001 mmol), platinum acetylacetonate (0.0056

g, 0.0142 mmol) and dioctyl ether (20 mL) were heated and stirred under nitrogen flow to 160 °C over 68 minutes. The heat rate was then increased, and the solvent reached reflux temperature after 7 minutes. The solution was kept at 286 °C for 10 minutes, and then was removed from the mantle, but left to stir in the inert atmosphere. Particle formation was noted at 230 °C. Prior to this synthesis, the oleic acid and oleylamine surfactant mixture was prepared by weighing 1:1 molar quantities of both components and then combining these with moderate heating and vigorous stirring. The quantities of both surfactants were accurately weighted on a four figure balance. The density difference of both surfactants when melted, meant that vigorous stirring was required to ensure they were sufficiently mixed with one another and two separate layers of surfactant did not form.

5.4.4 Synthesis of $Co_{80}Ni_{20}$ particles with trioctylphosphine oxide (TOPO)

Several experiments were carried out in order to synthesise TOPO stabilised $Co_{80}Ni_{20}$ nanoparticles. The following synthesis is one of four described in Chapter 2 (section 2.6.5.1) and illustrates the manner by which those particular syntheses took place. Cobalt tetrahydrate acetate (1.6 mmol), nickel tetrahydrate acetate (0.4 mmol), 1,2-hexadecanediol (3.98 mmol), trioctylphosphine oxide, platinum acetylacetonate (molar amounts in Table 3) and dioctyl ether (30 mL) were heated to 160°C over a 75 minute period in an inert atmosphere with magnetic stirring. The solution was then heated to 286°C, the solvent boiling temperature. The heating profile adopted for these reactions was identical to that of other syntheses where surfactant-type has been varied, apart from the OA/OY synthesis described in section 5.4.3. Nanoparticle formation, characterised by a change in colour of the reaction solution from deep purple to black, occurred at between 204 – 209 °C for the various TOPO-coated $Co_{80}Ni_{20}$ particles that were made. The reaction conditions of several nanoparticle syntheses that used TOPO as sole surfactant, are documented in section 2.6.5.1 (Table 3), as are the results and discussion relating to these.

5.4.5 Synthesis of Co$_{80}$Ni$_{20}$ particles with tributylphosphine (TBP)

Cobalt acetate tetrahydrate (0.3998 g, 1.6051 mmol), nickel tetrahydrate acetate (0.0999 g, 0.4015 mmol), 1,2-hexadecanediol (1.0018 g, 3.8763 mmol) and diphenyl ether (30 mL) were heated and stirred in an atmosphere of nitrogen. A nucleating agent was not used in this particular reaction. The reaction mixture was initially heated from room temperature to approximately 160 °C in 40 minutes. The colour of the solution changed from red to a deep purple during this time, due to reduction of the respective metallic ion species in solution. At this point, tributylphosphine (2.6240 g, 12.9695 mmol) was injected into the reaction mixture. Upon the addition of TBP, the mixture darkened in colour, so that the solution was dark brown with a purple hue at the meniscus. The addition of the TBP also led to a puff of vapour being expelled in the flask. The heat rate was then increased to a rapid rate of approximately 10 °C per minute. The reactant mixture reached 260 °C in 10 minutes, and was then left to reflux at this temperature for a further 10 minutes. The nanoparticle solution was subsequently cooled under nitrogen flow, with magnetic stirring, following the removal of the vessel from the mantle. Nanoparticle formation occurred at approximately 224 °C. On the day of synthesis, there was a slight response of the solution to a magnet. The particles did not maintain their stability in solution and settled to the bottom of the vial after a few days.

5.5 Compositional variation

Following detailed investigations into nucleation methods and suitable surfactants for the Co$_x$Ni$_{1-x}$ system, using the Co$_{80}$Ni$_{20}$ formulation as a basis, synthesis of the other alloys in this series was carried out. Experimental details are given in the following subsections. The various studies that had been carried out into this Co$_x$Ni$_{1-x}$ system, indicated that it was best to nucleate the particles heterogeneously. The best surfactant determined for these alloy nanoparticles was an OA/OY mixture. This particular mixture had shown that it was effective at stabilising the particles against oxidation and agglomeration, in addition to controlling their respective sizes. The syntheses described in the following section put into practice this optimised synthetic process, in order to fabricate particles within this compositional series.

5.5.1 Synthesis of cobalt nanoparticles

The synthesis of cobalt nanoparticles was carried out using similar methods to those described earlier for the OA/OY mixture synthesis of $Co_{80}Ni_{20}$. Cobalt (acetylacetonate)$_3$ (0.3557 g, 0.9843 mmol), 1,2-hexadecanediol (1.2923 g, 5.0003 mmol), oleic acid (0.8474 g, 3.0001 mmol), oleylamine (0.8025 g, 3.0001 mmol), platinum acetylacetonate (0.0058 g, 0.0147 mmol) and dioctyl ether (20 mL) was heated to 162°C over 70 minutes. The heat rate was then increased and ramped to a reflux temperature of 286°C in approximately 8 minutes. The solution was refluxed for 10 minutes at this temperature and then left to cool under nitrogen flow, with stirring. Nanoparticle formation occurred at 226°C, characterised by a change in the colour of the solution from deep olive green to black. Once cooled to room temperature, the solution was tested with a magnet, to determine whether magnetic particles had formed. The particles were attracted to the magnet very strongly and were drawn out of the solvent. The particles remained magnetic for several months in air, suggesting oxide shell growth had occurred and the particles were well passivated.

5.5.2 Synthesis of $Co_{80}Ni_{20}$ nanoparticles

$Co_{80}Ni_{20}$ nanoparticles were synthesised with cobalt (acetylacetonate)$_3$ (0.2858 g, 0.8022 mmol), nickel (acetylacetonate)$_2$ (0.0518 g, 0.2082 mmol), 1,2-hexadecanediol (1.2922 g, 5.0000 mmol), oleic acid (0.8474 g, 3.0000 mmol), oleylamine (0.8025 g, 3.0001 mmol), platinum acetylacetonate (0.0046 g, 0.0116 mmol) and dioctyl ether (20 mL). The reactant mixture was heated to 162°C over 70 minutes and then to the reflux temperature of 286°C in 8 minutes. The mixture was then left to reflux for 10 minutes at the solvent boiling temperature. The mixture was then removed from the heating mantle and allowed to cool, with stirring and nitrogen flow, down to room temperature. The solution turned black, indicating nanoparticle formation at approximately 230°C.The particles were strongly attracted to a permanent magnet with some being drawn out of solution. This effect remained even after several months of the nanoparticle solution being left out in air.

5.5.3 Synthesis of Co$_{60}$Ni$_{40}$ nanoparticles

Cobalt (acetylacetonate)$_3$ (0.2138 g ,0.6001 mmol) and nickel (acetylacetonate)$_2$ (0.1028 g, 0.4001 mmol) were used in a 3:2 ratio for the synthesis of Co$_{60}$Ni$_{40}$. Platinum (acetylacetonate)$_2$ (0.0050 g, 0.0127 mmol) was also used as the sample was heterogeneously nucleated. Oleic acid (0.8474 g, 3.0000 mmol) and oleylamine (0.8025 g, 3.0001 mmol) made up an OA/OY 1:1 mixture which was the surfactant stabiliser with dioctyl ether (20 mL) used as the solvent medium. The heating regime that had been used in previous syntheses was maintained. The mixture was steadily heated up to 160°C over 100 minutes, and then rapidly heated to the solvent boiling temperature over 8 minutes. Nanoparticle formation occurred at 228°C, and was characterised by the solution changing in colour from deep purple to black. The solution was initially variant shades of green due to the colour of the precursor salts, and eventually deepened in colour to purple followed by black. The black nanoparticle solution was isolated after cooling under nitrogen and stirring. The resultant nanoparticle solution was tested with a magnet. These particles also responded on the day of synthesis, and over subsequent weeks.

5.5.4 Synthesis of Co$_{50}$Ni$_{50}$ nanoparticles

The molar precursor ratio of the cobalt and nickel salts in this reaction, were varied to form the Co$_{50}$Ni$_{50}$ nanoparticulate alloy. Cobalt (acetylacetonate)$_3$ (0.1786 g, 0.5013 mmol) and nickel (acetylacetonate)$_2$ (0.1290 g, 0.5021 mmol) were therefore used in a 1:1 ratio. The growth of the particles was seeded with platinum (acetylacetonate)$_2$ (0.0048 g, 0.0122 mmol), with oleic acid/oleylamine used to stabilise the particles (1.6508g, 6 mmol) and dioctyl ether (20 mL) used as solvent. The reaction mixture was heated gradually to 160°C over 65 minutes, and then rapidly heated to 286 °C over 8 minutes. Nanoparticle formation occurred at 222°C. Repeat syntheses also yielded black nanoparticulate solutions at around the same formation temperature. These particles did respond to a magnet on the day of synthesis and fell out of solution.

5.5.5 Synthesis of Co₄₀Ni₆₀ nanoparticles

Nanoparticles of expected composition, $Co_{40}Ni_{60}$, were synthesised using similar methods to those described for the other samples in this compositional series. The molar ratios of the salts were adjusted accordingly. Cobalt (acetylacetonate)₃ (0.1432 g, 0.4020 mmol) and nickel (acetylacetonate)₂ (0.1530 g, 0.5955 mmol) were used in a 2:3 ratio. Platinum (acetylacetonate)₂ (0.0058 g, 0.0014 mmol) was used to seed particle growth and an oleic acid/oleylamine mixture stabilised the particles (1.6506 g, 6 mmol).The solvent used for these reactions was again dioctyl ether (20 mL). The reaction proceeded by heating the reactants for 75 minutes until the solution temperature was 158°C. The heat rate was then increased so that the boiling point of the solvent was attained in 8 minutes. The solution was heated for a further ten minutes at the reflux temperature of 286°C. Nanoparticle formation occurred at 224°C, characterised by change in solution colour from deep purple to black. The following day the nanoparticles had crashed out of solution and also responded strongly to a magnet.

5.5.6 Synthesis of Co₂₀Ni₈₀ nanoparticles

The molar ratios of the metallic precursors were altered so that $Co_{20}Ni_{80}$ nanoparticles could be formed (1:4 ratio). Cobalt (acetylacetonate)₃ (0.0703 g, 0.1973 mmol), nickel (acetylacetonate)₂ (0.2055 g, 0.7998 mmol), 1,2-hexadecanediol (1.2922 g, 5.0000 mmol), oleic acid/oleylamine mixture (1.6502 g, 6 mmol), nucleating agent; platinum acetylacetonate (0.0050 g, 0.0127 mmol) and dioctyl ether (20 mL) were used to make the particles. The reactants were heated to 161°C over a period of 50 minutes. The heat rate was increased so that the reflux temperature of the solvent was achieved after 8 minutes. Nanoparticle formation occurred at around 220°C. The solution was refluxed at this temperature for 10 minutes. Some vapour was evolved during this stage of the reaction. The reaction vessel was removed from the mantle and the nanoparticulate mixture was cooled with nitrogen flow. The nanoparticles in solution did not respond to a magnet on the day of synthesis or at any time over subsequent weeks. The particles had also fallen out of solution and did not remain as a stable liquid.

5.5.7 Synthesis of nickel nanoparticles

The nickel nanoparticles were made using similar methods to those described above for other samples in this compositional series. Nickel (acetylacetonate)$_2$ (0.2490 g, 0.9692 mmol), 1,2-hexadecanediol (1.2920 g, 4.9992 mmol), oleic acid/oleylamine (1.6497g, 6 mmol), platinum acetylacetonate (0.0050 g, 0.0127 mmol) and dioctyl ether (20 mL) were weighed out and placed in the two-necked round bottomed flask. The reactants were heated to 158°C in approximately 85 minutes, and then the heat was increased so that the reflux point of 286°C was reached in 7 minutes. The solution was held at this approximate temperature for a further 10 minutes. Nanoparticles were formed when the solution was at a temperature of 220°C. This was evident by the change in the appearance of the colour of the solution, which turned from a murky green/brown colour to black, in an instant at that particular temperature. The solution was then cooled, by maintaining the stirring condition, and removal of the flask from the heating mantle. The particles that were formed did not respond to a magnet on the day of synthesis, or few weeks later. These particles also did not form a stable nanoparticulate solution.

5.6 Post-Preparative Procedures

After cooling the reaction mixture to room temperature with magnetic stirring and N$_2$ flow, the following steps were performed in air. The crude solution of black Co$_x$Ni$_{1-x}$ nanoparticles was precipitated and separated via centrifugation. Ethanol (25 mL) was added to 5 mL of the nanoparticle solution and shaken. The ethanol acted as a flocculent which caused the particles to "crash out" of solution. The resultant precipitate was isolated by centrifugation (~ 10,000 rpm). This precipitate was then re-dispersed in toluene (10 mL) and centrifuged again. This cleaning cycle was carried out two times additional times, however, the amount of ethanol used in subsequent washes was reduced to 10 mL. This process ensured the washing and removal of excess stabilisers. Each time toluene was introduced to the nanoparticle solution, two drops of the specific surfactant used in the reaction was also added. This addition of surfactant ensured that any excess stabiliser that was washed away from the nanoparticle coatings was replaced, as this would result in aggregation of the particles. After the washings had

taken place, the resulting black precipitate which contained Co_xNi_{1-x} nanocrystals, was re-dispersed in various non-polar solvents in a variety of concentrations (toluene, hexane etc).The nature of the solvent used for the particle's storage was dependent upon the subsequent particle analysis that had to take place.

The nanoparticles were isolated in a powder form, by performing the cleaning cycles detailed above, and then in the final step, re-dispersing in acetone. The acetone-particle solution was decanted from the centrifuge tubes into glass sample vials or aluminium boats. These were then placed either in: (i) air to allow to air drying or (ii) the antechamber port of a glove-box or (iii) in a dessicator under the flow of nitrogen gas. The materials were left in this state for two days to allow the slow and controlled growth of an oxide shell. After initial investigations into the oxidative processes using magnetic studies detailed in later chapters. It was found that the best method of drying, in order to encourage the growth of an oxide shell, was by using antechamber of the glove-box. Therefore, for all of the particles discussed in this thesis, this particular method was used to dry the particles. The resultant dry powders were stored in glass screw-cap vials in air, or in their native liquid solutions also within the glass vials. The samples were dried, as required, for particle analysis. This was because the particles were less susceptible to oxidation in their native liquid form, in comparison to a nanoparticulate powder, as the solvent and surfactant provided a barrier to surface oxidation.

5.7   Characterisation of nanoparticles

The structural morphology, composition and magnetic properties of the Co_xNi_{1-x} nanoparticles were analyzed using transmission electron microscopy (TEM), elemental analysis (EA), energy-dispersive X-ray analysis (EDX) and a superconducting interference device (SQUID). Each sample described in this thesis was characterised using a number of techniques. Some of the samples were characterised further because of their possible magnetic functional properties. The additional techniques used in these instances included: High–resolution transmission electron microscopy (HRTEM); electron energy loss spectroscopy (EELS); thermogravimetric analysis (TGA), x-ray photoelectron spectroscopy (XPS) and x-ray diffraction (XRD). Fourier transform

infrared spectroscopy (FTIR) was also used to characterise surfactant interactions with the nanoparticles.

Samples were cleaned and prepared for TEM analysis by re-dispersion of the nanoparticles into hexane. A droplet of the nanoparticle hexane dispersion was dropped onto an amorphous carbon copper grid. All observational analysis was carried out using a JEOL 100KV instrument. Electron film images were taken of different areas of the grid to give an accurate representation of particle size and shape in a particular sample. These were scanned to obtain digital images and the contrast adjusted to improve particle visibility, in Adobe Photoshop[1] software. This was necessary in order to be able to view detail in the particle structure. Particle size distributions were calculated using the Image J programme,[2] which correlates pixel coverage of the nanoparticles with size, using the magnification used in the image capture to calculate size. The particles are identified by the difference in contrast between the individual nanoparticle and the background. Analysis was made of at least 200 particles in a sample, in different areas of the amorphous carbon grid. The samples were each viewed carefully and incidences where particles had aligned themselves on top of one another lead to the software counting them as a single particle. Therefore, these were not included for purposes of a size distribution count. The software measured the particles' major and minor axes, and these were then averaged to obtain an approximate nanoparticle diameter. This accounted for the imperfect shapes of the particles, so they could not be modelled to that of a perfect sphere.

Igor Pro[3] data analysis software was used to fit the data to appropriate distribution functions, so that average particle sizes and standard deviations could be obtained. Multi-peak fitting was implemented for samples that had a variable distribution i.e bimodal distribution. This was carried out in order to determine accurately the mean particle size in samples that had multiple nucleation events, resulting in large populations of particles in two or three dominant size ranges.

Elemental microanalysis was carried out at UCL, on milligram quantities of sample. The elements tested for were carbon, hydrogen and nitrogen as they were present in the surfactants. The technique was used to quantify the amount of sample mass that was due to surfactant stabiliser.

---

[1] http://www.adobe.com/
[2] http://rsb.info.nih.gov/ij/
[3] http://www.wavemetrics.com/

EDX was carried out in conjunction with a scanning electron microscope (SEM), as an additional analytical package to the SEM set-up. SEM and EDX measurements were carried out on a Field Emission JEOL 6301F using the keV system. The SEM was calibrated with standard reading from a cobalt calibration. The calibration was performed frequently between a number of measurements. An elemental study was carried out on samples to establish relative quantitative atomic ratios between the components of the nanoparticles. EDX provided an average quantification of an area of nanoparticles, which correlates with the electron beam size of the SEM. The beam size was approximately several microns in diameter. A much more precise method of analysis was carried out on a few samples using EELS which is described in detail on the next page. However, this method was sufficient in obtaining a relative ratio between the cobalt and nickel elements.

Samples were prepared in the following way: (i) a carbon background sticker was placed onto an aluminium stub (ii) the stub was dipped into the dried nanoparticulate powder and excess powder was shaken off (iii) the powder was carbon coated to ensure accurate quantitative results. The samples were then placed on a stage and introduced into the electron microscope chamber, having first been place under vacuum in an antechamber compartment. On each sample stub, quantitative analysis was conducted on five different areas or spots by rotating the stage, and an average of these was taken to ensure reproducibility. The values that are quoted in this thesis are atomic percentages. Images were also taken using the SEM; however the quality of the TEM images is much better for nanoparticle analysis, as it allows clear resolution of individual particles. Whereas the SEM displays aggregation in the particles, due to clumping that occurs in sample preparation.

Magnetic studies were carried out on a commercial superconducting quantum interference device. A Quantum Design MPMS7 was used to collect low temperature magnetic measurements, including zero field cooled curves to determine particle blocking temperatures and hysteresis loops on field cooled samples to investigate exchange bias effects in the samples. Samples were prepared by packing milligram quantities of the black nanoparticle powder into 5mm diameter agar gel capsules. The powders were fixed in place by packing down with cotton wool to ensure they were rendered immobile. Different types of measurement were made to elucidate various specific magnetic properties associated with that particular material. Initially, measurements were made at 280 K of magnetisation versus the applied magnetic field.

This type of measurement is a field-dependent measure of the moment of a sample, as the magnetic field is systematically increased and decreased, in hysteretic fashion.

The materials were initially cooled from room temperature to 5 K in a zero-applied magnetic field. The temperature was subsequently ramped to 280 K at 10 K intervals (ZFC measurement). Upon reaching 280 K the applied field was maintained and the temperature was decreased to 5 K. The temperature was then increased again to 280 K at 10 K intervals in order to perform the field-cooled measurement. During the ZFC measurement the magnetic dipoles are randomly oriented at room temperature and remain thus when the sample is cooled. At 5 K the spins do not possess enough thermal energy to allow rotation to occur. During the ZFC measurement, as the temperature is decreased, the kT also increases and the magnetic dipoles align parallel to the field that has been applied. This leads to an increased magnetic moment. During the field-cooled measurements the dipoles are aligned with the magnetic field at 280 K and remain configured in this position when the sample is cooled to 5 K. Whilst the temperature increases, kT provides energy for the magnetic dipoles, enabling randomisation in their orientation and hence a resultant decrease in magnetic moment. The temperature dependent decrease is observed in both ZFC and FC curves, as the temperature increases past the blocking temperature T_B.

Electron energy loss spectroscopy (EELS) was carried at Glasgow University on pre-selected specimens, which were chosen due to their interesting magnetic functional properties and hence indicated the formation of an oxide shell. The aim of this exercise was to establish the nature of the oxide shell, and gain an approximate shell thickness and particle core diameter. Due to the accuracy of this technique is quantifying oxygen content in a individual particle, it was also used to prove shell formation, and alloy formation in the core. The specimens were examined in an FEI Tecnai F20 TEM/STEM equipped with a field emission gun and a Gatan ENFINA electron spectrometer. Spectrum imaging was performed using Gatan Digital Micrograph and DigiScan software. A ~0.5 nm diameter probe with a convergence semi-angle of 13 mrad and a spectrometer collection semi-angle of 18 (or 30 mrad in some of the datasets) was used for the EELS data presented here. The energy range ~430 eV to ~1368 eV (1340 channels at 0.7 eV/ch) was recorded at a dispersion of 0.7 eV/ch and a typical dwell time of 5 sec per pixel. Although on occasion, a dwell time of 10 sec per pixel was also used.

Thermogravimetric magnetic analysis was also attempted. In the measurements discussed in this thesis, the instrument was used to ascertain an approximate Curie transition temperature (T_c) for the CoNi nanoparticles. The aim was to prove the nanoparticles were true solid solutions, with magnetic properties that could be varied with the alloy composition. The TGA could also be used to determine the amount of surfactant bound to the nanoparticle surface as mentioned earlier. Measurements were carried out on a Netzsch STA 660 instrument, with a rhodium furnace, in an inert atmosphere. During measurement runs, argon flow to the furnace was maintained, to protect the highly sensitive balance from the effects of the furnace being heated to elevated temperatures. Nitrogen was passed over the sample during the heating process to prevent oxidation. Due to the nature of the sample, alumina (Al_2O_3) crucible pans were used in all calibrations and measurement runs. This was to prevent any reaction between the metal alloy nanoparticles and the aluminium pan which are used in conventional TGA measurements. Temperature and sensitivity calibrations were performed on a series of standards over the temperature range where measurements were to be made. All sample measurements were standardised against the experimental calibration curve for the instrument using the melt temperatures as the calibration point. The highest temperature calibration standard used was gold which has a melting point of 1064 °C. The lowest melting temperature standard used was for indium with a melting point of 156 °C. The percentage of weight loss due to surfactant was apparent within the first 400 °C, dependent on the decomposition temperature of the surfactant. An example of a typical TGA run with a nickel calibration sample is shown in Appendix B. The TGA could also be used to determine the amount of surfactant bound to the nanoparticle surface.

X-ray photoelectron spectroscopy was carried out on a few samples to enable characterisation of elements in the sample, the oxidation state of these elements, and also to indicate the nature of connectivity between these particular elements. Information collected from this technique also gave confirmation of the core-shell structure of the particles when surface etching was carried out.

The sample was prepared for XPS by taking a large quantity of the dried powder, and pressing it into a pellet of approximately half a millimetre in thickness, using an infrared pellet press at a 7 kPa setting. Measurements were carried out using a VG ESCALAB 220iXL instrument with a monochromatic Al K_α radiation source. Binding energies were referenced to surface elemental carbon at 284.6 eV. Depth-

profiling was carried out using a 3kV argon ion gun operating at 0.5 μA to sputter the surface of the sample. The binding energies were correlated with results on the NIST database.[4]

The powder XRD technique was carried out to confirm the crystalline nature of the particles and to characterize the phases present. The measurements were made on a Bruker D8 Discover reflection diffractometer, with Cu-K$_\alpha$ (λ =1.5406 Å) in reflection mode. Where possible, Scherrer analysis of the full width half maximum (FWHM) of the most intense peak on a diffractogram was carried out. Scherrer analysis yields an approximate crystallite size for particles which can be compared to the mean particle size garnered from TEM studies. Therefore, this is a very useful technique that provides interesting information about the particles. Samples were prepared for XRD by packing down the nanoparticles powder onto the substrate. Measurements of the particles were made on a variety of substrates which included silicon, glass and wood. The particles had been pressed into a pellet for the purpose of an XRD measurement. A 13 mm die was used to press the black nanoparticulate powder into a small pellet. A pressure of 7kPa was applied in order to achieve the necessary compaction, and ensure a homogeneous surface from which to take the measurements. These peaks arose because of the long collection time for the data and the weak signal given from the sample. XRD studies have presented challenges in this particular study due to the nature of the samples.

---

[4] http://srdata.nist.gov/xps/

APPENDIX A

Theoretical X-ray diffraction peak positions for fcc Co, fcc Ni, fcc CoO and hcp Co obtained from the Powder Data File 2 database.
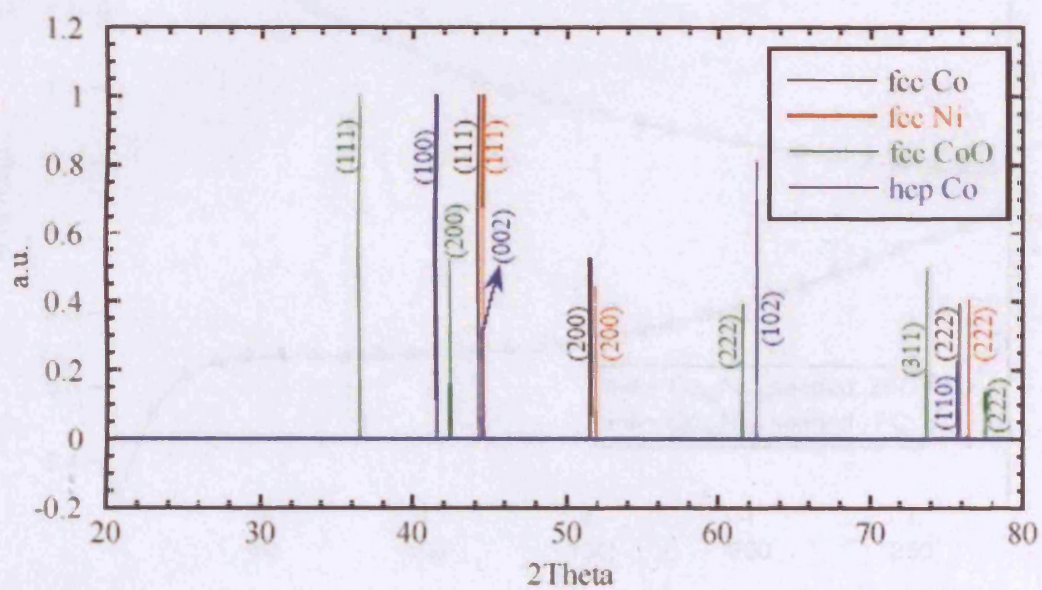
APPENDIX B

ZFC/FC curves for $Co_{80}Ni_{20}$ nanoparticles made with premade $Co_{80}Ni_{20}$ nanoparticle seeds.